SEPTEMBER 2018 Ph.D. in CIVIL ENGINEERING BARAA JABBAR MAHMOOD AL-ELIWI

UNIVERSITY OF GAZİANTEP

GRADUATE SCHOOL OF

NATURAL & APPLIED SCIENCES

CONCRETE-FILLED STEEL TUBE COLUMNS AND THE CONFINMENET EFFECT

Ph.D. THESIS

IN

CIVIL ENGINEERING

BY

BARAA JABBAR MAHMOOD AL-ELIWI

SEPTEMBER 2018

Concrete-Filled Steel Tube Columns and the Confinement Effect

Ph.D. Thesis

in

Civil Engineering

University of Gaziantep

Supervisor

Assoc. Prof. Dr. Talha EKMEKYAPAR

by

Baraa Jabbar Mahmood AL-ELIWI

September 2018

REPUBLIC OF TURKEY
UNIVERSITY OF GAZİANTEP
GRADUATE SCHOOL OF NATURAL & APPLIED SCIENCES
CIVIL ENGINEERING DEPARTMENT

Name of the thesis: Concrete-Filled Steel Tube Columns and the Confinement Effect

Name of the student: Baraa Jabbar Mahmood AL-ELIWI

Exam date: September 7, 2018

Approval of the Graduate School of Natural and Applied Sciences.

Prof. Dr. A. Necmeddin YAZICI
Director

I certify that this thesis satisfies all the requirements as a thesis for the degree of Doctor of Philosophy.

Prof. Dr. Hanifi ÇANAKCI
Head of Department

This is to certify that we have read this thesis and that in our consensus/majority opinion it is fully adequate, in scope and quality, as a thesis for the degree of Doctor of Philosophy.

Assist. Prof. Dr. Talha EKMEKYAPAR
Supervisor

Examining Committee Members:	Signature
Prof. Dr. Mustafa ÖZAKÇA	…………………………
Assist. Prof. Dr. Fatih ÇELİK	…………………………
Assist. Prof. Dr. Hasan Erhan YÜCEL	…………………………
Assist. Prof. Dr. Mehmet Tolga GÖĞÜŞ	…………………………
Assoc. Prof. Dr. Talha EKMEKYAPAR	…………………………

I hereby declare that all information in this document has been obtained and presented in accordance with academic rules and ethical conduct. I also declare that, as required by these rules and conduct, I have fully cited and referenced all material and results that are not original to this work.

Baraa Jabbar Mahmood AL-ELIWI

ABSTRACT

CONCRETE-FILLED STEEL TUBE COLUMNS AND THE CONFINEMENT EFFECT

AL-ELIWI, Baraa Jabbar Mahmood
Ph.D. in Civil Engineering
Supervisor: Assoc. Prof. Dr. Talha EKMEKYAPAR
September 2018
250 Pages

Concrete-filled steel tube (CFST) columns are one of the pioneering types of composite columns and are increasingly used in applications that require the support of large loads such as tall buildings, bridges, and offshore structures. CFST columns are used due to their high strength, high stiffness, high ductility, and high energy absorption capacities besides high speed of construction, relatively low economic cost, and compatibility with different types of connections.

These advantages result due to the composite action between the steel and the concrete where the concrete and the steel act together to combine the best features of both the steel tube and concrete to yield efficient performance. The steel tube confines the infilled concrete and serves as a perpetual formwork. Also, it works as longitudinal and transverse reinforcement. The circular cross-section offers enhanced confinement to the concrete compared to other shapes.

This thesis examines the conduct of circular CFST columns and the confinement effect with different types of strengths of concrete. In addition to classical CFST columns, a new configuration, concrete-filled double circular steel tube (CFDCST) stub columns were also studied, which provides an effective improvement in compression, ductility, and stiffness capacities relative to classical CFST columns of the corresponding size. Furthermore, the possibility of the CFDCST column concept for repairing deformed CFST columns was examined and gave good results. For assessment, test results were compared with the estimates of the AISC360-16, EC4, AS5100.6, and AIJ2001 design specifications.

Key Words: Circular concrete filled-steel tube columns, composite columns, confinement, composite action, design specifications.

ÖZET

İÇİ BETON DOLDURULMUŞ ÇELİK TÜP KOLONLAR VE SARGI ETKİSİ

AL-ELIWI, Baraa Jabbar Mahmood
Doktora Tezi, İnşaat Mühendisliği Bölümü
Tez Yöneticisi: Doç. Dr. Talha EKMEKYAPAR
Eylül 2018
250 sayfa

İçi beton doldurulmuş çelik tüp (CFST) kolonlar, kompozit kolonların öncü tiplerinden biridir ve yüksek binalar, köprüler ve açık deniz yapıları gibi büyük yükler taşıması gereken uygulamalarda giderek daha fazla kullanılmaktadır. Bu kolonlar, yüksek mukavemet, yüksek rijitlik, yüksek süneklik, yüksek enerji yutma kapasiteleri, yüksek inşaat hızı, nispeten düşük ekonomik maliyet sağladıkları ve farklı bağlantı türlerine uygulanabildiklerinden dolayı kullanılır.

Bu avantajlar, çelik tüp ve betonun en iyi özelliklerini bir araya getirerek verimli performans elde etmek için birlikte hareket ettiği, kompozit etki nedeniyle ortaya çıkar. Çelik tüp, içindeki betonu sargılar ve sürekli bir kalıp görevi görür. Ayrıca çelik tüp boyuna ve enine donatı olarak çalışır. Dairesel kesit, diğer şekillere kıyasla beton için daha fazla sargı etkisi ortaya çıkarır.

Bu tez, dairesel içi beton doldurulmuş çelik tüp kolonlarının davranışını ve farklı beton mukavemeti ile sargı etkisini incelemektedir. Klasik kolonlara ek olarak, yeni bir konfigürasyon olan beton doldurulmuş çift dairesel çelik tüp kolonlar da çalışılmıştır. Bu tip kolonlar klasik kolonlarına göre basınç, süneklik ve rijitlik kapasitelerinde etkili iyileştirmeler sağlar. Ayrıca, deforme olmuş kolonlarının onarımı için içi beton doldurulmuş çift çelik tüp kolon şeklinin kullanımı incelenmiş ve iyi sonuçlar elde edilmiştir. Değelendirmeler yapabilmek için test sonuçları AISC360-16, EC4, AS5100.6 ve AIJ2001 tasarım şartnamelerinin tahminleriyle karşılaştırılmıştır.

Anahtar Kelimeler: İçi beton doldurulmuş dairesel çelik tüp kolonlar, kompozit kolonlar, sargı etkisi, kompozit etkisi, tasarım şartnameleri.

ACKNOWLEDGEMENTS

At the very outset, all praises to **Allah** the lord of mankind.

I express my honest thanks and appreciation to Dr. Talha EKMEKYAPAR, my supervisor, for his support and invaluable guidance all through my study. I also admiringly thanks to Dr. Mehmet Tolga GÖĞÜŞ, for the great help and guidance. Also, I express my thank the examining committee members for their participation and valuable criticism.

The author would also like to thank the Iraqi Ministry of Higher Education and Scientific Research and the University of Mosul for providing this scholarship to finish my Ph.D study. Also, special thanks to the scientific research unit of the Gaziantep university for the financial support within the project MF 14.06.

The experimental research was conducted in the structural mechanic laboratory in the Department of Civil Engineering at Gaziantep University. I convey my thanks to all the people participated in the work.

I would also take this chance to thank my close friend Ahmed Abdalhafedh Mustafa AL-SHAAR for his help and immense contribution to my study.

I leave to the end to people to whom I have heartfelt thankfulness my lovely parents, brothers, and sisters for the endless and unconditional support and love. Special thanks to my wife for accompanying me through the tough times and lighting up my life with her smile, finally to my life candles my children. This work is granted to them with all my love.

TABLE OF CONTENTS

Page

LIST OF FIGURES

Page

LIST OF TABLES

Page

LIST OF SYMBOLS

Scalars

A_1	Constant coefficient of the concrete mix (= 4.1)
A_2	Constant coefficient of the lateral pressure $(= 5A_1)$
A_c	The cross-sectional area of the concrete core (mm^2)
A_e	the effective area of the cross-section (mm^2)
A_g	The gross area of the CFST cross-section (mm^2)
A_s	The cross-sectional area of the steel tube (mm^2)
A_{sr}	The cross-sectional area of the steel bar reinforcement (mm^2)
D, D_{outer}	The outer diameter of the steel tube (mm)
D_{inner}	The inner diameter of the steel tube (mm)
D_{sr}	The longitudinal steel bar reinforcement diameter (mm)
E_c	The tangent modulus of elasticity of the concrete (MPa)
EI_{eff}	Effective stiffness of the CFST column (MPa)
E_s	The modulus of elasticity of steel tube (MPa)
E_{sec}	The tangent modulus of elasticity of the concrete $= f_{cc}/\varepsilon_{cc}$ (MPa)
E_{sr}	The modulus of elasticity of steel bar reinforcement (MPa)
F_{cr}	the critical buckling stress (MPa)
f_c	Unconfined concrete compressive strength (MPa)

f_{cc}	Confined concrete compressive strength (MPa)
$f_{cube.100}$	The concrete compressive strength of standard cube 100×100 mm (MPa)
$f_{cube.150}$	The concrete compressive strength of standard cube 150×150 mm (MPa)
$f_{cyl.100}$	The concrete compressive strength of standard cylinder 1000×200 mm (MPa)
$f_{cyl.150}$	The concrete compressive strength of standard cylinder 150×300 mm (MPa)
f_y	The yield strength of the steel tube (MPa)
f_{yr}	The yield strength of the steel bar reinforcement (MPa)
I_c	moment of inertia of concrete core (mm^4)
I_s	moment of inertia of steel tube (mm^4)
I_{sr}	moment of inertia of steel bar reinforcement (mm^4)
K	the end fixity coefficient of the column
L	Length of the column (mm)
$N_{pl.Rd}$	The plastic resistance of the column of EC4 specification
N_{us}	The plastic resistance of the column of AS5100.6 specification
P_e, N_{cr}	The elastic critical buckling load (kN)
P_{no}	The nominal axial strength (kN) of AISC360-16 speciation
P_p	Plastic capacity of the section (kN) of AISC360-16 speciation
P_y	The yielding strength (MPa) of AISC360-16 speciation

r	Radius of the concrete core (mm), or, radius of gyration (mm)
r_{uc}	the reduction factor for concrete strength of AIJ2001 specfication
t_{inner}	Inner steel tube thickness (mm)
t, t_{outer}	Outer steel tube thickness (mm)

Greek

α	the imperfection factor of EC4 specification
α_a and α_b	the appropriate section constants
α_c	Compression member slenderness reduction factor
ε_c	Strain at unconfined concrete compressive strength (mm/mm)
ε_{c1}	Concrete strain at maximum compressive strength (mm/mm)
ε_{cc}	Strain at confined concrete compressive strength (mm/mm)
ε_y	Steel tube yield strength (mm/mm)
η_a	the steel reduction factor
η_c	the concrete enhancement factor
ν_c	Poisson's ratios for concrete
ν_e	Poisson's ratios for steel tubes
ρ_s	longitudinal steel reinforcement ratio
σ_{ah}	the circumferential tensile stress (MPa)
σ_{al}	the axial compressive stress (MPa)
σ_c	The concrete stress

σ_{crc}	the critical stress of a concrete column (MPa)
σ_{lat}	The confining stress
δ	the steel contribution ratio according to EC4
λ	the column's relative slenderness
ξ	The confinement coefficient
ρ	Concrete density (kg/m^3)
χ	The reduction factor of CFST column capacity

LIST OF ABBREVIATIONS

ACI	American Concrete Institute
AIJ	Architectural Institute of Japan
AISC	American Institute of Steel Construction
AS	Australian Standard
ASTM	American Society for Testing and Materials
CFDCST	Concrete Filled Double Circular Steel Tube
CFST	Concrete Filled Steel Tube
DI	Ductility Index
EC4	European Code
EFNARC	European Federation Dedicated to Specialist Construction Chemicals and Concrete Systems
FA	Fly Ash
FE	Finite Element
HPC	High Performance Concrete
HSC	High strength Concrete
HSS	High Steel Strength
LWC	Lightweight Aggregate Concrete
LWCFST	Lightweight Aggregate Concrete Filled Steel Tube

MSS	Mild Steel Strength
NSC	Normal strength Concrete
NWC	Normal Weight Concrete
RC	Reinforced Concrete
RLWCFST	Reinforced Lightweight Aggregate Concrete Filled Steel Tube
SCC	Self-Compacting Concrete
SCCFST	Self Compacted Concrete Filled Steel Tube
SF	Silica Fume
SI	Strength Index
SP	Super Plasticizer
TS	Turkish Standard
UHSC	Ultra High Strength Concrete

CHAPTER 1

INTRODUCTION

1.1 Background and Context

Composite columns are deemed the major significant structural members in multiple applications such as high-rise structures, marine structures, and long-span bridges, among others. Thus, concrete-filled steel tube (CFST) columns, which belong to the composite column family, provide excellent and economical solutions to support the heavy loads of these structures. These composite columns succeed due to their characteristics, such as small cross-section dimensions, high strength, high ductility, high energy absorption capacities, and economic cost. In the construction process of CFST columns, concrete is used to fill the hollow steel tube; the process allows production of composite columns with different geometrical and material properties.

The most significant structural features distinguishing this type of composite column from reinforced concrete columns and bare steel columns are that in CFST: (1) the steel tube confines the core concrete, this confinement increases the compressive strength of the concrete and improves characteristics of the concrete such as ductility; (2) the existence of concrete infill increases the stability of the steel tube and lags the local buckling of the steel tube, preventing inward local buckling of steel tube and allowing only local outward buckling; (3) the composite action between the steel tube and the core concrete significantly increase the stiffness and compression capacity of the columns. In addition, the presence of the steel tube can support load prior to the pouring of concrete.

In addition, in this type of column, unreinforced concrete can be used to fill the steel tube. This feature helps reduce the needs for tools, labor, as well as the time and cost of construction, and facilitates the fabrication and assembly of the composite columns.

The steel tube works as longitudinal and transverse reinforcement and a perpetual formwork for the infill concrete. In turn, the use of longitudinal reinforcement improves the compressive behavior of the CFST columns and helps to create connections with other members, e.g. beams and other columns.

The general consensus in the literature is that a circular cross-section offers robust confinement to core concrete compared to square and rectangular cross-sections. Sections of the latter shapes are significantly used in CFST columns applications due to their ease of use in beam-to-column connection applications, and their ability to provide higher cross-sectional bending stiffness and meet aesthetic requirements (Han *et al.*, 2014). In this thesis, all the studies have been performed with steel tubes possessing circular cross-sections.

In addition to the classical CFST form, a new technique was introduced to improve the compressive behavior of these composite columns. This new technique, called concrete filled double steel tubes (CFDST) columns, can also be used as a repair form for deformed CFST columns. As shown in the literature (Lu *et al.*, 2015a, 2015b), CFST columns can be used to strengthen reinforced concrete columns.

There are a several of design code specifications appropriate for CFST column design. These code specifications adopt different theories and philosophies according to the country or region of origin. In this thesis, four such codes were considered. The experimental results were compared to the predictions of these codes and their appropriateness for use in the design of CFST columns was assessed. All codes formulations have limitations for the geometrical and mechanical properties of CFST columns where the experimental data may be within or beyond these limitations.

The specific design specifications adopted in this thesis were AISC360-16, EC4, AS5100.6, and AIJ2001. AISC360-16 is the code for steel structures in the United States, EC4 is the European code for composite structures, AS5100.6 is the Australian code for the steel and composite construction, and AIJ2001 is the Japanese standard for structural calculations of steel reinforced concrete structures. These codes were selected to allow study of the design considerations of a wide variety of regions.

1.2 Aims and Scope of the Thesis

The structural steel and filled concrete are essential elements of CFST columns. Therefore, the mechanical characteristics of these materials have a superior impact on the compressive behavior and confinement effect of circular CFST columns.

Specifically, concrete type and compressive strength affect the compressive capacity and failure modes of the final column. Thus, the confinement effect and failure modes differ between columns constructed using normal-strength and high-strength concrete. These behaviors also differ between columns built using lightweight aggregate concrete and self-compacted concrete.

Similar to the choice of concrete type, the properties of the steel tube have a direct action in the behavior of CFST columns. A thick steel tube provides higher confinement compared to a thinner steel tube; additionally, the yield strength combined with the steel tube thickness affects the compressive behavior and failure modes of CFST columns. Therefore, the combination of the impacts of the steel tube and the core concrete determines the final compressive response and failure modes of any given CFST column.

The main goal of this work is to expand the research experience of the compressive behavior of the CFST columns and the confinement effect under axial loading. To achieve this aim, CFST columns with different materials properties and configurations were used.

In hollow steel tube columns, the critical factor is the stability. Therefore, in CFST, the existence of concrete infill offers more stability and strength for the steel tube. The performance of the confined concrete itself will improve in this case, and this improvement in materials leads to improved performance of the composite column.

The topics of interest were to explore several areas. The first was the efficiency of the circular steel tube with various lengths, thicknesses, and material properties in confining different types of concrete with dissimilar compressive strength classes. The second was the applicability of the design codes for estimating the compression capacity of the CFST columns. For this aim, large experimental database of 1036 columns were collected from literature. The data in this database were selected to involve a vast number of the geometrical and material properties of circular CFST columns, a range both within and beyond the limitations of the specification codes examined. In the third, in addition to the aim of collecting the database, the applicability of the design specification to each type of concrete was also assessed. The calculations and limitations of these specifications do not cover all the types of infill concrete. Fourth and finally, the possibility of concrete-filled double steel tube stub columns as a new CFST configuration to support loads and using this new technique in repairing process was assessed.

This thesis deals with only the full concrete-filled circular steel tube sections without any mechanical improvements to the bond between steel tube and concrete. Only steel-bar reinforced concrete was used. Furthermore, all experimental tests described in this thesis are considered short-term tested, with the steel and concrete loaded together simultaneously under axial compressive loading.

1.3 Layout of the Thesis

This thesis involves nine chapters. These chapters were prepared to satisfy the goals of this search.

Chapter Two presents an introduction to the types and classifications of composite structures and the advantages of CFST columns. It also introduces the structural behavior of CFST columns and provides an inclusive literature review on the performance of circular CFST columns. Many published works on CFST columns with different parameters—configuration, geometric and material characteristics were highlighted and discussed.

Chapter Three introduces selected design codes specifications. It explains the theories involved in their definition and discusses limitations relative to the assessment of their predictions of the compression capacities of circular CFST columns under axial compressive loading.

The experimental studies of CFST columns are supported by design code specifications. In this thesis, four design codes (AIJ2001, 2001; AS5100.6-2004, 2004; Eurocode4, 2004; ANSI/AISC360-16, 2016), were selected to guess the capacities of CFST columns loaded axially and compared with experimental data.

Chapter Four introduces the experimental procedure followed for each test in this thesis. It involved preparation of the steel tube specimens according to the required lengths, machining process for the specimens' ends, and specimens required to get the steel yield strength. In addition, it describes the preparation of concrete mixes and all steps after pouring the concrete for concrete crushing specimens, such as curing and capping. These steps were carried out before compressive testing to record the concrete compressive strength. The preparation of CFST specimens from pouring fresh concrete to testing is fully described. This chapter also introduces the concrete types used throughout this thesis and describes their properties as well as the tests required for each type.

Chapters Five through *Eight* present the experimental studies. *Chapter Five* studies the impact of the geometrical and mechanical characteristics of the steel tube and the core concrete—i.e., *L/D* ratio, *D/t* ratio, steel tube yield strength (f_y), and concrete compressive strength (f_c) on the performance of the circular CFST columns and the confinement effect. Eighteen specimens were prepared, representing three *L/D* ratios, two *D/t* ratios, two steel yield strengths, and three concrete compressive strengths. Each of these specimens was tested under concentric compression loading. Additionally, a large database was collected from the literature. The collected data were both within and beyond the limits of the AISC36-16, EC4, AS5100.6, and AIJ2001 design codes to allow evaluation of the predictions of these codes and study the behavior of circular CFST columns under the effect of the different factors.

Lightweight aggregate concrete (LWC) and self-compacting concrete (SCC) are two innovative concrete types which provide significant advantages for CFST columns. LWC is considered the best way to minimize the self-weight of CFST columns and improve their seismic resistance. SCC offers the desirable feature of flowing in the formwork under its own weight. Although these concrete types offer advantages, few studies have examined the performance of CFST columns which incorporate them.

Therefore, *Chapter Six* studies the compressive response of circular CFST columns filled with LWC and SCC. It examines the efficiency of these types of concrete when used in CFST columns, in addition to investigating the efficiency of the design code predictions for LWC and SCC filled steel tube columns. This is particularly relevant as the design codes were established for CFST columns of normal weight concrete.

For this objective, sixteen hollow steel tubes columns filled with LWC or SCC were tested to study the performance of lightweight aggregate concrete filled steel tube (LWCFST) and self-compacted concrete filled steel tube (SCCFST) columns under axial compressive loading. Four different *L/D* ratios to observe the behavior of the short, medium, and long columns, and three different *D/t* ratios were used in this experimental study. The accuarcy of the AISC36-16, EC4, and AIJ2001 design codes predictions for LWC and SCC were also evaluated.

Steel-bar reinforcements are sometimes used to enhance the potential of the CFST columns and facilitate the connection of the CFST columns to other structural elements. In spite of these advantages, few experimental studies have studied the performance of steel-bar reinforced CFST columns. The combination of features of LWC and steel-bar reinforcement provides an excellent solution to improve the behavior of the LWC and leads to improve the compressive behavior of LWCFST columns.

Therefore, *Chapter Seven* discusses the response of reinforced lightweight aggregate concrete-filled steel tube columns. To that end, eighteen circular hollow steel tube specimens with various *D/t* ratios, *L/D* ratios, and yield strengths (f_y) were filled with LWC with different reinforcement conditions. These specimens were used to study the performance of reinforced lightweight aggregate concrete-filled steel tube (RLWCFST) columns loaded axially and compare the experimental results to the predictions of AISC360-16 and EC4 design codes.

Chapter Eight presents a new configuration of CFST columns and consist of two main parts. In general, the main function of CFST columns is to support loads. Heavier loads require increasing the cross-section of the CFST columns, which increases the self-weight and the cost of construction. These costs led to the suggestion of a new concept: placing a CFST column in a bigger hollow steel tube and filling the part between the two tubes with concrete. This new configuration is called concrete-filled double steel tube columns (CFDCST). It improved the strength, ductility, and stiffness over a CFST column capable of supporting an equivalent load. In addition, the interaction between steel tube and core concrete in the elastic phase improved these columns' fire resistance. In this thesis, both the inner and outer tubes are circular and stub columns, resulting in CFDCST stub columns.

This chapter is in two parts. The first part investigates the performance of CFDCST stub columns. The cross-sectional feature of this configuration allows use of different materials and geometric characteristics for the steel tube and shell and core concretes. The second part investigates the possibility of the CFDCST column concept for repairing deformed CFST columns. Distorted CFST stub columns were centered in larger steel circular tubes and fill the shell zone between the inner and outer steel tubes with concrete. This wet concrete can take the same shape of the deformed inner steel tube. Various concrete types and classes for shell zone can be used; additionally, an outer steel tube with different properties from the inner steel tube, such as thickness and yield strength, can be used. After curing of the shell concrete, the repaired column was tested and compared with corresponding CFDCST stub columns.

Chapter Nine presents a summary of the research work described in this thesis and lays out the conclusions drawn from this work. It also provides recommendations for further studies in this direction.

CHAPTER 2

LITERATURE REVIEW

2.1 Introduction

Steel and concrete are the most prevalent materials which used in the erection of structures and different civil engineering implementations. While steel is distinguished by its high tensile strength, excellent ductility, and high elastic modulus, for smaller cross-sections and slender members its buckling behavior often needs to be considered in design. In turn, concrete is distinguished by it is higher compressive but lower tensile strength, relatively lower material cost per unit weight, and lower thermal conductivity than steel (Liew and Xiong, 2015).

The composite structures combine the features of steel and concrete to obtain optimum performance, combining both strength and stiffness. In comparison to structural steel columns and conventional reinforced concrete columns, CFST columns offer many advantages. Among them, the steel tube confines the inner concrete, and this restriction improves the strength and ductility of columns. The maximum moment of inertia can be accomplished due to the existing of the steel tube on the farthest location to the centroid of the CFST column. The existence of a concrete precludes inward local buckling which has a comprimising effect on empty tubes.

In the case of a hollow steel tube column, this buckling may take place before the applied load equals the squash load of the column. In contrast, for CFST columns, local buckling occurs at a higher load. This behavior is clear in the mode of the failure for the different types of columns, as denoted in Figure 2.1. The steel tube can also bear a significant portion of erection loads and perpetual loads even before the pouring of fresh concrete (Uy and Liew, 2003; Yu *et al.*, 2007; Han *et al.*, 2014).

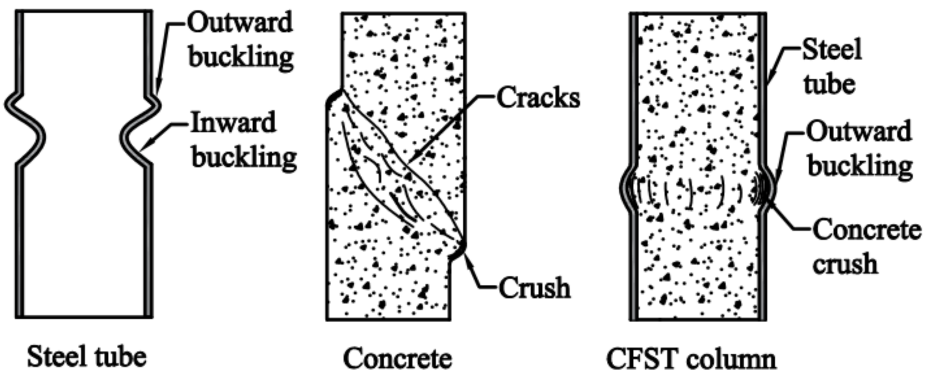

Figure 2.1 Failure modes of columns types adapted from Han *et al.* (2014)

Australian consulting engineers compared the cost of the CFST columns against other types of columns for buildings which are greater than thirty levels. This comparison indicated that the CFST columns will be more adequate for structures which are greater than fifty levels compared to other columns (as summarized in Table 2.1) (Uy and Liew, 2003).

Table 2.1 Cost comparison for different column types (Uy and Liew, 2003)

Column type	**RC**	**Concrete with steel erection column**	**Concrete-encased steel strut**	**RCFST**	**CFST**	**Steel column**
proportional cost, 10 levels	1.0	1.22	1.53	**1.14**	**1.1**	2.27
proportional cost, 30 levels	1.0	1.13	1.85	**1.11**	**1.02**	2.61

CFST columns also provide superior structural characteristics for seismic resistance, like large capacity of energy absorption and superior ductility. The presence of steel tube surrounding the core concrete works as longitudinal and transverse reinforcement; the concrete is under triaxial stress due to the confining pressure, and steel tube is under biaxial stress and stiffened by the concrete. These structural characteristics are caused by the steel-concrete composite action (Shams and Saadeghvaziri, 1997; Uy and Liew, 2003; Patel, 2013).

Composite action means the shear stress is transferred from one material to other (Mathias, 2003); this action is considered key for the satisfactory structural response of CFST columns. Composite action may be achieved via natural bond formation between steel and concrete, as a bond between steel reinforcing bars and surrounding concrete, or with the aid of shear connectors of various types, including structural bolts, nails, threaded bars, self-tapping screws, and tab stiffeners (Qu *et al.*, 2013).

The properties of CFST columns are higher than the sum of properties of their parts; a synergistic effect arises from their combination"; Figure 2.2 clarifies the capacities of steel tube and reinforced concrete (RC) columns and summation of them compared to the capacity of CFST columns. Note that the ductility of CFST columns is remarkably increased in comparison to the ductility of a steel tube and a concrete column together or each one alone (Han *et al.*, 2014).

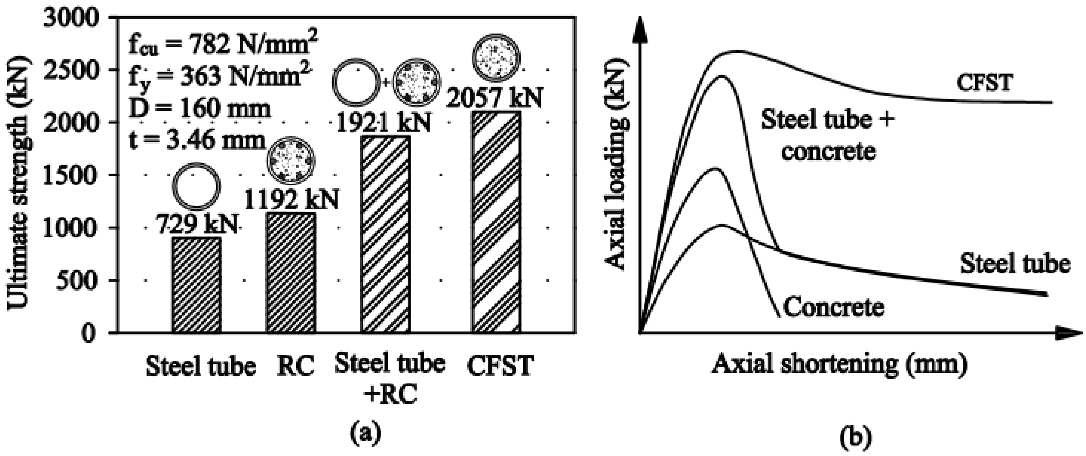

Figure 2.2 Performance of CFST stub columns adapted from Han *et al.* (2014)

2.2 Advancement of Concrete-Filled Steel Tube Columns

Figure 2.3 shows several types of steel tube cross-sections, but the most common types are circular, square, and rectangular sections. A circular shape offers the most powerful confinement to the concrete infill in comparison to square and rectangular cross-sections, while local buckling in a circular section is similar to that happen in columns with square or rectangular cross-sections. To meet aesthetic and functional requirements, other cross-sectional types also used, including elliptical polygons and round-ended rectangles. (Han *et al.*, 2014; Liew *et al.*, 2016).

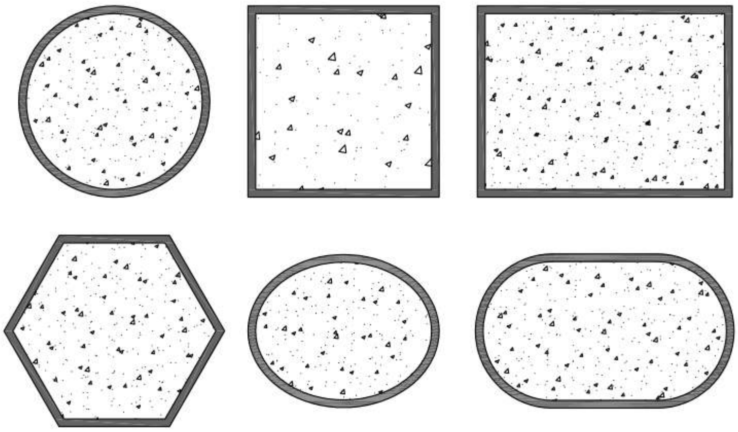

Figure 2.3 Common shapes for CFST columns adapted from Han *et al.* (2014)

In actual applications, the function and type of structure specify which type of CFST column will be suitable: single-wall or classical CFST columns (Figure 2.3); Infilled concrete may be reinforced by steel fiber or steel-bars to improve ductility behavior and fire resistance of the columns. An additional inner tube can be used instead of steel reinforcement, or use of steel sections. Solid steel sections or I-sections can serve to provide higher confinement to the infilled concrete, in addition to increasing the compression capacity and reducing column size, (Figure 2.4) (Yu *et al.*, 2007; Han *et al.*, 2014; Cai *et al.*, 2015; Liew *et al.*, 2016; Ekmekyapar and AL-Eliwi, 2017).

Applications such as fire resistance and columns with large cross-section may require special solutions, the double-skin and double-tube columns provide a good solution. Where a double-tube column provides higher flexural strength with lower self-weight (Ekmekyapar and AL-Eliwi, 2017). Also for large CFST columns section, the use of stiffeners via welding them to the inner surface of steel tube can increase its capacity and control local buckling of steel tube. Shear connectors can be applied to increase the bond between outer steel and inner concrete (Wang *et al.*, 2017b), (Figure 2.4).

Different columns are appropriate for different applications. To meet specific architectural or structural requirements, the CFST members used in construction may be not prismatic, but inclined or non-prismatic members. Inclined columns work as load-transfer members in structures with irregular architectural styles, while tapered columns could be used for architectural or economic causes. In some long span structures, curved members are suitable (Figure 2.5) (Han *et al.*, 2014).

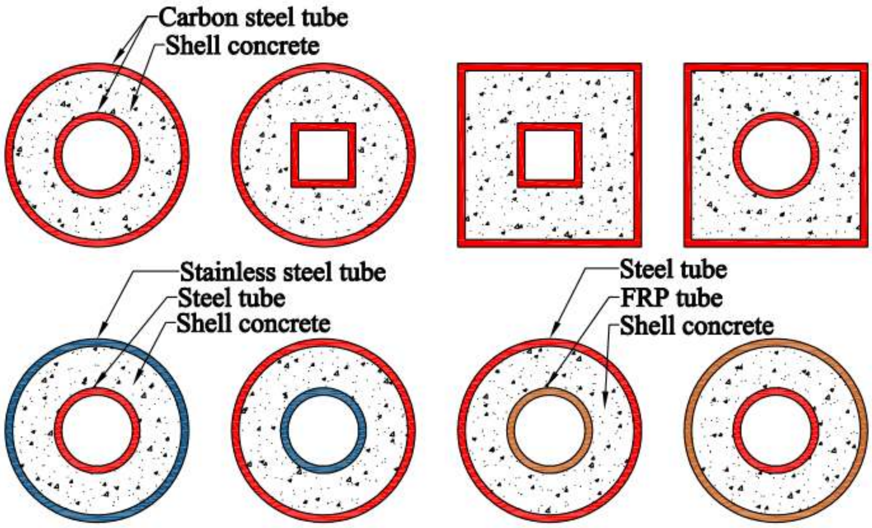

(a) Concrete-filled double skin tubes (CFDST)

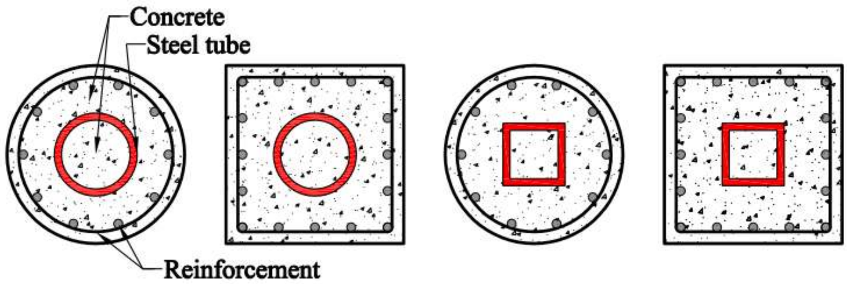

(b) Concrete-encased CFST

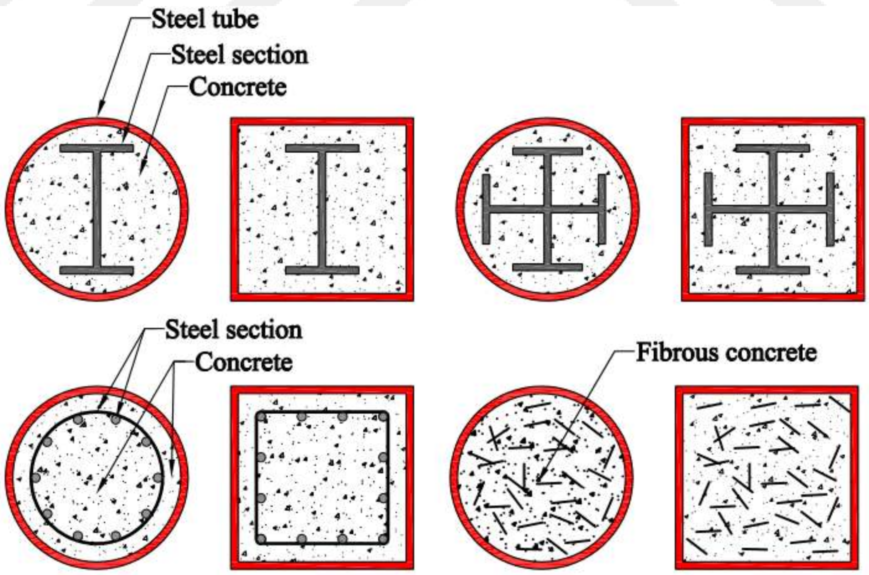

(c) CFST with additional reinforcement

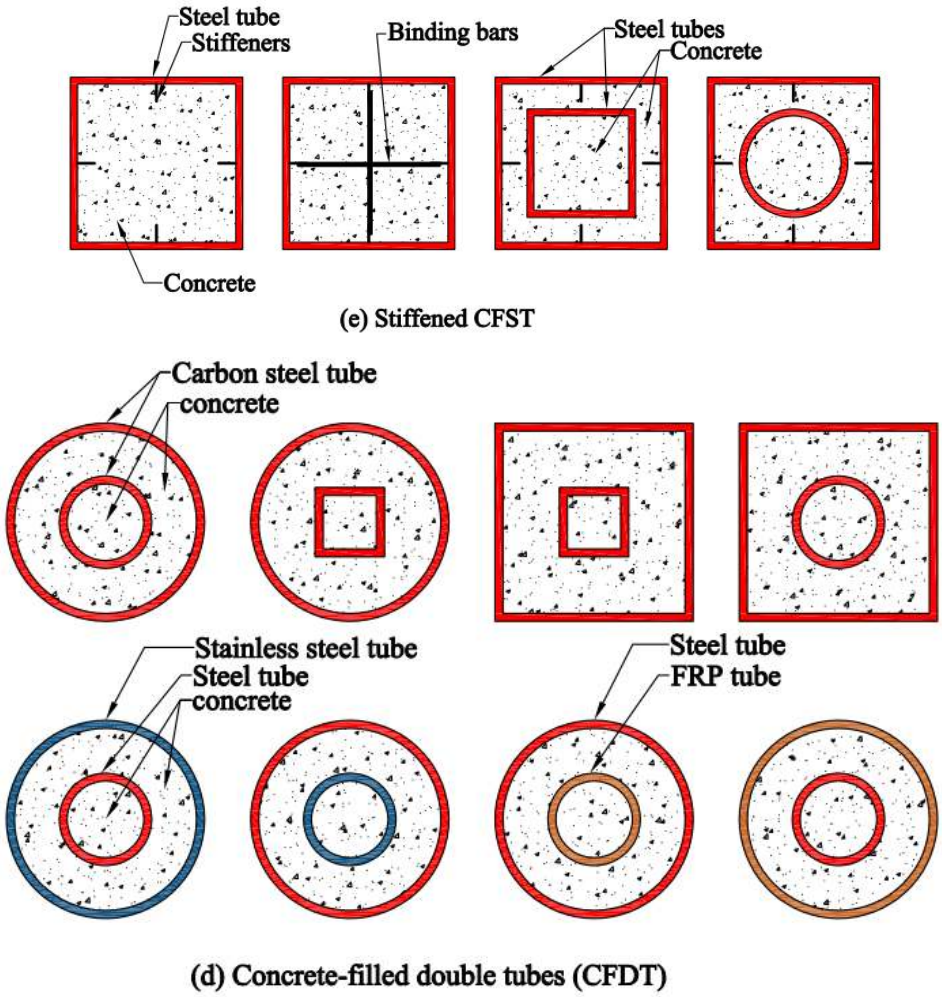

Figure 2.4 General types of CFST column adapted from Han *et al.* (2014)

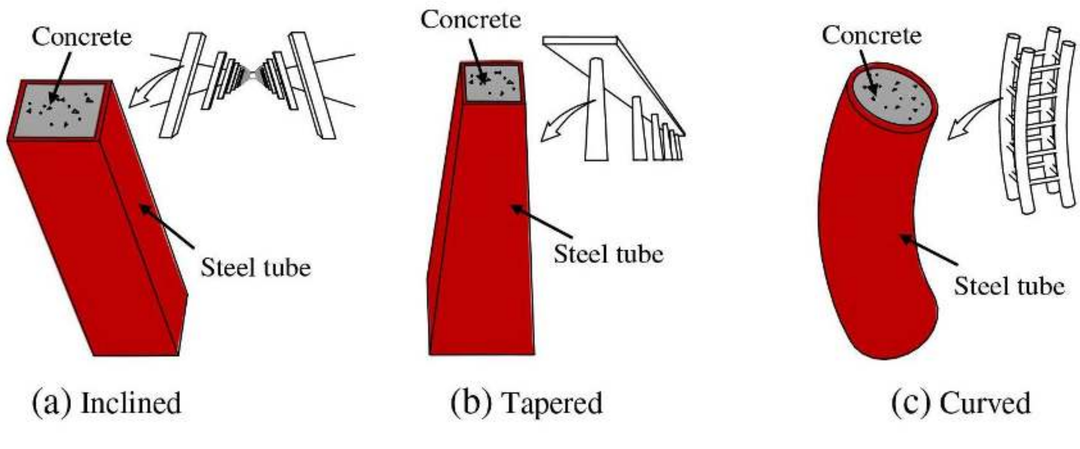

Figure 2.5 Non-prismatic of CFST columns (Han *et al.*, 2014)

2.3 Structural Behavior of CFST Columns

2.3.1 Composite Column Classifications

Composite columns are usually classified as short and long, but these terms do not refer to the ratio of cross section dimensions by length, but to their modes of failure:

1. Short or stocky (very short) columns do not experience from flexural buckling, while the local bucking will take in consideration of the design. These columns fail via squashing under control of the materials' strength: concrete strength f_c and steel yield strength f_y; therefore, the capacity of the cross-section to resist the axial load and moment depends purely on the material strength of the section.

2. Long or slender columns fail by flexural buckling, where the column becomes unstable or suffers overall buckling effects. There are two ways to improve the strength of these columns: first, the use of reinforced concrete columns, and second, the use of steel columns. In this case, the load resistance is depended on the geometric properties of the column in addition its material properties. If the load resistance is affected by second-order moment due to column deflections, the column is classified as slender; in all other cases it is classified as short (Oehlers and Bradford, 1995; Mathias, 2002a; Oehlers and Bradford, 2002) .

2.3.2 Bonding Between Steel and Concrete

The most attractive features of composite structures depend on sufficient connection between steel and concrete elements. This connection allows transfer of forces between the different elements and gives composite members their enhanced behavior. Composite structures are susceptible to bond failure between their components: steel tube buckling and crack of the concrete and this behavior leads to failure in the bond between them which often called debonding, a behavior that gives composite construction its unique distinctiveness (Oehlers and Bradford, 1995, 2002).

To ensure composite action, sufficient shear strength must exist at the steel-concrete interface; the quality of this interaction is the bond strength. Overall bond strength is a result of the (1) natural bond, which includes chemical adhesion and frictional resistance, and (2) mechanical bond, which typically requires auxiliary tools to improve bonding of steel to concrete. When possible, depending on the steel-concrete natural bond, instead of the mechanical bond, facilitates construction of CFST elements, since it results in less interference during concrete pouring. (Oehlers and Bradford, 1995; Roeder *et al.*, 1999; Oehlers and Bradford, 2002; Roeder *et al.*, 2009).

There are many parameters that affect bond strength, including cross-section shape and dimension, interface roughness, and compaction and shrinkage of the concrete core. The bond strength not affected directly by the length of the interface, while concrete compressive strength may also increase bond strength, or not be as a result of the increased shrinkage of high-strength concrete. This is especially true for circular sections where the confining pressure is reduced due to shrinkage of concrete (Roeder *et al.*, 1999; Tao *et al.*, 2011; Qu *et al.*, 2013).

Circular CFST columns have a larger bond stress than those with other sections such as rectangular or square cross-sections where the circular section reaches full composite resistance compared to rectangular and square sections. Figure 2.6 presents the relation between concrete strength (f_c) and bond stress capacity for columns with circular and rectangular shapes. The bond stress of rectangular CFST columns has been reported to be 70% lower than that for those with circular cross-sections (Roeder *et al.*, 1999; Roeder *et al.*, 2009).

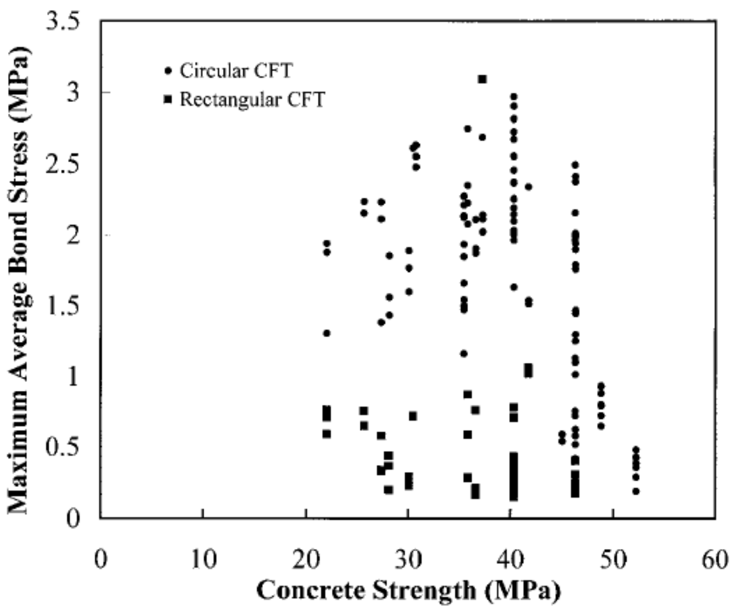

Figure 2.6 Bond stress versus f_c for CFST columns (Roeder *et al.*, 1999)

Bond strength increases when diameter-to-thickness *D/t* ratio decreases; reducing the *D/t* ratio enhances the confinement effect and leads to increased contact pressure at the steel-concrete interface, resulting in higher bond stresses. For large-diameter tubes, the a big gap can appear between steel and concrete due to concrete shrinkage, leading to a decrease in bond stresses (Roeder *et al.*, 1999; Tao *et al.*, 2011). However, bond strength can decrease with increasing length-to-diameter *L/D* ratio (Tao *et al.*, 2011).

According to Tao *et al.* (2011), concrete type also affects bond strength, but the effect is crossed; it depends on the binder material of the concrete mix, especially the fly ash. Where the recycled aggregate concrete and the expansive concrete have bond strength more than the bond strength of the normal concrete. Also, the normal strength concrete has bond strength more than high strength concrete where the bond strength decreases as concrete compressive strength increases (Tao *et al.*, 2016). The bond strength decreases after 90 min exposure to fire (Tao *et al.*, 2011).

Also, the steel tube type affects the bond strength where the carbon steel CFST columns have higher bond strength compared to stainless steel CFST columns (Tao *et al.*, 2016)

The bond between steel and concrete can be deemed a result of three mechanisms:

1. Chemical adhesion (bond) or natural bond.
2. Micro-locking or interface-interlocking.
3. Macro-locking or friction.

The chemical bond (natural bond) defines as an elastic-brittle shear transfer technique that is effective at the early phase of loading when the proportional displacements are small. It is influenced by many parameters such as the cement content and the water/cement ratio; moreover, the shrinkage of concrete gives a reverse impact on adhesion, and the contribution of this adhesion to transfer the shear stress is lost if the adhesion stress is surpassed at a value of slip lower than 0.01 mm or if the bond stress is higher than 0.1 MPa. When shear increases, the adhesion resistance is exceeded, and subsequent strength depends on mechanical characteristics at the interface. After this point, two characteristics, the bond provided by the micro-locking of the steel and concrete, and the bond that depends on the interface pressure and the coefficient of friction control, as shown in Figure 2.7 a and b (Mathias, 2002a, 2003).

Micro-locking is associated with the surface roughness of the steel tube. In CFST elements, the separation is prevented by the confinement which the steel tube exerts on the concrete. This mechanism is significant when the two surfaces are tied together. Micro-interlocking is caused due to the steel tube inner surface roughness and it breaks when the concrete interface reaches the compressive crushing strain of the concrete. Macro-interlocking or friction occurs between the steel and the concrete because of the normal forces, such as the expansion of concrete under axial loading or due to the roughness of the inner surface of the steel tube (Mathias, 2002a, 2003). The frictional shear resistance depends on the coefficient of friction, μ, which ranges from 0 to 0.6 (Rabbat and Russell, 1985; Baltay and Gjelsvik, 1990; Mathias and Gylltoft, 2003; Tao *et al.*, 2013), and is related to the roughness of the streel surface and the condition of the interface. Figure 2.7 shows the mechanism of shear transfer for steel–concrete interfaces (Mathias, 2003).

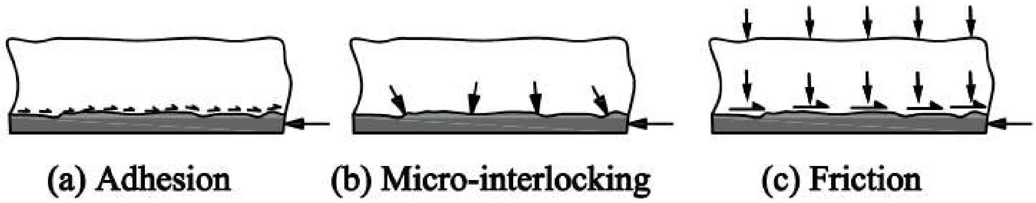

Figure 2.7 Shear transfer mechanisms adapted from Mathias (2003)

To provide more details about this mechanism, Figure 2.8 presents the response of CFST column under a push-out force test. In it, the three stages of bond strength at the different stages of loading are shown as an idealized force–slip curve. Due to adhesion and micro-interlocking, the bond is broken, and the macro-interlocking is started, the adhesion and micro-interlocking govern the linear part and contribute to satisfying the maximum bond stress, whereas the macro-interlocking defines the residual bond stress that remains at the final stage of bond–slip curve (Qu *et al.*, 2013).

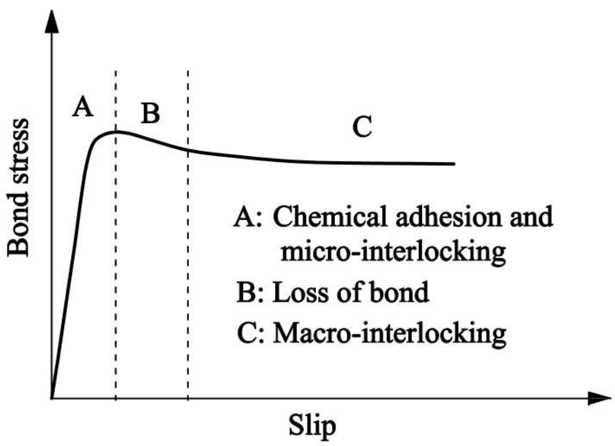

Figure 2.8 Push-out test response of a CFST column adapted from Qu *et al.* (2013)

In finite element simulation of a CFST column, software like the ABAQUS package, it is difficult to include the three forces mechanism of bonding mentioned above. Therefore, to simplify the simulation, many studies only consider the friction case (Hu *et al.*, 2003; Mathias and Gylltoft, 2003; Ellobody and Young, 2006; Ellobody *et al.*, 2006; Yu-Feng *et al.*, 2012; Tao *et al.*, 2013; Pagoulatou *et al.*, 2014). In these studies, the simulation of bond behavior in the tangential and normal direction is uses the "Coulomb friction" model and a contact pressure model, ignoring the effects of chemical bond and micro-interlocking. According to the good agreement of the numerical simulation in these studies compared to experimental results, ignoring the contributions of chemical and micro-interlocking bonds is reasonable.

2.3.3 Concrete Under the Confinement Effect

When concrete under multiaxial compression both strength and ductility are considerably improved, which delays damage in the microstructure due to the application of confining stress (Imran and Pantazopoulou, 1996). Concrete is naturally brittle, but can be made ductile if properly confined. Sufficient transverse reinforcement must be provided to successfully confine compressed concrete in reinforced concrete columns. The lateral reinforcement prevents the concrete from cracking and failing due to brittleness and gives it higher load resistance and deformation capacity. This confinement effect increased when the spacing of stirrups decreases for post-peak behavior especially for high-strength concrete (Mander *et al.*, 1988; Mathias, 2002b). The CFST column system provides the best solution to eliminate the hazard of the precocious spalling of the concrete cover compared to ordinary reinforced concrete columns (Mathias and Gylltoft, 2003).

Confinement is classified into two forms: active and passive confinements. For the active one, the confinement effects apply from the beginning, and constant lateral pressure is applied on the column. For passive confinement, the confining stress is not constant; reinforced concrete columns and CFST columns are examples of concrete under passive confinement (Mander *et al.*, 1988; Mathias, 2002a).

In the state the triaxial compression, there is one main difference between active confinement by fluid pressure and passive confinement by spirals, ties, or steel tube: when the confinement is passive, the confining pressure is variable and based on lateral dilation of the concrete and the stress-strain model for the steel tube. The behavior of confined concrete depends on uniaxial compressive strength and level of the applied confining pressure (Attard and Setunge, 1996; Liew and Xiong, 2012).

The behavior of concrete under triaxial compression is investigated using an axially loaded concrete cylinder subjected to active lateral confining pressure. Using a triaxial test cell, the confining pressure is applied around the cylinder, after which the axial pressure is increased until failure. The confining pressure is supplied using fluid with a constant level. Two of the principal stresses are equal ($\sigma_1 = \sigma_2 = \sigma_{lateral} = \sigma_{lat}$), and the third principal stress is axial stress, referred to as $\sigma_3 = f_{cc}$ (Wang *et al.*, 2016), (Figure 2.9) shows concrete under triaxial compressive stresses.

As mentioned before, the axial capacity of RC columns or CFST columns improves due to the lateral confinement; therefore, the excess of concrete compressive strength and corresponding strain as a result of active hydrostatic fluid pressure depends on the Mohr-Coulomb failure criterion and can be expresed by Equations 2.1 and 2.2 (Mander *et al.*, 1988; Candappa *et al.*, 1999):

$$f_{cc} = f_c + A_1\sigma_{lat} \tag{2.1}$$

$$\varepsilon_{cc} = \varepsilon_c\left(1 + A_2\frac{\sigma_{lat}}{f_c}\right) \tag{2.2}$$

where f_{cc} and ε_{cc} are the compressive strength and the corresponding strain, respectively for confined concrete. The variables f_c and ε_c are the compressive strength and corresponding strain, respectively, for unconfined concrete and coefficients A_1 and A_2 represented the concrete mix and the lateral pressure (Mander *et al.*, 1988). According to Richart *et al.* (1928) the average values of A_1 and A_2 are $A_1 = 4.1$ and $A_2 = 5A_1$.

Many models of confined concrete are appropriate, depending on the results of column tests under triaxial strain; these stress-strain relationships are based on the degree of confinement (Attard and Setunge, 1996). Where these stress-strain models involve of two parts, ascending and descending, the ascending part gives the parameters of materials, such as Young's modulus of concrete, and the descending or softening part indicates the ductility of concrete (Candappa *et al.*, 1999). Figure 2.10 shows the compressive stress-strain model for confined and unconfined concrete (Mander *et al.*, 1988). Where, E_c is the tangent modulus of elasticity of the concrete (MPa) and E_{sec} is the secant modulus of elasticity of the concrete ($E_{sec} = f_{cc}/\varepsilon_{cc}$) (MPa).

In a CFST column, the steel tube works as reinforcement in both longitudinal and transverse directions and offers confining pressure to the concrete. This means the concrete is subject to a state of the triaxial stress, and the steel under a biaxial state of stress (Hu *et al.*, 2003).

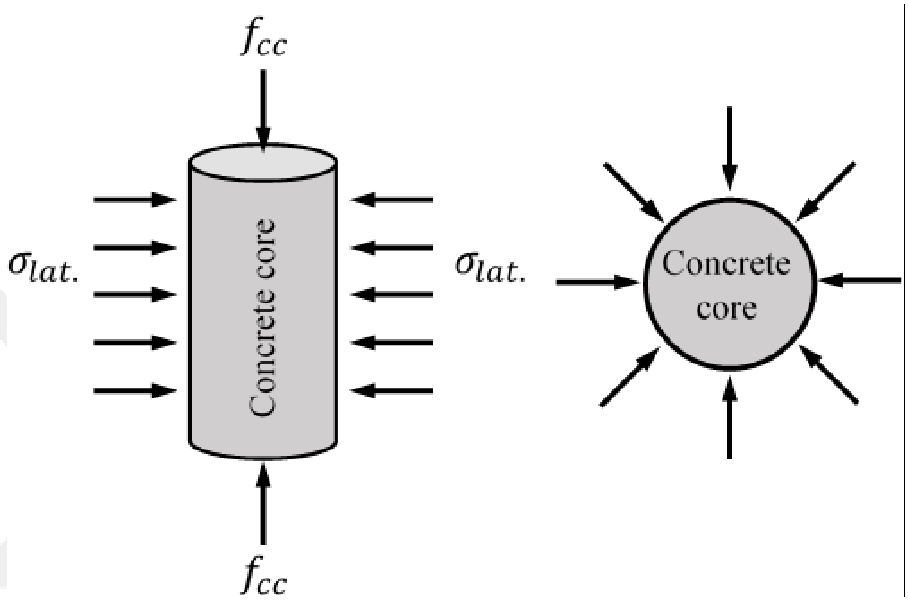

Figure 2.9 Concrete under triaxial compressive stresses

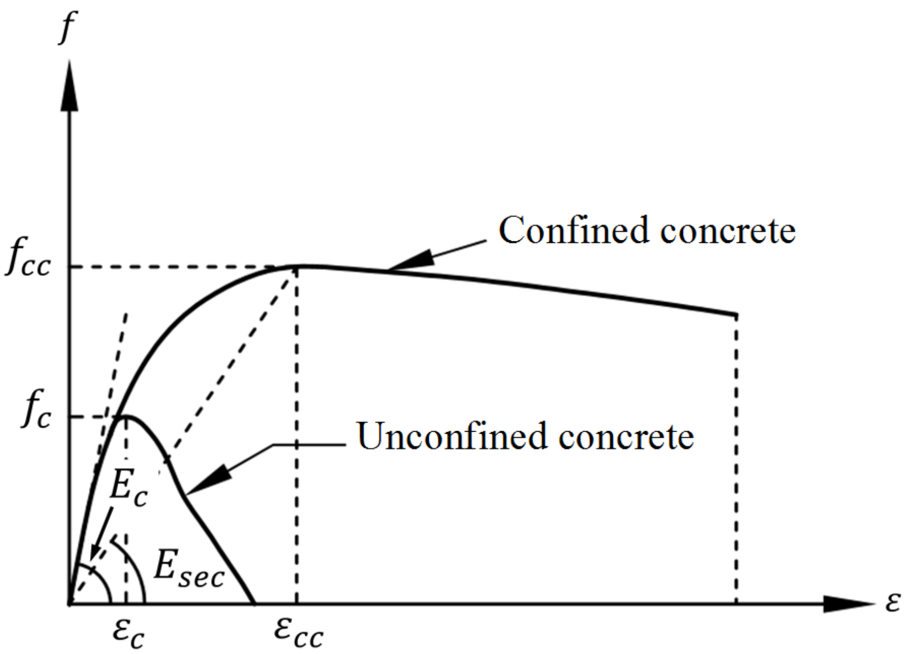

Figure 2.10 Stress-strain curves for concrete adapted from Mander *et al.* (1988)

2.3.4 Confinement Mechanism of CFST Columns

As mentioned in the previous section, the compression strength and the ductility of CFST columns enhance due to the lateral restriction of the inner concrete by the outer steel tube. However, for short composite columns, the confinement effect is one of the significant parameters which affect their behavior. In that case, failure is governed by material strength, namely compressive strength of concrete, f_c, and yield strength of the steel tube, f_y. In long composite columns, the confinement effect is insignificant unlike short composite columns. On the other hand, long composite columns tend to develop lateral displacement leading to global buckling; in that case, failure is governed by geometrical properties of the composite column.

The steel tube restricts the infilled concrete and provides longitudinal and lateral reinforcement. This configuration of composite column eliminates premature spalling of the infilled concrete. As stated by previous experimenters, such as Schneider (1998), Shanmugam and Lakshmi (2001), and Shams and Saadeghvaziri (1997), the circular cross-section of CFST column provides improved confinement over rectangular or square cross-sections. The flat edges of square or rectangular cross-sections are not stiff sufficiently to bear the internal pressures as a result of volumetric increase of the concrete core, so only the center and corners of square and rectangular cross-sections are effectively confined. However, circular cross-sections are rigid against internal pressures; Figure 2.11 shows the differences in confinement (Mathias, 2002a; De Oliveira *et al.*, 2009).

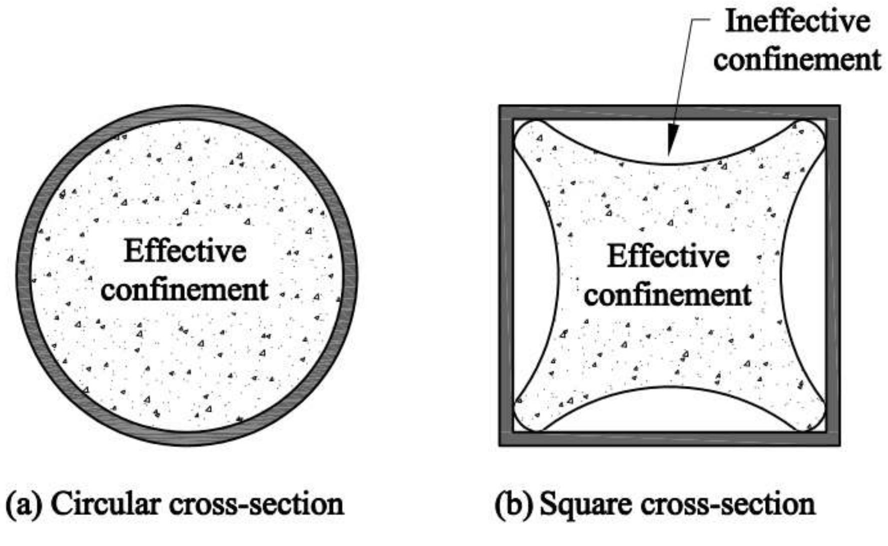

Figure 2.11 Confinement of CFST columns adapted form De Oliveira *et al.* (2009)

Passive confinement in CFST columns is based on the lateral expansion of the outer steel tube in addition to the lateral deformations of the inner concrete. The steel and the concrete support the axial compressive loading simultaneously; therefore, the mechanical behavior of CFST columns directly affected due to the difference in dilatation of these materials. In CFST columns the steel tube is under a state of biaxial stress due to the combination of lateral tension and axial compression loading.

Figure 2.12 shows the forces applied to half cross-sections of CFST columns. The effective circumferential hoop tensile stresses, σ_{ah}, can develop in the steel to provide uniform distributed confining stress, σ_{lat}, which ensures the whole concrete section will be confined effectively over the length of the circular CFST column. The relation between them can be calculated by equilibrium calculations:

$$\sigma_{lat} = \frac{t}{r}\sigma_{ah} \tag{2.3}$$

Where *r* and *t* are the radius of the inner concrete and t the thickness of the outer steel tube, respectively. The equations for compressive strength of confined concrete, f_{cc}, and the corresponding strain, ε_{cc}, Equations 2.1 and 2.2, can be rewritten by using the definition of $\sigma_{lat.}$ from Equation 2.3

$$f_{cc} = f_c + A_1\frac{t}{r}\sigma_{ah} \tag{2.4}$$

$$\varepsilon_{cc} = \varepsilon_c\left(1 + A_2\frac{t}{r}\frac{\sigma_{ah}}{f_c}\right) \tag{2.5}$$

It can be noted from Equations 2.4 and 2.5 that the increase in hoop stress will increase the compressive strength of concrete. An increase in steel thickness or a reduced concrete diameter will also give the same results (Mathias, 2002a).

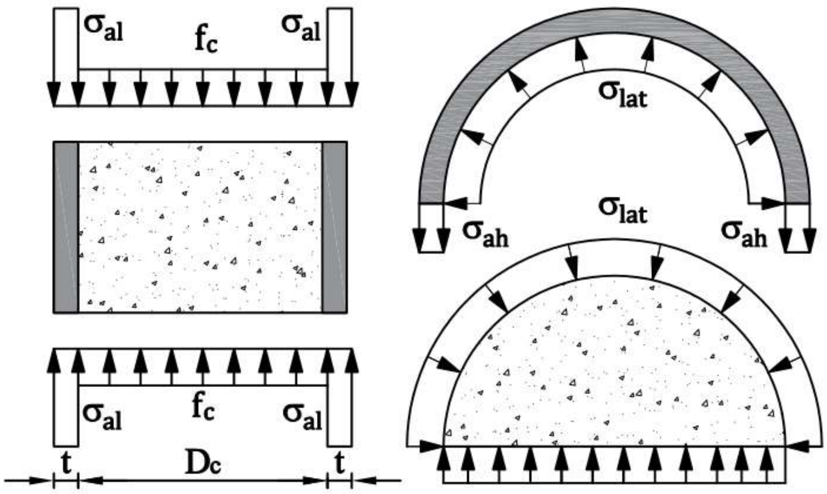

Figure 2.12 Stress states in CFST columns adapted from Mathias (2002a)

The confining stress σ_{lat} on the concrete cannot be easily derived. It is based on the relation between the axial compressive stress, σ_{al}, and the circumferential tensile stress, σ_{ah}, which also change during the loading. Thus, many formulations have been derived to calculate the confining stress, σ_{lat}. In numerical analysis of circular CFST columns, the accuracy of the solution is based on the selection of a suitable model for confined concrete.

Passive confinement in CFST columns relies on lateral deformation of both the concrete and the steel. These materials have different dilatation features, represented by Poisson's ratios for steel tubes, ν_e, which is typically equal to 0.3 (Eurocode3, 2005), and concrete core, ν_c, typically equal to 0.2 (Eurocode2, 2004). This difference has a superior impact on the mechanical response of the CFST columns (Mathias, 2002a, 2002b).

The ideal loading use case to take advantage of the full composite behavior between steel tube and core concrete is to load both of them simultaneously. Then the load sharing between the steel and concrete is as a result of their axial response from the beginning of loading (Mathias, 2002a; Mathias and Gylltoft, 2003).

The mechanical behavior of a short CFST column subjected to axial compressive loading applied to an entire section primarily depends on the difference in Poisson's ratios between steel and concrete. In the elastic phase of loading, and prior to the formation of micro-cracks in the concrete core. The concrete core expands slower than the steel tube in the radial direction because the Poisson's ratio of concrete is lower than that of the steel tube. In this phase of loading, there is no confinement effect and the bond between steel and concrete is not broken. The initial circumferential steel hoop stresses are compressive stresses, $\sigma_{ah} < 0$, and the concrete is under lateral tension (Figure 2.13a and Figure 2.14a, b). As the load continues to increase and stress in the concrete core reaches the unconfined compressive strength f_c, microcrack propagation starts to localize and the formation of macrocracks begins. At this phase, the lateral deformations of concrete and steel become equal. For a more increase in load, the steel tube restricts the concrete core and the hoop stresses in the steel become tensile, $\sigma_{ah} > 0$ (Figure 2.13b and Figure 2.14a, c). At this phase and later phases, the concrete is under triaxial stress and the steel is under biaxial stress. This means that before the concrete stress approaches the unconfined concrete compressive strength f_c, the steel tube has no obvious restriction impact on concrete core. So, before this point there is no effect of confinement and the total responses that could be expected are those for the uniaxial cases of the concrete and steel tube, respectively. However, with increased confinement of the inner concrete, the steel stress in the circumferential direction σ_{ah} increases. The steel tube then cannot bear the plastic resistance in the axial direction σ_{al} and the force carried by the steel tube decreases (Mathias, 2002a, 2002b; Mathias and Gylltoft, 2003; De Oliveira *et al.*, 2009).

With increased damage, the mechanical resistance in the shear zone decreases. However, at some specific point, the damage is so comprehensive that the present confining pressure is not enough to restrain unstable cracking and the maximum concrete compressive strength, f_{cc}, is reached. After this stage, the descending branch starts (Figure 2.14a, d). At this stage, the shear failure plane is completely formed, reaching a residual strength $f_{c.res}$. The residual load resistance of the CFST column can be maintained for large deformations, and represents the axial force taken by the steel tube and carried by friction across the shear plane in the concrete core. Softening behavior due to the shear failure is generally observed for most CFST columns filled with high strength concrete (HSC), while normal strength concrete (NSC) generally shows hardening behavior during crushing. The residual stresses and the ductility have been observed to increase with greater steel tube thickness, and in some cases, almost perfectly plastic behavior was obtained (Mathias, 2002a, 2002b; Mathias and Gylltoft, 2003; De Oliveira *et al.*, 2009; Ekmekyapar and AL-Eliwi, 2016).

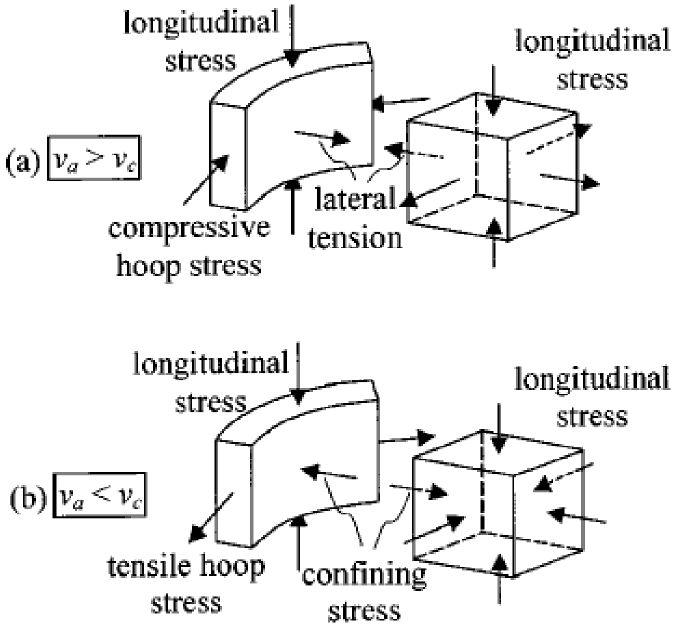

Figure 2.13 Stresses in steel and concrete at different phases of loading (Mathias and Gylltoft, 2003)

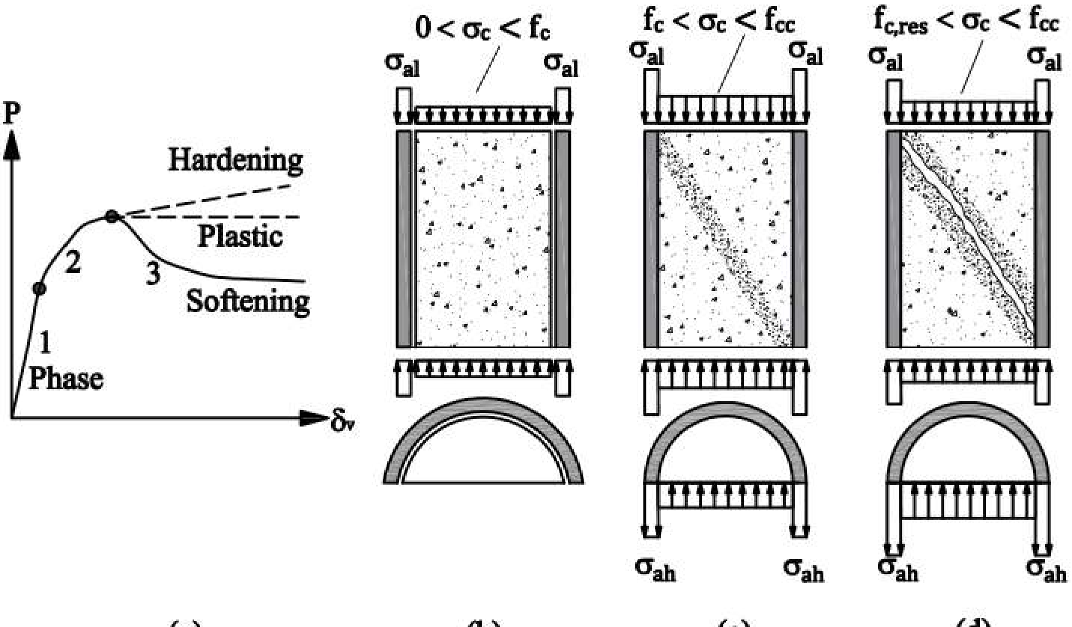

Figure 2.14 (a) Schematic load-deformation for a CFST column, (b, c, and d) Fracture process in the concrete at different phases of load adapted from De Oliveira *et al.* (2009)

In the CFST column, the performance of the post-yield phase is majorly affected by the failure of the inner concrete, which depends on factors including the strength and degree of confinement. Mathias (2002b) stated that the post-yield behavior can be classified into three classes: strain softening response, perfectly plastic behavior, and strain hardening behavior (as shown in Figure 2.14a).

According to Han (1998), Han *et al.* (2001), and Han (2002), an unified theory was used to specify the composite action between steel and concrete by using confinement factor ξ. When confinement factor ξ increases, so does the ductility of the CFST column. Confinement factor ξ is defined as:

$$\xi = \frac{A_s f_y}{A_c f_c} \tag{2.6}$$

where A_s and A_c are the cross-sectional areas of the outer steel tube and inner concrete, respectively, f_c is the compressive strength of concrete, and f_y is the steel tube yield strength.

When $\xi < 1$, the concrete core bears a bigger part of the total load, and the response of the concrete will be more apparent. When $\xi > 1$, hardening behavior develops, and the strain hardening of the steel tube becomes more apparent. While $\xi = 1$ performs perfect plastic response.

For high-strength unconfined concrete (HSC) the confinement factor will be small. This is because the increase in concrete unconfined compressive strength means there will be less microcracking, resulting in a need for less lateral expansion to mobilize the restraint action offered by the steel tube. It also results in less ductility of CFST column as a whole. Normal-strength unconfined concrete (NSC) provides a higher confinement factor and leads to CFST columns with higher ductility as a result of its higher deformation capacity than HSC (Han, 1998; Mathias, 2002b; De Oliveira *et al.*, 2009).

The experimental results of De Oliveira *et al.* (2009); Uy *et al.* (2011); Abed *et al.* (2013) Ekmekyapar and AL-Eliwi (2016) showed that the degree of the confinement of the concrete core by the steel tube has a major effect on the capacity of the CFST columns loaded axially, where the capacity of column increases when the confinement increased. The confinement depends on many parameters, including geometrical and material properties such as length-to-diameter ratio (*L/D*), diameter-to-thickness ratio

(D/t), cross-section shape, concrete compressive strength f_c, and steel tube yield strength f_y.

Xiong *et al.* (2017) reported that the degree of confinement depends on the steel tube yield strength and concrete compressive strength. It is formulated by the ratio of confining stress to concrete compressive strength, which can be derived based on the equilibrium state between a steel tube and infilled concrete, as illustrated in Figure 2.12. The stress in the radial direction is canceled because the steel tube is considered as a thin-walled member. The following equations can be obtained taking into account the equilibrium and Von Mises failure criteria for the steel tube:

$$N = A_c\sigma_c + A_s\sigma_{al} \tag{2.7}$$

$$\sigma_{al}^2 + \sigma_{al}\sigma_{ah} + \sigma_{ah}^2 = f_y^2 \tag{2.8}$$

Equation 2.9 represents the degree of confinement (σ_{al}/f_c) derived by Xiong *et al.* (2017). It shows that the degree of confinement grows as the steel tube yield strength increases, and is in inverse proportion to the concrete compressive strength. As shown in Equation 2.9, the value of confining stress, σ_{al}, is not related to the compressive strength of concrete f_c, but to the area of concrete cross-section A_c.

$$\frac{\sigma_{lat}}{f_c} = \frac{A_s f_y}{A_c f_c}\frac{A_1 - 1}{\sqrt{9 + 3(A_1 - 1)^2}} \tag{2.9}$$

2.4 Past Research

Many experimental and numerical studies have been done to examine the response of the CFST columns with different materials and geometrical characteristics. These characteristics include features such as the shape of the steel tubes (e.g. circular, square, rectangular, elliptical, octagonal), the cross-section dimensions, and the overall length of the specimens. Different material characteristics that have been studied include the concrete infill type (normal compacting concrete, self-compacting concrete, lightweight concrete, geopolymer concrete, etc.), the concrete's compressive strength (including normal-strength concrete, high and ultra-high-strength concrete, high-performance concrete, etc.). In addition, the characteristics of the steel tubes such as yield strength (mild steel strength, high steel strength); type of steel tube (e.g. carbon steel, stainless steel, aluminum, bimetallic, high performance fire-resistant steel, weathering steel) have been studied.

There many other parameters that affect the response of composite columns, such as the method of loading (loading one entire section, steel section only, and concrete section only); type of loading (constrict compression loading, eccentric compression loading, tension loading, flexure loading, shear forces, torsion forces, combined loading, dynamic loading, impact loading, seismic loading, cyclic loading, etc.).

In addition to experimental studies, computational studies have been done to offer the best comprehension of the performance of CFST columns and the confinement effect. They also serve to expand the investigation of more real cases which cannot be easily carried out in the laboratory due to high costs and difficulty of execution. These studies are conducted using commercial finite element software programs such as ABAQUS (ABAQUS, 2014) and ANSYS (ANSYS, 2016), or by using classical finite element analysis techniques.

Moreover, investigators have suggested analytical methods and design strategies for CFST members. These approaches have formed the basis for formulation of the existing design codes. Such codes are written according to different theories and design philosophies, limitations, and practices in their respective countries.

There are many design codes and specifications that describe the design of CFST columns. For example, ANSI/AISC 360 is the American specification for steel structures (ANSI/AISC360-16, 2016); Eurocode 4 is the European code for composite structure (Eurocode4, 2004); AS5100.6 is the Australian standard for steel and composite construction (AS5100.6-2004, 2004); and the AIJ guide is the Japanese guide for reinforced concrete structures (AIJ2001, 2001).

The earliest experimental tests of CFST columns were conducted by Kloppel and Goder (1957) to investigate the axial capacity of CFST columns with different cross-sectional shapes and *D/t* ratios. Gardner and Jacobson (1967) conducted a theoretical and experimental study of CFST columns under axial loading. Their experimental results were compared to loads allowed by NBC and ACI recommendations.

Furlong (1968) tested 30 circular and 22 square CFST short columns. They were subjected to axial load and bending to derive the ultimate load interaction diagrams.

Neogi *et al.* (1969) tested CFST columns under eccentric loading. The columns had *D/t* ratios from 40 to 80. A software model was suggested to estimate the capacity of slender columns.

Knowles and Park (1969, 1970) examined 21 circular and 7 square CFST specimens with *D/t* ratios of 15, 22, and 59, and *L/D* ratio ranged between 2 and 21. The results concluded that the tangent modulus method accurately estimated the capacity of CFST columns with *L/D* > 11, but not for *L/D* < 11. This difference was as a result of the effect of the confinement where the capacity of CFST specimens increased especially for short column with a circular cross-section. Buckling failure occurred in long columns before the strains needed to cause a dilation in concrete core were reached.

Tomii and Yoshimaro (1977) examined the influence of the cross-sectional shape, aspect ratio, *D/t* ratio, and specimen length on the behavior of 286 CFST specimens loaded axially. The specimens studied included six sizes of circular, square, and octagonal steel tubes with different wall thicknesses. The results indicated that the columns fail in two cases: for long columns, global buckling controlled, while for short columns, crushing concrete was the controlling failure mode. The capacity of the specimen was affected by the slenderness ratio, the thickness of steel tube, and the cross-sectional shape. Circular columns showed significant confinement, while square columns presented no excess in capacity due to the confinement effect.

Lin (1988) tested 18 concrete infilled cold-formed steel columns loaded axially. The factors were cross-sectional shape and the thickness of the outer steel, *L/D* ratio, and compressive strength of inner concrete. The results concluded that the cross-sectional shape and the thickness of the outer steel had a direct impact on the compression capacity of composite columns, and the circular cross-section offered the best confinement.

O'Shea and Bridge (1994) experimentally studied the effect of local buckling on circular CFST columns under axial loading. The specimens used had a *D/t* ratio of 165, *L/D* ratio of 3.5, and used concrete with very high-strength of 120 MPa and a steel tube with a yield strength of 200 MPa. The results indicated that local buckling has a significant effect on bare steel tubes, while for CFST columns steel only contributes a maximum of approximately 4% of total axial capacity. Therefore, any reduction in the total capacity a result of local buckling of the steel tube is small, and a steel tube filled with concrete with a very high strength offers uneffective confinement to the concrete.

O'Shea and Bridge (1997) studied the impact of local failure of the steel tube on the response of short circular CFST columns. They examined two failure modes: local buckling and yield failure. The outcomes showed that these failure modes were independent of the *D/t* ratio, while the bond between steel and the concrete controlled the failure mode of the specimen. They also proposed a design method according to the recommendations of EC4 (Eurocode4, 2004)

Schneider (1998) conducted an experimental and computational investigation into the performance of short circular, square, and rectangular CFST columns. Fourteen specimens were tested; they possessed *D/t* ratios ranged from 17 to 50, *L/D* ratios between 4 and 5, and were fabricated of normal-strength concrete, and a mild-strength steel tube. The experimental results concluded that a circular cross-section provides better post-yield strength and ductility compared over square and rectangular sections. The numerical analysis was done by using ABAQUS program and verified by experimental results; the ultimate column strength was also compared with the predictions of various design codes and provided acceptable predictions.

O'Shea and Bridge (2000) investigated the capacity of circular short CFST columns with small eccentricities under different loading conditions. The specimen columns had an *L/D* ratio of 3.5, *D/t* ratios varied from 60 to 220, and were constructed using concrete compressive strengths of 50, 80, and 120 MPa. They concluded that the loading condition had a direct effect on the confinement level; the highest confinement happens when loaded the inner concrete only and the outer steel tube acts as an only circumferential barrier. They found that the EC4 specification offered the best method with predicting the capacity of circular short CFST columns for entire section loading condition (the steel and concrete loading together).

Mathias and Gylltoft (2001) examined the structural behavior of 11 slender circular CFST columns both experimentally and computationally. The columns were studied under three different types of loading: entire section, concrete core only, and steel section only. The results revealed that the performance of CFST column is majorly affected by the method of loading. For the natural bond case, the full composite action was observed only when applying the load to the entire section of the CFST column. For slender columns, increasing the compressive strength of concrete had no impact on the column capacity.

Mathias and Gylltoft (2003) investigated the mechanical behavior of 13 circular tube CFST columns both experimentally and computationally (using ABAQUS). Three loading types were adopted: the entire section, concrete core section only, and steel tube section only. The results showed that the response of CFST specimens was impacted by the method of loading. In addition, the bond strength did not effect on the behavior for the "entire loading" condition, while the bond strength highly effect on the confinement effect and the behavior of column in only the condition of concrete core loading.

Han and Huo (2003) studied the structural performance of CFST specimens under fire condition: they tested 12 circular and square CFST specimens subjected to concentric and eccentric loading with fire protection or without it after subjected to the conditions of the ISO-834 fire standard. The circular sections were filled with high-strength concrete with a strength of 71.3 MPa and a steel tube yield strength of 365 MPa, while the square sections were filled with normal-strength concrete with a strength of 34.8 MPa and a steel tube yield strength of 294 MPa. They concluded that fire exposure increases the deflection of CFST columns and reduces their strength, but that if the fire duration is under ten minutes, there is no reduction in strength. Furthermore, they developed a theoretical model for the relationship between load–midspan deflection for a composite column that gave acceptable agreement with test results. Depending on the numerical model, the slenderness ratio, cross-sectional dimensions and the fire duration had a significant effect on residual strength index. The steel ratio, the load eccentricity ratio, and the materials characteristics have a moderate impact on residual strength index. Also, models for the calculation of the residual strength of CFST after exposure to ISO-834 fire standard have been suggested.

By using ABAQUS software Hu *et al.* (2003) proposed a numerical model to simulate the nonlinear response of CFST columns. Convenient material constitutive models for concrete cores were proposed and verified against the experimental results. Three cross-sectional columns were classified into three sets: circular, square, in addition to square sections strengthened by reinforcing ties. The outcomes showed that circular section provides better confinement, and the confinement of the square specimens with reinforcing ties are better than square specimens without reinforcing ties. No considerable confinement effect was observed for square sections especially for specimens which have the high width-to-thickness ratio (say > 30).

Sakino *et al.* (2004) tested 114 short hollow steel tubes and CFST columns under axial loading to study the steel-concrete interaction and derived formulas to describe the relationship between applied load and deformation of the CFST columns. They examined a variety of parameters: tube cross section (circular and square), cross-sectional dimensions, (for circular section, the diameter ranged from 122 mm to 450 mm, for square section, the width ranged from 120 mm to 324 mm), steel tube tensile strength (mild steel strength, and high steel strength: 400, 600, and 800 MPa), concrete compressive strength as use of normal- or high-strength concrete (20, 40, 80 MPa). They proposed design formulas to specify the capacity of CFST columns for both sections. A linear function was derived to simulate the relation between the ultimate capacity and squash load of circular cross-sections.

Han and Yao (2004) tested 38 self-compacting CFST members to search the impact of concrete compaction methods on the capacity of CFST members. Concrete was compacted by vibrator machine, by hand, and by self-compacting without any vibration. The main factors in the tests were cross-sectional shape (circular and square), *D/t* ratios, from 33 to 67, and eccentricity from 0 to 0.3. The results revealed that the features of the specimens that used different methods of concrete compaction were similar. The results were also compared with the predictions of different design codes; it was found that the predictions of the design codes are acceptable for self-compacting CFST members.

Georgios and Lam (2004) examined the effect of the wall thickness of the steel tube, bond between steel and concrete, and the confinement effect on the response of short circular CFST columns with normal and high strength concrete under concentric loading. The compressive strength of concretes used were 30, 60, and 100 MPa; the steel tube yield strength was 343 and 365 MPa, and the specimens had D/t ratios from 22.9 to 30.5. According to results, the shrinkage is significant for concrete with high strength but negligible for concrete with normal strength. In addition, the bond between steel and concrete become more critical when concrete strength increased. The authors affirmed that for short columns under concentric loading the EC4 code provides the best prediction for both types of concrete.

Han *et al.* (2005b) examined the behavior of self-compacted concrete-filled steel stub columns loaded axially. The factors of the test were cross-sectional shape type, circular and square, with diameter- or width-to-thickness ratio: ranged between 30 to 134, and steel tube yielding strength, with values from 282 MPa to 404 MPa. The average compressive strength of concrete was 60 MPa. The theoretical model was adopted to evaluate the impact of the variables of the study on the capacity of composite columns. Furthermore, the results were compared with the predictions of different design codes which used for normal compacting concrete and offered the same predictions compared with the self-compacting concrete.

Ellobody *et al.* (2006) conducted an experimental and numerical research of circular short CFST columns loaded axially. The concrete compressive strength varied between 30 to 110 MPa, and *D/t* ratios ranged from 15 to 80 to cover the compact range. A comprehensive parameter study was done to examine the effect of compressive strength of concrete and cross-sectional shape on the capacity of circular compact CFST short columns. The computational results were verified versus the experimental results and compared to the estimations of some design codes.

Yang and Han (2006b) tested circular and square hollow steel tubes filled with two types of concrete; normal concrete and recycled aggregate concrete. The varied parameters were cross-sectional shape, concrete type, and load eccentricity (from 0 to 0.53). The results outlined that failure modes were similar for both types of concrete, and that the capacities of all columns decreased when load eccentricity increased. However, in general, the capacities of composite columns with recycled aggregate concrete were smaller than those made with normal concrete, and the compression capacities decreases as load eccentricity increases. Also, the results showed that failure modes of the CFST columns for both concrete types were the global buckling. The compression capacities were compared with some design codes and the results were acceptable. Also, the theoretical model which used for normal concrete is also convenient for recycled aggregate CFST columns.

Ellobody and Young (2006) used ABAQUS package to simulate the nonlinear conductance of square and rectangular CFST columns under axial loading. The confined concrete model was adopted to simulate the core concrete, and a constitutive model was used for the steel tube. The computational results were verified versus experimental results, followed by a comprehensive parametric study. The parametric study examined the impact of different concrete compressive strength, and of cross-sectional shape on the response of CFST columns. The study parameters were concrete compressive strength (30 to 110 MPa) and width-to-thickness ratio (10 to 40). The outcomes of the parametric study were compared with American, European, and Australian codes. The results of American and Australian codes were conservative, while the results of European code were accurate except specimens with a width-to-thickness ratio more than 40.

Lachemi *et al.* (2006a, 2006b) examined the behaviors of self-compacted CFST columns and normal CFST columns. It was stated that the use of self-compacted CFST columns significantly minimized the pouring time compared to normal concrete processing. On the other hand, they observed that normal concrete exhibits a superior confinement strength over self-compacted CFST columns. They also suggested a model to estimate the capacity of self-compacted CFST columns.

Yu *et al.* (2007) experimentally studied the performance of seventeen circular stub hollow steel tubes columns filled with normal and self-compacted concrete under axial loading. The effect of other parameters on the compression behavior was studied, such as concrete strength, presence or absence of notched holes or slots, and the condition of loading which including; (1) entire section, (2) entire section but after the concrete section was compressed initially, (3) entire section but after the steel section was compressed initially, and (4) the concrete section only. The results reported that the existence of slots reduced the stiffness of the column. An increase in strength for both type of concrete led to an increase in capacity; the confinement effect changed with different loading conditions. Compared to the entire section, when the steel section initially loaded, the confinement occurred earlier but decreased and provides approximately same compression capacity, when the concrete section initially loaded or only the concrete section, the confinement occurred later but improved and the compression capacity increased slightly. Furthermore, they reported that the EC4 code provides a good prediction of capacity for both types of concrete when the entire section was loading.

Tao *et al.* (2008) discussed the applicability of approaches used in the Australian code AS5100 for the design of CFST columns, beams, and beam-columns. They compared the predictions of this standard with the results of available test data including 2194 test results. In addition, other design codes were also compared with this database of results. They concluded the method in AS5100 provides accurate estimations and that therefore, it is also suitable for building construction.

Yu. *et al.* (2008) used a self-compacting concrete as a high-performance concrete infilled hollow steel column, to examine the response of very high-strength self-compacting CFST columns. The principal parameters of the study were cross-sectional shape (circular and square sections), slenderness ratio (from 12 to 120) short to long columns, and load eccentricity (from 0 to 0.6), with a compressive strength of concrete of 121.6 MPa. The results show that the failure mode was different between stub specimens with circular and square shapes. The failure mode for square sections was local buckling, while circular sections suffered shear failure. The ductility of very high-strength self-compacting CFST columns is smaller than that of normal strength CFST columns. Furthermore, the results were compared with different design codes; the comparison showed acceptable results for prediction for very high strength self-compacting CFST columns.

De Oliveira *et al.* (2009) experimentally examined confinement in 16 circular CFST columns loaded axially. The experimental parameters were concrete compressive strength (30, 60, 80, and 100 MPa, covering normal- and high-strength concrete), and *L/D* ratios (3, 5, 7, and 10, covering short and long columns). The results were compared with four design codes and the codes predictions were accurate compared to test results. As the results reported, the capacity of composite columns decreases when the *L/D* ratio increases, and the opposite is true of increasing the compressive strength of the core concrete.

Beck *et al.* (2009) presented a study of design code provisions for CFST columns; their investigation includes the national building specification codes of the United States, Canada, Brazil, and Europe. Reliability analysis was used to evaluate the safety level of the codes, the study adopted on test results of 93 columns axially loaded. The results showed that Canadian and European codes are appropriate to predict the column capacity, because the calculations of these codes take the confinement effect in their considerations. While American and Brazilian codes do not take the confinement effect in detail in their calculations, therefore their results become more conservative for short columns. The results also showed Eurocode was least successful in providing uniform reliability, a consequence of the partial factors used in load combinations. The reliability index of the European code was 2.2, below the target reliability levels of the Eurocode specification.

Portolés *et al.* (2011) tested thirty-seven slender circular CFST columns subjected to eccentric loading to explore the suitability of use of HSC with compared to NSC by comparing the results of: concrete contribution ratio, strength index, and ductility index. The test parameters were concrete compressive strength (30, 70, and 90 MPa), *D/t* ratios, load eccentricity ratios (20 or 50 mm), and *L/D* ratios. The nominal cross-section ($D \times t$) were 100×3 mm, 100×5 mm, and 160×6 mm. The columns lengths were 2135 mm and 3135 mm. However, the strength index of columns constructed using NSC is better than that of those using HSC. The concrete contribution ratio is a combination of the relative slenderness and the confinement index. However, the columns with an eccentricity of 20 mm have a greater effect than 50 mm in the reduction of the compression capacity due to the second-order effects and imperfections which are more for the smaller eccentricities than greater ones. The predictions were compared with Eurocode 4 design codes and were in line with the experimental results.

Work begun in Portolés *et al.* (2011) was continued in Portolés *et al.* (2013), which reports the results of testing 24 slender circular CFST columns. They used normal, high, ultra-high strength concrete for plain, steel-bar reinforced, and steel fiber reinforced concrete columns that were under axial and eccentric loading. The variables were concrete compressive strength (30 MPa, 90 MPa, and 130 MPa), load eccentricity (0, 20 mm, and 50 mm), and type of reinforcement. The results showed that high- and ultra-high concrete compressive strength was more beneficial for columns loaded axially than for eccentrically loaded columns. For the reinforcement condition, steel-bar reinforcement was better than reinforcement by steel fiber. Furthermore, steel-fiber reinforcement was useful with normal-strength concrete, but not with high-strength concrete. The ductility of slender columns improved load eccentricity but was not related to the concrete type. The results were compared with the predictions of Eurocode 4 specifications and the comparisons indicated that the Eurocode 4 can be safely used for high and ultra-high strength concrete with eccentric axial loading.

Dundu (2012) experimentally examined the performance of 24 circular CFST columns loaded axially. The variables of the study were length of the column (1000 to 2500 mm), column diameter (114.85 to 193.70 mm), concrete compressive strength (30 and 40 MPa), and steel tube yield strength (355 to 475 MPa). The results showed long columns failed via global buckling, while short columns failed via crushing of the concrete and yielding of the steel tube. However, when the results were compared with the European and the South African code, it was discovered that both codes had conservative results.

Abed *et al.* (2013) examined both experimentally and computationally the behavior of circular short CFST columns concentrically loaded with a low rate of loading of 0.6 kN/s. The variables of the study were *D/t* ratios (54, 32, and 20) and concrete compressive strength (44 and 60 MPa). The results were compared with four different design codes. The computational study was conducted using the software package (ABAQUS) and gave good agreement compared to the test results. The impact of *D/t* ratios on the capacity of CFST columns were found to be more significant than other parameters. The ductility of the column reduces when the concrete compressive strength increases for higher *D/t* ratios, and vice versa for the smaller *D/t* ratios. The ductility and the capacity for higher *D/t* ratios decrease due to decreases in the confinement effect.

Moon *et al.* (2014) used fuzzy logic techniques to estimate the confinement effect on the axial compression capacity of stub CFST columns. The variables that affected the confinement were *D/t* ratios and the concrete compressive strength to steel tube yield strength ratio. he suggested a fuzzy-based model was compared with design codes and the results of the past research and good agreement were obtained.

Ekmekyapar (2016) tested 18 CFST columns under concentric loading; the steel tubes were welded laterally and longitudinally. The main variables of the study were *L/D* ratios, *D/t* ratios, and different locations of the lateral weld. The results indicated that a seam-weld had a small effect on the capacity and failure mode, though the ductility was reduced. Presence of a lateral weld was very significant in transmitting compression and bending effects. The failure mode of short columns was local buckling, while intermediate and long columns suffered both local and global buckling. Lateral weld joints could be used for CFST columns with thin and thick steel tubes; however, the location of the lateral weld did not impact on the column capacity.

Ghannam *et al.* (2004) compared the performance of nine hollow steel tubes columns and thirty-six filled with lightweight or normal concrete. The columns were long, with different cross-sectional sizes and shapes. The results showed that the specimens filled with lightweight aggregate concrete (LWC) suffered local buckling, and global buckling occurred when the column approached failure load. Global buckling was the demonstrated failure mode of specimens with the normal concrete core. The specimens with lightweight concrete presented more lateral displacement and more axial deformation than hollow steel tube columns. The authors suggested that these columns offer a good chance to use lightweight aggregate concrete and the low specific gravity and thermal conductivity of this type of concrete.

Mouli and Khelafi (2007) explored the bond strength and the axial capacity of short rectangular CFST with normal and lightweight aggregate concrete core. The parameters of the test were the cross-sectional dimensions, length of the specimen, and the type of concrete infill. The results showed that the bond strength of lightweight concrete higher than that of normal concrete, while the load-slip behavior was similar for both types of concrete. Cross section was not found to affect the bond strength.

Abdelgadir *et al.* (2011) studied the performance of 54 hollow steel tube columns infilled with lightweight aggregate concrete subjected to eccentric loading. The variables of the study were load eccentricity ratio (10, 20, and 35), steel ratio (11.4 and 13.5), and *L/D* ratios (3, 7, and 14). In the first part of the study, the test results were compared with predicted bearing capacities of different design codes. The second part of the study suggested a method to calculate the maximum compressive strength of confined concrete. The study presented the load eccentricity had a direct impact on the capacity; in addition, an increase in steel ratio increased the column capacity.

Zhongqiu *et al.* (2011a) tested 33 short and long hollow steel tubes columns filled with lightweight aggregate concrete and compared them with columns filled with normal concrete. The results showed that the slenderness ratio had a considerable impact on the capacity of columns. The capacity of these columns decreases when the slenderness ratio increases. The results were also compared with Eurocode 4 estimations and concluded that the formulations of the Eurocode 4 can be used to predict the compression capacity of the columns filled with lightweight concrete.

Zhongqiu *et al.* (2011b) tested 18 columns filled with the lightweight aggregate concrete loaded concentrically. The variables of the test were concrete compressive strength and steel ratio. The results presented that the failure mode was related to the compressive strength of concrete. The confinement increased when the concrete compressive strength decreased; the steel ratio also increased but was smaller than that of specimens with normal concrete.

Zhongqiu *et al.* (2011c) investigated the response of 24 stub columns filled with lightweight aggregate concrete under compression loading. The variables of the test were the yield strength of the steel tube, compressive strength of concrete, and steel ratio. The confinement factor is a significant factor for short composite columns, where the failure mode of the specimens depended on the confinement ratio. The strength of lightweight aggregate concrete core increased due to confinement, and the improvement in strength was related to the confinement coefficient.

Bohai *et al.* (2013) studied the response of long columns filled with lightweight aggregate concrete. The slenderness ratio of the test specimens varied between 64 and 96. The study revealed that the long composite columns were failed due to instability. Furthermore, the capacity and factor of stability decrease when the slenderness ratio increases. The bound of the slenderness ratio was calculated based on the Euler formula; this bound value was smaller than of that of the specimens with normal concrete.

Chan *et al.* (2015) tested twenty-four circular and elliptical stub columns filled with lightweight aggregate concrete loaded concentrically. from the hot-rolled circular hollow sections, the cold-formed elliptical hollow sections were formed. The compressive strength of the lightweight aggregate concrete was 39 MPa, and the yield strength of the steel tube ranged from mild steel strength to high steel strength. Due to this process, the capacity and the ductility of the composite columns decreased. The approaches of Eurocode 4 could be adopted for lightweight circular aggregate filled steel tube columns, and a simple superposition can be considered for the elliptical sections. The concrete contribution for circular sections was higher than that for elliptical sections.

Yu *et al.* (2015) experimentally examined stub CFST columns infilled with five different types of concrete under axial loading. the content of cement and the w/c ratio were same for all concrete types. The study revealed that the type of concrete had a high impact effect on the performance of the composite column. Columns built using lightweight aggregate concrete had reduced capacity and ductility due to the weakness of lightweight aggregate compared with normal concrete. The nonlinear analysis was used to investigate the response of CFST columns with various types of concrete infill by using ABAQUS software and compared the results with the estimations of Eurocode 4 and gave acceptable results.

Zhou *et al.* (2017) used LWC as shell concrete in fiber-reinforced polymer (FRP)-concrete-steel double-skin tubular columns (DSTC). They compared the results with FRP confined full lightweight aggregate concrete (FLAC). The results report that when DSTC were tested under axial loading, shell LWC was efficiently confined, resulting in high ductility and increasing the ultimate capacity of the column. The capacity of FLAC-filled DSTC is higher than the total capacities of the unconfined FLAC and the steel tube. The capacity increases 40-55% for FRP-confined FLAC specimens and 52-65% for DSTC specimens.

AL-Eliwi *et al.* (2017) explored the performance of LWCFST columns and compared their behavior with that of self-compacted concrete-filled steel tube (SCCFST) columns loaded axially. The results revealed differences in behavior between LWCFST and SCCFST columns, especially in their ductility and failure modes. However, all of the SCCFST columns, including the long columns, presented good composite action between steel and SCC. This behavior indicates that SCC is appropriate for use in composite structures. The short and medium LWCFST columns provided good composite action, while the long columns did not. Therefore, the LWC is not appropriate for use in long composite columns.

Chang *et al.* (2013) studied concrete-filled stainless steel–carbon steel tubular columns as a new composite structural member. In these columns, the outer tube was stainless steel and the inner tube was carbon steel; they were filled with high-strength concrete for both inner tube and shell concrete, as clarified in Figure 2.15. This study tried to provide columns with higher corrosion resistance, higher load capacity, and lower cost. A computational analysis was performed and verified with the experimental results. The results illustrated the inner carbon steel tube provided higher confinement and higher capacity. A parametric study was done and concluded that the capacity increased when the diameter ratio, thickness ratio, steel yield strength ratio, and strength of concrete increased. Furthermore, the use of carbon steel had an evident beneficial effect on the behavior of such composite columns.

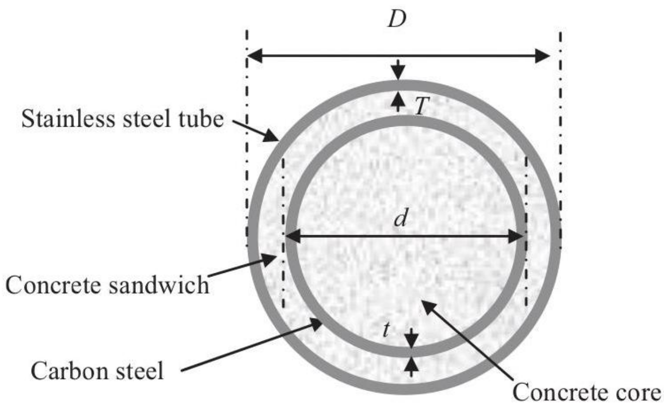

Figure 2.15 Cross-section of a composite column (Chang *et al.*, 2013)

Hassanein *et al.* (2013) conducted a theoretical investigation of the behavior of short circular concrete-filled lean duplex stainless steel–carbon steel tubular columns. In their study, the external tube was stainless steel and the inner tube was carbon steel; concrete filled all sections. Material constitutive models were used to simulate the confined concrete and the stainless steel and carbon steel tubes. A parametric study was carried out to study the effect of the compressive strength of concrete, yield strength of the carbon steel, and geometry of the cross-section of the composite columns. The proposed design model produced perfect predictions of the capacity of columns with many different values of *D/t* ratios for the stainless-steel tubes.

Hassanein *et al.* (2017) performed a computational study of the overall buckling of concrete-filled slender composite columns formed with an outer stainless-steel tube and inner carbon steel tube (CFDST). The parameters studied were the slenderness ratio, the confinement effect, and the compressive strength of concrete. However, the results were compared with the Eurocode 4, and Eurocode 4 gave unsafe predictions. Therefore, the modified European formulation was suggested to calculate the capacity of the slender CFDST columns. The intermediate columns failed by elastic-plastic buckling, while the failure of the long columns was elastic buckling. The confinement of the external stainless-steel tube provided different behavior between intermediate and long columns; no confinement effect was observed for long columns. The use of high- and ultra-high strength concrete cores in slender composite columns did not affect their properties.

Lu *et al.* (2015a) used SCCFST columns to strengthen square reinforced concrete columns under concentric loading. They tested three reinforced concrete columns without any strengthening, one reinforced concrete strengthened with a concrete jacket, and thirteen reinforced concrete columns strengthened with SCCFST columns. The study concluded that the strengthening process by using CFST columns improved the ductility and capacity of the strengthened columns. The degree of enhancement was significantly affected by steel wall thickness, concrete compressive strength, and the length-to-width (*L/B*) ratio. Furthermore, the results were compared with the predictions of different design codes.

Lu *et al.* (2015b) used SCCFST columns to strengthen square RC columns under eccentric loading. The experimental results presented that the use of CFST in offered significant strengthening of reinforced concrete columns. This behavior depends on factors including column cross-section (circular and square), thickness of the outer tube, compressive strength of the concrete, and the eccentricity of the load. A simple design formula was suggested to calculate the maximum capacity of columns according to finite element analysis by using a generic fiber element model, and the results of formula were verified with experimental results.

Wang *et al.* (2017b) tested concrete-filled stiffened double tube (CFSDT) stub columns loaded concentrically. The factors of the research were the presence or absence of an inner steel tube, the compressive strength of core concrete (42.1 and 69.8 MPa), and *D/t* ratio of the inner steel tube. The results showed that the existence of the inner circular CFST component enhanced the ductility and the capacity of the composite column. A nonlinear analysis was done and confirmed the results of the experimental results; it specified that the inner circular tube provides significantly confinement to the core concrete. For outer concrete, the improvement in capacity was limited due to the small confinement produced by the outer tube. A superposition model was suggested to estimate the maximum capacity of CFSDT stub columns.

Liao *et al.* (2013) explored the response of stub CFST columns with initial concrete imperfection under concentric loading in a computational study. The imperfections in the concrete were represented by a circumferential gap or spherical-cap gap (Figure 2.16). The computational results gave a good acceptance compared to the test results. The parametric study discussed the impact of different variables on the capacity of composite columns with gaps. The results presented that the presence of the gap had a direct impact on failure mode, capacity, and load-deformation response because its presence means there is no contact between the concrete and steel at maximum load. A spherical-cap gap only affected the confinement of concrete in the area near the gap. The authors proposed a maximum limit of the circumferential gap ratio for CFST stub columns. Furthermore, they suggested a simplified function to calculate the influence of spherical-cap gap on the maximum capacity of CFST stub columns.

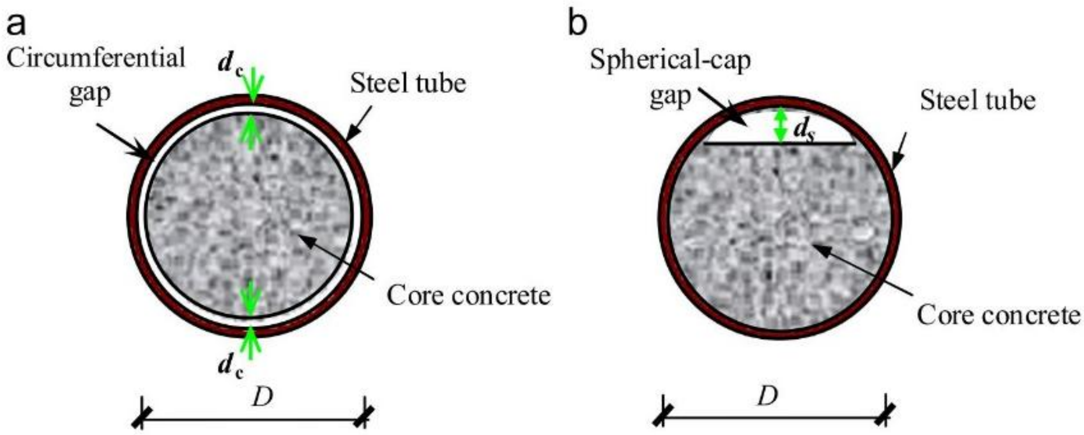

Figure 2.16 A graphical view of gaps in CFST columns (Liao *et al.*, 2013)

Lai and Varma (2015) developed the stress-strain relationships derived from parametric studies by using finite element methods to study noncompact and slender circular CFST columns. The computational model included the influences of inelastic local buckling of steel tubes, concrete cracking, and compression inelasticity. A nonlinear fiber-based analysis model was used to verify the conservatism of the effective stress-strain relationships to estimate the load-deformation behavior of noncompact and slender CFST columns.

Using ABAQUS, Cai *et al.* (2015) explored the behavior and mechanism of failure of steel–reinforced CFST columns under concentric loading (Figure 2.17). Their results were verified with experimental results. The factors of the study were the steel tube ratio, section steel ratio (section steel area-to-core concrete area), compressive strength of the concrete, and yield strength of the steel tube and steel section. Furthermore, a new model was suggested to determine the capacity of these columns. As reported by the results, the capacity of columns and their initial stiffness improve when all parameters are increased. The section steel provided a "strength reserve" for the full column, which has a direct impact on fire resistance for the composite columns. Local buckling of steel sections can be avoided because of the presence of outer CFST columns. The results of the predictions of the Eurocode 4 were underestimates due to the absence of the strength of the core concrete and section steel caused by confinement effect.

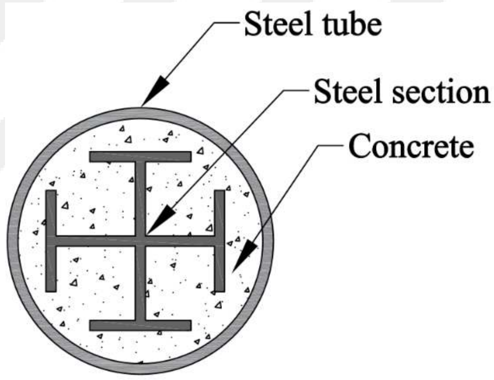

Figure 2.17 Steel-reinforced CFST column adapted from Cai *et al.* (2015)

Yang and Han (2012) presented the response of CFST columns subjected to partial axial compression (Figure 2.18). The parameters of the study were cross-sectional shape, *L/D* (*B*) ratio, partial compression area, and the thickness of the endplate. The results showed ductile behavior of CFST columns under partial compression. A numerical analysis was done to simulate the response of CFST columns subjected to partial compression. The results indicated that such analysis was able to predict their failure modes and load deformation. A simplified model was suggested to estimate the capacity of CFST columns under partial compression; this model and gave credible results.

2.5 Construction of Concrete-Filled Steel Tube Columns

In CFST construction, hollow steel tube columns are erected before pouring the infill concrete. The steel tube works as the perpetual and complete formwork for the concrete. Therefore, the steel tube columns will be under preload from the applied load, additionally the self-weight of the steel tube and the weight of fresh concrete. This preload could cause additional deformation and increased initial stress to the steel tube, which would affect the bearing capacity of the final composite columns (Han and Yao, 2003; Li *et al.*, 2012; Han *et al.*, 2014).

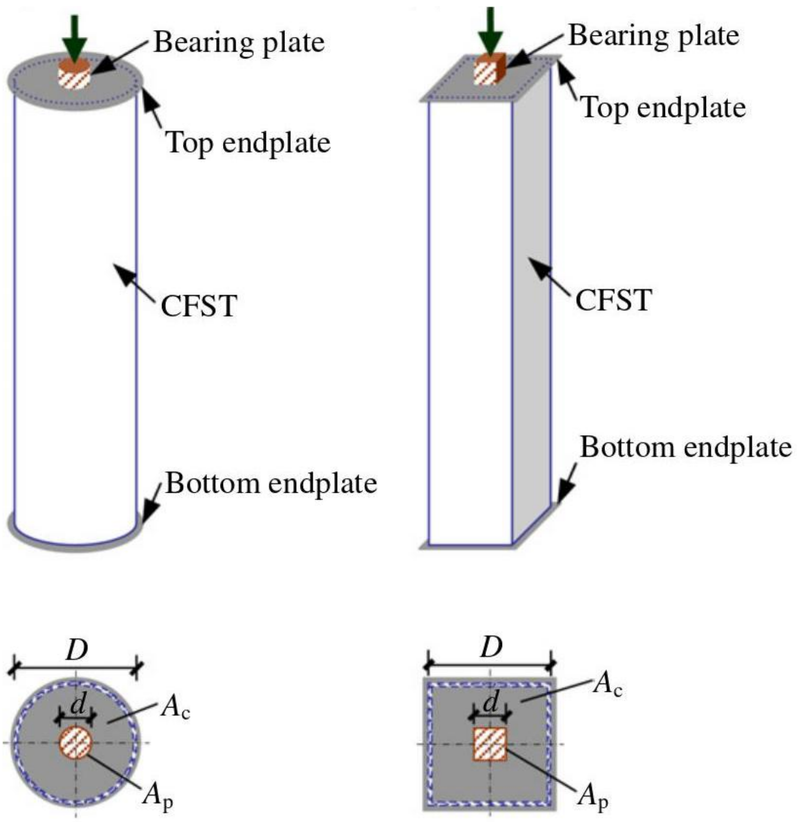

Figure 2.18 Partially loaded CFST columns (Yang and Han, 2012)

The significant factor is the preload ratio (PLR), which is known by the applied preload divided by the maximum strength of the hollow steel tube. The preload on the steel tube excesses its deformation and reduces the final capacity of the composite column. This decline in capacity depends on the PLR. If the PLR was about 0.7, the reduction would be about 20%, and a PLR < 0.3 the reduction would be less than 5% (Han and Yao, 2003; Li *et al.*, 2012). However, the preloading influence has an insignificant effect on short columns, and the effect can be eliminated if the amplified relative column slenderness or the PLR is less than 0.2. The preload effect may have a more obvious impact on the capacity of the composite columns with a slender cross-section because local failure of these steel tubes is more possible during preload (Liew and Xiong, 2009).

On the other hand, the imperfection occurred through the placement of concrete. These imperfections may appear as gaps in addition to cavities in the concrete. These imperfections could also effect on the response of the CFST column. Liao *et al.* (2013) studied the impact of the initial concrete imperfection on the response of the stub CFST columns and found that the loss of the capacity of the column is less than 3.5% if the gap ratio is smaller than 0.05%.

2.6 Pouring of Concrete

The hollow steel tubes columns and beams are erected before the pouring the infill concrete. It is difficult to examine the poured concrete poured, but the strength and the compaction of the infilled concrete is vital.

There are many ways to pour fresh concrete into a steel tube. However, there are two main concrete pouring methods: (1) Pumping, such as pouring concrete from the bottom. In this case the pumping holes should be closed after concrete hardening. (2) Gravity method, pouring the concrete from the top of the column. These methods are illustrated in Figure 2.19 (Han *et al.*, 2014).

Before casting the concrete, the steel tube from inside must be clean and free from any undesirable thing such as water, dust, and oil. Where no particular cleaning method is needed. The quantity of concrete mix must be checked to be certain that the infilled concrete is adequate for the tube.

The poured concrete may be normal compacting concrete or self-compacting concrete; the latter may be preferred in construction processes. Normal compacting concrete should be poured in steps with depths of 300 or 500 mm, and should be vibrated (Han *et al.*, 2014).

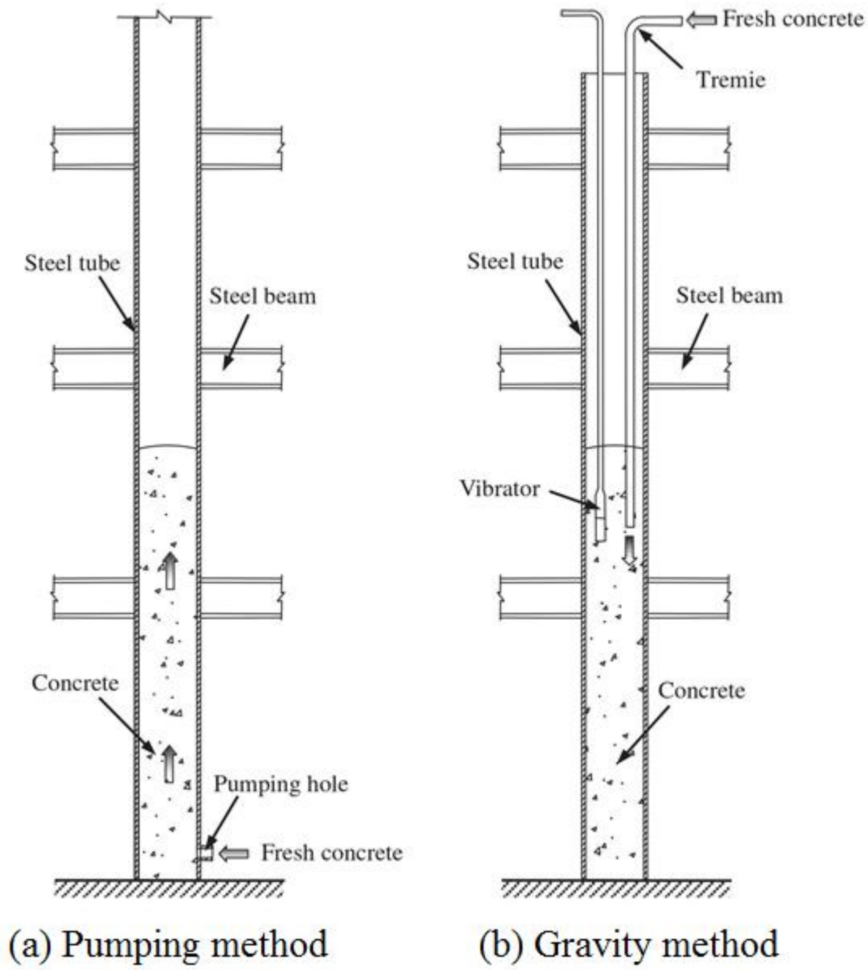

Figure 2.19 Pouring of concrete (Han *et al.*, 2014)

2.7 Manufacturing Processes of Tubular Members

The manufacturing of hollow steel tube members is like that of other structural steel members; the dimensional tolerances follow the general specifications of steel manufacturing.

Many steps are involved in the manufacture of steel tube members (Figure 2.20) (Zhao *et al.*, 2005):

1. Uncoiling and joining coils.
2. Forming: the steel strip forms into a circular shape by passing through a set of forming rollers.
3. Welding; for a circular shape, the edges formed together by pressure rollers and they are welded by electric resistance welding.

4. Sizing and shaping; a series of rolls are utilized for sizing the circular hollow section or formed the rectangular or square sections from the circular hollow section.
5. Cutting and bundling; the tube is cut into specific proper lengths and prepared for dispatch.

The basic dimensions of cold-formed tubes are shown in Figure 2.21. In this thesis, hollow steel tubes were manufactured according to the EN10219 (2006) specification for cold-formed welded structural hollow sections of non-alloy and fine grain steels. As reported by that specification, the steel tubes are produced without consequent heat treatment. Table 2.2 shows the cross-section tolerance of circular hollow steel tubes, and Table 2.3 shows the tolerance of length and straightness of circular hollow steel tubes.

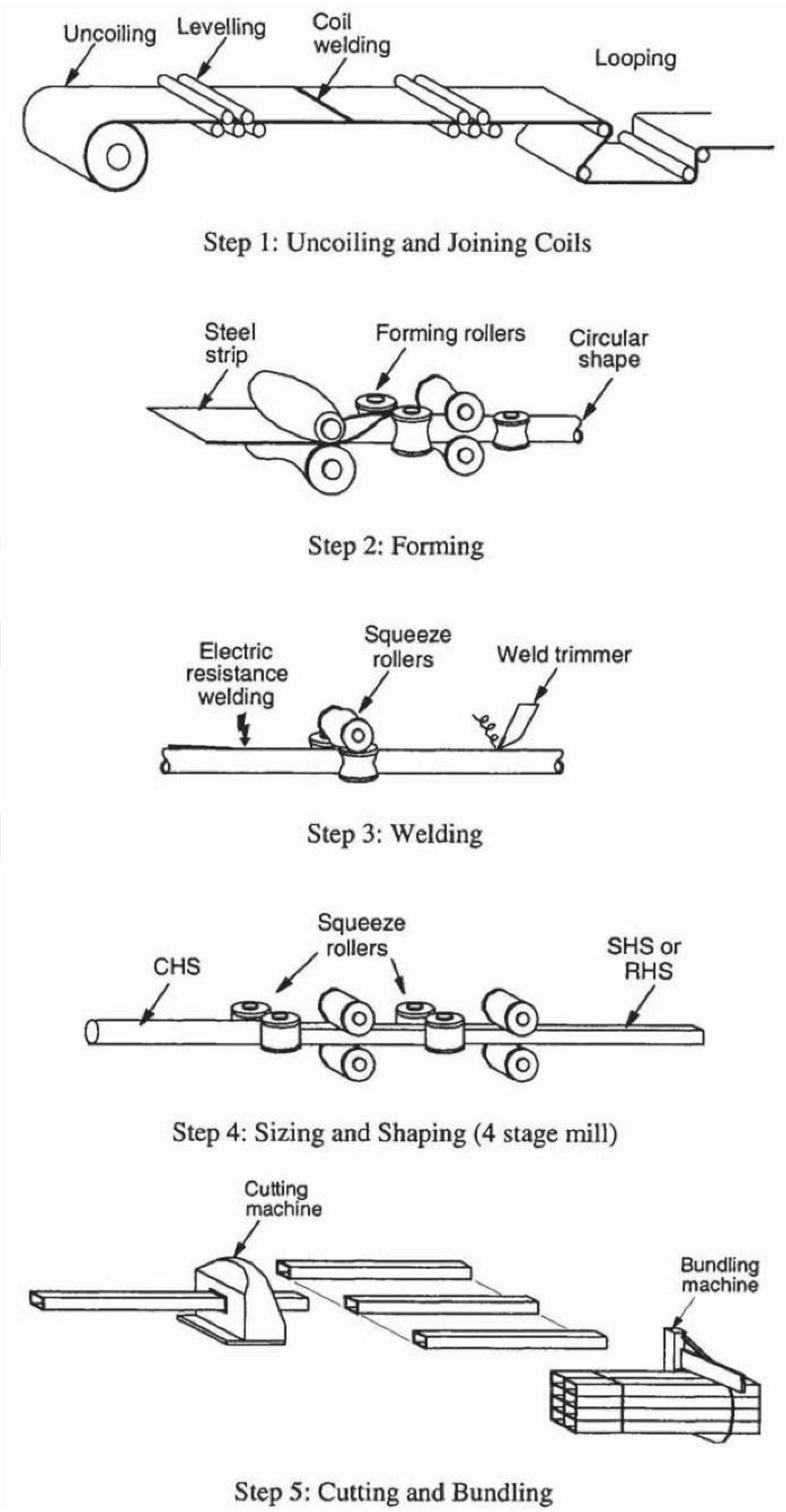

Figure 2.20 Main steps in manufacturing processes (Zhao *et al.*, 2005)

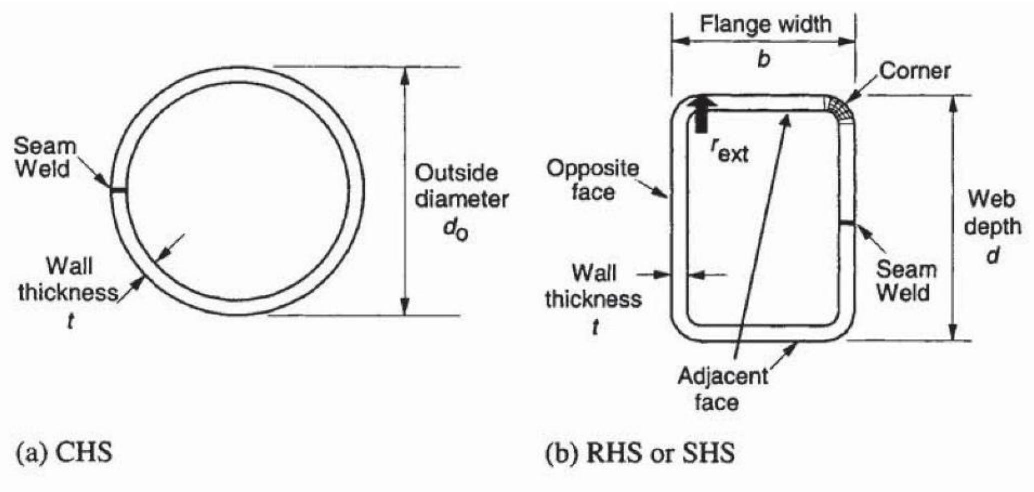

Figure 2.21 Basic dimensions of cold-formed tubes (Zhao *et al.*, 2005)

Table 2.2 Tolerance of circular cross-section (Zhao *et al.*, 2005)

Tolerance	EN 10219
Outside dimension	$\pm 0.01D$, but $\geq \pm 0.5\ mm$ and $\leq \pm 10\ mm$
Thickness	For $D \leq 406.4\ mm$: $\pm\ 0.1t$ For $t \leq 5\ mm$: $\pm\ 0.5\ mm$ For $D > 406.4\ mm$: $\pm\ 0.1t$ but $\leq 2\ mm$

Table 2.3 Tolerance of length of circular hollow tube (Zhao *et al.*, 2005)

Tolerance	EN 10219
Length	$+5\ mm$, and $0\ mm$ for length $< 6\ m$ $+15\ mm$, and $0\ mm$ for $6\ m <$ length $\leq 10\ m$ $+5\ mm + 1\ mm/m$, and $0\ mm$ for length $> 10\ m$
Straightness	$\pm L/500$

2.8 Concrete-Filled Steel Tube Elements Applications

CFST members have been utilized in various constructions worldwide, including tall structures, bridges, subway stations, workshops, and power plants.

2.8.1 Concrete-Filled Steel Tube Elements in Constructions

CFST has been utilized to carry member-supported compressive loads; it is commonly joined to steel or RC beams to produce a composite frame structure.

Figure 2.22 describes a high-rise building with an inner wall offering lateral bracing to the steelwork during construction. Figure 2.23 reveals the steel tube columns before concrete was poured into the columns (Liew and Xiong, 2012).

Figure 2.24 shows the Ruifeng International Commercial Building built in China in 2001; square CFST columns were used in its construction. The structure includes a composite frame and reinforced concrete shear walls.

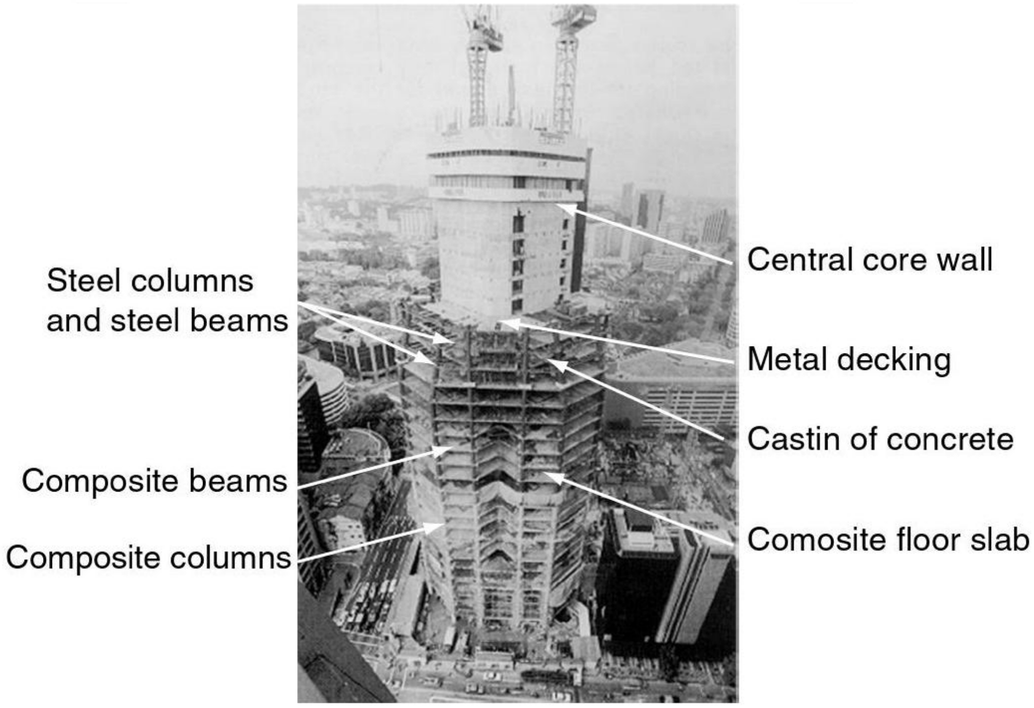

Figure 2.22 High-rise building under construction (Liew and Xiong, 2012)

Figure 2.23 Circular steel tubes before pouring concrete (Liew and Xiong, 2012)

Figure 2.24 Ruifeng building, China, 2001 (Han *et al.*, 2014)

2.8.2 Concrete-Filled Steel Tube Elements in Bridges

CFST members have been utilized in different bridges including truss bridges, suspension bridges, and cable-stayed bridges. They can serve as piers, bridge towers, and arches, among other applications (Han *et al.*, 2014).

In arch bridges such as this, the use of hollow steel tubes is a significant feature: during construction, the tubes work as the formwork for pouring concrete, which lowers the cost. Also, due to the stability of the hollow tubes, the arch bridge can be constructed without any temporary bridging.

2.8.3 Concrete-Filled Steel Tube in Other Structures

Many other structures are also constructed using CFST columns, including subway stations, electricity pylons, and industrial buildings. Subway stations in particular experience high axial loading, which a CFST system particularly well-suited to support (Han *et al.*, 2014).

In another application, CFST members have been used to erected a long-span transmission tower with a height of 370 m, CFST diameter of 2000 mm, and concrete filling up to 210 m in height (Han *et al.*, 2014).

However, through the erection of transmission towers, the use of concrete-filled double skin steel tubes (CFDST), with lighter self-weight and higher bending stiffness in comparison with the more-usual CFST columns. Figures 2.32 and 2.33 show a real example of the utilization of CFDST columns in the erection of transmission towers. The internal and external tubes are constructed first, then pouring of the concrete (Li *et al.*, 2012; Han *et al.*, 2014).

2.9 Summary

This chapter focused on several different subjects. The characteristics of CFST columns were compared to RC and steel columns; the effects of concrete type and cross-section shape on CFST columns were described, and applications of CFST columns were discussed. The structural performance of CFST columns under axial compressive loading, the classification of CFST columns as short and long columns, the steel-concrete interaction, and the mechanism of the confinement of these composite columns were also discussed.

A wide-ranging literature review examined the body of work on CFST columns with different material and geometric characteristics under different loading and boundary conditions. It was concluded that more test and numerical studies should be conducted to explore the performance of the CFST columns constructed using self-compacted concrete, lightweight concrete, high- and ultra-high-strength concrete, and concrete-filled double steel tube columns under different loading conditions. The construction of CFST columns, placement of concrete, and manufacturing processes of tubular structural members were also discussed in this chapter.

At the end of the chapter, the use of CFST members in different field applications, such as buildings, bridges, and other structures subjected to different loading conditions were presented. This wide range of uses for CFST members indicates their efficiency in these types of these types of structures.

CHAPTER 3

DESIGN SPECIFICATIONS

3.1 Introduction

Many published research and design codes have suggested empirical formulas for the assessment of the section and ultimate capacities of CFST columns. These design codes depend on different theories and design philosophies. They have limitations because of the material characteristics of steel and concrete, section slenderness, and columns slenderness ratio. Outside these limitations, design codes may provide less exact estimates of capacity. However, even within the limitations, the estimates provided by design codes can present large deviations from experimental results (Wang *et al.*, 2017a). Nevertheless, experimental studies of CFST columns are supported by different codes.

In this thesis, several design codes have been adopted to evaluate the axial compressive capacity of CFST columns and compare them with experimental results. They are ANSI/AISC360-16 (2016) —AISC360-16—, the American specification for steel structures; Eurocode4 (2004) —EC4—, the European sepecifcation for composite structures; AS5100.6-2004 (2004) —AS5100.6—, the Australian code for steel and composite construction; and AIJ2001 (2001) —AIJ2001—, the Japanese specification for steel reinforced concrete structures.

In comparing the estimation of codes with experimental results, the material partial safety factors were adjusted to one. Moreover, all limitations of codes were ignored to check their applicability in estimating capacities relative to experimental results. The codes provide two stages of prediction for CFST capacity: (1) prediction of the section capacity, for the short columns, the capacity depends on the material strength of the section and local buckling is taken into consideration; (2) prediction of ultimate capacity, where for long columns the section capacity was reduced due to the effect of the slenderness ratio, and global buckling occurred in addition to local buckling (De Oliveira *et al.*, 2009; Aslani *et al.*, 2015).

All of these codes take the confinement effect into consideration, but some of them—namely ASIC360-16 and AIJ2001—consider confinement as a constant, while EC4 and AS5100.6 provide formulations to predict the confinement effect.

3.2 Axial Compressive Capacity of the Circular CFST Columns

3.2.1 Limitations of the Design Codes

As addressed in the previous section, all codes apply some limitations on the mechanical features of the materials and geometrical characteristics used in their formulation. It is noteworthy that significant variations exist in the limitations of each of the design codes. Table 3.1 presents the limitations of the design codes included in this thesis.

Table 3.1 Limitations of CFST design codes

Parameter	AISC 360-16	EC4	AS5100.6	AIJ2001
f_y (MPa)	$f_y \leq 525$	$235 \leq f_y \leq 460$	$f_y \leq 350$	$235 \leq f_y \leq 355$
f_c of NWC (MPa)	$21 \leq f_c \leq 70$	$20 \leq f_c \leq 60$	$25 \leq f_c \leq 65$	$f_c \leq 60$
f_c of LWC (MPa)	$21 \leq f_c \leq 41$			
D/t	$\leq 0.31\left(E_s/f_y\right)$	$\leq 90\left(235/f_y\right)$	$\leq 82\left(250/f_y\right)$	$\leq 1.5\left(23500/f_y\right)$
Steel amount	$\geq 1\% A_g$	$0.2 \leq \delta \leq 0.9$	$0.2 \leq \delta \leq 0.9$	-
Longitudinal steel amount		$0 \leq \frac{A_{sr}}{A_c} \leq 6\%$		
Slenderness	$KL/r \leq 200$	$\lambda \leq 2$	$\lambda \leq 0.5$	-

In Table 3.1, E_s refers the elastic modulus of the steel tube, K is the end fixity coefficient of the column, λ refers to the column's relative slenderness, and δ is the steel contribution ratio defined in EC4 (Equation 3.1).

$$\delta = \sqrt{\frac{A_s f_y}{N_{pl.Rd}}} \tag{3.1}$$

$$N_{pl.Rd} = A_s f_y + A_{sr} f_{yr} + A_c f_c \tag{3.2}$$

where $N_{pl.Rd}$ is the plastic resistance of column, A_s is the cross-section area of the structural steel tube, A_{sr} is the cross-section area of the longitudinal steel-bar reinforcement if used, A_c is the cross-section are of the concrete core, f_y is the yield strength if the structural steel tube, f_{yr} is yield strength of the longitudinal steel-bar reinforcement, and f_c is the core concrete compressive strength.

The elastic modulus of the concrete, E_c, is calculated in each design code as presented in Table 3.2.

Table 3.2 Calculating the Elastic Modulus of Concrete

Specification	E_c (MPa)	Details
AISC 360-16	$0.043\rho^{1.5}\sqrt{f_c}$	ρ: Concrete density (NWC and LWC)* $(1500 \leq \rho \leq 2500\ kg/m^3)$
EC4	$22000\ ((f_c + 8)/10)^{0.3}$	NWC
	$(22000\ ((f_c + 8)/10)^{0.3})(\rho/2200)^2$	LWC According to Eurocode2 (2004)
AS5100.6	$0.043\sqrt{f_c}\ \rho^{1.5}\ \ f_c \leq 40\ MPa$	
	$\rho^{1.5}(0.024\sqrt{f_c} + 0.12)\ f_c > 40\ MPa$	
AIJ 2001	$3.35 \times 10^4 (\rho/2400)^2 (f_c/60)^{\frac{1}{3}}$	

*NWC: normal weight concrete; LWC: lightweight aggregate concrete

3.2.1 AISC 360 – 16 (American Institute of Steel Construction)

In this code, the calculations of the sections' capacity depend on the plastic stress distribution method. This approach supposes that the steel element has reached a yield strength f_y of steel tube while the concrete core is about $0.95f_c$, where f_c is concrete compressive strength. The AISC360-16 specification permits an increase of concrete compressive strength from $0.85f_c$ for rectangular tube sections to $0.95f_c$ for circular sections due to increasing of the hoop stress arising from the transverse confinement effect. Local buckling of the steel tube is taken into consideration in the plastic stress distribution method, where local buckling is considered according to the section slenderness ratio (*D/t* ratio); however, the elastic local buckling of the hollow steel tube is remarkably affected by the presence of core concrete. Core concrete changes the buckling mode of the CFST column compared to that of a hollow steel tube, whether for the cross-section and along the length of the column, as shown in Figure 3.1 and Figure 3.2.

Local buckling is calculated according to the classification of a section of the CFST column. A section may be classified as compact, noncompact, or slender in accordance with its *D/t* ratio. Table 3.3 shows the classification of sections of CFST columns by their *D/t* ratios.

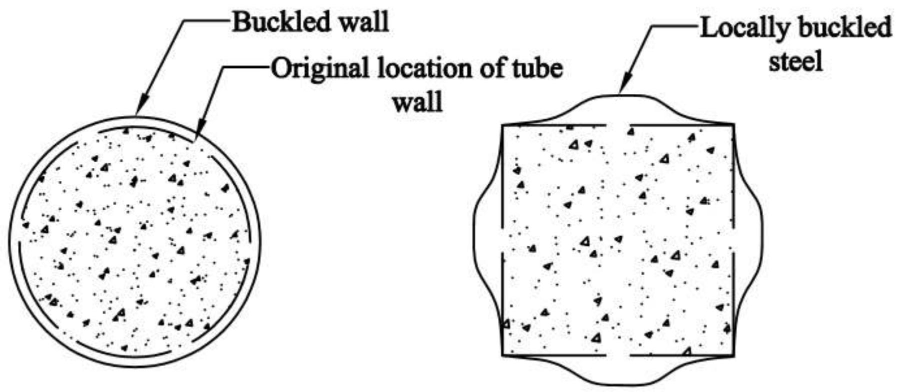

Figure 3.1 Cross-sectional buckling of CFST column adapted from ANSI/AISC360-16 (2016)

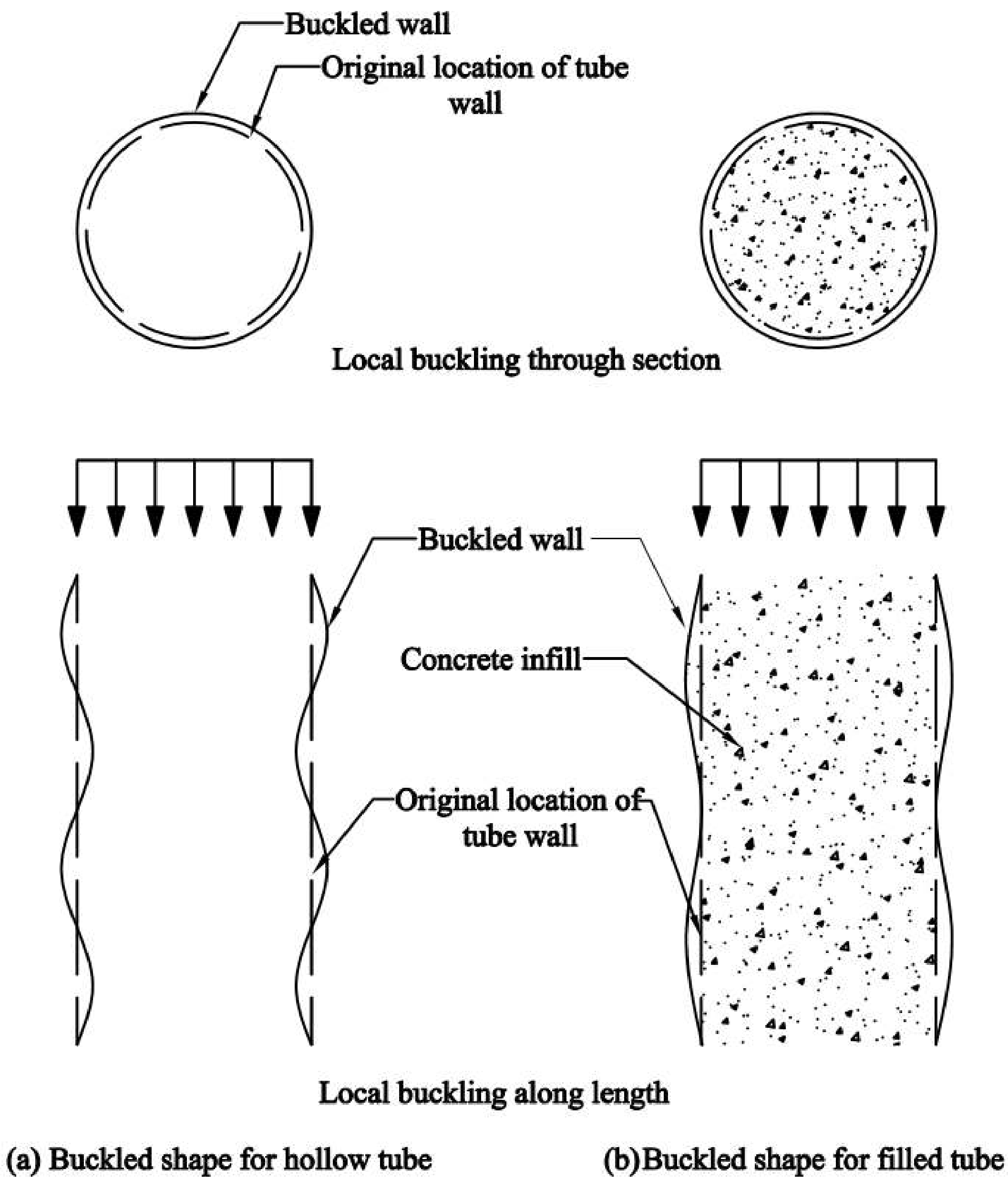

Figure 3.2 Buckling shape along hollow and filled steel tube column adapted from Lai and Varma (2015)

Table 3.3 Limitations of *D/t* of circular steel tube (ANSI/AISC360-16, 2016)

Compact section	Non-compact section	Slender section	Maximum permitted
$D/t \leq \lambda_p$	$\lambda_p < D/t \leq \lambda_r$	$D/t > \lambda_r$	$D/t < 0.31\dfrac{E_s}{f_y}$
$\lambda_p = 0.15\dfrac{E_s}{f_y}$	$\lambda_r = 0.19\dfrac{E_s}{f_y}$		

Nominal compressive strength, N_{AISC}, for CFST columns subjected to axial loading can be calculated for the limit state of flexural buckling based on member slenderness according to Equation 3.3:

$$N_{AISC} = \begin{cases} P_{no} \times 0.658^{\frac{P_{no}}{P_e}} & if \ \frac{P_{no}}{P_e} \leq 2.25 \\ 0.877P_e & if \ \frac{P_{no}}{P_e} > 2.25 \end{cases} \tag{3.3}$$

P_e, the elastic critical buckling load, can be calculated as:

$$P_e = \pi^2 \frac{EI_{eff}}{(KL)^2} \tag{3.4}$$

EI_{eff} is the effective stiffness of the CFST columns section (N/mm^2), and can be calculated as:

$$EI_{eff} = E_s I_s + E_{sr} I_{sr} + C_3 E_c I_c \tag{3.5}$$

$$C_3 = 0.45 + 3\left(\frac{A_s + A_{sr}}{A_g}\right) \leq 0.9 \tag{3.6}$$

$$A_g = A_s + A_{sr} + A_c \tag{3.7}$$

Where A_g is the gross area of the CFST cross-section, A_s, I_s, A_{sr}, I_{sr}, and A_c, I_c, are the area of the section, and moment of inertia about the elastic neutral axis of CFST column section of steel tube, steel reinforcing bars, and concrete core, respectively.

P_{no} is the nominal axial strength and can be calculated according to the formula for the appropriate cross-section type:

Compact sections:

$$P_{no} = P_p \tag{3.8}$$

where P_p is the nominal, plastic capacity of the section (at zero length strength). It is calculated as the superposition of the yield strength of the steel tube and compressive strength of core concrete; in a compact section, the steel tube wall offers adequate thickness to evolve yielding of the steel tube before local buckling and produce a proper confinement to the concrete core to reach its compressive strength of $0.95f_c$.

$$P_{no} = f_y A_s + 0.95 f_c \left(A_c + A_{sr} \frac{E_s}{E_c} \right) \tag{3.9}$$

Noncompact sections:

A noncompact CFST section is thick enough to reach the yielding strength of the steel tube, f_y, in the longitudinal direction with local buckling, but it cannot provide appropriate confinement to the concrete core when f_y reaches $0.7f_c$.

In this case, P_{no} can be calculated as

$$P_{no} = P_p - \frac{P_p - P_y}{\left(\lambda_r - \lambda_p\right)^2} \left(\lambda - \lambda_p\right)^2 \tag{3.10}$$

where λ, λ_p and λ_r are slenderness ratios calculated from Table 3.3.

$$P_y = f_y A_s + 0.7 f_c \left(A_c + A_{sr} \frac{E_s}{E_c} \right) \tag{3.11}$$

Slender sections:

When a slender CFST section is subjected to elastic buckling, the steel tube neither yields nor provides appropriate confinement to the concrete core when its yielding strength reaches $0.7f_c$. After reaching this compressive strength, the concrete core undergoes significant volumetric expansion, increasing the post-local buckling collapse of the steel tube. The steel tube is also incapable of confining the concrete.

$$P_{no} = F_{cr} A_s + 0.7 f_c \left(A_c + A_{sr} \frac{E_s}{E_c} \right) \tag{3.12}$$

where the F_{cr} is the critical buckling stress:

$$F_{cr} = \frac{0.72 f_y}{\left[\left(\frac{D}{t} \right) \frac{f_y}{E_s} \right]^{0.2}} \tag{3.13}$$

Figure 3.3 presents the difference of the nominal axial compressive strength P_{no} of the circular CFST columns versus the section slenderness ratio (*D/t*). Compact sections can provide full plastic strength, P_p, under compression. In noncompact sections, the nominal axial compressive strength P_{no} can be calculated by a quadratic variation between the plastic strength, P_p, and yielding strength, P_y, with respect to the *D/t* ratio. This nonlinearity occurs due because the steel tube must to be closer to the compactness limit λ_p and increase the concrete compressive strength from $0.7f_c$ at P_y to $0.95f_c$ at P_p. The results of considering the relation between P_y and P_p linear has been found unconservative by some experimental results. However, slender sections are limited to reaching the critical buckling stress, F_{cr}, of the steel tube and $0.7f_c$ of the concrete core (Lai and Varma, 2015; ANSI/AISC360-16, 2016).

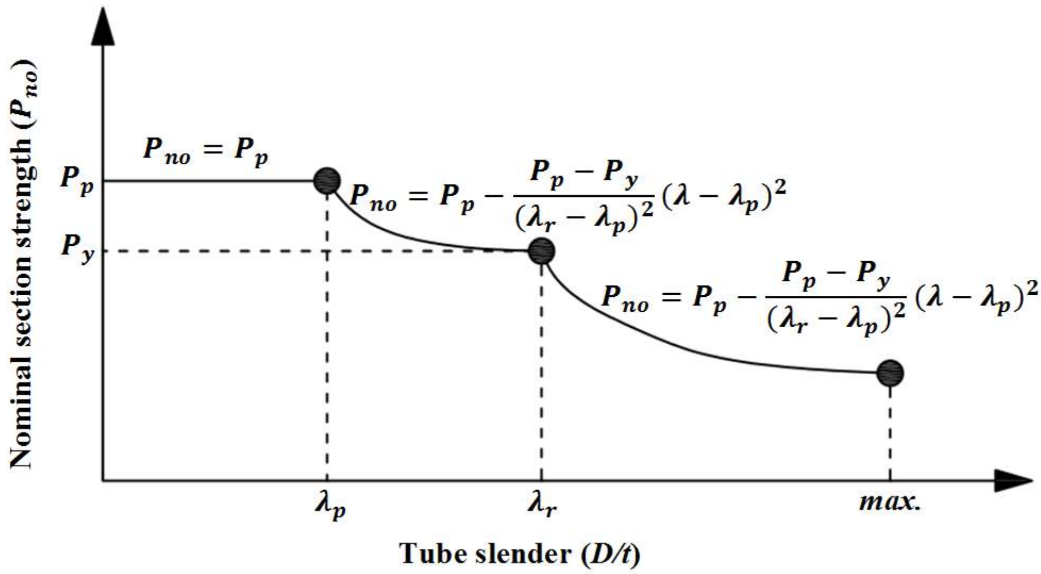

Figure 3.3 P_{no} versus *D/t* ratio adapted from Lai and Varma (2015)

Equations 3.3 to 3.6 are applied to calculate the nominal compressive strength N_{AISC} of circular CFST columns with consideration of length effects; P_{no} is the nominal compressive strength of the section including the factor of tube slenderness and calculated using Equations 3.9, 3.10, and 3.12.

3.2.2 European Standard – Eurocode 4 (EC4)

EC4 depends on a simplified method to predict the axial capacity of CFST columns. the simplified method depends on assumptions belonging to the geometric characteristics of the CFST cross-section. It also be based on the European buckling curves for steel columns as the principle of column buckling design. This technique is limited to members of doubly symmetrical and uniform cross-section along the member length with rolled, cold-formed, or welded steel sections. To use the simplified method, there are some limitations must be satisfied, stated in Table 3.1. Among them, the steel contribution ratio must meet the condition $0.2 \leq \delta \leq 0.9$. If $\delta < 0.2$, the column may be designed under EC2 (Eurocode2, 2004), while if $\delta > 0.9$, the column may be designed as a bare steel section, neglecting the effect of the concrete core, and the design may follow EC3 (Eurocode3, 2005). However, the *D/t* ratio of CFST must be satisfy the limit of EC4 to preclude precocious local buckling of the steel tube (Eurocode4, 2004).

The plastic resistance of a CFST column under axial compression (also called the squash load, $N_{pl.Rd}$) is calculated as shown in Eq. 3.2. This value denotes the maximum load that can be used to the CFST column in section. For circular sections, the augmented strength of concrete core because of the confinement effect. The capacity of a CFST column is enhanced by up to 15% under simple concentric loading when the effect of triaxial confinement is taken in account. This improvement in capacity also depends on the slenderness ratio of the CFST column and is significant only in short columns with relative slenderness ratio $\bar{\lambda} \leq 0.5$. For other columns, this improvement should be ignored and it should be treated as a rectangular section (Hicks and Newman, 2002; Eurocode4, 2004; Liew and Xiong, 2015). Thus, the plastic resistance of circular CFST columns with $\bar{\lambda} \leq 0.5$ is calculated as:

$$N_{EC4-1} = \eta_a f_y A_s + f_{yr} A_{sr} + A_c f_c \left(1 + \eta_c \frac{t}{D} \frac{f_y}{f_c}\right) \tag{3.14}$$

where η_a is the steel reduction factor and η_c is the concrete enhancement factor. If eccentricity is smaller than 10% of the outer dimeter of steel tube, the steel reduction factor and concrete enhancement factor are calculated as follows:

$$\eta_a = 0.25(3 + 2\bar{\lambda}) \leq 1.0 \tag{3.15}$$

$$\eta_c = 4.9 - 18.5\bar{\lambda} + 17\bar{\lambda}^2 \geq 0.0 \tag{3.16}$$

$$\bar{\lambda} = \sqrt{\frac{N_{pl.Rd}}{N_{cr}}} \tag{3.17}$$

$N_{pl.Rd}$ is the plastic resistance of the columns, given in Equation 3.2, and N_{cr} is the elastic (Euler) critical buckling load, calculated as follows:

$$N_{cr} = \pi^2 \frac{EI_{eff}}{(KL)^2} \tag{3.18}$$

EI_{eff} is the effective stiffness of the CFST columns section (N/mm^2), and can be calculated as:

$$EI_{eff} = E_s I_s + E_{sr} I_{sr} + 0.6 E_c I_c \tag{3.19}$$

However, for slender columns, EC4 does consider the effects of global buckling. The buckling resistance of a slender column is described as a reduction factor χ, which is calculated using buckling curves (Figure 3.4) according to Eurocode3 (2005):

$$\chi = \frac{1}{\phi + \left(\phi^2 - \bar{\lambda}^2\right)^2} \leq 1.0 \tag{3.20}$$

$$\phi = 0.5\left[1 + \alpha\left(\bar{\lambda} - 0.2\right) + \bar{\lambda}^2\right] \tag{3.21}$$

In which α is an imperfection factor, if the circular CFST column containing longitudinal steel reinforcement as $\rho_s = A_{sr}/A_c \leq 3\%$, α equal to 0.21, curve a; or if containing longitudinal steel reinforcement as $3\% \leq \rho_s \leq 6\%$, α equal to 0.34, curve b, see Figure 3.4. Then, the resistance of CFST column subjected to axial compression with global buckling is estimated as:

$$N_{EC4} = N_{EC4-1}\,\chi \tag{3.22}$$

For values of $\bar{\lambda} \leq 0.2$ (Figure 3.4), the buckling effects are neglected and only cross-sectional N_{EC4-1} is considered.

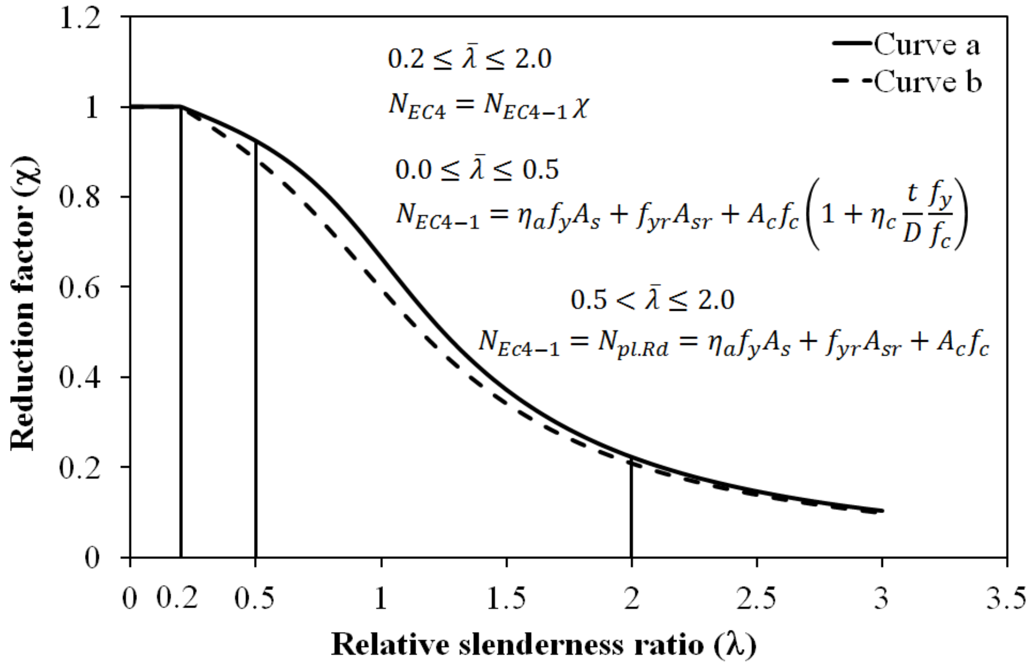

Figure 3.4 European buckling curve according to Eurocode3 (2005)

3.2.3 Australian Standard – AS5100.6-2004

The Australian bridge design standard, AS5100 part 6, is interested with the design of steel and composite construction. In it, approaches are given for the design of CFST columns, which take into account the composite action between the steel and concrete core (AS5100.6-2004, 2004; Tao *et al.*, 2008).

To estimate the nominal section capacity of CFST columns under axial loading under this standard, an assumption is applied that the steel tube yields before the concrete core reaches its ultimate stress. Therefore, the nominal section capacity for rectangular section can be estimated as follows:

$$N_{us} = A_s f_y + A_{sr} f_{yr} + A_c f_c \tag{3.23}$$

For circular CFST columns, the excess in the concrete compressive strength because of the confinement impact may be counted if the relative slenderness ratio $\lambda_r \leq 0.5$, and the load eccentricity is not greater than 10% of the outer diameter of steel tube; otherwise, the N_{us} should be determined according to Eq. 3.22. For a circular section with confinement effect, N_{us} may be determined as follows:

$$N_{AS-1} = \eta_a f_y A_s + f_{yr} A_{sr} + A_c f_c \left(1 + \eta_c \frac{t}{D} \frac{f_y}{f_c}\right) \quad (3.24)$$

where η_a is the steel reduction factor, and η_c is the concrete enhancement factor. If eccentricity is smaller than 10% of the outer dimeter of steel tube, the steel reduction factor and concrete enhancement factor are calculated as follows:

$$\eta_a = 0.25(3 + 2\lambda_r) \leq 1.0 \quad (3.25)$$

$$\eta_c = 4.9 - 18.5\lambda_r + 17\lambda_r^2 \geq 0.0 \quad (3.26)$$

$$\lambda_r = \sqrt{\frac{N_{us}}{N_{cr}}} \quad (3.27)$$

N_{us} is the nominal resistance of the columns, given in Eq. 3.22, N_{cr} is the elastic (Euler) critical buckling load, and determined as follows:

$$N_{cr} = \pi^2 \frac{EI_{eff}}{(KL)^2} \quad (3.28)$$

EI_{eff} is the effective stiffness of the CFST columns section (N/mm^2), can be calculated as:

$$EI_{eff} = E_s I_s + E_{sr} I_{sr} + E_c I_c \quad (3.29)$$

Calculations of the nominal section capacity according to AS5100.6 are practically similar to those used in the EC4 code unless various values have been used for the capacity parameters (Tao *et al.*, 2008).

The nominal member capacity (N_{AS}) for circular CFST columns under axial loading can be estimated as follows:

$$N_{AS} = \alpha_c N_{AS-1} \leq N_{AS-1} \quad (3.30)$$

where N_{AS-1} is the nominal section capacity (Equation 3.24). The coefficient α_c is a compression member slenderness reduction factor used to show the relationship between the strength and stability for CFST column. Its value is determined using Equation 3.31:

$$\alpha_c = \zeta\left[1 - \sqrt{1 - \left(\frac{90}{\xi\lambda}\right)^2}\right] \tag{3.31}$$

$$\zeta = \frac{\left(\frac{\lambda}{90}\right)^2 + 1 + \eta}{2\left(\frac{\lambda}{90}\right)^2} \tag{3.32}$$

$$\lambda = \lambda_\eta + \alpha_a\alpha_b \tag{3.33}$$

$$\eta = 0.00326(\lambda - 13.5) \geq 0 \tag{3.34}$$

$$\lambda_\eta = 90\lambda_r \tag{3.35}$$

$$\alpha_a = \frac{2100(\lambda_\eta - 13.5)}{\lambda_\eta^2 - 15.3\lambda_\eta + 2050} \tag{3.36}$$

α_a and α_b are the appropriate section constants and λ_η is modified compression member slenderness and calculated as follows:

$$\lambda_\eta = \left(\frac{L_e}{r}\right)\sqrt{k_f}\left(\frac{f_y}{250}\right) \tag{3.37}$$

L_e/r is geometrical slenderness ratio of the member, where, L_e is the effective of the member and r is the radius of gyration. k_f is form factor and calculated as $k_f = A_e/A_g$, where A_g is the gross area of the section and A_e is the effective area of the cross-section, which depends on the effective outer diameter. The effective outer diameter d_e of a circular section in turn depends on the element slenderness, λ_e, and the element yield slenderness limit, $\lambda_{ey} = 82$.

$$\lambda_e = \frac{D}{t}\left(\frac{f_y}{250}\right) \tag{3.38}$$

the effective outer diameter d_e shall be the lesser of:

$$d_e = D\sqrt{\frac{\lambda_{ey}}{\lambda_e}} \leq D \tag{3.38}$$

or

$$d_e = D\left(\frac{3\lambda_{ey}}{\lambda_e}\right)^2 \tag{3.39}$$

Finally, $\alpha_b = -1$ if $k_f = 1$, and $\alpha_b = -0.5$ if $k_f < 1$ (according to Table 10.3.3 A, or 10.3.3 B, in the AS5100.6-2004 (2004) code).

3.2.4 Japanese Code – AIJ2001

The AIJ2001 code uses the allowable stress design method, which relies on the elastic analysis of structures. This code classifies CFST columns as short, medium, and long according to their *L/D* ratio: if $L/D \leq 4$, the column is short, if $4 < L/D \leq 12$, the column is medium, and if $L/D > 12$, the column is long.

In this code, the effect of confinement is constant (0.27), as determined by regression analysis between experimental data for the capacity of hollow steel tubes, $N_{so} = A_s f_y$, as presented in Figure 3.5 (Sakino *et al.*, 2004).

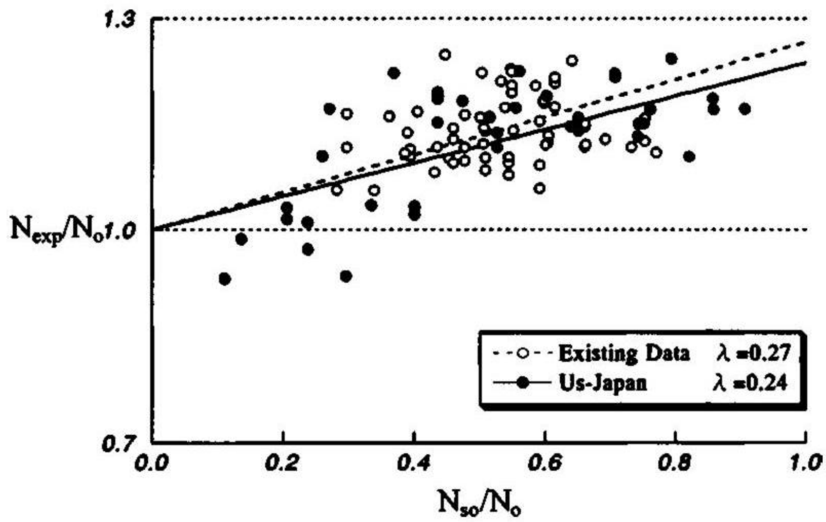

Figure 3.5 Axial capacity of the circular hollow steel tube (Sakino *et al.*, 2004)

In this standard, the ultimate capacity of a CFST column is calculated by a different formula depending on its classification:

For short CFST columns, $L/D \leq 4$:

$$N_{AIJ-short} = N_{cuc} + (1+\xi)N_{cus} \tag{3.40}$$

Where, ξ is the confinement factor and equal to 0.27.

For intermediate CFST columns, $4 < L/D \leq 12$:

$$N_{AIJ-inter.} = N_{AIJ-short} - 0.125\left(N_{AIJ-short} - N_{AIJ-long}\right)\left(\frac{KL}{D} - 4\right) \tag{3.41}$$

For long CFST columns, $L/D > 12$:

$$N_{AIJ-long} = N_{crc} + N_{crs} \tag{3.42}$$

where N_{cuc} and N_{cus} are the ultimate strength of concrete column and steel tube column, respectively, and N_{crc} and N_{crs} are the buckling strength of a concrete column and a steel tube column, respectively.

$$N_{cuc} = A_c r_{uc} f_c \tag{3.43}$$

$$N_{crc} = A_c \sigma_{crc} \tag{3.44}$$

where σ_{crc} is the critical stress of a concrete column, and $r_{uc} = 0.85$ is the reduction factor for concrete strength.

$$\text{if } \lambda_{1c} \leq 1.\ \sigma_{crc} = \frac{2r_{uc}f_c}{1+\sqrt{\lambda_{1c}+1}} \tag{3.45}$$

$$if\ \lambda_{1c} > 1.\ \sigma_{crc} = 0.83 r_{uc} f_c e^{(C_c(1-\lambda_{1c}))} \tag{3.46}$$

$$\lambda_{1c} = (\lambda_c/\pi)\sqrt{\varepsilon_{uc}} \tag{3.47}$$

$$\varepsilon_{uc} = 0.93(r_{uc}f_c)^{1/4} \times 10^{-3} \tag{3.48}$$

$$C_c = 0.568 + 0.00612 f_c \tag{3.49}$$

$$\lambda_c = KL/r_c \text{, and } \lambda_s = KL/r_s \tag{3.50}$$

$$if\ \lambda_{1s} < 0.3,\ N_{crs} = A_s f_y \tag{3.51}$$

$$if\ 0.3 \leq \lambda_{1s} < 1.3,\ N_{crs} = N_{Es}/1.3 \tag{3.52}$$

$$\lambda_{1s} \geq 1.3,\ N_{crs} = [1 - 0.545(\lambda_{1s} - 0.3)]A_s f_y \tag{3.53}$$

$$\lambda_{1s} = \lambda_s/\pi \sqrt{f_y/E_s} \tag{3.54}$$

$$N_{Es} = \frac{\pi^2 E_s I_s}{(kL)^2} \tag{3.55}$$

where λ_c and λ_s are the slenderness of the concrete and steel columns, respectively.

3.3 Summary

Many design codes are used in the design of CFST columns. Only four codes were selected for discussion in this work: AISC360-16, EC4, AS5100.6, and AIJ2001. These codes represent different regions of the world and are based on different theories and design criteria. In addition, the limitations due to the material characteristics of steel and concrete contained in these codes also differ. The main significant parameter in CFST columns is the confinement effect. AISC360-16 and AIJ2001 represent confinement as a constant factor, while, both EC4 and AS5100.6 provide formulations to calculate the confinement effect.

In the experimental work of this study, CFST columns with various types of concrete (normal-weight concrete including compacted and self-compacted concrete and lightweight aggregate concrete) and grades of concrete (normal-, high- and ultra-high-strength concrete) have been carried out. The predictions of each of the selected design codes provided different predictions vied to the test results; the variations between the outcomes of the codes are due to differences in their formulations. In addition, it is found that the formulations of these design codes should be extended to cover different types of concrete; their current formulations all essentially focus on normal-weight concrete. The boundaries of both the current material (f_c and f_y) and geometric (*D/t* and *L/D*) limitations should be extended.

CHAPTER 4

EXPERIMENTAL WORK AND MATERIAL PROPERTIES

4.1 Introduction

The major goal of the experimental work addressed in this thesis was to determine the performance of circular CFST columns loaded axially. This chapter reports the experimental program, material properties, specimen preparation, and testing setup.

4.2 Experimental Program

The experimental program of this thesis was divided into four parts. Each part studied the effect of different geometric characteristics of the steel tube and different type and characteristics of the inner concrete on the response of the columns loaded axially compression. Three of them deal with single CFST and the fourth one deals with concrete-filled double steel tube (CFDCST) columns.

4.3 Material Properties

4.3.1 Structural Steel Tube and Steel-Bar Reinforcement

The steel tubes used in all studies in this thesis were cold-formed, seam-welded circular hollow sections. They were provided by Borusan Mannesmann company for steel pipe industry/Turkey and cut from a stock 6.0 m length to the required length. Before pouring the concrete, the hollow steel tube specimen ends were treated by a machining process to guarantee flat ends and the applied load will be equal over the cross-section where the steel and concrete loaded together. This machining process which applied to the specimen ends is a critical procedure to obtain reliable test results (Ziemian, 2010). Figure 4.1 presents the machining process of steel tube specimens, and Figure 4.2 shows the specimens before concrete was poured.

ASTME8/E8M-16 (2016) standard was followed for sampling, cutting tensile coupons, and testing to measure mechanical properties of the steel tubes specimens.

Figure 4.3 describes the dimensions of the tensile coupons, and Figure 4.4 shows a representative sample of the tensile coupon samples used in this work.

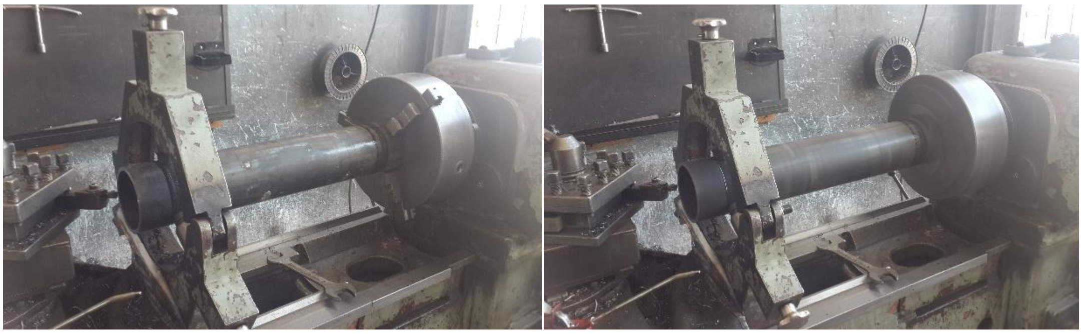

Figure 4.1 Machining of steel tube specimens

Figure 4.2 Steel tube specimens before pouring concrete

For steel reinforcing bars if present (Chapter Seven), ASTMA370−17a (2017) standard was followed for testing to measure mechanical properties of the steel-bar reinforcement.

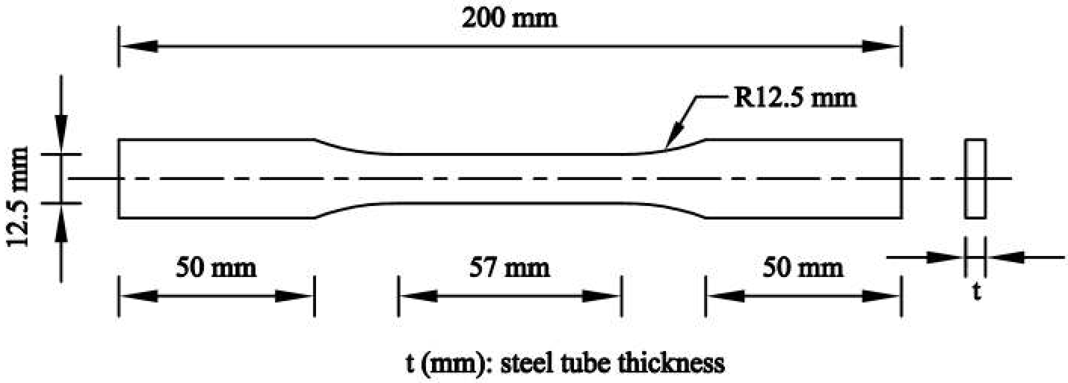

Figure 4.3 Tensile coupon dimensions adapted from ASTME8/E8M-16 (2016)

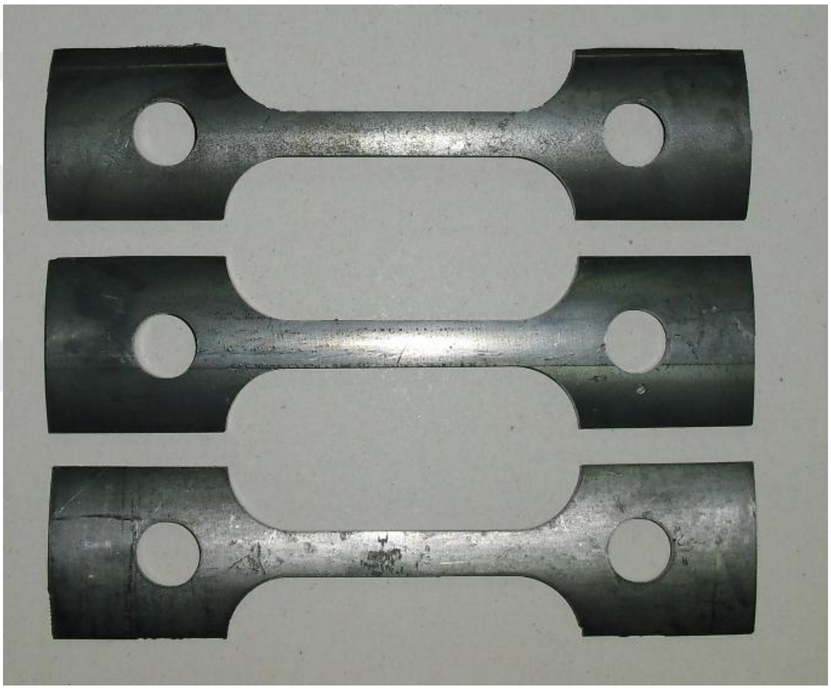

Figure 4.4 Representative tensile coupon specimens

4.3.2 Concrete

In this thesis, various concrete kinds were used: normal-strength concrete (NSC), self-compacted concrete (SCC), high-strength concrete (HSC), Ultra high-strength concrete (UHSC), and lightweight aggregate concrete (LWC). These types of concrete, each with a different compressive strength, were adopted to explore the impacts of concrete choice on the performance of CFST columns.

Concrete is produced principally of Portland cement, aggregate (coarse and fine), and water, with chemical admixtures and supplementary cementitious materials added to provide the required workability and strength.

The components of concrete mix used in this work were:

- **Cement:**

Ordinary Portland cement (Type I) produced according to Turkish Standard (TS) 197-1.

- **Fine aggregate:**

Natural sand and crushed sand types.

- **Coarse aggregate:**

Natural gravel and crushed gravel types.

- **Water:**

Ordinary faucet water was utilized in the stage of mixing of the concrete mix components and the curing stage of the concrete specimens.

- **Supplementary cementitious materials:**

They are frequently added to the concrete mix by combining them with cement to reduce the heat of hydration and enhance workability, strength, durability, and economy under expected service conditions. These materials include fly ash (FA) and silica fume (SF) (ACI211.1-91, 2002).

FA is a byproduct of coal-fired power plants, consisting of fine particles emitted from the boiler along with flue gases. There are two main classes: Class F and Class C. The main difference between them is the quantity of silica and calcium oxide. The surface area of FA is around 300–500 m^2/kg, and its specific gravity ranges from 1.9–2.8 (Mo *et al.*, 2017).

Essentially, FA is added as a partial mass or replace it with a part of cement volume. The inclusion of FA improves many properties of concrete, including its workability and permeability among others. The appropriate amount of FA in concrete mix depends on the required level of strength and the age at which that strength is required. Where it affects to increase the strength of concrete at ages over 28 days, when replacing an equal mass of cement with FA, and the compressive strength at less than

7 days may be lower, especially for Class F FA. To achieve the same strength, the proportions of the mix must be modified, by reducing the *w/c* ratio, modifying the cementitious material content, or modifying the admixture content (ACI211.4R-08, 2008; ACI363R-10, 2010; Darwin *et al.*, 2016).

SF is a very fine material ($< 1\ \mu m$) and it is highly like cement when combined with cement. It is a by-product of silicone metal production. The specific gravity of SF is around 2.2–2.5 and its surface area approximately 20000 m^2/kg. In contrast to FA, SF mainly helps cement to gain strength in the early stages, from 3 to 28 days after mixing (Darwin *et al.*, 2016; Mo *et al.*, 2017).

The fundamental role of SF in a concrete mix is the enhancement of the paste-aggregate interface, the weakest zone of the concrete matrix. The use of SF is mandatory in the manufacturing of HSC, where it increases the concrete compressive strength and modulus of elasticity. However, the use of SF increases the required water for concrete due to its very fine particle size and because it is added directly to the concrete, not used as a replacement for cement. Therefore, SF is used simultaneously with a superplasticizer to obtain the required workability (Köksal *et al.*, 2008). Wille *et al.* (2011); Wille *et al.* (2012) have recommended SF be used as 25% by weight when mixing cement.

- **Materials used for chemical admixture:**

Nowadays, the use of chemical admixture has become a part of current concrete technology. Before the use of chemical admixture, the production of HSC was not as simple as it is now. The accurate use of the chemical admixture enhances the characteristics of both fresh and hardened concrete (Caldarone, 2008). Chemical admixtures may be water-reducers (plasticizers), wet-retarders or accelerators; they are classified according to their objective when mixed in concrete. ASTMC494/C494M−17 (2017) classified the chemical admixtures as follows:

- "Class A: Water-reducing admixtures,
- Class B: Retarding admixtures,
- Class C: Accelerating admixtures,
- Class D: Water-reducing and retarding admixtures,
- Class E: Water-reducing and accelerating admixtures,

- ❖ Class F: Water-reducing, high range admixtures or superplasticizer,
- ❖ Class G: Water-reducing, high range, and retarding admixtures, and
- ❖ Class S: Specific performance admixtures".

Admixtures may be used in the liquid or solid state. The use of the liquid type is more common, as it can be more rapidly dispersed uniformly during mixing of concrete. However, the dosage of admixture is typically given as a percentage of the cement by weight in instructions from manufacturers (Neville, 2011).

The use of chemical admixtures are summarized according to the functions that they perform, such as (Ramachandran, 1996):

- ❖ "Increasing workability without increasing water content or decreasing the water content at the same workability,
- ❖ Accelerating the rate of concrete strength increase shortly after pouring.
- ❖ Increasing the compressive, tensile, or flexure strength of concrete.
- ❖ Accelerating or retarding the initial setting time of concrete.
- ❖ Reducing the segregation of concrete.
- ❖ Increasing the durability of concrete.
- ❖ Decreasing the permeability of concrete".

Superplasticizers (SP), Type F, help in separating cement particles, and the can reduce mixing water demand by more than 30%, then increasing concrete compressive strength (Ramachandran, 1996; ACI211.4R-08, 2008). However, the enhancement in workability can be achieved by two approaches: producing concrete with high workability or concrete with high strength (Neville, 2011). The dosage of SP depends on its function, where, for improving the workability, the normal dosage is between 1 to 3 letter per cubic meter of concrete, while for reduce the water content of the mix, the dosage is between 5 to 20 liters per cubic meter of concrete (Neville, 2011).

The superplasticizer (hyperplasticizer) type F which used in this thesis is known commercially as Master Glenium 51 (old name is Glenium 51).

4.3.2.1 High-performance concrete (HPC)

High-performance concrete (HPC) surpasses normal concrete in features and construction abilities. To produce this type of concrete and to satisfy design requirements, many featured materials are used. Additional processes are needed for the use of high-performance concrete, such as specific mixing, placing and curing (Caldarone, 2008; Kosmatka and Wilson, 2011).

The ACI committee has the following definition and commentary for HPC (Russell, 1999; Caldarone, 2008):

> Definition: "*High-performance concrete meeting special combination of performance uniformity requirements that cannot always be achieved routinely using conventional constituents and normal mixing, placing, and curing practices*".
>
> Commentary: "HPC *is concrete in which certain characteristics are developed for a particular application and environment. Examples of characteristics that may be considered critical for an application are*":
>
> - "*Ease of placement*
> - *Compaction without segregation*
> - *Early age strength*
> - *Long-term mechanical properties*
> - *Permeability*
> - *Density*
> - *Heat of hydration*
> - *Toughness*
> - *Volume stability*
> - *Long life in severe environments*".

Any type of concrete possesses fresh characteristics or hardened characteristics better than normal concrete can be named HPC. Additionally HSC, many different types of HPC are available, such as (Caldarone, 2008):

- "Self-compacting concrete (SCC)
- Lightweight aggregate concrete (LWC)
- Heavyweight concrete
- No-fines concrete

- Low permeability concrete; and
- Shrinkage-compensating concrete".

4.3.2.2 High-Strength Concrete (HSC)

HSC is of increasing interest due to its economic and constructional merits. The greater the concrete strength, the minimize the member size can be; in turn, a reduction in member size reduces the amount of construction materials needed. HSC is predominantly used for compression members, such as columns in tall structures; where the use of such concrete contributes significantly to minimize the final cost of these structures (Liew *et al.*, 2016).

Though HSC offers many advantages, it has some significant shortcomings. One of these is its high brittleness; its brittleness becomes more as its strength rises, presenting low tensile strength to compressive strength ratio (Xincheng, 2012). When HSC is used in structural applications, the cross-section of a member is reduced but its slenderness and buckling are increased (Portolés *et al.*, 2013).

The use of a composite structure is one solution to compensate for these shortcomings. CFST columns are a type of composite structure in which the ductility and the compressive strength of the column can be improved as a result of the confinement of the steel tube to the inner concrete. Columns filled with HSC have many advantages, like high compression capacity and stiffness. Also, the brittle behavior of the HSC in the post-peak phase can be minimized due to the presence of the outer steel tube (Portolés *et al.*, 2011; Liew *et al.*, 2016). In addition, the fire resistance of composite columns is improved, particularly if the HSC is reinforced with steel bars (Portolés *et al.*, 2011).

ACI363R-10 (2010) defines HSC as concrete with a cylinder compressive strength greater than 55 MPa. Eurocode2 (2004) defines concrete as HSC when concrete cylinder compressive strength greater than 50 MPa, and as ultra-high strength concrete (UHSC) when the compressive strength is higher than 90 MPa (Portolés *et al.*, 2011).

The *w/c* ratio is the significant parameter influencing the strength of the resulting concrete. HSC is fabricated by a higher content of cementitious materials and lower water content; however, in general, the use of high quantities of cementitious materials increases the quantity of water required. In such a case, the use of chemical admixtures as superplasticizers is required to control the increase in water demand (ACI363R-10, 2010). The water to cementitious materials ratio or water to binder (*w/b*) ratio of HSC is commonly between 0.3 to 0.4 and for UHSC is commonly between 0.2 to 0.3 or less (Wille *et al.*, 2012; Xincheng, 2012).

4.3.2.3 Self-Compacting Concrete (SCC)

Self-compacting concrete (SCC) is a highly flowable high-performance concrete that can be poured into place, filling a formwork under its own weight. It can achieve acceptable consolidation without application of internal or external vibration and does not face problems due to segregation and bleeding. SCC is also known as self-consolidation concrete, self-placing concrete, and self-leveling concrete (Lachemi *et al.*, 2006b; ACI237R-07, 2007).

SCC technology was developed in Japan in the late 1980s and is used in different applications in the field of civil engineering. This technology depends on increasing the amount of fine material, such as cementitious materials and superplasticizer, to obtain the required workability without changing the water content. According to ACI237R-07 (2007), there are three practical conditions that must be met for concrete to be considered SCC: filling ability, passing ability, and resistance to segregation.

These terms are defined as (EFNARC, 2005):

"Filling ability: *Ability of fresh concrete to flow into and fill spaces within formwork, under its own weight*";

"Passing ability: *Ability of fresh concrete to flow through tight openings, such as spaces between steel reinforcing bars, without segregation or blocking*";

and

"Segregation resistance: *ability of fresh concrete to remain homogeneous in composition while in its fresh state*".

To satisfy these requirements it is necessary to adjust the conventional concrete mix. The first adjustment is for fine and coarse aggregates; it requires changing the proportion from the 60% coarse aggregate and 40% fine aggregate mixture used in conventional concrete to a 50% proportion of each, or less for coarse aggregate when the maximum aggregate size is less or equal to 10 mm and when the reinforcement steel bars are overcrowded. The second adjustment is to the amount of fine materials, which can enhance the filling and passing ability of SCC. The goal of the second adjustment is to minimize free water and enhance the cohesiveness of the mixture, improving the stability of the SCC. This goal can be achieved by using cementitious materials, as silica fume and fly ash, in addition to materials crushed to sizes less than 0.125 mm (processed with no. 100 sieves) (Yahia and Aïtcin, 2016).

Four characteristics are typical of SCC in the fresh state: flowability, viscosity, passing ability, and segregation. Each of these features can be defined by one or more test approaches:

1. Flowability: slump-flow test.
2. Viscosity: T_{500} slump-flow test or V-funnel test.
3. Passing ability: L-box test.
4. Segregation: Segregation resistance (sieve) test.

According to the requirements of a project, the desired characteristics of SCC in the fresh state should be selected from one or more of these and follow its classifications (Table 4.1) (EFNARC, 2005).

Table 4.1 SCC tests and limitations

Characteristic	Test	Class	Limitations
Flowability	Slump-flow (SFL)	SF1	$550\ mm \leq SF1 \leq 650\ mm$
		SF2	$660\ mm \leq SF2 \leq 750\ mm$
		SF3	$760\ mm \leq SF3 \leq 850\ mm$
Viscosity (V)	V-funnel (VF): T_{500}	V1	$VF < 8\ s: T_{500} \leq 2\ s$
		V2	$9\ s \leq VF \leq 25\ s: T_{500} > 2\ s$
Passing ability (PA)	L-box	PA1	$PA \geq 0.8\ s$: two bars
		PA2	$PA \geq 0.8\ s$: three bars
Segregation resistance (SR)	Sieve segregation	SR1	$SR1 \leq 20\ \%$
		SR2	$SR2 \leq 15\ \%$

1. Slump-test and T_{500} time is a test to check the flowability and the flow rate of SCC without obstructions. These test results are suggestive of the filling ability of SCC, and the T_{500} time is also a measure of the speed of flow and the viscosity of the SCC. This test follows the test described in EN 12350-2 (Figure 4.5).
2. The V-funnel test is used to estimate the viscosity and filling ability of SCC, and it is not appropriate when the maximum aggregate size is greater than 20 mm. A funnel with a V shape (Figure 4.6) is filled with fresh concrete and the time required for the concrete to flow out of the funnel measured; this time is the "V-funnel flow time".
3. The L-box test is used to estimate the passing ability of SCC to flow through narrow spaces between two or three reinforcing bars (to simulate crowded reinforcements) and other objections without segregation of blocking (Figure 4.7).
4. The sieve segregation test is used to estimate the resistance of SCC to segregation.

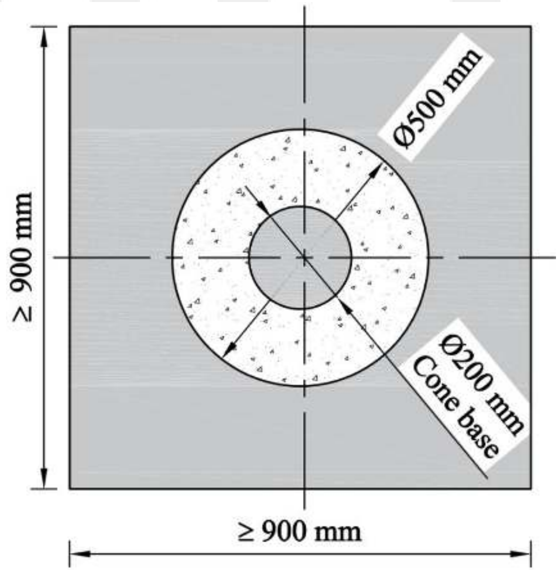

Figure 4.5 Schematic of plate used for slump-test adapted from EFNARC (2005)

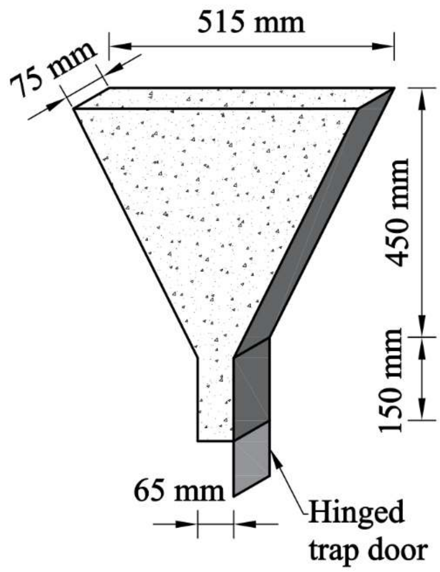

Figure 4.6 Schematic of V-funnel test adapted from EFNARC (2005)

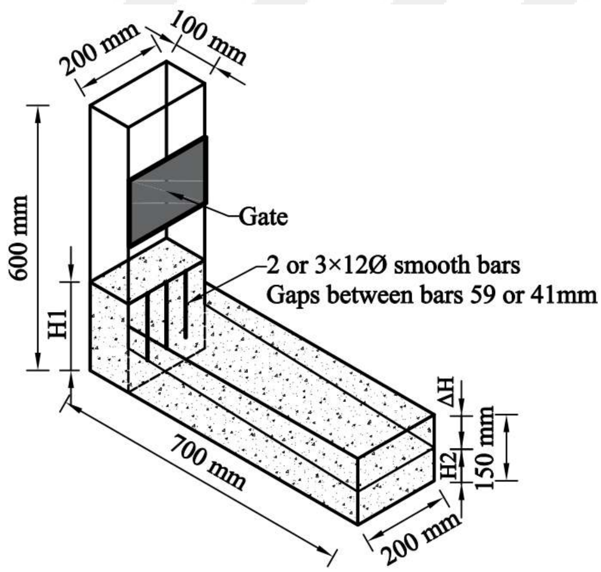

Figure 4.7 Schematic of L-box test adapted from EFNARC (2005)

4.3.2.4 Lightweight Aggregate Concrete (LWC)

Lightweight aggregate concrete (LWC) is can be defined as a type of concrete produced by introducing lightweight materials as conventional coarse or fine aggregate substitute (Mo *et al.*, 2017) .

Structural lightweight aggregate concrete has lower density than normal-weight concrete (NWC). When manufactured with lightweight aggregate (LWA) or with a mix of lightweight- and normal-weight aggregate, according to the ACI213R-03 (2003) specification, the LWC must gain a minimum compressive strength of 17 MPa and a density varied from 1120 to 1920 kg/m^3 at 28 days. The concrete strength is affected by the density of the aggregates used; there are two different types of LWA: natural and artificial lightweight aggregate. The natural type includes materials such as pumice, oil palm shell, coconut shell, etc. These types of natural LWA are ready to use after only preparation, such as crushing and sieving. The artificial type includes materials such as expanded shale, expanded clay, and sintered fly ash, among others (Chandra and Berntsson, 2002; ASTMC330/C330M-14, 2014).

In any structure, self-weight has a big share of the gross load to which the structure is subjected. Therefore, there are the important advantages of minimizing the concrete density, consequently, reducing the weight of the different structural members. The use of LWC can reduce the size of concrete structural members, which reduces the load on the foundation and also has economic consequences (Neville, 2011).

LWC has several shortcomings compared with NWC, such as high shrinkage, a tendency to develop creep deformations, brittle failure, and low rigidity. Even with these shortcomings, however, there are many merits to its use, for instance, the low density of LWC (LWC is 20% to 30% lighter than NWC) results in lower dead weight in structures, which leads to cost savings in construction. LWC also provides low thermal conductivity, about 12% to 33% that of NWC. This allows it to provide superior fire resistance as well as sound and heat insulation due to the presence of air voids, all while reducing the risk of earthquake damage (Zhongqiu *et al.*, 2011a; AL-Eliwi *et al.*, 2017).

In summary, some properties of LWC compared to NWC are (Neville, 2011):

- The modulus of elasticity of LWC is lower by 25% to 50% for the same strength.
- Due to the greater porosity of LWC, its resistance to freezing and thawing is greater. The porosity results because LWA is not saturated before mixing.
- LWC has a lower sensitivity to spall, while the fire resistance of LWC is greater; the loss in strength in LWC is smaller with increase in temperature.
- At the same concrete compressive strength, the shear strength of LWC is lower by 15% to 25%, and its bond strength is lower by 20% to 50%.
- Creep is about equal for both types of concrete.

There are many approaches to improve the mechanical properties of LWC, such as add the supplementary cementitious materials (SF, FA, etc.) as partial cementing materials in LWC. The use of the optimum amount of SF as a cement replacement gives a good impact on the LWC compressive strength due to its high reactivity and micro-filler effect; the optimum content of SF in pumice LWC has been reported as 20%. When using FA as a partial cement replacement up to the optimum limit, the workability of the resulting concrete improves, but beyond the allowable limit, its workability could be significantly reduced (Mo *et al.*, 2017). However, the use of reinforced LWC with steel fiber or steel bar reinforcement can improve the mechanical properties of the LWC.

Many different mixes were prepared for all concrete types used in this study. From each concrete mix, cylinder specimens of 100×200 mm in size were poured. After curing, ASTMC39/C39M−15a (2015) specification followed to test these cylindrical specimens to determine the concrete compressive strength. Three concrete specimens were tested to allow determination of mean values for each mix.

4.4 Test Instruments

All CFST columns experiments were performed on a device with a capacity of 3000 kN. The specimens were centered accurately in the machine to cancel any eccentric loading. A displacement-controlled load was applied to drive the hydraulic actuator for all specimens at constant rate, the displacement loading control mode allows to investigate the post-peak behavior of the column, and the results of the axial loading against end shortening were saved, Also, two displacement transducers were affixed to record the axial deformation of the specimens to study the behavior of specimens in the pre-peak and post-peak regions. Figure 4.8 shows the testing machine and a schematic view of the experimental setup. Strain gauges were used to measure the strain at mid-height of the specimen.

For concrete specimens, the crushing test was conducted using a universal testing machine with a capacity of 3000 kN with load-controlled loading at a rate of loading 1.5 kN/sec. After curing and before testing, the specimens were capped with sulfur to provide planar surfaces on both ends of each concrete specimen; this was essential to provide accurate results from crushing testing (ASTMC617/C617M−15, 2015). Figure 4.9 shows the testing machine used for concrete specimens and Figure 4.10 shows representative concrete specimens. All tests were done in the Civil Engineering Department at Gaziantep University.

(a) The testing machine

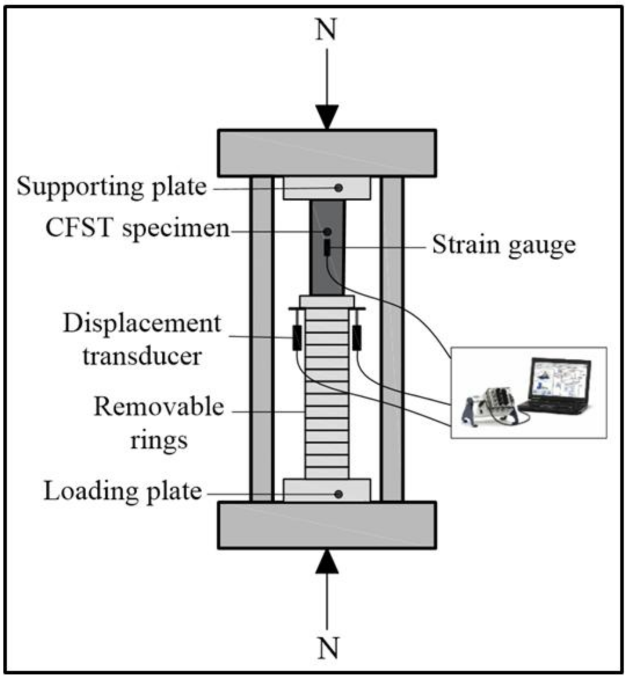

(b) The schematic view

Figure 4.8 Testing setup for CFST specimens

Figure 4.9 Testing machine used for concrete specimens

Figure 4.10 Samples of concrete specimens before crushing

4.5 Preparation of CFST Columns

After cutting the steel tube specimens to the desired length, the ends of the specimens were machined to get a flat surface, then cleaning the inner surface of each specimen. The clean inside of the steel tube allows positive steel-concrete interaction. A stiff mica plate was fixed by using silicone to close the base end of each tube during concrete pouring, and this guarantee that there is no adhesion between the concrete surface and base plate. This procedure guaranteed that a flat concrete surface was easily obtained at the bottom end upon removing the mica plates. To achieve a flat, level top, the last 5 mm of the steel tube left empty and leveled using high-strength leveling epoxy during concrete pouring, this epoxy-based repair, anchorage and adhesive mortar with two components, Table 4.2 shows the properties of the used epoxy. This procedure is to guarantee that the load will be distributed simultaneously to the whole section. When the specimens are ready for testing, the mica plates are separated, and silicone residues cleaned off.

Table 4.2 Properties of the used epoxy

Property	Data
Components	A: epoxy resin; B: epoxy hardener
Compressive strength	1 day: 30 MPa; 7 days: 75 MPa
Flexure strength	1 day: 17 MPa; 7 days: 25 MPa
Bonding strength	To concrete > 3.0 MPa, To steel > 3.5 MPa
Application thickness	Min.: 2 mm; Max.: 30 mm
Full cured	7 days

4.6 Summary

In this chapter, the test program, material (steel and concrete) properties, CFST specimen preparation, and testing procedures have been explained. The steps explained in this chapter are typical of those followed in all experimental studies described within this thesis.

These steps include the preparation of the steel tube specimens: taking them from stock, cutting specimens to the required length and calculating the basic mechanical properties with a coupon tensile test. Preparation of reinforcing steel bars (if present in the desired column) also involved calculation of the basic mechanical properties using a tensile test.

For concrete, all procedures, including preparing the required mix design, casting in the standard cylinder specimens, curing and capping procedures, and estimating the concrete compressive strength using a uniaxial compression test conducted at the same time as CFST columns were tested, were described. The properties and required tests for all types of concrete used in this thesis have been explained.

The testing procedures for all CFST columns using a displacement-loaded control approach with a slow rate of loading were described. Compression loading and end-shortening data were saved for all specimens to allow study of their compression behavior.

CHAPTER 5

IMPACT OF MATERIAL AND GEOMETRIC PROPERTIES ON THE BEHAVIOR AND CONFINEMENT EFFECT OF CFST COLUMNS

5.1 General

Structural steel tubes and concrete cores are the basic components of CFST columns. Therefore, the geometrical and mechanical properties of these materials have the significant impact on the CFST columns performance subjected to axial compressive loading. The behavior of short columns is diverse from that of long columns in different attributes such as failure modes, compression capacity, confinement effect, and ductility. In addition to the steel tube transverse section dimensions. The type and compressive strength of the core concrete also effect on these behaviors.

However, the main goal of this chapter is to examine the effect of various parameters: the length-to-diameter (*L/D*) ratio, diameter-to-thickness (*D/t*) ratio, steel tube yield strength (f_y), and concrete compressive strength (f_c) on the response of circular CFST columns and the confinement effect.

Eighteen circular CFST specimens were prepared, representing three *L/D* ratios, two *D/t* ratios, two steel grades, and three concrete compressive strengths. All columns were tested under axial concentric loading. Table 5.1 shows the details of these specimens.

The naming system utilized in this study, as shown in Table 5.1, contains the outer diameter of the hollow circular tube (*D*), wall thickness (*t*), a specimen length (*L*), and compressive strength of core concrete (f_c), respectively. As an example, 114.3-2.74-300-56 refers to CFST column with a diameter of 114.3 mm, 2.74 mm wall thickness, 300 mm specimen length, and a concrete core compressive strength of 56.20 MPa.

Additionally, 1018 experimental data were collected from the literature about circular CFST columns under axial compression loading. This database (in a total of 1036 specimens) was used to assess the predictions within and beyond the limits of the AISC36-16, EC4, AS5100.6, and AIJ2001 design codes, and also to explore the influence of variables on the response of circular CFST columns and the confinement effect.

5.2 Material Properties of Current Experimental Work

5.2.1 Steel Tube

All column specimens were fabricated with the same outer diameter of 114.3 mm. Two different steel qualities were used: European S235 with a tube thickness of 2.74 mm, and European S355 with tube thickness of 5.90 mm. The manufacturing processes used to prepare the steel tube columns is as described in Chapter Four.

5.2.2 Concrete

Three different normal weight concrete mixes were used. For first two mixes, cement, crushed coarse and fine aggregates—with a maximum aggregate size less 10 mm due to the small diameter of the steel tubes—were combined with water and hyperplasticizer.

The third mix was produced by using a very fine sand like a powder as a fine aggregate ($FS \leq 0.3$ mm) and crushed sand ($0.3 < CS \leq 2$ mm) as coarse aggregate mixed with cement, silica fume, water, and hyperplasticizer to achieve ultra-high compressive strength. Although this mix somewhat looked like a mortar mixture due to the absence of normal coarse aggregate. However, several researchers define such type of mixtures as high-performance concrete (HPC) (Guler *et al.*, 2012; Wille *et al.*, 2012).

The results of cylinder compression of 100×200 mm specimens of the three mixes were 56.20 MPa, 66.75 MPa, and 107.20 MPa, respectively. Detailed concrete properties and the preparation of concrete specimens was as described in Chapter Four.

According to ACI363R-10 (2010), the concrete compression strengths of all specimens fall within the category of high-strength concrete. Tables 5.2–5.4 show the details of these mixes.

Table 5.1 Properties of CSFT specimens

No.	Specimen	*L* (mm)	*t* (mm)	*L/D*	*D/t*	f_y (MPa)	f_c (MPa)
1	114.3-2.74-300-56	300	2.74	2.62	41.71	235	56.20
2	114.3-2.74-300-66						66.75
3	114.3-2.74-300-107						107.20
4	114.3-5.90-300-56	300	5.90	2.62	19.37	355	56.20
5	114.3-5.90-300-66						66.75
6	114.3-5.90-300-107						107.20
7	114.3-2.74-600-56	600	2.74	5.25	41.71	235	56.20
8	114.3-2.74-600-66						66.75
9	114.3-2.74-600-107						107.20
10	114.3-5.90-600-56	600	5.90	5.25	19.37	355	56.20
11	114.3-5.90-600-66						66.75
12	114.3-5.90-600-107						107.20
13	114.3-2.74-900-56	900	2.74	7.87	41.71	235	56.20
14	114.3-2.74-900-66						66.75
15	114.3-2.74-900-107						107.20
16	114.3-5.90-900-56	900	5.90	7.87	19.37	355	56.20
17	114.3-5.90-900-66						66.75
18	114.3-5.90-900-107						107.20

Table 5.2 Mix proportions of concrete with f_c of 56.20 MPa

Cement	Coarse aggregate	Fine aggregate	Water	Hyperplasticizer
1	2.70	1.85	0.4	0.01

Table 5.3 Mix proportions of concrete with f_c of 66.75 MPa

Cement	Coarse aggregate	Fine aggregate	Water	Hyperplasticizer
1	2.85	1.65	0.35	0.015

Table 5.4 Mix proportions of concrete with f_c of 107.20 MPa

Cement	*Coarse sand (CS)	*Fine sand (FS)	Silica fume	Water	Hyperplasticizer
1	0.575	0.370	0.25	0.165	0.06

*($FS \leq 0.3$ mm), ($0.3 < CS \leq 2$ mm)

5.2.3 CFST Column Specimens

After preparation, the eighteen hollow steel tubes specimens with lengths of 300 mm, 600 mm, and 900 mm were filled with fresh concrete in 3, 5, and 7 layers, respectively. After each layer was added, a shaking table was used to eliminate entrapped air from the fresh concrete. The vibration also served to reduce internal friction between concrete materials as well as the between the surfaces of steel and concrete. After finishing the curing process, the concrete surface was flatten using high-strength epoxy. The CFST columns specimens were then ready for testing (Figure 5.1).

For all specimens, displacement-control mode was applied to drive the hydraulic actuator at a constant rate of 0.4 mm/min, the displacement loading control mode allows to investigate the post-peak behavior of the column and this rate was adopted to permit the complete development of buckling failure. The data of end-shortening versus compression loading data were recorded to allow discuss of the results. Figure 5.2 shows a specimen during the test.

Figure 5.1 CFST column specimens before testing

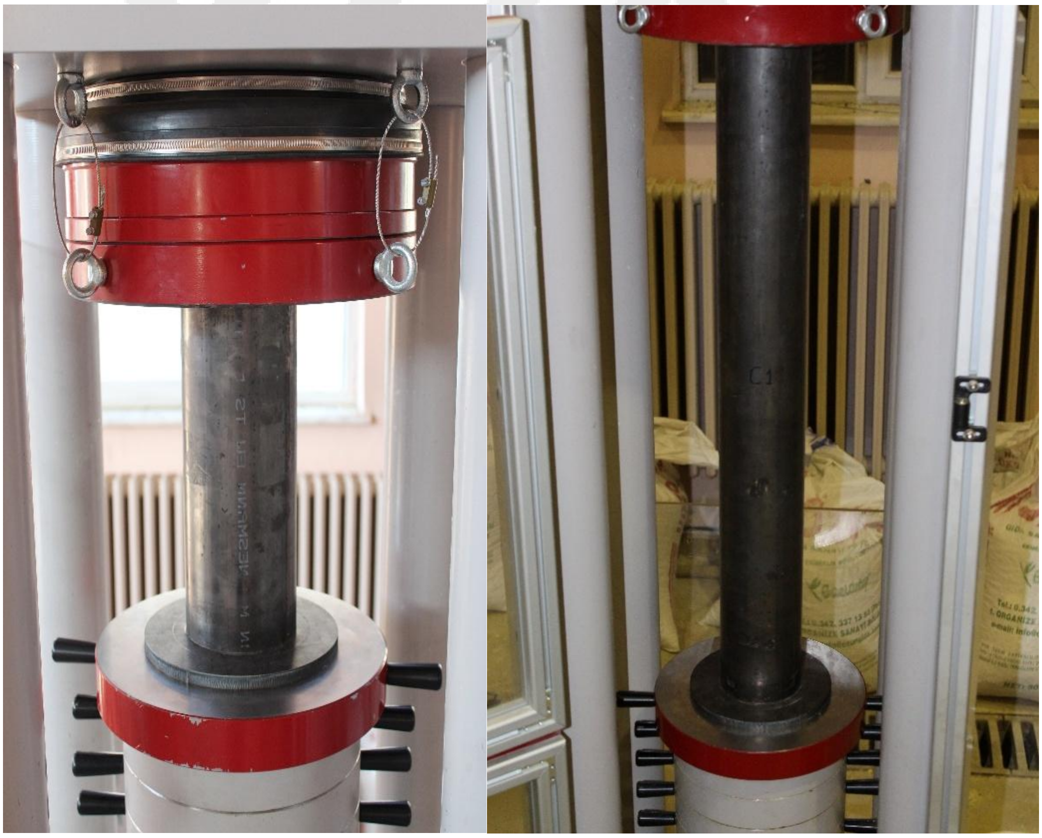

Figure 5.2 CFST column specimen testing setup

5.3 Test Results and Discussions

The results of the test are represented as compression loading against end-shortening curves and failure modes according to the impact of the geometrical and mechanical properties of the CFST column specimens. The relationship between loading against axial deformation provide information about the stiffness, ductility, and toughness capacities of the columns tested. Performance indices, such as the strength index (*SI*), ductility index (*DI*), and confinement index (ξ) were also calculated to explore the response of CFST columns.

The *SI* is a significant parameter which applied to assess the strength improvement due to composite action and the confinement effect in composite columns, especially circular columns. It can be defined as (Han *et al.*, 2005b; Han *et al.*, 2014):

$$SI = \frac{N_u}{A_s f_y + 0.85 A_c f_c} \tag{5.1}$$

where N_u is the maximum compression loading of a CFST specimen section, obtained by test or drawn from codes. The denominator in Equation 5.1 is called the "squash load" of a section, which is the maximum load capacity of the composite section without any confinement effect. Higher values of *SI* indicate an effective or positive composite action between the steel and concrete.

"Ductility" is known as the ability of the structure to bear deformations beyond its elastic limit while providing a desired load-carrying capacity until failure. The ductility index (*DI*) is a method uses to estimate section ductility; in other words, *DI* can be used to assess the ability of a CFST column to bear plastic deformation without any considerable reduction in strength. Thus, the definition of *DI* depends on the required ductility of a specific CFST column (Yu *et al.*, 2015). Different definitions used by many researchers depend on curves of compression loading vs. end-shortening. The first formulation has been provided by multiple sources (Han, 2002; Yang *et al.*, 2008; Chan *et al.*, 2015):

$$DI = \frac{\Delta_{85\%}}{\Delta_u} \tag{5.2a}$$

where Δ_u is the end-shortening at the maximum compression loading and $\Delta_{85\%}$ is the axial shortening when the compression loading drops to 85% of the maximum load (Figure 5.3a). It must be noted that when the loading failed to catch 85% of N_u, $\Delta_{85\%}$ was considered as the final value of end-shortening.

The second formulation of *DI* is (Lin and Tsai, 2001; Tao *et al.*, 2004; Yu *et al.*, 2015):

$$DI = \frac{\Delta_{95\%}}{\Delta_y} \tag{5.2b}$$

where $\Delta_{95\%}$ is the axial shortening when the load drops to 95% of N_u, and Δ_y is equal to $\Delta_{75\%}/0.75$, $\Delta_{75\%}$ the axial shortening when the load gets 75% of the N_u in the pre-peak region, as shown in Figure 5.3b.

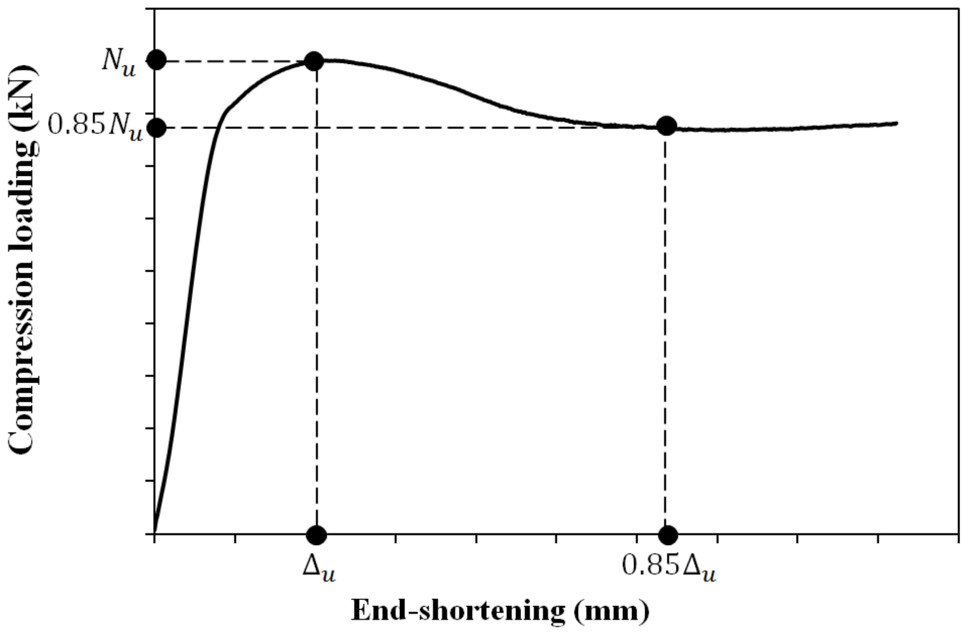

(a) The curve of the first definition of *DI*, corresponding to Equation 5.2a

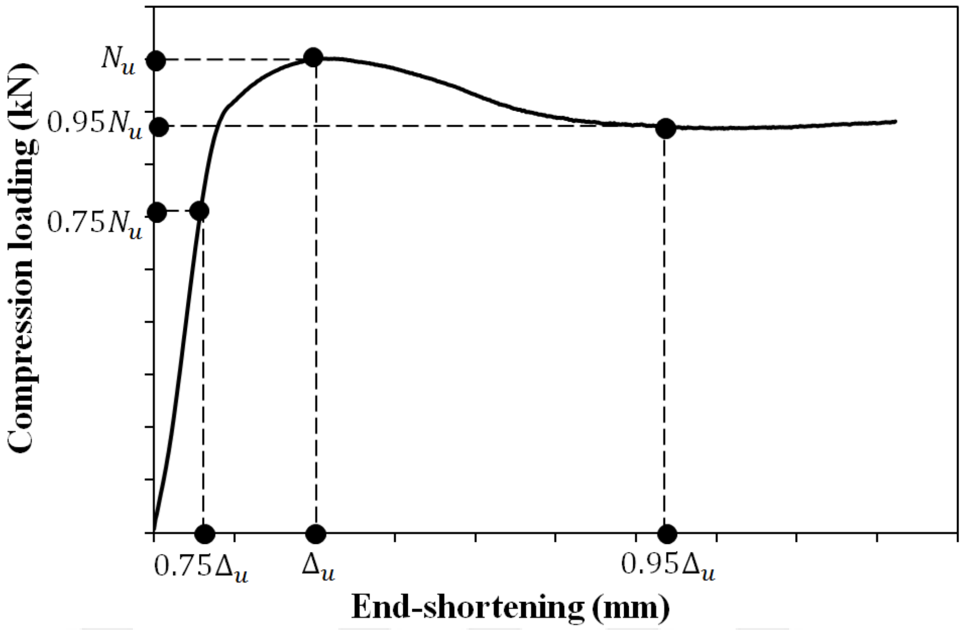

(b) The curve of the second definition of *DI,* corresponding to Equation 5.2b

Figure 5.3 Two definitions of the ductility index (*DI*)

To more easily discuss test results, it is convenient to classify CFST columns according to their *L/D* ratios. According to the consensus in the literature, columns with $L/D \leq 4.0$ are defined as short, while when $L/D > 4.0$ they are defined as long (Han *et al.*, 2014; Li *et al.*, 2015; Hoang and Fehling, 2017a, 2017b). In this thesis, to be more specific and discuss the results clearly, CFST columns were classified as short, medium, or long. Table 5.5 clarifies a summary of the results of this study.

5.3.1 Short CFST Column Specimens

Material failure was the dominant failure mechanism among short columns, a category that includes yielding of outer steel and crushing of inner concrete. Specimens with a length of 300 mm (*L/D* = 2.62) were treated as short or stub columns. The conventional failure mode of short specimens was a local failure of the steel tube (outward buckling), but this failure mode was affected by the compressive strength of concrete and the yielding of the steel tubes in addition to the *D/t* ratio.

Table 5.5 Summary of experimental results

No.	Specimen	$N_{exp.}$ (kN)	$\Delta_{exp.}$ (mm)	ξ	*SI*	*DI*	Initial stiffness (kN/mm)
1	114.3-2.74-300-56	901.82	5.17	0.43	1.35	2.12	416.56
2	114.3-2.74-300-66	981.23	5.29	0.36	1.30	2.13	363.05
3	114.3-2.74-300-107	1295.06	3.96	0.23	1.21	1.67	343.17
4	114.3-5.90-300-56	1753.77	25.74	1.54	1.58	1.18	463.18
5	114.3-5.90-300-66	1818.62	12.08	1.30	1.54	2.58	455.57
6	114.3-5.90-300-107	1989.86	4.92	0.81	1.36	3.62	439.77
7	114.3-2.74-600-56	947.75	15.66	0.43	1.41	1.38	285.79
8	114.3-2.74-600-66	1031.92	9.29	0.36	1.37	1.50	321.00
9	114.3-2.74-600-107	1296.61	5.58	0.23	1.21	1.51	248.76
10	114.3-5.90-600-56	1723.19	25.25	1.54	1.56	1.21	337.47
11	114.3-5.90-600-66	1810.94	21.20	1.30	1.53	1.43	366.34
12	114.3-5.90-600-107	1968.06	6.71	0.81	1.34	4.44	348.18
13	114.3-2.74-900-56	877.28	11.95	0.43	1.31	1.92	243.02
14	114.3-2.74-900-66	983.84	9.29	0.36	1.30	1.78	263.36
15	114.3-2.74-900-107	1233.24	6.96	0.23	1.15	1.24	212.05
16	114.3-5.90-900-56	1592.48	17.91	1.54	1.44	1.70	305.36
17	114.3-5.90-900-66	1713.35	15.16	1.30	1.45	1.99	330.91
18	114.3-5.90-900-107	1907.29	7.46	0.81	1.30	4.04	296.08

5.3.1.1 Failure Modes and Compression Behavior of Short Columns

All short specimens showed a local buckling failure of the steel tube. The *D/t* ratio is the main parameter which affected failure mode behavior. A crippling failure mode was observed for thin columns (t = 2.74 mm, D/t = 41.72), but not for thick columns (t = 5.90 mm, D/t = 19.37). Figure 5.4 shows the failure modes of the short specimens.

(a) 114.3-2.74-300-56 (b) 114.3-2.74-300-66 (c) 114.3-2.74-300-107

(d) 114.3-5.90-300-56 (e) 114.3-5.90-300-66 (f) 114.3-5.90-300-107

Figure 5.4 Failure modes of short columns

As presented in Figure 5.4, the failure modes differed between the thin (Figure 5.4a–c) and thick (Figure 5.4d–f) steel tubes. In addition, specimens with $f_c = 107.20$ MPa exhibited behavior different from that of those with $f_c = 66.75$ MPa and $f_c = 56.20$ MPa, which had similar behaviors to each other. Specimens 114.3-2.74-300-56 and 114.3-2.74-300-66 showed shear failure modes and a low confinement effect (Table 5.5 Nos. 1–2). The specimen 114.3-2.74-300-107, however, showed different behavior because of the highly brittle nature of concrete with a strength of 107.20 MPa; that concrete gave lower confinement in its group (Table 5.5 No. 3).

For the second group of this set, (Figure 5.4d, e, f), the specimen with 5.90 mm thickness and 355 MPa yield strength gave higher response. Specimens 114.3-5.90-300-56 and 114.3-5.90-300-66 (Figure 5.4d and e) did not show any crippling, as appeared in the other set. Specimen 114.3-5.90-300-107 showed signs of shear failure (Figure 5.4f). The CFST columns constructed using thin steel tubes faced failure via local buckling combined with crushing of concrete at a higher rate than CFST columns constructed with thick steel tubes.

For steel tube columns filled with HSC, it is important to guarantee that the steel tube reaches the yielding before the HSC core reaches its maximum compressive strength due to the brittle nature of HSC. This consideration ensures full plastic behavior of the composite section. Therefore, the compressive strain of the HSC core must be higher than the yield strain of the steel tube. Eurocode2 (2004) and Eurocode3 (2005) describe the strain for concrete and steel as follows (Liew *et al.*, 2016):

- Steel yield strain (ε_y)

$$\varepsilon_y = \frac{f_y}{E_s} \tag{5.3}$$

- Concrete strain at maximum compressive strength ($\varepsilon_{c1}\%$):

$$\varepsilon_{c1} = 0.7 f_c^{0.31} \tag{5.4}$$

where E_s is the elastic modulus of steel tube, $E_s = 200000$ MPa.

Figure 5.5 shows the compression loading against end-shortening curves for all short column specimens, while Table 5.5 shows the maximum compression capacity ($N_{exp.}$), corresponding end-shortening ($\Delta_{exp.}$), and the performance indices. The $N_{exp.}$ and $\Delta_{exp.}$ of specimen 114.3-2.74-300-56 were 901.81 kN and 5.17 mm, respectively, and showed very smooth curve and soft behavior in the post-peak region due to shear failure modes. The *SI* of that specimen is 1.35 which indicates a significant steel-concrete interaction. For specimen 114.3-2.74-300-66, the $N_{exp.}$ and $\Delta_{exp.}$ were 981.23 kN and 5.29 mm, respectively, the load-shortening curve was also smooth and exhibited slightly lower confinement compared to 114.3-2.74-300-56, with *SI* equal to 1.30. However, the specimen 114.3-2.74-300-107, identical except for concrete strength, had different behavior; due to the higher compressive strength, this specimen exhibited more brittleness and reached the maximum compression capacity with lower shortening—with $N_{exp.}$ equal to 1295.06 kN and $\Delta_{exp.}$ equal to 3.96 mm. As shown in the load-shortening curve, unsmooth movement from the pre-peak to post-peak regions, in addition to unsmooth behavior in the post-peak region, where the steel tube of this specimen did not provide significant confinement to the concrete core compared to specimens with concrete strengths of 56.20 MPa and 66.75 MPa. This behavior is clear with *SI* of 1.20. This specimen also had lower ductility, with *DI* equal 1.67, compared to 56.20 MPa- and 66.75 MPa-strength specimens with *DI* equal to 2.12 and 2.13, respectively.

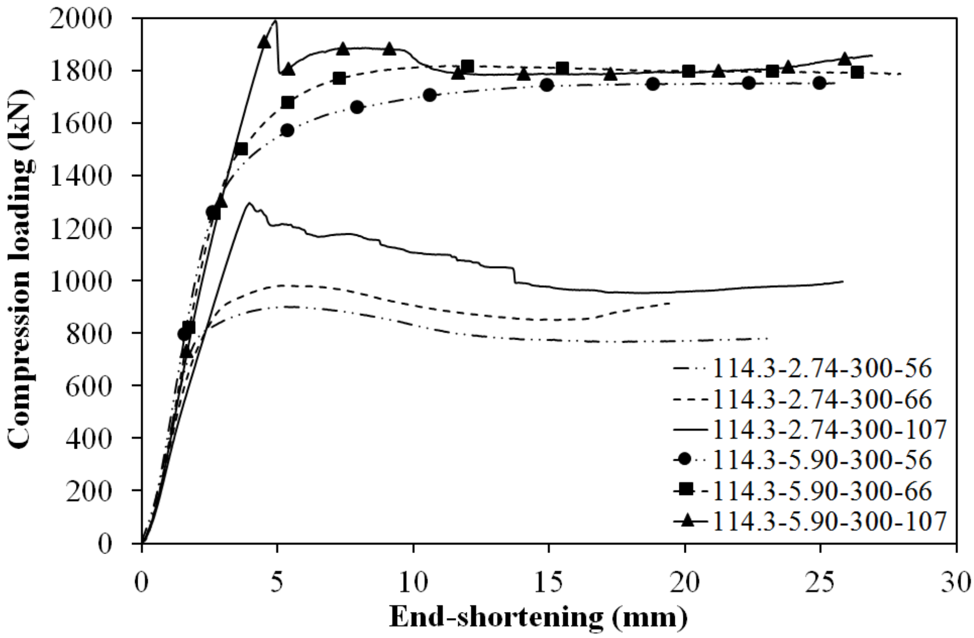

Figure 5.5 Load–shortening curves for short columns

The specimens with a tube thickness of 5.90 mm and steel yield strength of 355 MPa exhibited higher performance (Figure 5.5 and Table 5.5). This is clear from their higher initial stiffness, toughness capacity, strength enhancement, confinement effect, and ductility. The maximum compression loading $N_{exp.}$ and corresponding shortening $\Delta_{exp.}$ of specimens 114.3-5.90-300-56, 114.3-5.90-300-66, and 114.3-5.90-300-107 are 1753.77 kN and 25.74 mm, 1818.62 kN and 12.08 mm, 1989.86 kN and 4.92 mm, respectively. The 56.20 MPa and 66.75 MPa specimens experienced high plastic behavior before reaching the maximum compression loading as shown in their end-shortening, while the 107.20 MPa specimen exhibited less-plastic behavior before reaching the maximum compression capacity due to high brittleness nature of 107.20 MPa concrete core. In addition to $N_{exp.}$, the corresponding SI index values were also greater than those of specimens with 2.74 mm tube thickness and 235 MPa steel yield strength. It can be seen from these results that the strength and the confinement indices increase as the thickness of tube and steel yield increase; this mean the composite action of the composite column becomes larger. But for columns with the same steel tube properties, the increase in compressive strength of concrete decreases the confinement effect ξ of the steel tube to concrete core, Table 5.5, Nos. 4, 5, and 6.

5.3.2 Medium Length CFST Column Specimens

Columns with a length of 600 mm (*L/D* = 5.25) were considered medium columns. These columns developed behavior that combined the features of short and long columns due to the geometric and material properties' effects.

5.3.2.1 Failure Modes and Compression Behavior of Medium Columns

The specimens with a steel tube thickness of 2.74 mm showed failure modes that combined local buckling and overall buckling; this thickness could not prevent local crushing of the concrete core for specimen 114.3-2.74-600-56 in addition to global buckling failure, as shown in Figure 5.6a. Specimens 114.3-2.74-600-66 and 114.3-2.74-600-107 showed evidence of a shear failure mode and slight overall buckling (Figure 5.6b and c).

Specimens with a tube thickness of 5.90 mm failed via global buckling; this was the mode of failure for all such specimens. The 56.20 MPa and 66.75 MPa specimens presented the same failure modes, though in addition to global buckling, local buckling appeared at the top of the specimens (Figure 5.6d and e). For the 107.20 MPa specimens, in addition to local buckling at the top, due to the higher brittleness of 107.20 MPa concrete, another area of local buckling developed near the middle of the specimen (Figure 5.6f). Composite columns with a tube thickness of 2.74 mm and steel yield strength of 235 MPa acted like short columns, where the failure modes were governed by the material failure. On the other hand, for the composite columns with a steel tube thickness of 5.90 mm and steel yield strength of 355 MPa, the failure modes were governed by the geometric characteristics of the column and the effects of concrete compressive strength, leading to either local crushing or shear failure of concrete.

(a) 114.3-2.74-600-56 (b) 114.3-2.74-600-66 (c) 114.3-2.74-600-107

(d) 114.3-5.90-600-56 (e) 114.3-5.90-600-66 (f) 114.3-5.90-600-107

Figure 5.6 Failure modes of medium columns

Figure 5.7 shows the compression loading against end-shortening curves for medium specimens. The 56.20 MPa and 66.75 MPa specimens had smooth transitions from the pre-peak region to post-peak region, while the 107.20 MPa specimen had a drop in capacity after reaching the maximum compression capacity, which caused an unsmooth transition, though it was not as sharp as that of the corresponding short column (114.3-2.74-300-107, as shown in Figure 5.5). The 56.20 MPa and 66.75 MPa specimens showed higher plastic deformation before reaching maximum compression capacity compared to the 107.20 MPa specimen due to the brittleness of the high-strength concrete core.

As shown in failure mode section, the specimens with a thickness of 2.74 mm and steel yield strength of 235 MPa performed as short columns. As shown in Table 5.5, the compression capacities N_{exp}, and strength indices *SI* of the specimens 114.3-2.74-600-56, 114.3-2.74-600-66, and 114.3-2.74-600-107 increased with 5.09%, 5.17%, and 0.12%, respectively, compared to their counterpart specimens in short columns. They also developed more plastic behavior before reaching their compression capacities, according to the corresponding end-shortening $\Delta_{exp.}$, 203.08%, 75.58%, and 41.02%, respectively. It can be noted from these comparisons that the specimens of 107.2 MPa concrete offered poorer performance compared to specimens with 56.2 MPa and 66.75 MPa. Although these improvements in behavior of medium columns set, they gave lower initial stiffness and ductility compared to short specimens.

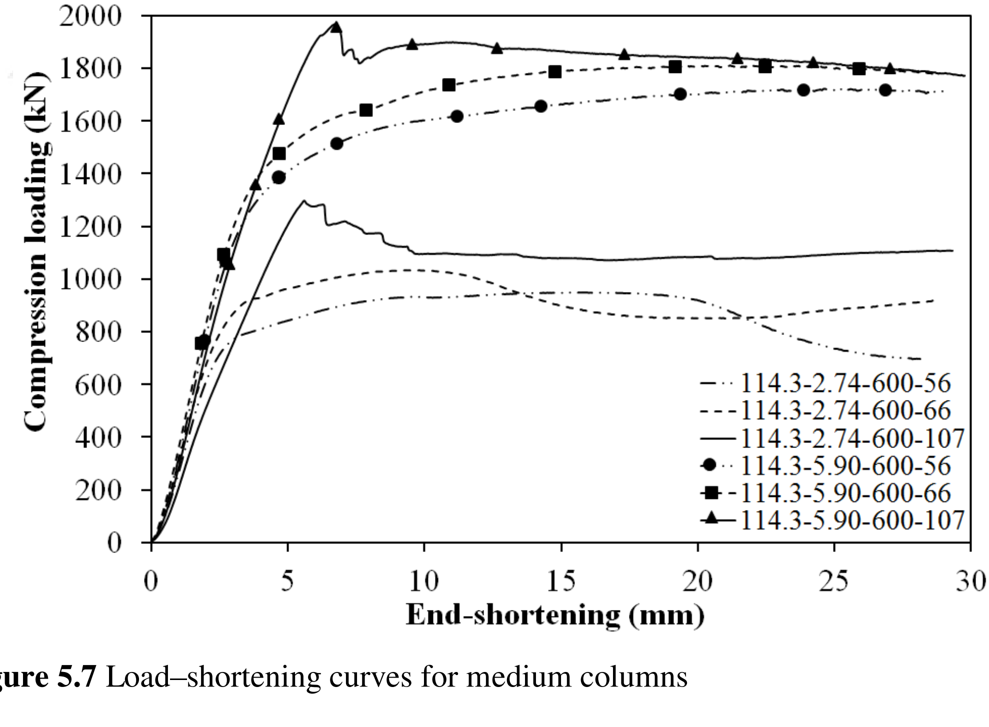

Figure 5.7 Load–shortening curves for medium columns

Again, as shown in Figure 5.7, and Table 5.5, an increase in the thickness of steel tube to 5.90 mm and steel yield strength to 355 MPa led to an increase in the compression capacities, strength improvement, initial stiffness, toughness capacity and ductility of the resulting columns. The compression capacities, N_{exp}, and the corresponding strength indices, *SI*, of specimens 114.3-5.90-600-56, 114.3-5.90-600-66, and 114.3-5.90-600-107 are 1723.19 kN, 1.56, 1810.94 kN, 1.53, and 1968.06 kN, 1.34, respectively. Also, as in the short columns, the loading–shortening curves of specimens with 56.20 MPa and 66.75 MPa are smoother than that of the 107.20 MPa specimen, which had a decreased capacity due to its brittleness after reaching the maximum compression capacity. That curve was not sharp, and the column offered more plastic behavior compared to the corresponding short column (114.3-5.90-300-107). All columns in this set exhibited a remarkable increase in confinement effect, with increases of 56%, 53%, or 34% compared to squash load.

As mentioned in the discussion of failure modes, the specimens with 5.90 mm tube thickness and 355 MPa steel yield strength behaved as long columns. For a comparison to their counterpart short specimens, see Table 5.5. There is a reduction in compression capacities and strength indices due to the failure pattern of these columns, which follow the behavior of long columns.

5.3.3 Long CFST Columns Specimens

Columns with a length of 900 mm (*L/D* = 7.87) were considered long columns. Global buckling failure governed the failure modes of these columns.

5.3.3.1 Failure Modes and Compression Behavior of Long Columns

Figure 5.8 presents the failure modes of long columns. Besides the overall buckling, local buckling also developed in specimens with a thickness of 2.74 mm. Specimen 114.3-2.74-900-56 failed by global instability and local buckling appeared at the top and mid-length of the specimen, where global instability was very clear (Figure 5.8a). Specimen 114.3-2.74-900-66, on the other hand, failed by global instability and crippling failure at the upper part of the specimen (Figure 5.8b). For the specimen 114.3-2.74-900-107 failed by slight global instability and also experienced crippling failure at the upper part of the specimen (Figure 5.8c). In this set of specimens, the effect of concrete by its compressive strength and brittleness dominated the failure patterns.

The behavior of specimens with a thickness of 5.90 mm and steel yield strength of 355 MPa was different (Figure 5.8c, d, and f). There was no clear effect of local failure for these specimens. Also, due to the effect of the high brittleness of 107.20 MPa concrete, specimen 114.3-5.90-900-107 showed different behavior compared to other specimens in this set.

(a) 114.3-2.74-900-56 (b) 114.3-2.74-900-66 (c) 114.3-2.74-900-107

(d) 114.3-5.90-900-56 (e) 114.3-5.90-900-66 (f) 114.3-5.90-900-107

Figure 5.8 Failure modes of long columns

Figure 5.9 shows the compression loading against end-shortening curves for long columns. In this group, the *L/D* ratio showed an effect on both compression capacities and the confinement effect. For both steel tube thicknesses and corresponding steel tube yield strengths reduction in the compression capacities and the confinement effect compared to short and medium columns were observed.

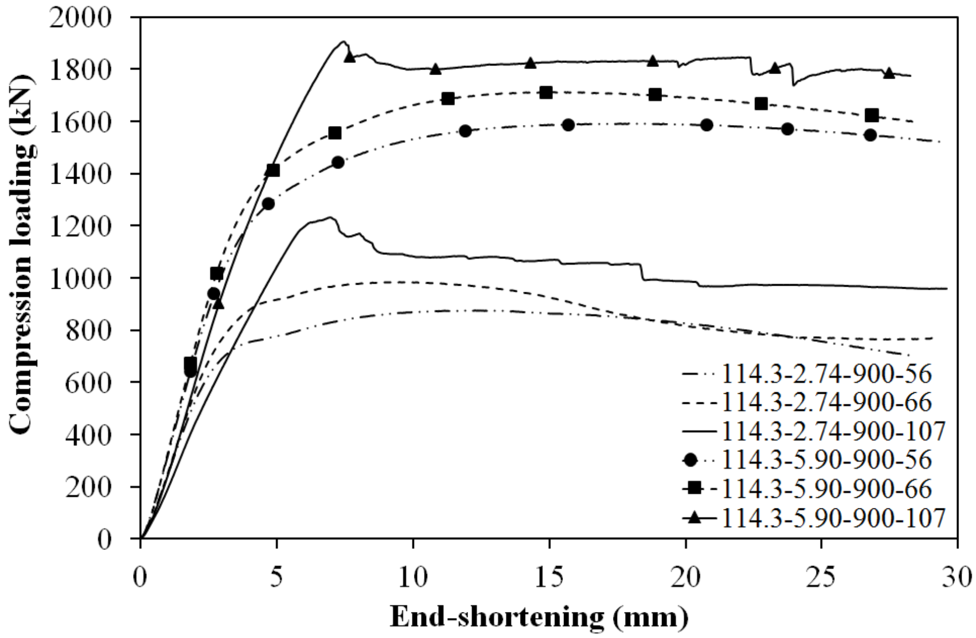

Figure 5.9 Load–shortening curves for long columns

Specimens 114.3-2.74-900-56 and 114.3-2.74-900-66 had lower compression capacities and higher *SI* with smooth loading–shortening curves compared to specimen 114.3-2.74-900-107 which developed higher compression capacity and lower *SI*, (Table 5.5, Nos. 13, 14, and 15). According to the loading–shortening curve of this specimen, the conversion from pre-peak zone to post-peak region is smoother than those counterparts of short and medium specimens. Long specimens gave more plastic behavior before reaching peak load; $\Delta_{max.}$ in this case was 6.96 mm, compared to 3.96 mm and 5.58 mm for short and medium specimens, respectively.

The same trend was observed here as seen in the results for short and medium columns: long columns with steel tube thickness of 5.90 mm and steel yield strength of 355 MPa presented higher compressive capacities, initial stiffness, toughness capacities, ductility, and confinement improvement compared to specimens of thickness 2.74 mm and yield strength 235 MPa, as shown in Figure 5.9. The loading-shortening curves of the specimens 114.3-5.90-900-56 and 114.3-5.90-900-66 are smooth compared to that of specimen 114.3-5.90-900-107; the specimens of 107.20 MPa concrete at all columns lengths, short, medium, and long, showed unsmooth behavior in the post-peak region.

According to Table 5.5 and Figure 5.9, specimens 114.3-5.90-900-56, 114.3-5.90-900-66, and 114.3-5.90-900-107 developed the maximum compression capacities, and the trend in *SI* decreased with increase in concrete strength. These values of *SI* are smaller than those of short and medium columns; this explain the contribution of *L/D* ratio to the confinement effect, where an increase in *L/D* ratio led to a decrease in the confinement effect.

All the specimens containing 107.20 MPa-strength concrete showed lower initial stiffness compared to other specimens; this is due to higher quantity of fine materials which used in the 107.20 MPa concrete mix.

5.4 Assessment of the Design Specifications

In this Chapter, four design specifications (AISC360-16, EC4, AS5100.6, and AIJ2001) previously introduced in Chapter Three were used. These codes adopt different theories and models to determine the compression capacity of CFST specimens. This section aims to appraise the applicability of these codes for estimating the compression capacity of CFST specimens.

To build a sense about the impact of each factor on the response of CFST specimens loaded axially, a large experimental database including data on 1018 columns was collected from fifty published references; with the addition of results from the 18 novel columns presented in this chapter, the database included a total of 1036 column. The columns were chosen to include a vast variety of the geometrical and material features of circular CFST specimens, as reviewed in Table 5.6. Table 5.7 presents the details of this database.

To facilitate comparison between test results and codes predictions, the partial safety factors were considered equal to one for all design codes and all limitations of the codes were ignored. When the elastic modulus (E_s) of the steel tube is not provided in the reference, it was taken as 200000 MPa, and the modulus of elasticity (E_c) of the concrete core calculated according to the corresponding code.

Table 5.6 The limits of the selected tested data

Property	From	To
D (mm)	25.40	1020.0
D/t	8.2	221.0
L/D	1.84	51.5
f_c (cylinder $150 \times 300\ mm$) MPa	13.20	187.67
f_y MPa	185.70	853.0
Slenderness ratio (according to EC4)	0.06	2.21
Steel contribution (according to EC4)	0.03	0.93

Table 5.7 Database of the circular CFST specimens

Reference	# of tests	D (mm)	D/t	L/D	f_c (MPa)	f_y (MPa)
Abed *et al.* (2013)	6	114-167	20.36-53.87	2.1-2.19	44-60	300
Dundu (2012)	24	114.85-193.70	38.28-64.57	5.16-21.77	25.33-33.04	345.2-488.2
Chitawadagi *et al.* (2010)	27	44.45-63.50	22.23-50.80	7.87-22.50	34.76-55.84	250
Beck *et al.* (2009)	36	114.3	19.05-34.12	3.0-10.0	21.84-100.17	287.33-342.95
Yu *et al.* (2007)	17	165-219	28.40-60.66	2.97-3.09	37.48-75.65	350
Li and Hao (2005)	12	159-164	25.24-43.16	3.17-3.27	25.92	342-379
Georgios and Lam (2004)	13	114.09-115.04	22.92-30.53	2.61-2.63	27.63-102.80	343-365
Li and Wen (2003)	14	219	31.29	4.52-9.13	34.08-35.87	272-275
Zeghiche and Chaoui (2005)	15	159.6-160.3	30.71-32.30	12.48-25.03	40-106	270-283
Sakino *et al.* (2004)	36	108-450	16.69-152.03	3.00	24.66-81.82	279-853
Han *et al.* (1999)	11	108	27.00	32.5-38.5	14.84-21.32	348.1
Han (1997)	14	111.3-250	19.78-125.0	2.01-3.29	29.41-49.64	248-482.5

Reference	# of tests	*D* (mm)	*D/t*	*L/D*	f_c (MPa)	f_y (MPa)
Bridge and O'Shea (1997)	15	165-190	58.51-220.93	3.47-3.52	41-108	185.7-363.3
Shaohuai and Wanli (1985)	23	108	27.00	6.0-51.48	28.99	338.88
Mathias (2002b)	9	159	15.90-33.13	4.09	36.6-93.8	355-433
Liew and Xiong (2012)	12	114.33-219.43	18.65-45.06	2.18-2.73	51.0-184.0	377.0-428.0
Liew *et al.* (2016)	29	114.3-219.1	12.0-43.82	1.84-3.0	50.09-187.67	380-779
O'Shea and Bridge (2000)	18	165-190	58.51-220.93	3.41-3.52	38.2-108	185.7-363.3
Yamamoto *et al.* (2000)	13	101.5-318.5	30.69-33.63	3.00	23.2-52.2	335-452
Han *et al.* (2005a)	12	60-240	40.54-162.16	3.00	37.48	307
Schneider (2006) reported in Tue *et al.* (2004)	9	164.2-189	20.75-65.68	3.82-4	36.2-167.87	363-452
Oliveira *et al.* (2010)	32	114.3	19.05-34.12	43376.00	26.79-100.17	287.33-342.95
Han and Yao (2004)	17	100-200	33.33-66.67	3.0-10.0	35.2	303.5
Han *et al.* (2005b)	26	60-250	30.0-133.69	3.00	88.2-83.496	282-404
Han (2000)	11	108	24.00	32.5-38.5	26.07-38.37	348.1
Gupta *et al.* (2007)	72	47.28-112.56	1.05-38.95	3.02-7.19	19.55-35.20	360
Kato (1996)	100	25.4-267.4	8.19-69.65	3.93-42.01	20.3-66.2	275-682
Gardner and Jacobson (1967)	12	76.4-152.6	29.54-49.71	2.00	20.9-43.4	363.3-633.4
Sakino and Hayashi (1991)	10	159.0-1020.	31.36-105.81	2.81-3.0	13.2-40.48	291.4-381.5
Sakino and Hayashi (1991)	12	174.0-179.0	19.78-58.0	2.01-2.07	22.1-45.7	249.0-283.0
Kato (1995)	12	297-301.5	25.0-67.0	3.00	26.90-79.23	347.90-471.4
Saisho *et al.* (1999)	29	101.6-139.8	33.87-59.0	3.00	24.66-128.82	341.0-462.6

Reference	# of tests	D (mm)	D/t	L/D	f_c (MPa)	f_y (MPa)
Yamamoto *et al.* (2002)	13	101.3-318.5	30.68-33.58	3.00	22.52-50.2	331.0-452.0
Yu *et al.* (2002)	28	149.0-165.0	19.88-165.0	3.03-3.36	80.13-84.45	338.0-438.0
Zhang and Wang (2004)	36	133.1-167.8	24.47-50.42	2.97-3.03	36.57-70.93	325.0-392.0
Tan (2006)	16	108.0-133.0	18.14-125.0	3.50	103.88-113.68	232.0-429.0
Fujii (1994)	15	114	18.57-66.28	7.46-24.12	24.0-37.0	266.0-486.0
Matsui and Tsuda (1996)	6	165.2	36.71	4.0-30.0	40.9	413.84
Tan *et al.* (1999)	16	108.0-133.0	18.14-125.0	3.50	77.40-84.70	232.0-429.0
Schneider (1998)	3	140.0-141.4	20.96-46.93	4.49-4.54	23.80-28.18	285-537
Yang and Han (2006a)	15	114.0-219.0	52.05-76.57	3.00	32.20-37.57	335.7-350.4
Chen *et al.* (2010)	22	88.0-113.1	33.03-67.70	3.18-3.24	18.83-25.69	342.70-357.20
Wang *et al.* (2015)	39	133.0-140.0	28.54-53.03	3.00	37.14-61.73	302.0-335.3
Chen *et al.* (2017)	15	137.63-137.91	50.46-51.20	3.05-12.20	42.64-44.60	299.4
Guler *et al.* (2013)	7	75.84-76.21	23.02-30.69	3.94-3.96	145	278.0-305.0
O'Shea and Bridge (1994)	7	190	165.22	3.45-3.49	94.7-110.3	202.8
Uy *et al.* (2011)	60	50.8-203.2	17.89-101.60	2.46-25.88	20.0-75.4	259.0-440.0
Lachemi *et al.* (2006a)	8	114	25.91	4.39-8.77	52-54	300
Lin (1988)	6	150	71.43-214.29	3.20-5.33	22.55-35.30	247.91
AL-Eliwi *et al.* (2017)	8	114.3-139.7	23.8-42.33	2.0-10.50	38.55	290.0-420.0
Ekmekyapar and AL-Eliwi (2016)	18	114.3	19.37-41.72	2.62-7.87	54.03-101.84	235.0-355.0

In the collected database, the concrete compressive strength f_c was obtained using different standard tests; therefore, to be compatible with the design codes standard all the collected concrete compressive strengths were converted to a standard cylinder size of 150×300 mm by using the approach suggested by Skazlić *et al.* (2008) for ultra-high-strength concrete (UHSC) and Yi *et al.* (2006) for normal-strength concrete (NSC) and high-strength concrete (HSC) and used by Hoang and Fehling (2017a) as follows:

For NSC ($f_c \leq 50$ MPa):

$$f_c = f_{cyl.150} = \frac{f_{cyl.100}}{1.03} = 0.88 f_{cube.150} = 0.82 f_{cube.100} \tag{5.5}$$

For HSC ($50 < f_c \leq 90$ MPa):

$$f_c = f_{cyl.150} = \frac{f_{cyl.100}}{1.04} = 0.98 f_{cube.150} = 0.92 f_{cube.100} \tag{5.6}$$

For UHSC ($f_c > 90$ MPa):

$$f_c = f_{cyl.150} = 0.95 f_{cyl.100} \tag{5.7}$$

where $f_{cyl.150}$ and $f_{cyl.100}$ are 150 × 300 mm and 100 × 200 mm standard cylinders, respectively, and $f_{cube.150}$ $f_{cube.100}$ are 150 × 150 and 100 × 100 mm standard cubes, respectively.

5.4.1 Database Results Compared with the Design Codes Predictions

Different theories underpin each design code, so their predictions are different. The results contained in the experimental database from 1036 circular CFST columns were compared to the predictions of each design code. Table 5.8 shows both averages ($\bar{x}$) and standard deviations (σ) of predicted capacity to experimental capacity ($N_{code}/N_{exp.}$) ratios derived from the database.

$N_{code}/N_{exp.}$ ratio represents the error ratio of the predicted results, where N_{code} is the predicted compression capacity according to the corresponding design code and $N_{exp.}$ is the tested compression capacity. An error ratio less than one represents an underestimate, or prediction on the safe side, while greater than one represents an overestimate, or prediction on the unsafe side.

Table 5.8 Comparison results of $N_{code}/N_{exp.}$

CFST type	# of tests (n) and %		AISC		EC4		AS5100.6		AIJ2001	
			$\bar{x}$	σ	$\bar{x}$	σ	$\bar{x}$	σ	$\bar{x}$	σ
Short	652	63.0%	0.79	0.11	1.00	0.13	1.01	0.12	0.85	0.10
Long	384	37.0%	0.82	0.17	0.87	0.18	0.93	0.20	0.82	0.17
$\bar{\lambda} \leq 0.5$	873	84.3%	0.79	0.12	0.97	0.14	0.98	0.14	0.85	0.12
$0.5 < \bar{\lambda} \leq 2.0$	159	15.3%	0.86	0.19	0.87	0.20	0.98	0.23	0.80	0.18
$\bar{\lambda} > 2.0$	4	0.40%	0.85	0.35	0.85	0.37	0.96	0.38	0.76	0.30
C*	964	93.0%	0.80	0.13	0.94	0.15	0.97	0.15	0.83	0.13
NC*	37	3.6%	0.73	0.18	0.89	0.24	0.91	0.23	0.78	0.19
SL*	35	3.4%	0.73	0.09	1.07	0.13	1.08	0.13	0.91	0.11
NSC	643	62.0%	0.77	0.15	0.92	0.18	0.95	0.18	0.81	0.15
HSC	266	25.7%	0.84	0.09	0.97	0.11	1.01	0.11	0.87	0.09
UHSC	127	12.3%	0.86	0.10	0.98	0.11	1.00	0.11	0.88	0.09
MSS	950	91.7%	0.79	0.12	0.94	0.14	0.97	0.14	0.83	0.12
HSS	86	8.3%	0.85	0.25	1.01	0.25	1.05	0.28	0.92	0.23
Safe predictions (%)			94.40		60.04		53.09		91.89	
Unsafe predictions (%)			5.60		39.96		46.91		8.11	
Total	**1036**	**100%**	**0.80**	**0.14**	**0.95**	**0.16**	**0.98**	**0.16**	**0.84**	**0.13**

* C: Compact section, NC: Non-compact section, SL: Slender section

As shown in Table 5.8, AS5100.6 generally gives values closest to the experimental results, with an average error ratio of 0.98. EC4, AISC360-16, and AIJ2001 also provided good agreement, with average error ratio of 0.95, 0.80, and 0.84, respectively; thus, the average predictions of all codes were safe.

However, it is worth noting that the experimental database studies have significant representation of short columns, NSC columns, and CFST columns with MSS tubes, with percentages of 63.0%, 62.0%, and 91.7%, respectively. Therefore, more studies should be achieved to long CFST columns, CFST with HSC and UHSC, and CFST with HSS to investigate their contributions in composite structures.

The standard errors of the mean ($\sigma/\sqrt{n=1036}$) of the design codes predictions for AISC360-16, EC4, AS5100.6, and AIJ2001are 0.00420, 0.00507, 0.00504, and 0.00422, respectively. This indicates that the predictions of AISC360-16 and AIJ2001 are close together, while the predictions of EC4 and AS5100.6 are close together.

5.4.1.2 Impact of *L/D* Ratio on Codes' Predictions

Figure 5.10 shows the effect of *L/D* ratio on error ratio. According to Table 5.8, for short columns, $L/D \leq 4.0$, EC4 and AS5100.6 gave the closet prediction, with average error ratio of 1.0 and 1.01, respectively. The AISC360-16 and AIJ2001 codes offered averages of 0.79 and 0.85, respectively. This divergence in predictions is due to the fact both the EC4 and AS5100.6 codes take the confinement effect into consideration; this effect is represented by the factor $\left(1+\eta_c\, t/D\, f_y/f_c\right)$. No significant confinement effect in represented in the calculations of AISC360-16, and AIJ2001 presents a constant factor 0.27 to represent the confinement effect. This allows AIJ2001 to offer better predictions than AISC360-16, though not as close as those of EC4 and AS5100.6.

For long columns, $L/D > 4.0$, all design codes recorded average error ratio less than unity, indicating underestimates. This means these design codes provided safe predictions for long columns. EC4 and AS5100.6 had a ratio of predictions to the experimental results with averages of 0.87 and 0.93, respectively, while both AISC360-16 and AIJ2001 recorded an average of 0.82.

The relative slenderness $\bar{\lambda}$ (Equation 3.17) described in EC4 can be used instead of *L/D* ratio to study the length effect, because it contains in its definition the material properties in addition to geometric properties. Figure 5.11 shows effect of $\bar{\lambda}$ on error ratio. In accordance with EC4, the effect of confinement is ignored when $\bar{\lambda} > 0.5$. As shown in Table 5.8, even for $\bar{\lambda} > 0.5$ all codes gave underestimates compared to experimental tests. These results confirmed the previous conclusion about the applicability of these codes for predicting the behavior of long columns. For $\bar{\lambda} > 2.0$, both AISC360-16 and EC4 provided very close predictions, where the Euler elastic buckling behavior demonstrated the prediction for long columns.

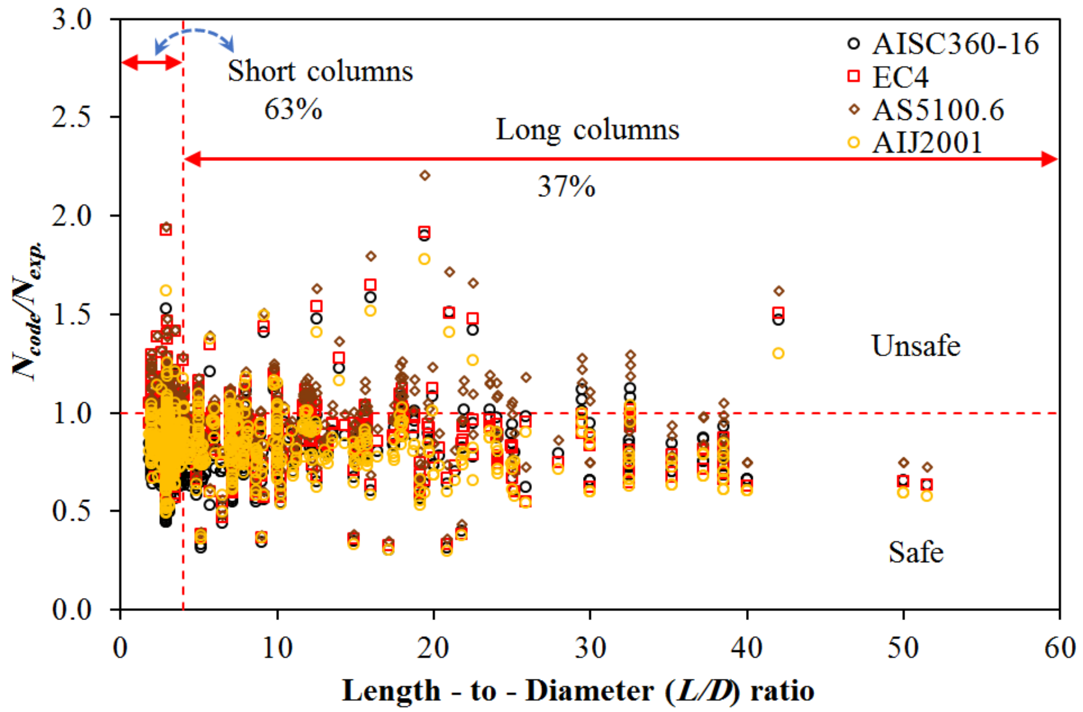

Figure 5.10 *L/D* ratio versus N_{code}/N_{exp}.

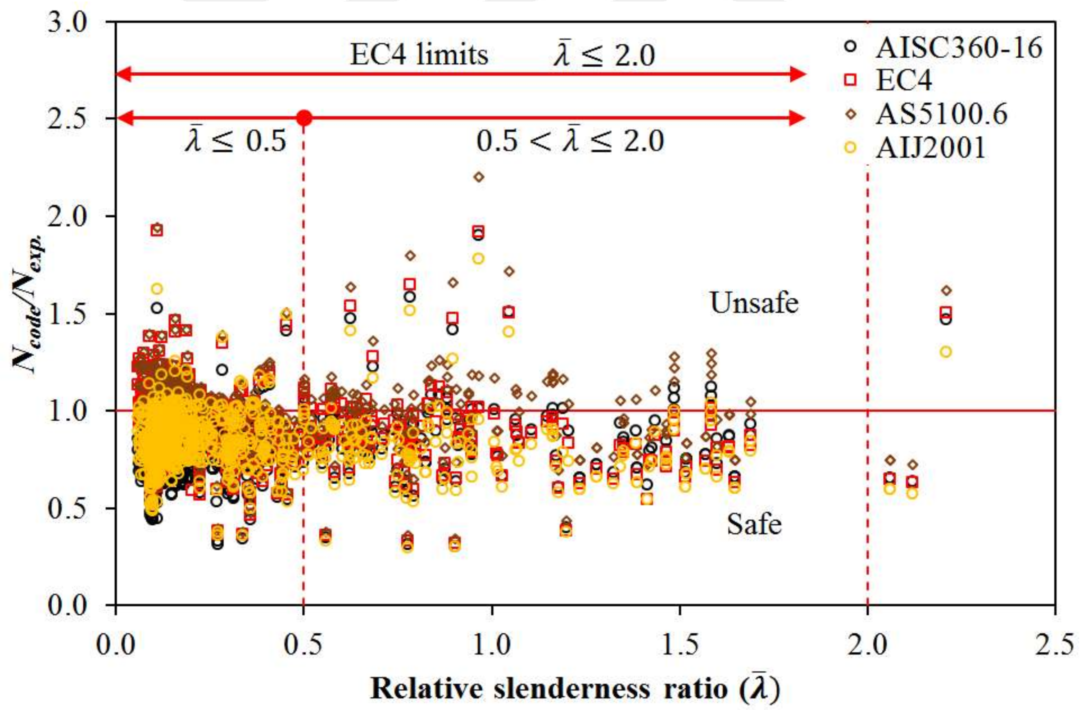

Figure 5.11 $\bar{\lambda}$ versus N_{code}/N_{exp}.

5.4.1.3 Impact of *D/t* Ratio on Codes' Predictions

D/t ratio is known as the slenderness of the cross-section, and it directly impacts the local buckling of CFST columns. Three codes (excluding AISC360-16) restrict *D/t* ratio to prevent local buckling. Figure 5.12 shows the effect of *D/t* ratio on N_{code}/N_{exp}.

To compare all four codes, Figure 5.13 shows the relation between the slenderness coefficient $\mu_{coffi.}$ of AISC360-16 and $N_{code}/N_{exp.}$. The value of $\mu_{coffi.}$ is obtained by dividing the slenderness ratio *D/t* by E_s/f_y (Lai and Varma, 2015).

The majority of the database (93.0%) contains data from experimental tests carried out on compact circular CFST columns, while fewer tests were carried out on the non-compact and slender columns (3.4% and 3.6%, respectively), as shown in Figure 5.13. As shown in Figure 5.12, the majority of experiments were conducted on specimens with *D/t* less than 100. More studies should be conducted on non-compact and slender sections to fill this gap in experimental results.

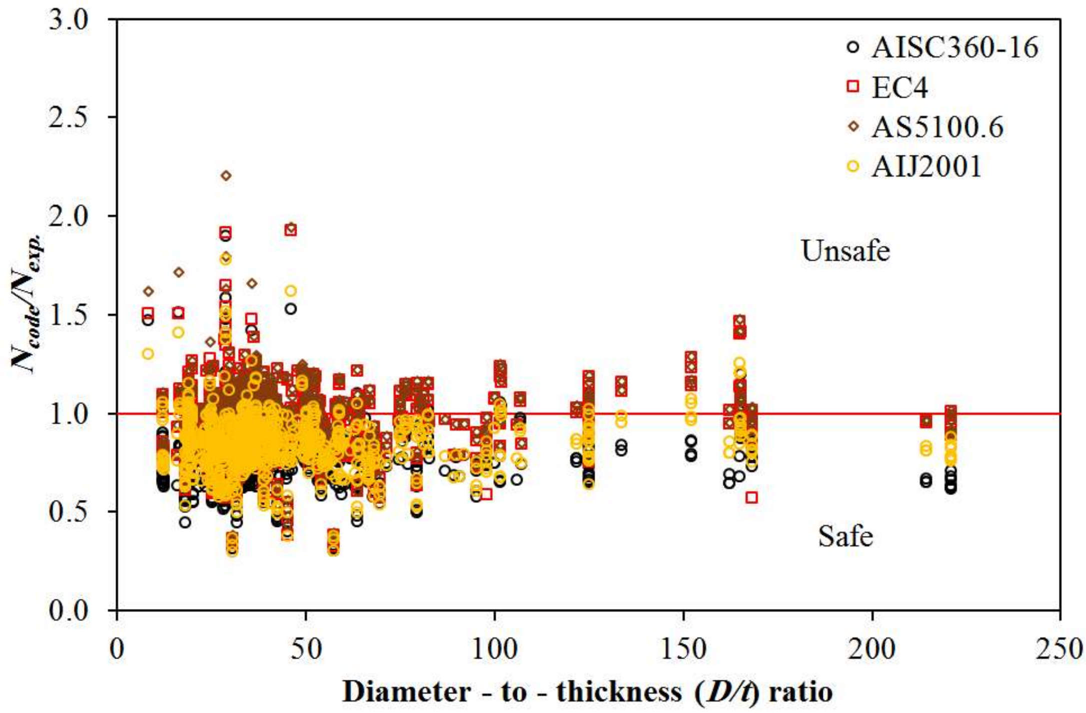

Figure 5.12 *D/t* ratio versus N_{code}/N_{exp}.

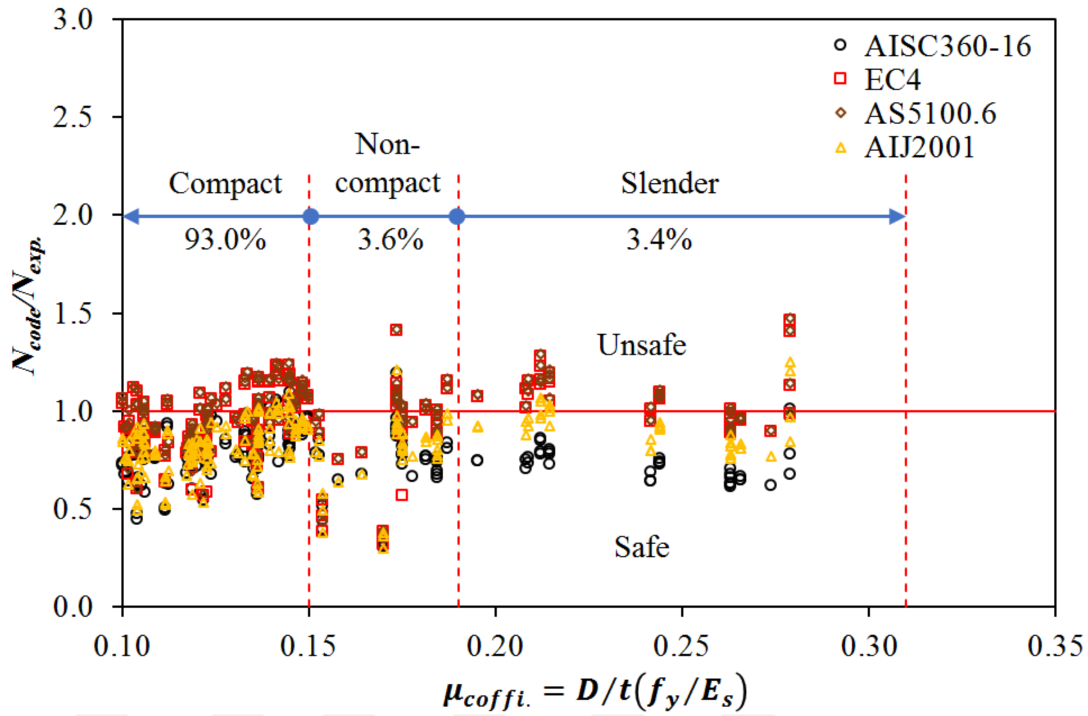

Figure 5.13 $\mu_{coffi.}$ versus N_{code}/N_{exp}.

Figure 5.14 shows the relation between $\mu_{coffi.}$ and $N_{code}/N_{exp.}$ for four codes separately. AISC360-16 and AIJ2001 represent the major percentages of $N_{code}/N_{exp.}$ less than or equal to unity, while results of EC4 and AS5100.6 are distributed around, both above and below, unity. Table 5.8 shows that AISC360-16 and AIJ2001 gave closer averages in compact and in non-compact regions, while their averages diverge in the slender region. In contrast, EC4 and AS5100.6 presented the same averages for compact, non-compact, and slender regions.

The minimum thickness of circular steel tube permitted by the four codes for S355 European steel is presented in Figure 5.15, where it can be noticed that EC4 and AS5100.6 provide relatively higher thicknesses. AISC360-16 provides lower thicknesses with different limits for compact, non-compact, and slender sections, while AIJ2001 provides thickness close to non-compact/slender section of AISC360-16. It can also be noticed from Figure 5.15 that when the diameter of steel tube increases the variation between permitted thicknesses also increases.

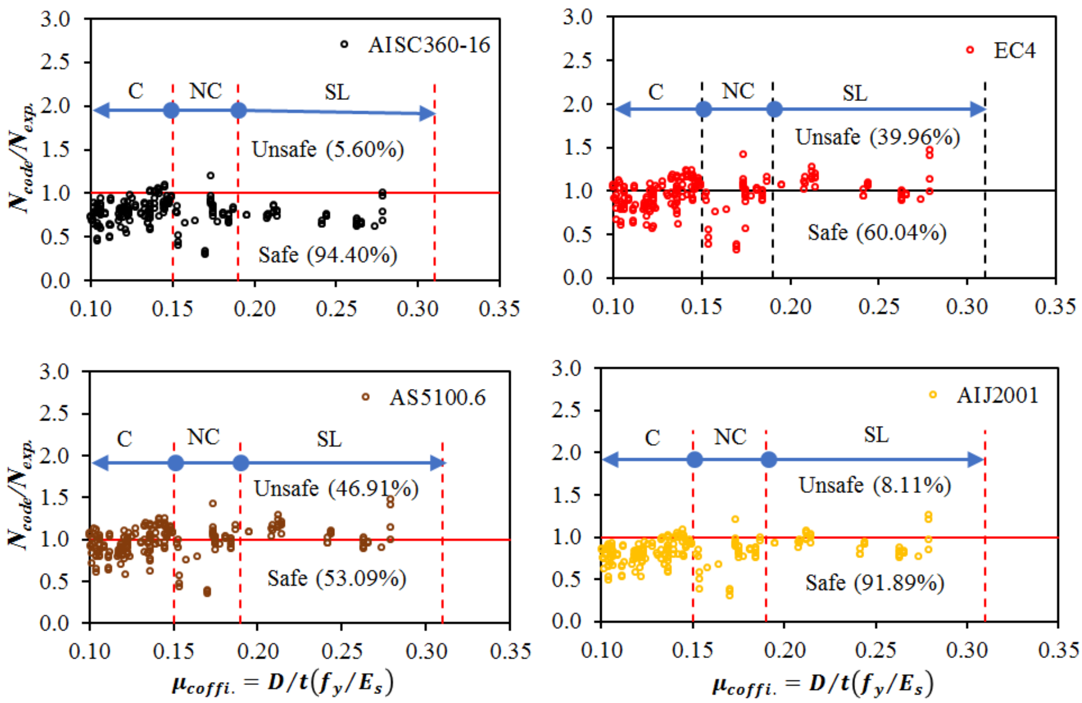

Figure 5.14 $\mu_{coffi.}$ versus $N_{code}/N_{exp.}$ for all codes

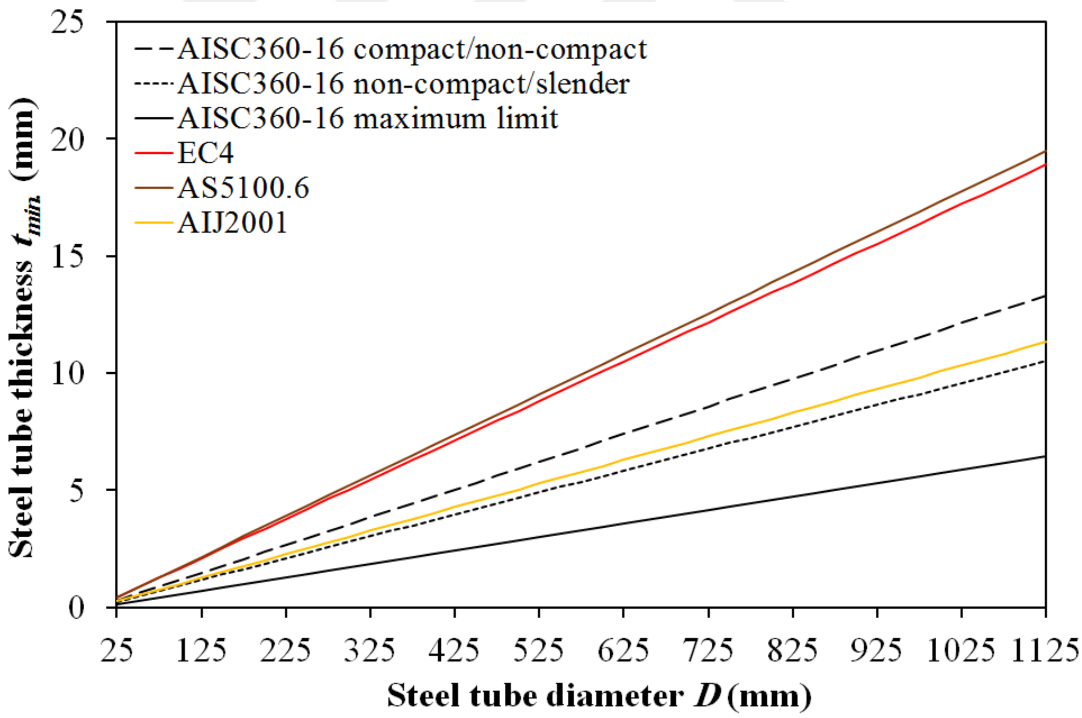

Figure 5.15 Permitted minimum thickness of design codes

Table 5.9 shows the number of CFST columns in the database with properties out the limits of the design codes. Some CFST columns share more than one design code limits.

Table 5.9 Specimens out limits of design codes

	AISC360-16			EC4			AS5100.6			AIJ2001		
	D/t	f_c	f_y	*D/t*	f_c	f_y	*D/t*	f_c	f_y	*D/t*	f_c	f_y
# of tests	---	307	14	186	317	111	197	412	471	47	296	446
$N_{code}/N_{exp.}$		0.81	0.72	0.97	1.08	1.01	0.98	0.97	0.99	0.9	0.87	0.86
SI (average)		1.27	1.45	1.30	1.27	1.20	1.30	1.30	1.30	1.19	1.22	1.31

Strength index *SI* is a convenient performance parameter to exam the appropriateness of design codes beyond their limitations. As mentioned before, the *SI* indicates the composite action between steel and concrete represented by concrete confinement. Table 5.9 shows the average *SI* for all tests beyond code limitations. It can be observed that all parameters have an *SI* larger than unity. Accordingly, it can be deduced that minimum thickness should be altered to allow the use of thinner circular steel tube, high-strength concrete, and high-strength steel calculations in these design codes. Otherwise, for AISC360-16, the average values of *SI* for 37 non-compact section specimens and 35 slender section specimens are 1.4 and 1.17, respectively. From this, it can be concluded that AISC360-16 limits for non-compact and slender should be improved. Comparing to response of codes as shown in Table 5.9, it can be deduced that the EC4 and AS5100.6 results are more felicitous and closer to the experimental results than those of AISC360-16 and AIJ2001, which gives more conservative results.

In EC4 and AS5100.6, the minimum limit steel contribution ratio (δ) is 0.2; 86 specimens had δ below 0.2, ranging from 0.0345 to 0.195. For EC4, $N_{code}/N_{exp.}$ ratios ranged from 0.57 to 1.46 with an average of 1.11, with an average SI_{exp} of 1.19. For AS5100.6, $N_{code}/N_{exp.}$ ratios ranged from 0.76 to 1.47, with an average of 1.03, and an average SI_{exp} of 1.19. The predictions of both EC4 and AS5100.6 are close to experimental results and could be used to expand the minimum limit of steel contribution ratio to involve CFST specimens with lower steel areas.

5.4.1.4 Impact of f_c on Codes' Predictions

The four design codes have limits for concrete compressive strength which range from $20 \leq f_c \leq 70$ MPa. Figure 5.16 shows the relationship between f_c and $N_{code}/N_{exp.}$.

Each code provided different predictions for NSC, HSC, and UHSC; as seen in Table 5.8, all codes provided safe predictions for a wide range of f_c in the database. For all values of compressive strength, EC4 and AS5100.6 gave closer predictions to experimental results than AISC360-16 and AIJ2001.

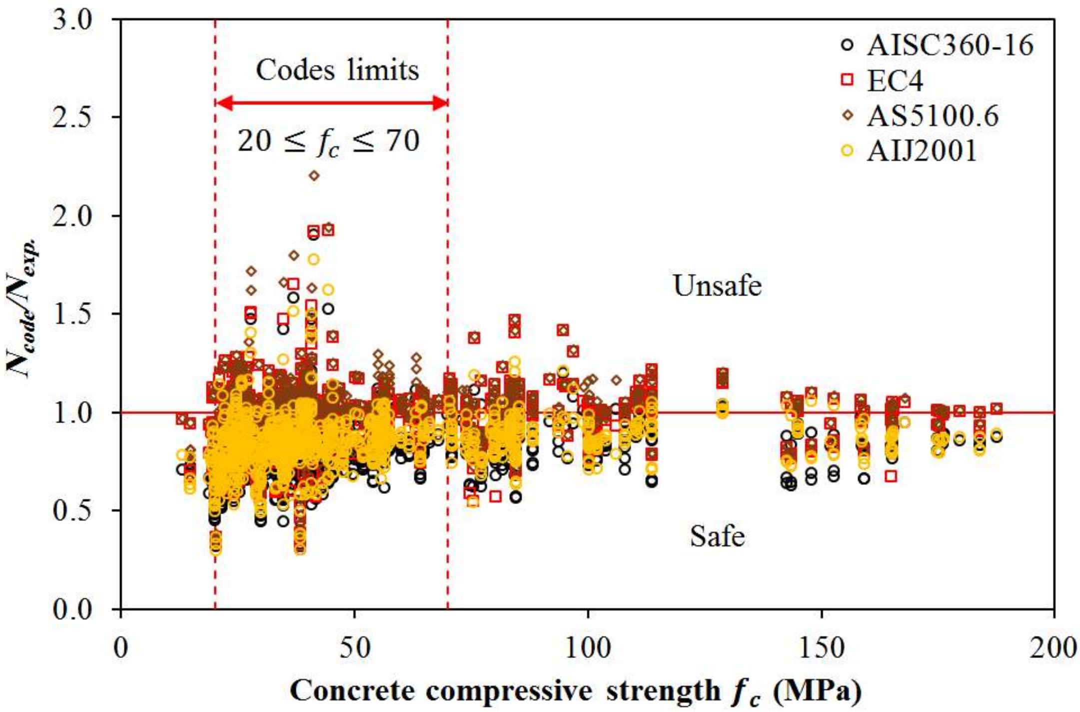

Figure 5.16 f_c versus $N_{code}/N_{exp.}$

5.4.1.5 Impact f_y on Codes Predictions

As shown in Table 5.8, all codes provided safe predictions for MSS ($f_y \leq 460$ MPa); AISC360-16 and AIJ2001 offered more underestimates than EC4 and AS5100.6. Similarly, for HSS, EC4 and AS5100.6 gave conservative predictions, and AISC360-16 and AIJ2001 again gave underestimates. Figure 5.17 shows the relationship between f_y and $N_{code}/N_{exp.}$.

According to Table 5.9, for specimens beyond the limits of codes, EC4 gave conservative results. AS5100.6 gave predictions closer to experimental results than AISC360-16 and AIJ2001, which both provided underestimates. However, all data beyond the codes' limits provided an average *SI* greater than unity.

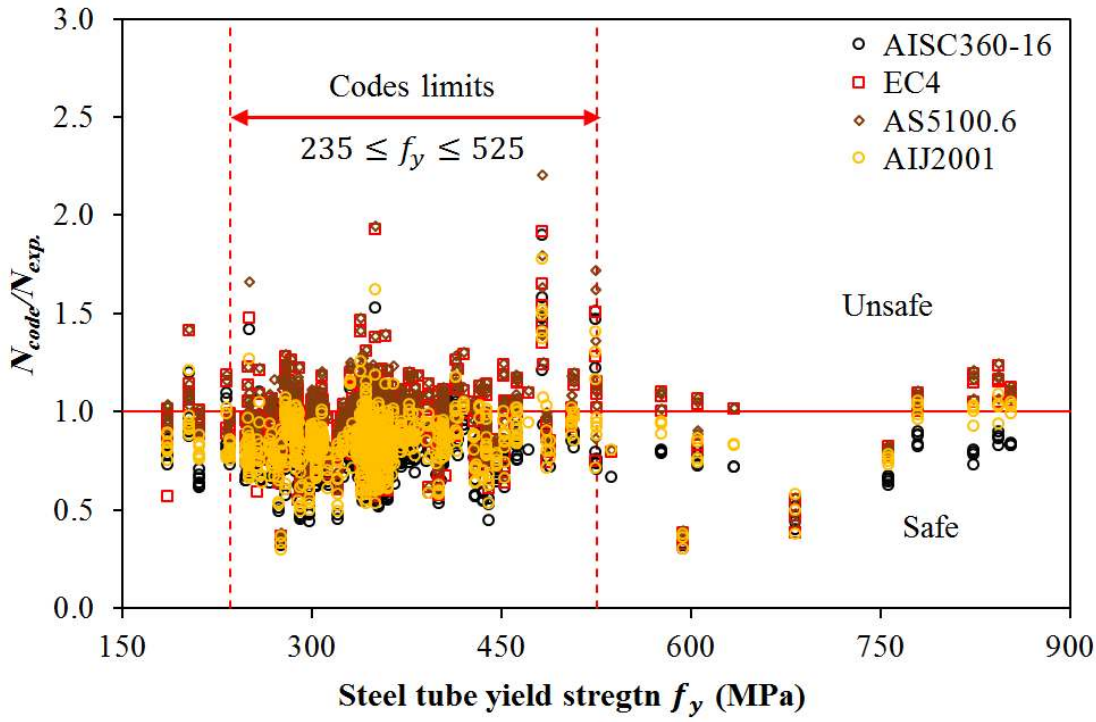

Figure 5.17 f_y versus $N_{code}/N_{exp.}$

5.5 Parameters' Impact on the Experimental Database Results

The database covers a wide range of geometrical and material properties of the circular CFST column loaded axially; therefore, it is important to study the influence of the significant parameters (*D/t* ratio, *L/D* ratio, f_c, f_y, and ξ) on the performance of the CFST columns.

5.5.1 Influence of *L/D* Ratio

CFST columns were categorized as short or long according to *L/D* ratio; this ratio affects the columns' failure modes. Generally, short columns fail by materials failure, while long columns fail geometrically; some columns show combinations of these two types of failures, and these columns are called medium columns. Most columns fall in medium length range.

To discuss the influence of *L/D* ratio on the compression response of CFST columns, Figure 5.18 describes the relationship between column *L/D* ratio and strength index, *SI*. As shown in Table 5.8, 63.0% of tested columns were short columns, while 37% were long. It can be noticed in Figure 5.18 that *L/D* ratio has a big influence on compression behavior of CFST columns. Capacity decreased as *L/D* ratio increased, as clear in the slope of the linear trendline; however, 71% of the short columns and

29% of the long columns possessed *SI* greater than unity. On the other hand, 7% of short columns and 92% of long columns had an *SI* less than unity. This result shows the direct impact of the *L/D* ratio on the capacity of CFST specimens.

Relative slenderness, $\bar{\lambda}$, as defined in EC4 also has an impact on the compression capacity of CFST specimens, where the strength decreases when $\bar{\lambda}$ increases. For $\bar{\lambda} \leq 0.5$, due to the effect of the confinement, 98% of tested columns have *SI* greater than unity, while for $\bar{\lambda} > 0.5$ without the effect of confinement only 32% of tested columns have *SI* greater than unity (Figure 5.19).

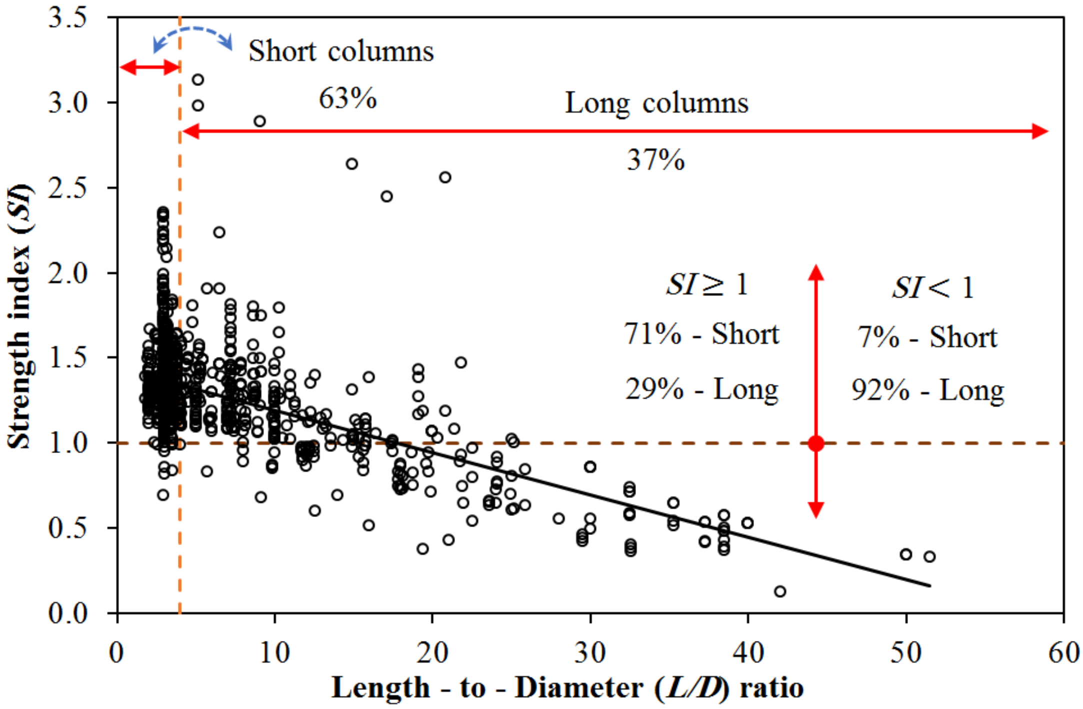

Figure 5.18 *L/D* ratio versus *SI* for all specimens

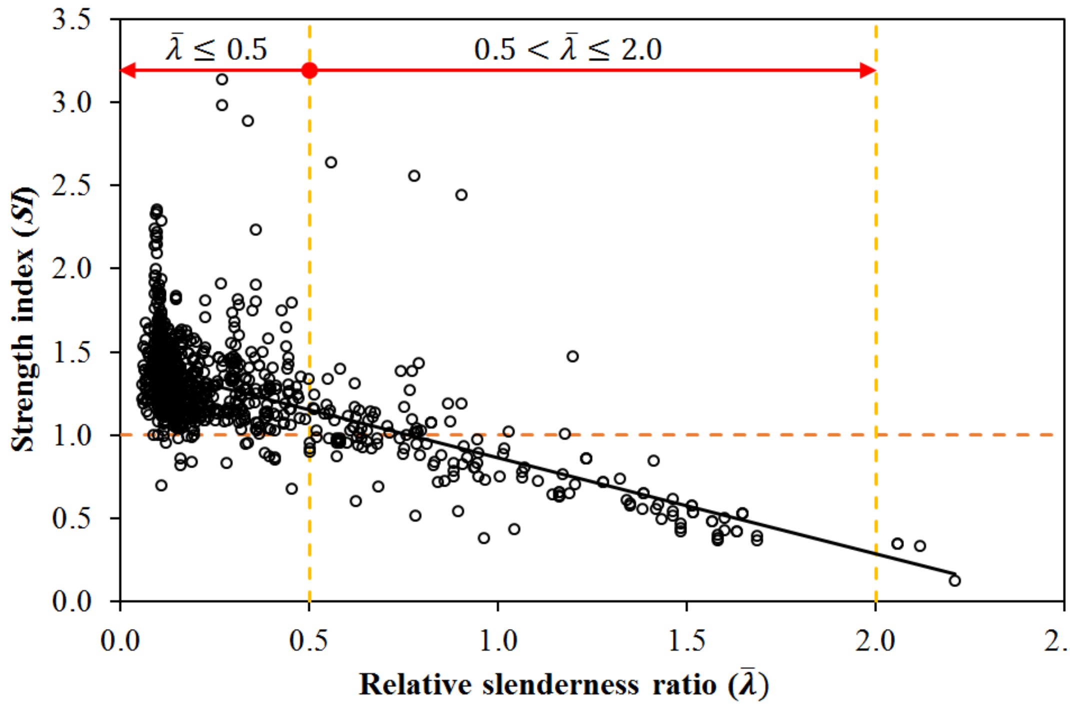

Figure 5.19 $\bar{\lambda}$ versus *SI* for all specimens

5.5.2 Influence of *D/t* Ratio

It is self-evident that an increase of *D/t* ratio not only decreases the stiffness of the CFST column but also decreases its compression capacity by reason of the decline in the confinement effect. The *D/t* ratio has a direct impact on the confinement index ξ: ξ decreases as *D/t* increases. The value of ξ represents the mechanical slenderness of the section and is known mathematically as the ratio capacity of steel to capacity of concrete. Figure 5.20 reveals the effect of *D/t* ratio on ξ.

Figure 5.21 presents the relation between *D/t* ratio and the strength index *SI*, and Figure 5.22 shows the relation between confinement index ξ and *SI*. It can be recognized that these factors have no direct influence on the compressive conduct of CFST columns loaded axially compared to the impact of *L/D* ratio. While the max value of *SI* is 3.13, gained at a *D/t* ratio equal to 57.35 and with *L/D* ratio equal to 5.14, the minimum *D/t* ratio is 8.19 with *SI* equal to 0.12 and maximum value of ξ equal to 14.09 but with *L/D* ratio equal to 42.01, and the maximum value of *D/t* ratio is 220.93 with average of *SI* equal to 1.27 and gives minimum ξ with average of 0.064 but with average *L/D* ratio equal to 3.48.

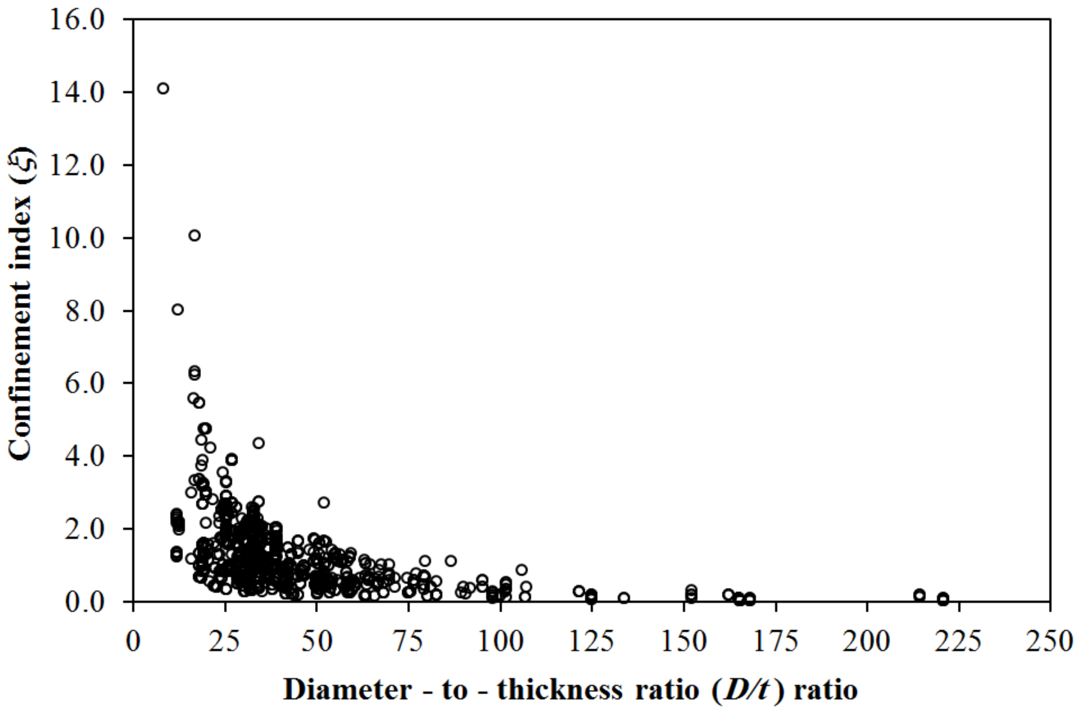

Figure 5.20 *D/t* ratio versus ξ for all specimens

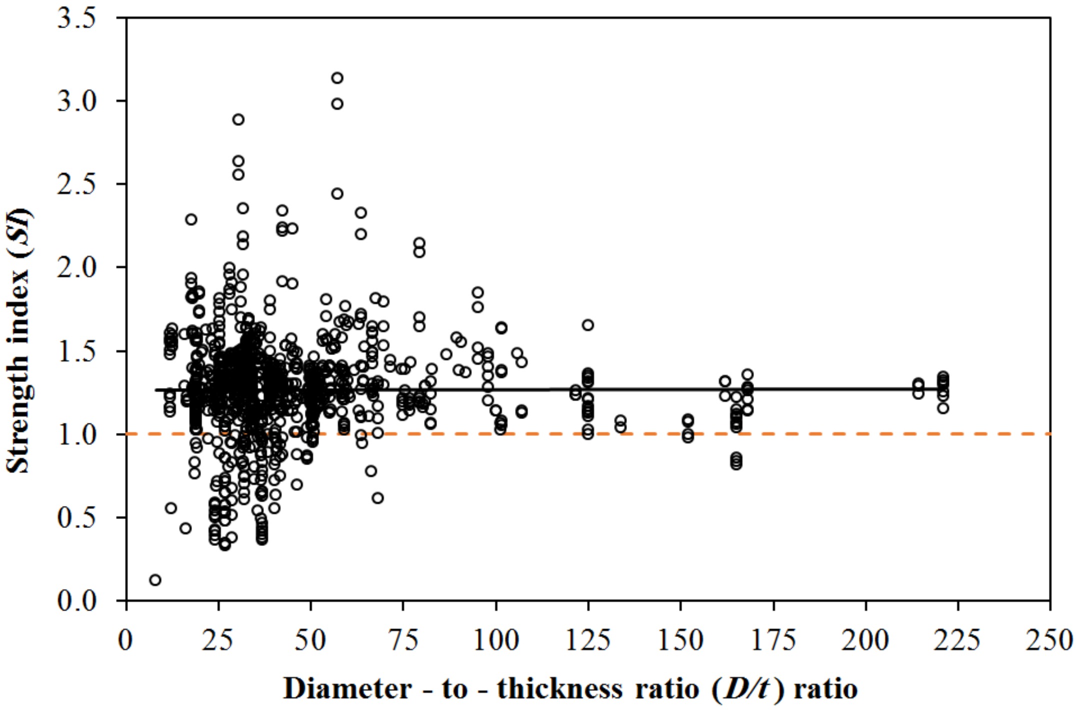

Figure 5.21 *D/t* ratio versus *SI* for all specimens

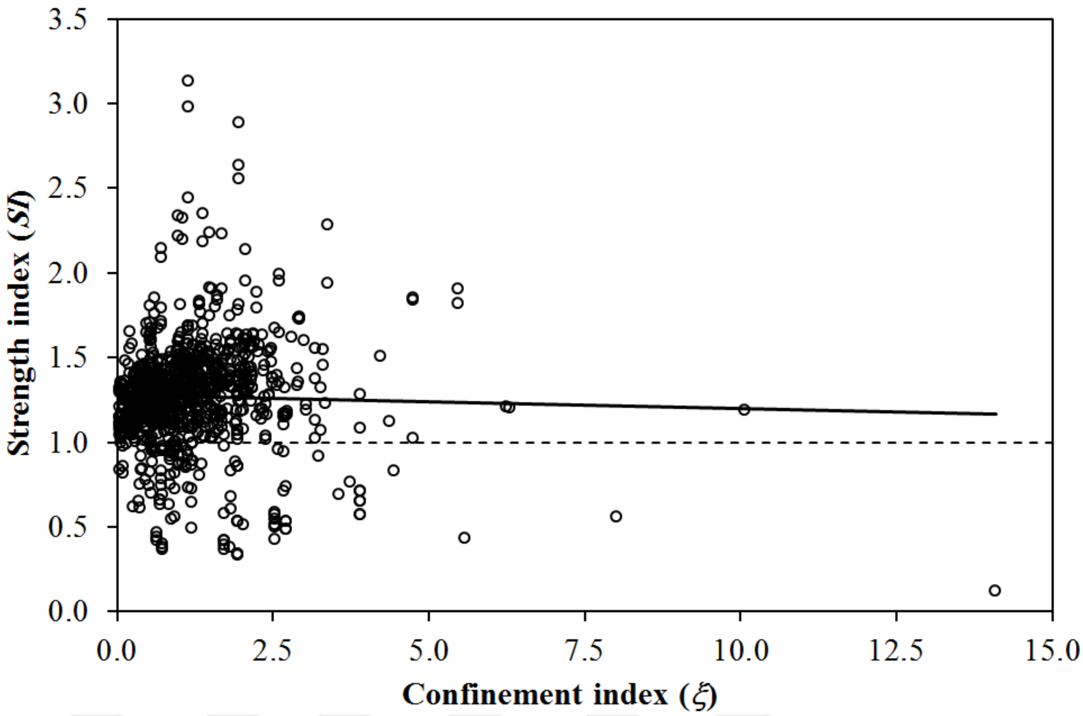

Figure 5.22 ξ versus *SI* for all specimens

5.5.3 Influence of Concrete Compressive Strength f_c

According to results of the database, and as shown in Table 5.8, 62% of CFST columns fell into the category of NSC, with $f_c \leq 50$ MPa; 25.7% of CFST columns were HSC, with $50 < f_c \leq 90$ MPa; and 12.3% of CFST columns were UHSC, with $f_c >$ 90 MPa. This survey of the literature shows a need for more research about CFST columns filled with HSC and UHSC.

Figure 5.23 presents the relationship between concrete compressive strength f_c and strength index *SI*; 87.64% of all data gave *SI* greater than unity, even for HSC and UHSC. The maximum value of *SI* is 3.13, with f_c equal to 38.4 MPa and *L/D* ratio equal to 5.14; the minimum value of *SI* is 0.12, with f_c equal 27.9 MPa and *L/D* ratio equal to 42.01. Both maximum and minimum values of *SI* were observed for NSC; CFST columns filled with NSC possessed more ductility and confinement than columns filled with HSC. This means the effect of *L/D* ratio has more of an effect than concrete type on the compression behavior of CFST columns.

5.5.4 Influence of Steel Tube Strength f_y

According to results of database analysis, and as shown in Table 5.8, 91.7% of CFST columns are in the range of mild steel strength (MSS) with $f_y \leq 460$ MPa, while 8.3%

of CFST columns were high strength steel (HSS) with $f_y > 460$ MPa (Figure 5.23). The test data are not enough to fill the gap in literature of using the high-strength steel.

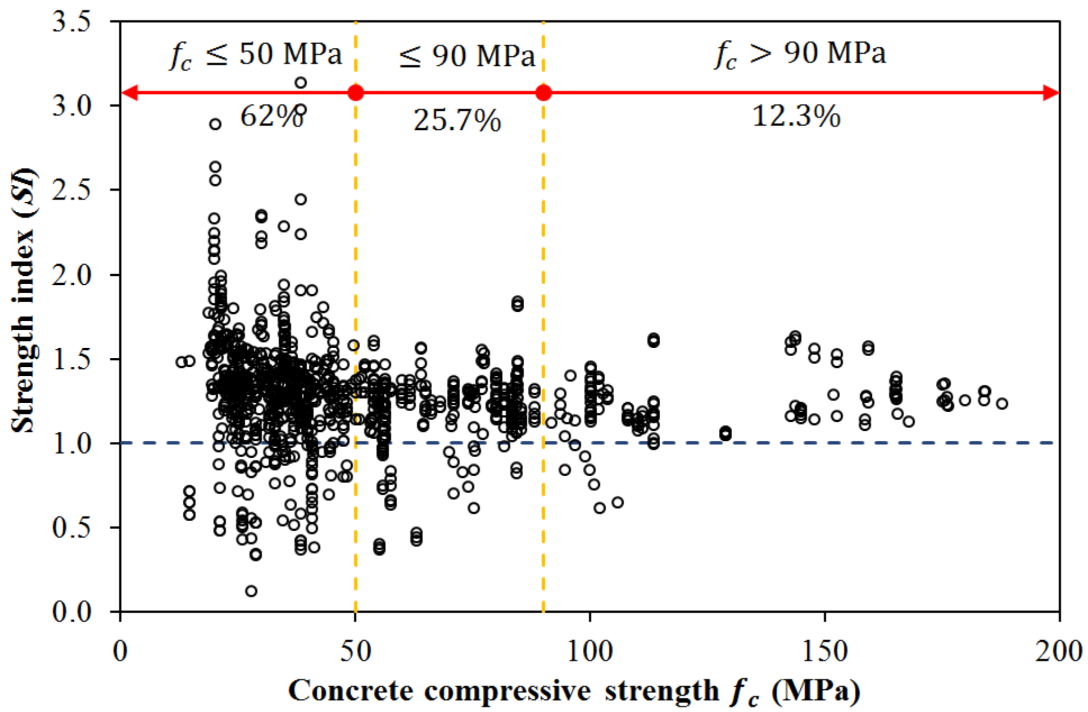

Figure 5.23 f_c versus *SI* for all specimens

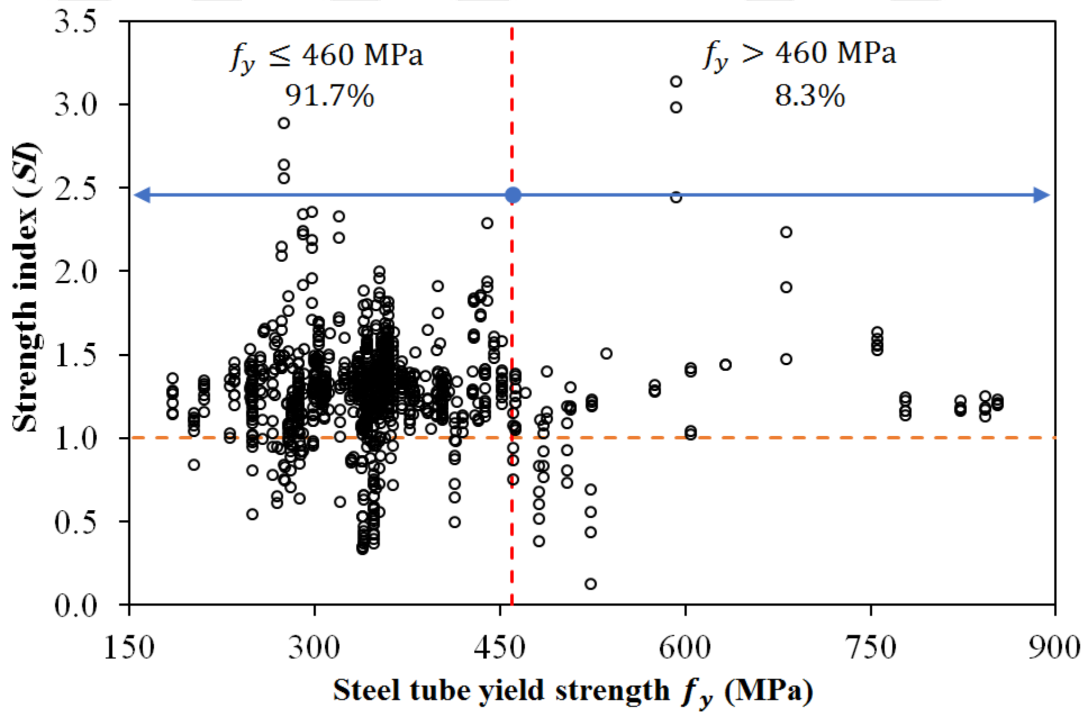

Figure 5.24 f_y versus *SI* for all specimens

5.6 Summary and Conclusions

This chapter addressed two goals. The first goal was to search the experimental performance of circular CFST columns loaded axially and to observe the contribution of the confinement effect.

Eighteen CFST specimens, with three *L/D* ratios of 2.62, 5.25, and 7.87, comprising short, medium, and long columns, and two *D/t* ratios, 19.37 and 41.71, were used. The properties of these composite columns are within or beyond the limitations of four selected design codes specifications, AISC16-360, EC4, AS5100.6, and AIJ2001.

To explore the concrete impact on the response of CFST columns, three grades of concrete strengths were selected, two of which were very close to upper limits of AISC360-16, EC4, AS5100.6, and AIJ2001 design codes, with f_c equal to 56.20 MPa, and 66.75 MPa. The third concrete strength selected was outside the limits of these codes, with its f_c equal to 107.20 MPa. Steel meeting two European steel specifications, S235 and S355, were used to address different confinement conditions.

Depending upon the geometrical and materials properties described above, the confinement index (ξ) of the tested CFST columns ranged between 0.230 and 1.540, and the steel contribution factor (δ) which used in EC4 from 0.185 to 0.606.

The second goal was to collect an experimental database from the literature, covering a wide range of parameters of circular CFST columns loaded axially. With literature data and the results of 18 columns tested in current research, a total of 1036 circular columns were examined to assess the predictions of design specifications codes and examine the influence of each factor on the performance of CFST columns and the confinement effect.

The following conclusions can be recorded:

- Concrete compressive strength affects the confinement behavior of CFST columns; *SI* decreases as concrete compressive strength increases.

- CFST specimens filled with concrete with strengths of 56.20 MPa and 66.75 MPa demonstrated larger deformation capacity, ductility, and confinement than CFST specimens with concrete strength of 107.20 MPa.

- The utilize of thicker steel tubes with higher yield strength works to increase the confinement effect of 107.20 MPa columns.

- The predictions of AISC360-16, EC4, AS5100.6, and AIJ2001 are different depending on which parameter is examined. In all cases these codes offered safe predictions.

- The predictions of EC4 and AS5100.6 were very close to the experimental results for short columns and columns with lower slenderness ($\bar{\lambda}$) due to the inclusion of confinement parameter in their calculations. On the contrary, no any confinement effect for AISC360-16 predictions and AIJ2001 has a constant factor for the confinement effect.

- The predictions of AISC360-16 and EC4 become closer when the relative slenderness $\bar{\lambda}$ increases, and AISC360-16 provides better predictions than EC4 in this slenderness zone.

- It is observed that *L/D* ratio and relative slenderness $\bar{\lambda}$ have a direct impact on the behavior of CFST columns, while other parameters do not have a direct impact on the response of CFST columns.

- The majority of the literature focused on short columns, columns fabricated with NSC, and columns fabricated with MSS; therefore, more studies should focus on long columns, columns fabricated with HSC and UHSC, as well as columns using HSS.

- In general, the predictions of AS5100.6 and EC4 have better agreement with the experimental results even for properties beyond their limits and could change their limits to cover a wider range of CFST column properties. While AISC360-16 and AIJ2001 give conservative predictions for CFST columns within and beyond the limits of the codes, this provides an indication that more attention should be paid to the confinement effect of circular CFST columns for both codes, and their calculations revised.

CHAPTER 6

EXPERIMENTAL INVESTIGATION OF LIGHTWEIGHT AGGREGATE AND SELF-COMPACTED CONCRETE IN CFST COLUMNS

6.1 General

Rapid development in structural engineering has increased demand for high-performance structural members to meet the design and construction requirements of massive constructions. Therefore, the progressions of concrete technology research have seen great growth in the manufacturing of high-performance concrete to intensify the mechanical behavior of such structural elements and decrease the difficulty of construction.

The development of lightweight aggregate concrete (LWC) and self-compacted concrete (SCC) are two of significant outcomes of such research, and they have been used in many of reinforced concrete applications. However, a literature review reveals that the use of these promising materials in composite construction, particularly CFST columns, has not yet been well covered (as mentioned in Chapter Two). Therefore, the experimental investigation of this chapter aimed to provide data to help to fill this research gap, while also assessing the ability of these materials to provide performance required for CFST columns. The efficiency of the design codes' predictions for LWC and SCC—which were established for normal-weight non-self-compacted CFST columns—were also examined.

6.2 Experimental Work

For this study, sixteen CFST columns were prepared. Half were filled with LWC, and half with SCC; all columns were then tested to compare the impact of the type of concrete on the compression response of the columns. In addition to the two types of concrete, four different *L/D* ratios were used to observe the behavior of short, medium, and long columns, and three different *D/t* ratios were used in this experimental study.

6.2.1 Material Properties

6.2.1.1 Structural Steel Tube

Two different steel tube outer diameters (139.70 mm and 114.30 mm) with three various sections (139.70 × 3.30 mm, 139.70 × 3.30 mm, and 114.30 × 3.38 mm) were used in this study. The geometrical characteristics of the tubes resulted in three different practical *D/t* ratios of 23.80, 33.82, and 42.33. For each tube, three tension coupons were cut and tested to measure the mechanical characteristics of the steel tube according to ASTME8/E8M-16 (2016) (see Chapter Four, Section 4.3.1). For steel tube yield strengths (f_y) of 290 MPa, 355 MPa, and 420 MPa, the corresponding ultimate stresses were 377 MPa, 430 MPa, and 520 MPa, respectively. The elastic modulus was measured as 200 GPa. The tensile stress–tensile elongation curves for the tests of coupons are shown in Figures 6.1–6.3.

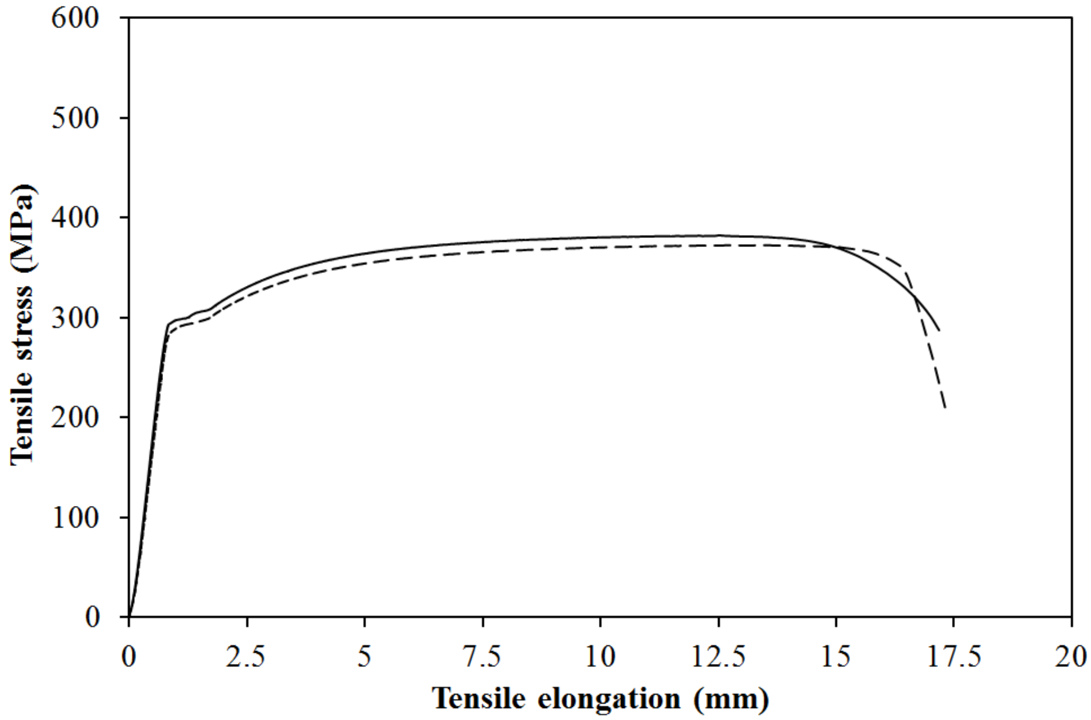

Figure 6.1 Coupons tests stress–elongation curves for 139.70 × 3.30 mm

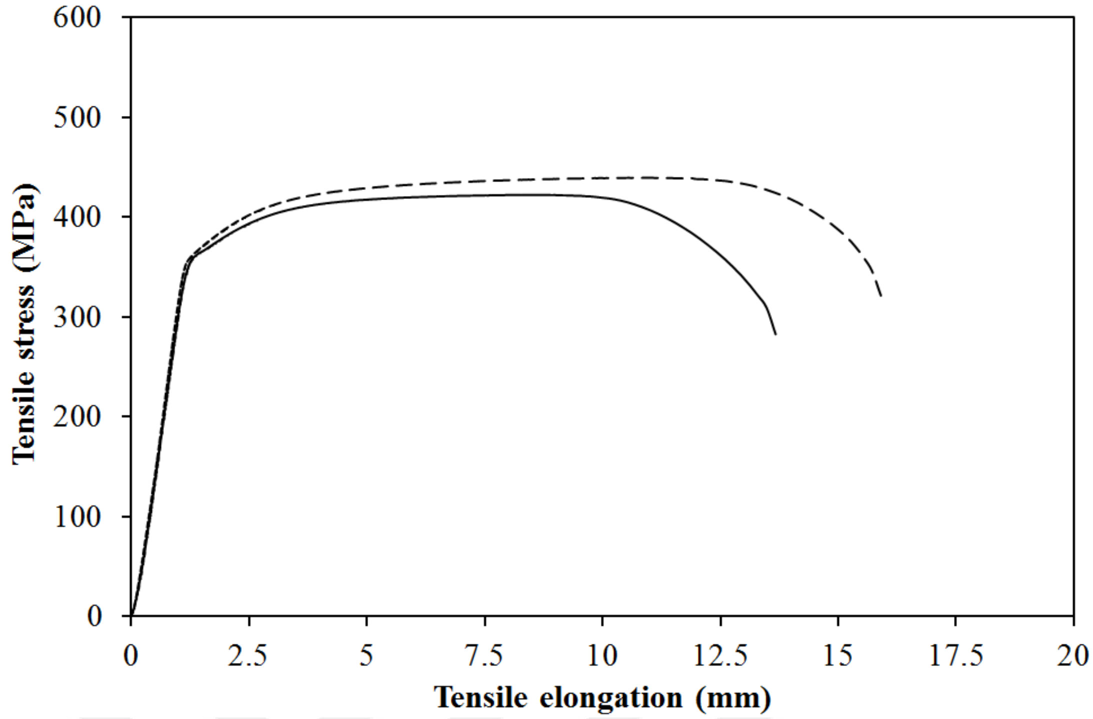

Figure 6.2 Coupons tests stress–elongation curves for 139.70 × 5.87 mm

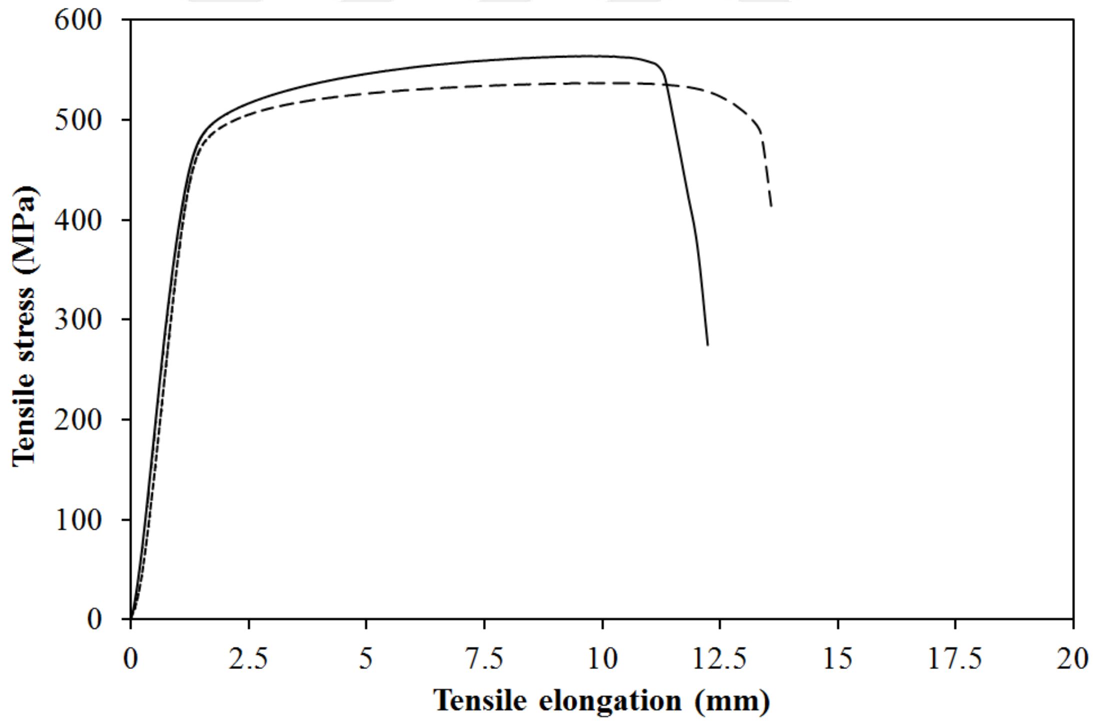

Figure 6.3 Coupons tests stress–elongation curves for 114.30 × 3.38 mm

6.2.1.2 Concrete

1. Lightweight aggregate concrete (LWC):

Pumice is used as lightweight aggregate in the manufacture of LWC with a maximum aggregate size of 10 mm. To obtain LWC with acceptable structural properties, the mix design of the LWC included cement, pumice LWA, water, silica fume (SF), fine crushed sand (CS), and hyperplasticizer (SP). Table (6.1) shows the details of LWC mix. The dry unit weight of this LWC was 1753 kg/m^3.

Table 6.1 LWC Mix proportions

Mix proportions	Cement	SF	LWA	Water	CS	SP
Ratio	1	0.25	0.395	0.25	0.592	0.013

2. Self-compacted concrete (SCC):

As mentioned in Chapter Four, the manufacture of SCC requires additional tests for fresh concrete which use additional materials. Fly ash (FA) is a significant material for this purpose; it has a spherical micro structure and provides high flowability to the final mix. The mix proportions of SCC are cement, fly ash type F (FA), water, hyperplasticizer (SP), coarse (RCA) and fine (RFA) river aggregates, and fine crushed sand (CS), Table 6.2 shows the details of SCC mix. The measured dry unit weight of SCC is 2324 kg/m^3.

Table 6.2 SCC Mix proportions

Mix proportions	Cement	FA	Water	RCA	RFA	CS	SP
Ratio	0.5	0.5	0.33	1.245	1.142	0.381	0.005

Two experiments were performed to define the properties of fresh SCC: a slump-flow test with T_{500} time check to measure the flowability and flow rate, and a V-funnel test to measure its viscosity and filling ability. These two tests were applied according to EN-12350-1 and 12350-2 (EFNARC, 2005). The fresh SCC mix properties were slump flow, 650 mm; T_{500} time, 4.5 sec; and T_v time (V-funnel test), 6 sec.

The 100×200 mm cylinder specimens were poured with LWC and SCC as prescribed by the ASTMC39/C39M−15a (2015) standard, and the average compressive strengths for LWC and SCC recorded as 33.47 MPa and 39.71 MPa, respectively. Despite the fact LWC and SCC had different measured compressive strengths, these values were in the same range and they can be addressed as normal-strength concrete.

The dry unit weight of LWC is about 24.57% lower than that of SCC. This reduction in weight offers the importance possibility to enhance the mechanical and thermal properties of the structural member. Due to this reduction in weight, the cross-sectional dimensions could be minimized, or the lower weight could allow workers to use smaller tools to handle larger structural units. These features would lead to savings of time as well as cost of transportation and construction, in addition to improving the thermal insulation properties of the final structure (Chandra and Berntsson, 2002). Furthermore, the reduction in structure self-weight possible by using LWC is appropriate for structures in seismically active regions, where these structures are liable to experience horizontal forces during an earthquake. The seismic response of a structure is a direct function of its mass (Mo *et al.*, 2016).

6.2.2 CFST Columns Specimens

After preparation of the hollow steel tubes according to the test requirements, sixteen specimens with different *L/D* ratios were filled with fresh concrete. Eight columns filled with LWC and another eight columns filled with SCC. The *L/D* ratios were selected to be able to observe local failure materials for short columns and global buckling failure for long columns in addition to medium length columns to mark the combined local materials and global failure modes.

Table 6.3 shows the details of CFST columns. The labeling system used in Table 6.3 includes concrete type, steel tube outer diameter *D*, steel tube thickness t, and *L/D* ratio of CFST columns, respectively. For example, the column specimen SCC-139.7-3.30-7.5 indicates a self-compacted concrete core, outer diameter of 139.7 mm, wall thickness of 3.30 mm, and *L/D* ratio of 7.5.

After completing the concrete pouring and curing processes, the surface of each column was leveled using high-strength epoxy, as described earlier in Chapter Four

(Section 4.5). The CFST columns specimens were then ready for testing, as shown in Figure 6.4.

Table 6.3 CFST column specimen details

Specimen	*D* (mm)	*t* (mm)	*D/t*	*L/D*	f_c (MPa)	f_y (MPa)	$N_{exp.}$ (kN)
LWC-139.7-3.30-2	139.7	3.30	42.33	2	33.47	290	920.31
LWC-139.7-5.87-2	139.7	5.87	23.80	2	33.47	355	1367.28
LWC-114.3-3.38-2	114.3	3.38	33.82	2	33.47	420	765.96
LWC-114.3-3.38-5	114.3	3.38	33.82	5	33.47	420	774.34
LWC-139.7-3.30-7.5	139.7	3.30	42.33	7.5	33.47	290	855.126
LWC-139.7-5.87-7.5	139.7	5.87	23.80	7.5	33.47	355	1318.2
LWC-114.3-3.38-7.5	114.3	3.38	33.82	7.5	33.47	420	717.39
LWC-114.3-3.38-10.5	114.3	3.38	33.82	10.5	33.47	420	725.81
SCC-139.7-3.30-2	139.7	3.30	42.33	2	39.71	290	989.2
SCC-139.7-5.87-2	139.7	5.87	23.80	2	39.71	355	1554.76
SCC-114.3-3.38-2	114.3	3.38	33.82	2	39.71	420	885.67
SCC-114.3-3.38-5	114.3	3.38	33.82	5	39.71	420	898.47
SCC-139.7-3.30-7.5	139.7	3.30	42.33	7.5	39.71	290	996.38
SCC-139.7-5.87-7.5	139.7	5.87	23.80	7.5	39.71	355	1481.5
SCC-114.3-3.38-7.5	114.3	3.38	33.82	7.5	39.71	420	861.57
SCC-114.3-3.38-10.5	114.3	3.38	33.82	10.5	39.71	420	815.87

Figure 6.4 CFST column specimens before testing

Specimens were cautiously placed and centered in the testing machine to preclude any eccentric behavior and bending effects. Displacement-controlled loading at a slow rate of 0.5 mm/min was applied to all columns and end-shortening versus compression loading data of all columns were acquired. Figure 6.5 describes a specimen during testing.

Figure 6.5 CFST column specimen test

6.2.3 Test Results and Discussion

The test results for lightweight aggregate concrete filled-steel tube (LWCFST) columns and self-compacted concrete filled-steel tube (SCCFST) columns are reported as end-shortening against compression loading curves and as failure modes according to the impact of the geometrical and mechanical properties of the CFST column specimens. Table 6.4 reviews the results of this study.

Table 6.4 Summarized results for LWCFST and SCCFST columns

Specimen	$N_{exp.}$ (kN)	$\Delta_{exp.}$ (mm)	SI	DI	K_i (kN/mm)	$\bar{\lambda}_{EC4}$
LWC-139.7-3.30-2	920.31	2.18	1.14	1.30	491.47	0.068
LWC-139.7-5.87-2	1367.28	3.15	1.10	1.35	493.78	0.069
LWC-114.3-3.38-2	765.96	2.25	1.02	2.04	395.06	0.074
LWC-114.3-3.38-5	774.34	3.07	1.03	1.29	305.19	0.185
LWC-139.7-3.30-7.5	855.126	4.95	1.06	1.60	252.25	0.254
LWC-139.7-5.87-7.5	1318.2	5.15	1.06	1.58	356.91	0.260
LWC-114.3-3.38-7.5	717.39	3.40	0.95	1.54	257.22	0.277
LWC-114.3-3.38-10.5	725.81	4.80	0.96	1.79	197.45	0.388
SCC-139.7-3.30-2	989.2	3.75	1.12	2.65	477.92	0.070
SCC-139.7-5.87-2	1554.76	7.50	1.19	4.92	543.09	0.071
SCC-114.3-3.38-2	884.12	4.52	1.10	6.62	436.67	0.076
SCC-114.3-3.38-5	898.47	13.32	1.12	7.46	321.38	0.190
SCC-139.7-3.30-7.5	996.38	12.80	1.13	5.17	222.85	0.264
SCC-139.7-5.87-7.5	1481.5	16.40	1.13	5.92	350.29	0.267
SCC-114.3-3.38-7.5	861.57	12.45	1.08	7.05	256.34	0.285
SCC-114.3-3.38-10.5	815.87	9.12	1.02	3.92	201.51	0.399

6.2.3.1 End-Shortening Against Compression Loading Curves

It is appropriate to address CFST columns according to the *L/D* ratio. Therefore, the discussion of the experimental results will be according to the following criteria:

- **Compression behavior of CFST columns with *L/D* ratio equal to 2:**

Figure 6.6 presents the end-shortening against compression loading curves for all CFST columns with *L/D* ratio equal to 2.

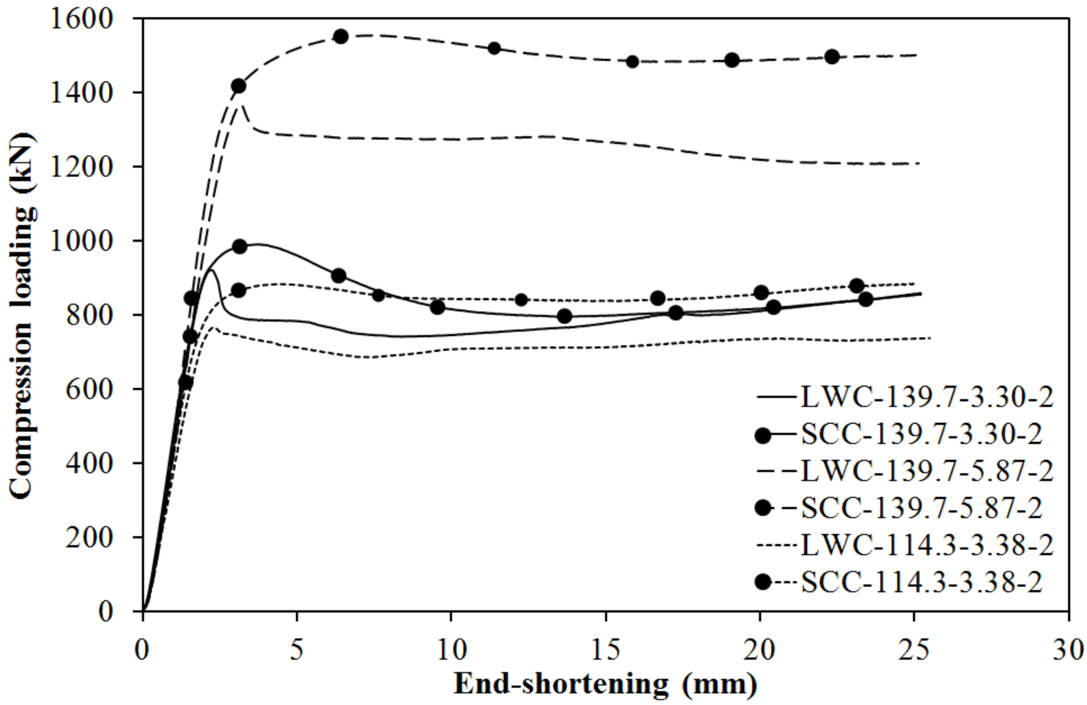

Figure 6.6 Load–shortening curves for columns with *L/D* = 2

Specimens with a diameter of 139.7 mm and a thickness of 5.87 mm had the highest value of compression capacity, 1367.28 kN and 1554.76 kN for LWCFST and SCCFST columns, respectively.

As expected, SCCFST columns gave greater compression capacities than the LWCFST counterparts because the compressive strength of SCC is greater than that of LWC. As shown in Figure 6.6, the performance of LWCFST columns was different than that of SCCFST columns. However, the LWCFST columns experienced very little plastic deformation before reaching compression capacity with very little end-shortening, while the results for SCCFST columns indicated higher plastic deformation capacities. In this regard, lightweight concrete specimen

LWC-139.7-3.30-2 reached its compression capacity with 2.18 mm end-shortening, while its counterpart SCC specimen, SCC-139.7-3.30-2, reached its compression capacity at an end-shortening of 3.75 mm. This behavior was observed for all specimens, as shown in Table 6.4 and Figure 6.6.

Furthermore, there was a significant difference in the performance of the LWCFST columns and SCCFST columns in the post-peak region. The LWCFST columns faced sudden loss of compression loading after reaching their compressive capacities, but the columns showed resistance against loading after a level of loss of loading.

On the other hand, the SCCFST columns presented smooth behavior after reaching their compression capacities, and these specimens exhibited higher ductility compared to the LWCFST columns. The behavior of the LWCFST could result from the physical properties of the lightweight aggregate. Lightweight aggregate has a porous structure, which is crushed when the load reaches compression capacity, leading to the formation of voids in the concrete core. These voids can cause a loss in compression capacity. However, under continuous loading, the crushed LWC re-fills the voids and the LWCFST columns regain their resistance.

It is noteworthy that the effect of the cross-sectional dimensions of CFST columns on their compression capacity is evident. Columns with a diameter of 139.7 mm with a tube thickness of 3.3 mm recorded a higher compression capacity ($N_{exp.}$) and higher initial stiffness (K_i) than columns with a diameter of 114.3 mm. Although the column with diameter of 114.3 mm has greater steel yield strength, this behavior is typical for both LWCFTS and SCCFST columns, as shown in Table 6.4 and Figure 6.6.

However, although LWCFST columns with a diameter of 114.3 mm showed lower compression capacities compared to LWCFST columns with a diameter of 139.7 mm, they provided a smoother transition from the pre-peak to the post-peak region and suffered less loss in capacity after reaching peak load. The same behavior could be seen for SCCFST columns; specimen SCC-114.3-3.38-2 had a smoother transition from the pre-peak to the post-peak region than specimen SCC-139.7-3.30-2, as shown in Figure 6.6.

- **Compression behavior of CFST columns with *L/D* ratio equal to 5:**

Figure 6.7 shows the end-shortening against compression loading curves for all CFST columns with *L/D* ratio equal to 5. This *L/D* ratio held only for CFST columns with a diameter of 114.3 mm. Also, the LWCFST column exhibits a sudden loss of loading after reaching its compression capacity, while the SCCFST column behaved with smooth behavior and higher ductility. LWCFST columns also provided little plastic deformation before reaching their compression capacity; the corresponding end-shortening was 3.07 mm, with lower initial stiffness. SCCFST specimens, though, had higher plastic deformation with the corresponding end-shortening equal to 13.32 mm (Table 6.4). The slight difference in initial stiffness between SCC and LWC specimens could due to the variation in the concrete compressive strength between them.

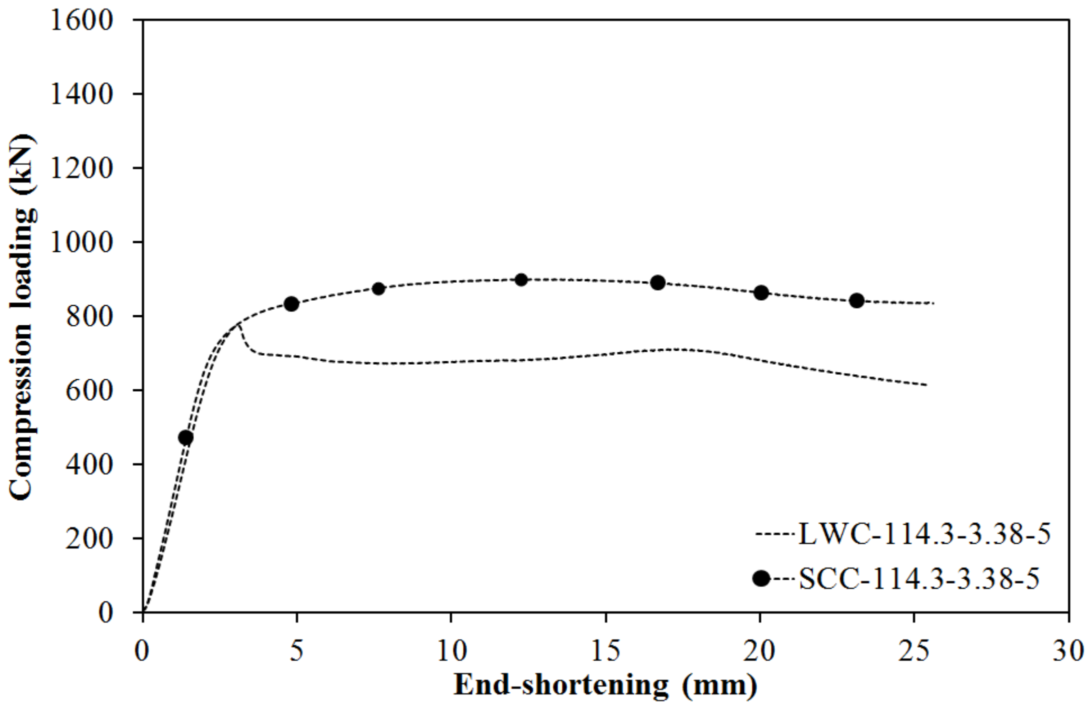

Figure 6.7 Load–shortening curves for columns with *L/D* = 5

- **Compression behavior of CFST columns with *L/D* ratio equal to 7.5:**

Figure 6.8 presents the compression behavior of CFST columns with *L/D* ratio equal to 7.5. In accordance with the classification of the CFST columns, the columns in this group tend to behave as long columns. Similar to specimens with *L/D* equal to 2, the compression capacity of the specimens with diameter of 139.7 mm is greater than the compression capacity of specimens with a diameter of 114.3 mm.

LWCFST columns with *L/D* equal to 7.5 showed more nonlinearity behavior in the pre-peak region compared to LWCFST columns with *L/D* equal 2 and 5 (Figures 6.6, 6.7). Also, the column length effect is clear on the loss of the load after reaching the compression capacity. There, specimens with *L/D* equal to 7.5 showed smoother and more gradual transition from pre-peak region to post-peak region than specimens with *L/D* equal to 2 and 5. SCCFST columns still showed better ductility behavior than LWCFST columns.

CFST columns with *L/D* equal to 7.5 show lower initial stiffness than CFST columns in previous groups. These columns present higher plastic deformation than counterpart specimens in the group of *L/D* equal to 2; the comparison of end-shortening corresponding to compression capacities supports this conclusion (Table 6.4 and Figure 6.8).

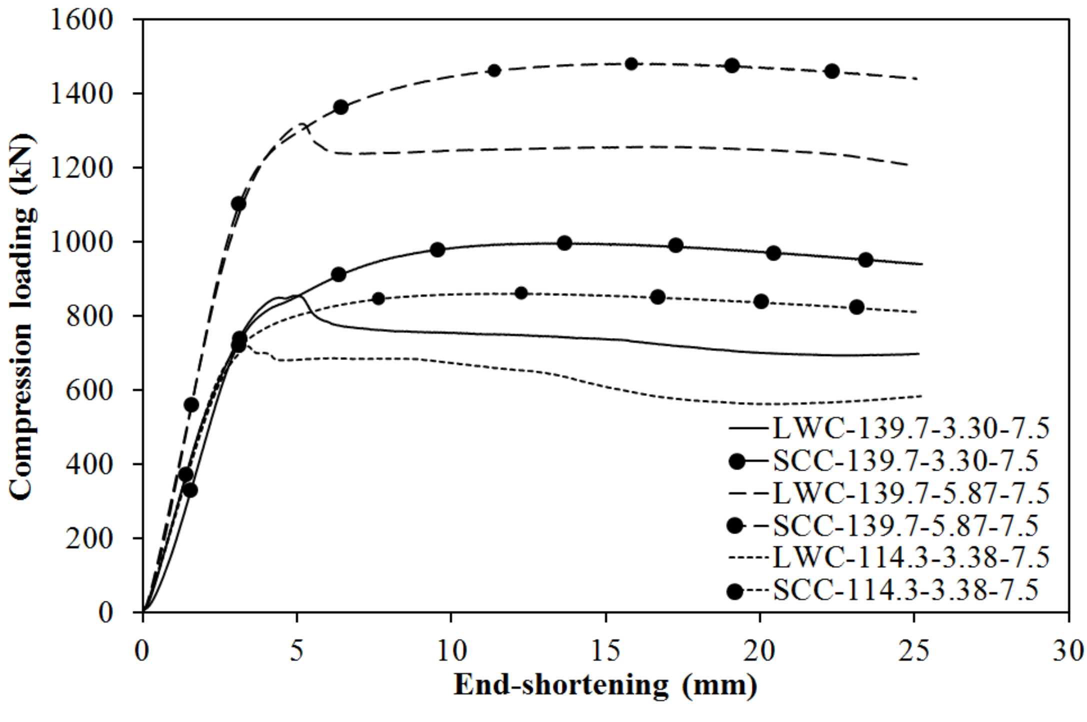

Figure 6.8 Load–shortening curves for columns with *L/D* = 7.5

- **Compression behavior of CFST columns with L/D ratio equal to 10.5:**

The behavior of CFST columns in this group was exactly like the behavior of long columns. Figure 6.9 illustrates the compression behavior of CFST columns with *L/D* equal to 10.5. Both LWCFST and SCCFST columns offered lower initial stiffness compared to the previous groups, with their values close to each other.

LWCFST and SCCFST columns showed a smoother and more gradual transition from the pre-peak to post-peak region compared to CFST columns of the previous groups. This type of behavior is because of the length effect of columns, which cause them to significantly diverge from the behaviors of the previous groups.

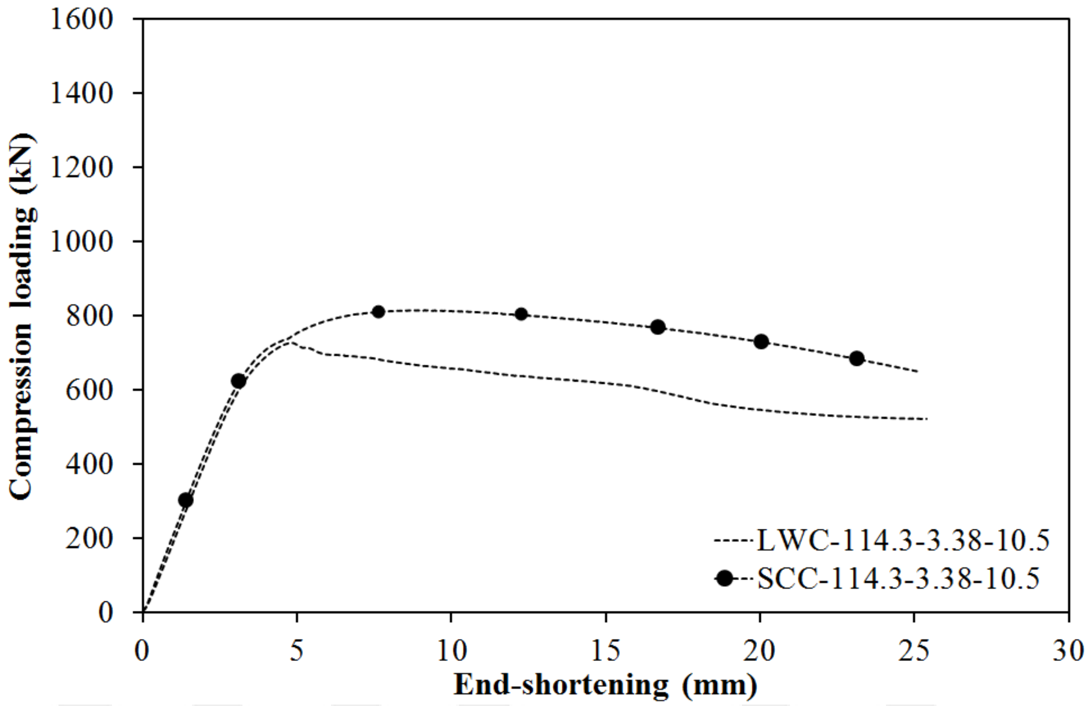

Figure 6.9 Load–shortening curves for columns with *L/D* = 10.5

6.2.3.2 Failure Modes

The failure modes of LWCFST and SCCFST columns are arranged in comparative form according to *L/D* ratio.

- **Failure modes of CFST columns with *L/D* ratio equal to 2:**

Figure 6.10 presents the failure modes of CFST columns with *L/D* equal to 2. These columns behave as short columns. In general, local buckling of the steel tube and local crushing of the concrete core mixed with the shear failure; the specimens with larger *D/t* ratios showed a concentrated effect of local materials failure. The sudden loss in capacity of LWC specimens led to different failure modes of LWCFST columns. The specimen LWC-114.3-3.38-2 exemplified different behavior than LWC specimens with a diameter of 139.7 mm.

(a) LWC-139.7-3.30-2 (b) LWC-139.7-5.87-2 (c) LWC-114.3-3.38-2

(d) SCC-139.7-3.30-2 (e) SCC-139.7-5.87-2 (f) SCC-114.3-3.38-2

Figure 6.10 Failure modes for columns with *L/D* = 2

- **Failure modes of CFST columns with *L/D* ratio equal to 5:**

Figure 6.11 illustrates the failure modes of CFST columns with *L/D* equal to 5. These specimens indicated combined local and overall failure modes, meaning these specimens could be classified as medium-length columns. The LWCFST specimen also showed obvious local buckling compared to SCCFST specimen, again due to the weakness of lightweight aggregate.

- **Failure modes of CFST columns with *L/D* ratio equal to 7.5:**

Figure 6.12 shows the failure modes of specimens with *L/D* = 7.5. In this group, the behavior of LWCFST columns differed from that of SCCFST columns. It was very clear that local materials failure governed the failure modes of the LWCFST columns, with a minimal contribution from overall buckling. In contrast, overall buckling governed the failure modes of SCCFST columns. From this difference in behavior, an interesting deduction arose: because of the porous structure of the lightweight aggregate, the LWC core did not have enough potential capacity to provide full inward support to the steel tube. However, this behavior would mean that the lightweight aggregate was crushed before the CFST column reached its compression capacity. In this group of LWCFST columns, the length has more effect on the failure mode than the *D/t* ratio, as shown the specimen LWC-139.7-5.87-7.5, with steel tube thickness of 5.87 mm. This behavior is not acceptable in the design of CFST columns which have this *L/D* ratio.

(a) LWC-114.3-3.38-5 (b) SCC-114.3-3.38-5

Figure 6.11 Failure modes of columns with *L/D* = 5

(a) LWC-139.7-3.30-7.5 (b) LWC-139.7-5.87-7.5 (c) LWC-114.3-3.38-7.5

(d) SCC-139.7-3.30-7.5 (e) SCC-139.7-3.30-7.5 (f) SCC-114.3-3.38-7.5

Figure 6.12 Failure modes of columns with *L/D* = 7.5

- **Failure modes of CFST columns with *L/D* ratio equal to 10.5:**

Figure 6.13 presents the failure modes of CFST columns with *L/D* equal to 10.5. These columns behave as long columns because the overall buckling behavior is governed the failure modes of both LWCFST and SCCFST columns. For LWC specimens, though, even those with *L/D* = 10.5, due to the porous structure of lightweight aggregate local buckling still contributed significantly to the failure mode columns. LWC could not enable the column to resist a full overall buckling failure. On another hand, SSCFST column confirmed full overall buckling mode of failure.

6.2.3.3 Performance Indices

The performance indices, like strength index *SI* and ductility index *DI*, are considered appropriate indices for comparison and evaluation of the performance of LWC and SCC in CFST columns. As mentioned in Chapter Five, *SI* indicates strength improvement due to confinement and composite action in the CFST column, and *DI* is used to evaluate the capability of CFST column to bear plastic deformation without significant degradation in capacity. Table 6.5 shows comparisons between LWCFST and SCCFST columns according to *SI* and *DI*.

(a) LWC-114.3-3.38-10.5 (b) SCC-114.3-3.38-10.5

Figure 6.13 Failure modes of columns with *L/D* = 10.5

Table 6.5 *SI* and *DI* for CFST column specimens

LWCFST specimen	*SI*	*DI*	SCCFST specimen	*SI*	*DI*
LWC-139.7-3.30-2	1.14	1.30	SCC-139.7-3.30-2	1.12	2.65
LWC-139.7-5.87-2	1.10	1.35	SCC-139.7-5.87-2	1.19	4.92
LWC-114.3-3.38-2	1.02	2.04	SCC-114.3-3.38-2	1.10	6.62
LWC-114.3-3.38-5	1.03	1.29	SCC-114.3-3.38-5	1.12	7.46
LWC-139.7-3.30-7.5	1.06	1.60	SCC-139.7-3.30-7.5	1.13	5.17
LWC-139.7-5.87-7.5	1.06	1.58	SCC-139.7-5.87-7.5	1.13	5.92
LWC-114.3-3.38-7.5	0.95	1.54	SCC-114.3-3.38-7.5	1.08	7.05
LWC-114.3-3.38-10.5	0.96	1.79	SCC-114.3-3.38-10.5	1.02	3.92

In general, for both columns, the strength and ductility indices decreased as the length of the column increased. A few specimens showed unexpected results that did not fit this trend; these unexpected results could be related to the uncertainty inherent in the concrete compressive strength.

The differences in ductility between LWCFST columns and SCCFST columns are very clear: SCCFST columns provide higher ductility than LWCFST columns. However, the short columns have higher ductility compared to medium length and long columns. Also, it is worth noting that SCCFST columns with a diameter of 114.3 mm have higher *DI* than columns with a diameter of 139.7 mm and the same *L/D* ratio.

For LWCFST columns, *SI* ranged from 0.95 to 1.14, while for SCCFST columns, *SI* range from 1.02 to 1.19. It can be concluded from these results that the composite action between steel tube and SCC is even better for long columns, likely because the steel tube yields better confinement to SCC. The value of *SI* for specimens LWC-114.3-3.38-7.5 and LWC-114.3-3.38-10.5 was less than 1.0 (0.95 and 0.96, respectively). The behavior expected for this ratio was observed in the failure mode of these columns, where a decrease in strength indicated premature crushing of lightweight aggregate at the local buckling region.

This result supports the previous conclusion, as mentioned in failure mode subsection, that LWC is not appropriate for use in long CFST columns, and does not provide any confinement in columns of this type. Indeed, the composite action between LWC and steel tube is insufficient for LWCFST columns with *L/D* ratios equal to 7.5 and 10.5 due to unexpected local buckling behavior in long columns.

In contrast, for the SCCFST column specimens, all values of *SI*, even for long columns, were greater than one. This means that SCCFST columns benefit from positive composite action between SCC and steel tube, behavior favorable for the design of composite columns using SCC.

6.2.4 Design Specifications Predictions Against Experimental Results

In this Chapter, only the AISC360-16, EC4, and AIJ2001 design specifications were adopted to assess the applicability of these codes to predict the compression capacity for the LWCFST and SCCFST columns. LWC is not the essential focus of the design specification methods (for details about calculations see Chapter Three). Table 6.6 presents the ratios of the experimental compression capacities to design codes' predicted compression capacities.

Table 6.6 Experimental results compared with design specification predictions

Specimen	$N_{exp.}$ (kN)	N_{AISC}/ $N_{exp.}$	N_{EC4}/ $N_{exp.}$	N_{AIJ}/ $N_{exp.}$
LWC-139.7-3.30-2	920.31	0.92	1142.35	0.81
LWC-139.7-5.87-2	1367.28	0.94	1827.30	0.75
LWC-114.3-3.38-2	765.96	1.02	1102.29	0.69
LWC-114.3-3.38-5	774.34	1.00	953.33	0.81
LWC-139.7-3.30-7.5	855.126	0.97	938.10	0.91
LWC-139.7-5.87-7.5	1318.2	0.95	1419.55	0.93
LWC-114.3-3.38-7.5	717.39	1.06	850.31	0.84
LWC-114.3-3.38-10.5	725.81	1.02	767.30	0.95
SCC-139.7-3.30-2	989.2	0.94	1225.45	0.81
SCC-139.7-5.87-2	1554.76	0.87	1902.76	0.82
SCC-114.3-3.38-2	884.12	0.94	1155.65	0.77
SCC-114.3-3.38-5	898.47	0.92	1004.01	0.89
SCC-139.7-3.30-7.5	996.38	0.91	1014.02	0.98
SCC-139.7-5.87-7.5	1481.5	0.89	1487.13	1.00
SCC-114.3-3.38-7.5	861.57	0.94	898.32	0.96
SCC-114.3-3.38-10.5	815.87	0.96	815.43	1.00
μ (LWC)		0.98	1.21	1.09
σ		0.05	0.13	0.06
μ (SCC)		0.92	1.12	1.01
σ		0.03	0.12	0.03
μ (Total)		**0.95**	**1.16**	**1.05**
σ		**0.05**	**0.13**	**0.06**

$\boldsymbol{\mu}$: Average and $\boldsymbol{\sigma}$: Standard deviation

The error ratio $N_{code}/N_{exp.}$ of the predicted results was estimated as described in Chapter Five. An error ratio less than one represents an underestimate, or conservative prediction on the safe side, while error ratio greater than one represents an overestimate or unconservative prediction on the unsafe side.

For the AISC360-16 design specification, the average of all $N_{AISC}/N_{exp.}$ ratios were 0.95. This means that AISC360-16 provides conservative predictions which are on the safe side for design purposes.

Figures 6.14 to 6.16 which represent the comparison between the experimental results and the estimations of both AISC360-16, EC4, and AIJ2001 respectively. The data which located above the equality line represent the unsafe predictions while the data located under the equality line represent the safe predictions.

The predictions of AISC360-16 for LWCFST columns and SCCFST columns were examined separately to provide more detail. The average $N_{AISC}/N_{exp.}$ for LWCFST and SCCFST columns was equal to 0.98 and 0.92, respectively. These predictions indicate that AISC360-16 provides acceptable predictions for LWCFST columns, with an average 2% difference on the safe side. The predictions of the AISC360-16 for SCCFST columns was much more conservative, understimating by 8% (Table 6.6 and Figure 6.14).

According to the EC4 method, the entire average of $N_{EC4}/N_{exp.}$ is 1.16. This means the EC4 predictions leads to unconservative predictions at an average rate of 16%. For LWCFST columns, the average of $N_{EC4}/N_{exp.}$ is equal to 1.21, which means that the EC4 predictions are even more unconservative, overestimating by 21%, while for SCCFST columns, the average of $N_{EC4}/N_{exp.}$ is equal to 1.12. This means that EC4 predictions for SCCFST columns overpredict by an average of 12%, Table (6.6 and Figure 6.15).

For AIJ2001, the entire average of $N_{AIJ}/N_{exp.}$ is 1.05; this code gives overpredicts by 5%. For LWCFST columns, the average value of $N_{AIJ}/N_{exp.}$ is equal to 1.09, and for SCCFST columns, the average $N_{AIJ}/N_{exp.}$ is equal to 1.01. These results give an indication that the AIJ2001 provides good predictions for SCCFST columns and deviates more for LWCFST than SCCFST columns, while still offering acceptable predictions for LWCFST columns, with an average deviation of 9% (Table 6.6 and Figure 6.16).

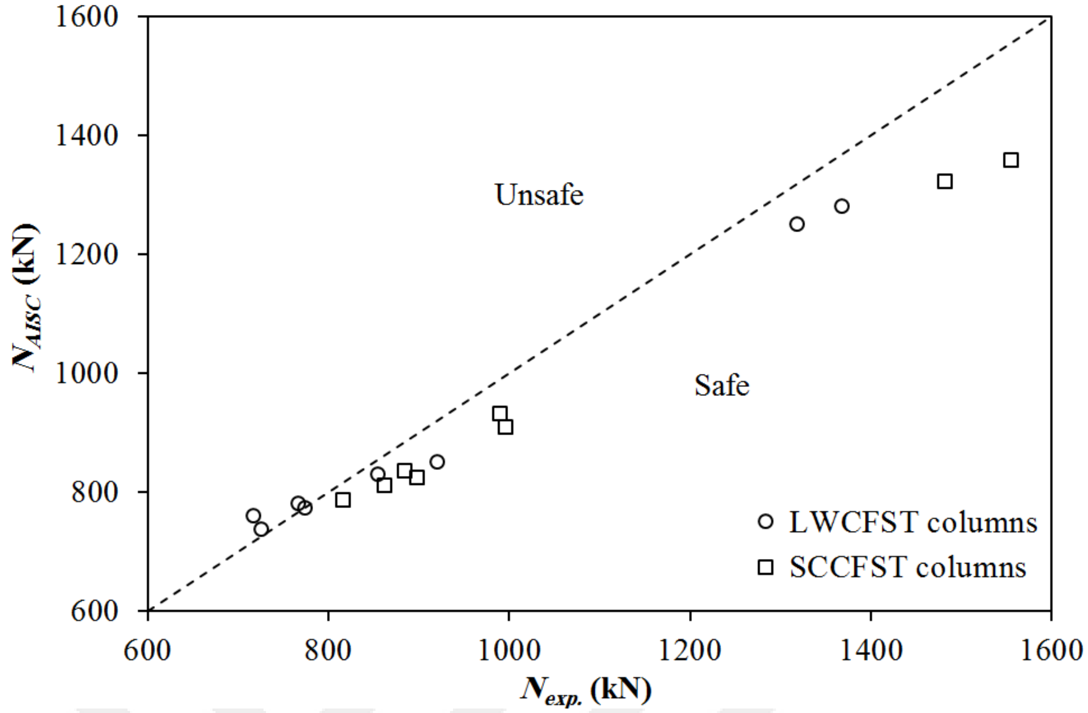

Figure 6.14 Comparison between $N_{exp.}$ and N_{AISC} predictions

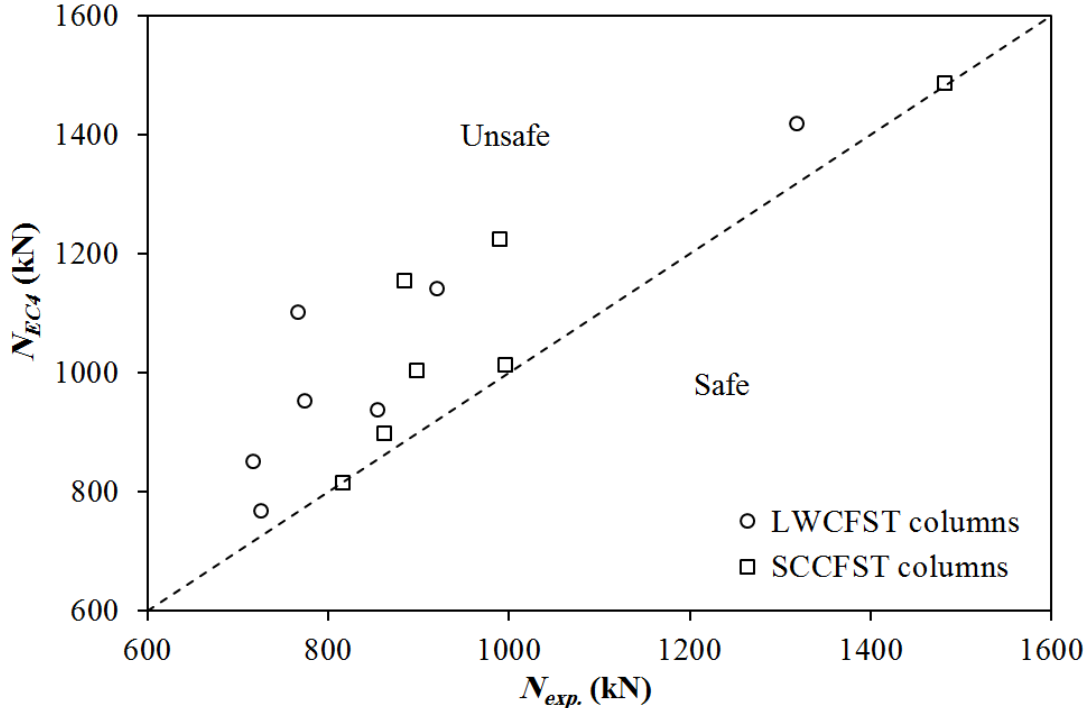

Figure 6.15 Comparison between $N_{exp.}$ and N_{EC4} predictions

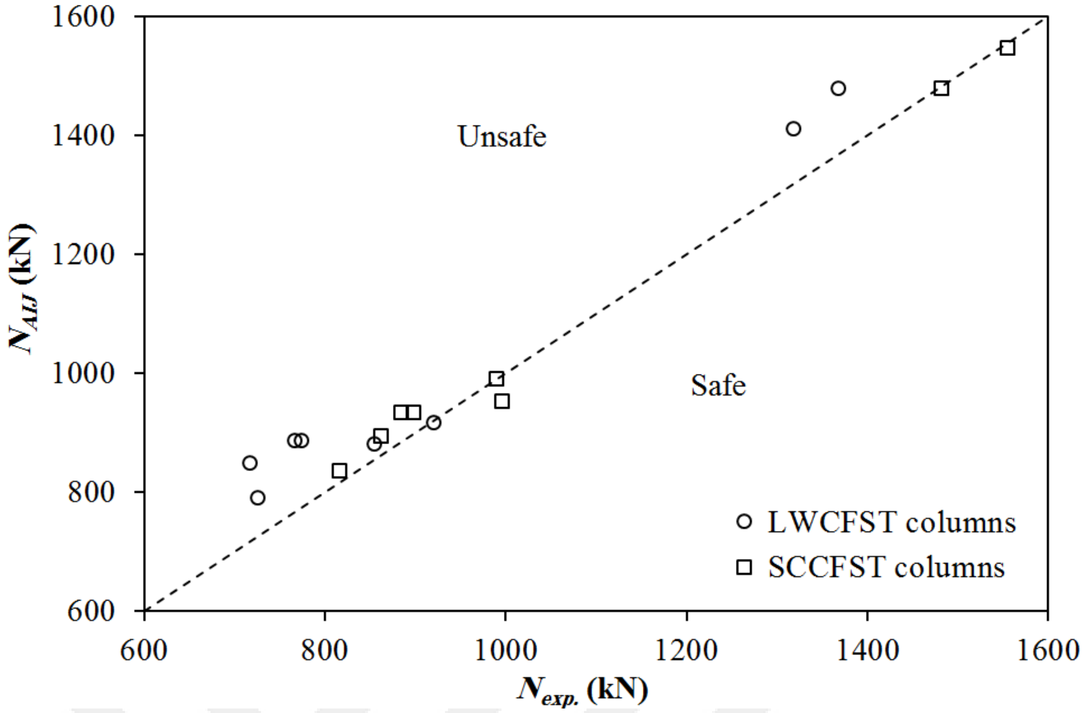

Figure 6.16 Comparison between $N_{exp.}$ and N_{AIJ} predictions

6.3 Summary and Conclusions

Composite structures used in multistory buildings, bridges piers, underground tunnels, subways stations, and towers, among other applications. These structures are designed to support different loading actions. CFST structural members have distinguishable characteristics compared to other structural members and even other composite structural members. Therefore, many studies about the response of CFST columns have been performed in the last decades. However, the majority of these studies treated steel tube columns filled with normal concrete. For this reason, as well as due to the wide use of CFST columns in civil engineering construction and to continue development of these constructions, further research must focus on others innovative types of concrete which offer superior engineering characteristics.

Lightweight aggregate concrete and self-compacted concrete are two innovative concrete types which provide excellent features for CFST column construction. Each material has advantages and disadvantages; therefore, this study tried to explore the appropriateness of using these materials in CFST columns.

To achieve this aim, sixteen hollow steel tubes columns, each filled with LWC or SCC, were tested to study the response of LWCFST and SCCFST columns subjected to axial compression loading. In the experimental study, four different *L/D* ratios were used to observe the behavior of the short, medium, and long columns, and three different *D/t* ratios were used. As reported by the results of testing, the following outcomes could be drawn:

- Both LWC and SCC exhibit properties significant to enhancing the behavior of structural members. The use of LWC causes a reduction in the self-weight of a structure and increases the strength to weight ratio. This merit of LWC is very important in heavy structures; in addition, the static, dynamic and thermal properties of the structures would also be improved. SCC, on the other hand, offers rheological properties that cause internal and external vibration to be canceled, and it can flow into place under its self-weight only. This ability is an advantage to the construction process, particularly for CFST because of the relatively small cross sections of the steel tubes.
- For short columns with an *L/D* ratio of 2, as expected, both LWCFST and SCCFST columns experienced local material failures. Short LWCFST columns offered less ductility and underwent sudden loss in loading after reaching compression capacity.
- For medium-length columns with an *L/D* ratio of 5, SCCFST showed a combined effect of local and overall failures. These were also observed in LWCFST, but local failure governed the behavior of those specimens.
- Among specimens with an *L/D* ratio of 7.5, those made with LWCFST exhibited the minimum effect of overall buckling, while local buckling followed by local concrete crushing were the dominant failure modes of such columns. LWCFST columns with an *L/D* ratio of 7.5 showed a less-severe loss in loading compared to those with *L/D* ratios of 2 and 5. On the other hand, all SCCFST column specimens experienced overall buckling failure modes with only a minimum effect of local failures.
- For long columns with *L/D* ratio of 10.5, SCCFST columns exhibit an overall buckling failure mode. Corroding LWCFST columns experienced interactions between local and overall buckling failure modes and showed smoother transition from the pre-peak to post-peak region.
- The major complication of using pumice lightweight aggregate in LWCFST columns is its structural weakness; its failure governed the collapse behavior

of columns that incorporated it, even long columns. This negative effect could be avoided either by reinforcement with steel bars, use of LWC reinforced with steel fibers, or by use of artificial lightweight aggregate with no or a less-porous structure.

- Among SCCFST columns, even long columns exhibited good composite action between steel tube and SCC; all columns had a strength index *SI* greater than one. This means SCC is an appropriate concrete type for use in CFST columns. LWCFST columns, though, only columns with *L/D* ratios equal to 5 and 7.5 offered acceptable composite action with *SI* index greater than one but still less than the *SI* offered by corresponding SCCFST columns. Long LWCFST column with *L/D* of 10.5 gave *SI* less than one; this behavior indicates that LWC is not suitable for use in long LWCFST columns.
- For LWCFST columns, the AISC360-16 design code gave the best prediction of compression capacity, with an average 2% conservative variation from the experimental results. For SCCFST columns, though, the AIJ2001 design code provided superior predictive power, with an average 1% unconservative variation from the experimental results. The EC4 design code offered predictions more conservative than experimental results, with averages of 21% and 12% for LWCFST and SCCFST columns, respectively.

CHAPTER 7

EXPERIMENTAL INVESTIGATION OF REINFORCED LIGHTWEIGHT AGGREGATE CONCRETE IN CFST COLUMNS

7.1 Introduction

Compared to reinforced concrete structures, the cross-section of CFST members is smaller, which markedly minimize their self-weight. Nonetheless, further minimization of the self-weight of CFST columns is of interest. The use of lightweight aggregate concrete to fill the hollow steel tube columns could reduce both the cross-section and self-weight of composite columns, leading to an improvement in their seismic performance and savings of construction time and cost (Fu *et al.*, 2011; Zhou *et al.*, 2017).

The use of LWC as a filling material for hollow steel tube columns could significantly enhance their characteristics beyond those of LWC-only columns (Fu *et al.*, 2011); moreover, the use of reinforced LWC in LWCFST columns should provide an even greater performance improvement for these composite columns.

Reinforced CFST columns are concrete-filled steel tubes with internal longitudinal reinforcement. This type of reinforcement is commonly used in piles, caissons, and bridge piers to improve strength and help connect them with other elements. In spite of widespread recognition of this approach as a structural engineering solution, few experimental studies have examined the performance of reinforced CFST columns (Roeder and Lehman, 2012; Moon *et al.*, 2013).

In reinforced CFST columns, the existence of the longitudinal steel reinforcement and lateral reinforcement works as a steel cage, causing an increase in the confinement effect on the concrete core.

The presence of the longitudinal steel reinforcement not only decreases crack propagation and reduces the risk of sudden loss of strength, it also improves the mechanical properties of the concrete core, such as its strength, toughness, and ductility. In addition, the fire resistance and seismic resistance of reinforced CFST columns are significantly increased (Kodur and Lie, 1995; Xiamuxi and Hasegawa, 2011, 2012; Hamidian *et al.*, 2016).

However, studies carried out by Endo *et al.* (2000), Xiamuxi and Hasegawa (2011, 2012), Hamidian *et al.* (2016) showed that the reinforced CFST columns have better compression capacity and greater toughness and ductility, in addition to improved anti-seismic response compared to CFST columns. The basic concept behind reinforced CFST is to combine the abilities of reinforced concrete columns and CFST columns; however, using steel-bar reinforcement may increase the difficulty of construction with reinforced CFST columns and increase its cost.

As mentioned in Chapters Two and Six, there have been numerous studies about LWCFST columns, though still fewer than those dedicated to normal CFST columns. In general, previous research dealt only with plain, unreinforced LWCFST columns. No studies have investigated the properties of steel-bar reinforced lightweight aggregate concrete-filled steel tube (RLWCFST) columns. Therefore, this study aimed to help fill this research gap by (1) exploring the properties and behavior of RLWCFST circular columns with three different *L/D* ratios, two different *D/t* ratios, and two different diameters of longitudinal steel bars; (2) comparing the response of RLWCFST columns to the corresponding LWCFST columns; and (3) investigating the appropriateness of the AISC360-16 and EC4 design codes, where these codes take the longitudinal reinforcement into consideration when predicting the compression capacity of LWCFST and RLWCFST columns.

7.2 Experimental Work

An experimental study was done to explore the performance of reinforced lightweight aggregate concrete-filled steel tube (RLWCFST) columns subjected to axial compression loading. Eighteen specimens were categorized into three groups according to their lengths; each group consisted of three specimens with the same thickness and three different reinforcement conditions.

7.2.1 Materials Properties

7.2.1.1 Steel

The steel tube specimens were prepared from a 6 m length of circular hollow steel tube; all steels were mild steel. Two different types of steel tubes with the cross-sections of 114.30×3.21 mm and 114.30×5.80 mm, respectively, were used to prepare RLWCFTS columns. Tensile coupon specimens were fabricated and tested according to the ASTME8/E8M-16 (2016) specification to determine the mechanical properties of the steel tubes. The longitudinal reinforcements were deformed steel bars with diameters of 8 or 12 mm, and the transverse reinforcements were deformed steel bars with a diameter of 5.5 mm. According to the ASTMA370−17a (2017), tensile test specimens were prepared and tested to determine the mechanical properties of the steel bars reinforcement. The mechanical properties of steel tube sections and steel reinforcing bar are summarized in Tables 7.1 and 7.2, respectively. The stress–elongation curves from tensile tests are shown in Figures 7.1–7.5.

Table 7.1 Mechanical properties of steel tube sections

Section (mm)	D (mm)	t (mm)	f_y (MPa)	f_u (MPa)	E_s (GPa)
114.3×3.21	114.3	3.21	465	520	200
114.3×5.80	114.3	5.80	440	513	200

Table 7.2 Mechanical properties of steel reinforcing bars

Steel bar	D (mm)	f_y (MPa)	f_u (MPa)	E_s (GPa)
Ø8	8	534	645	200
Ø12	12	470	586	200
Ø5.5	5.5	520	550	200

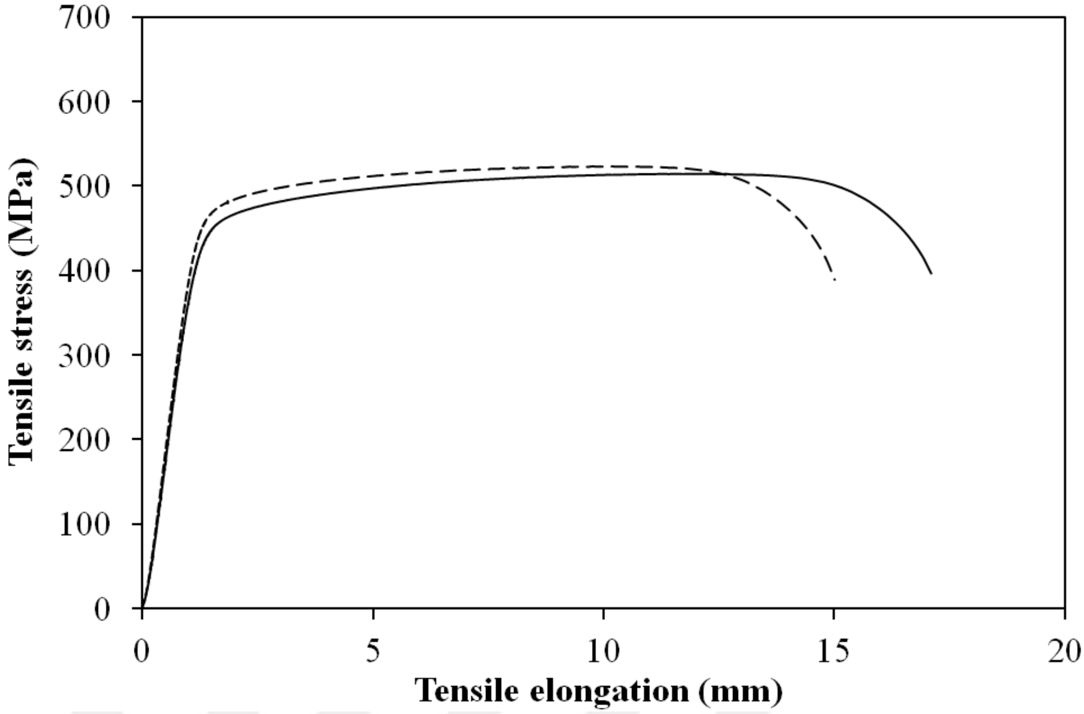

Figure 7.1 Coupon test stress–elongation curves for 114.3 × 3.21 mm

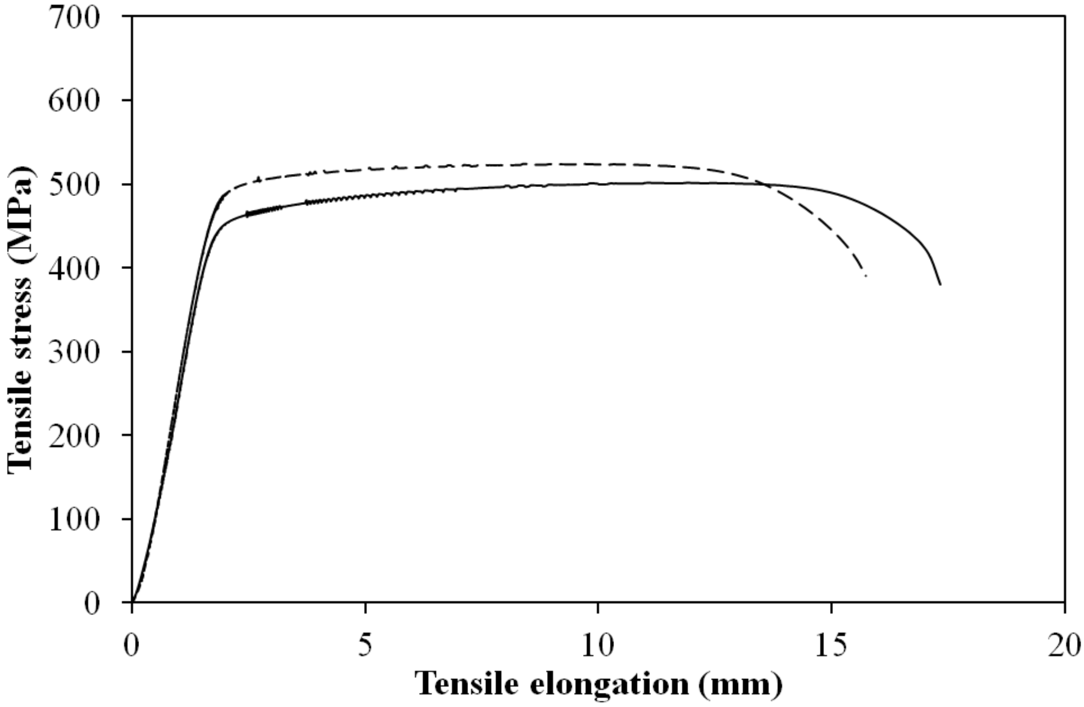

Figure 7.2 Coupon test stress–elongation curves for 114.3 × 5.80 mm

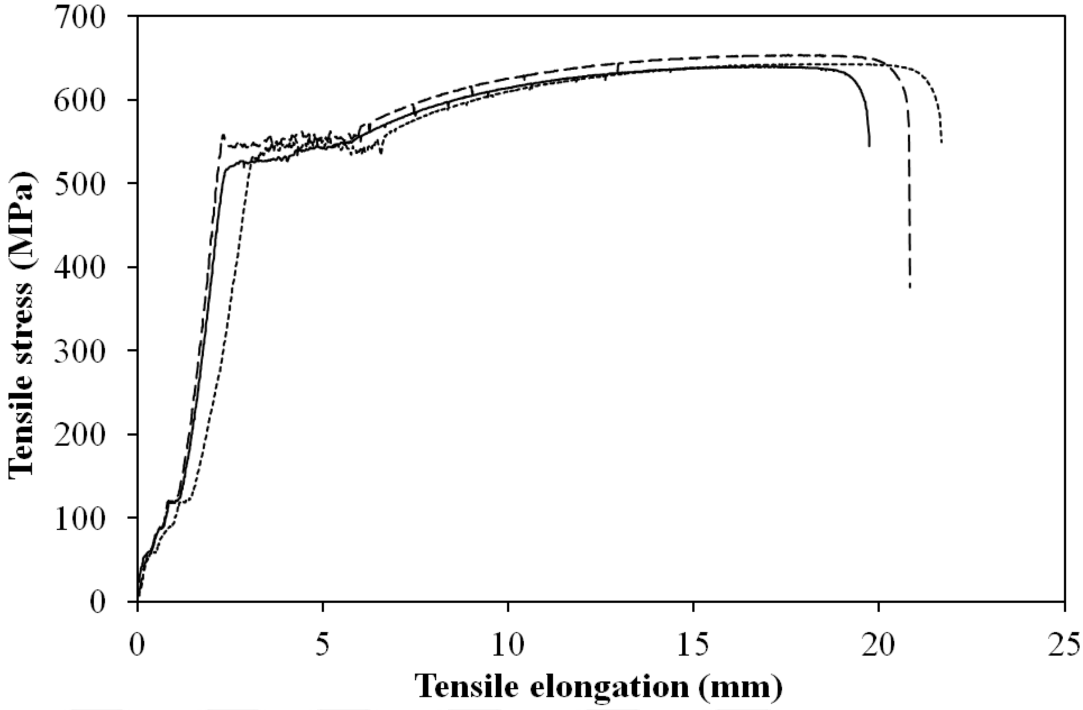

Figure 7.3 Coupon test stress-elongation curves for 8 mm steel bars

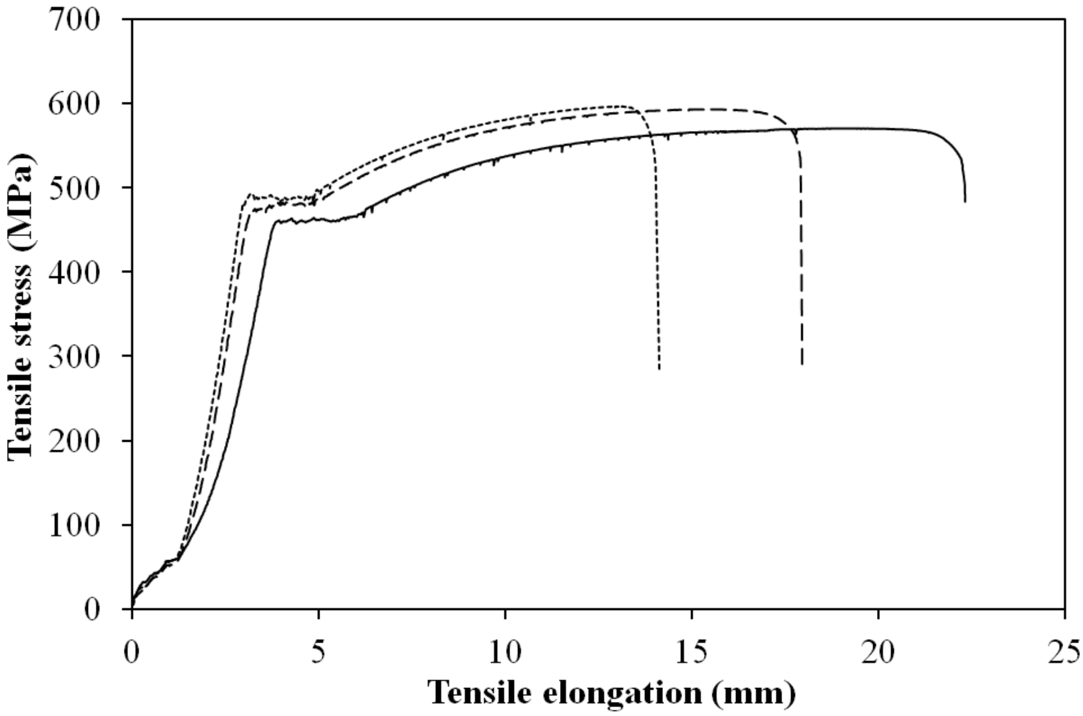

Figure 7.4 Coupon test stress–elongation curves for 12 mm steel bars

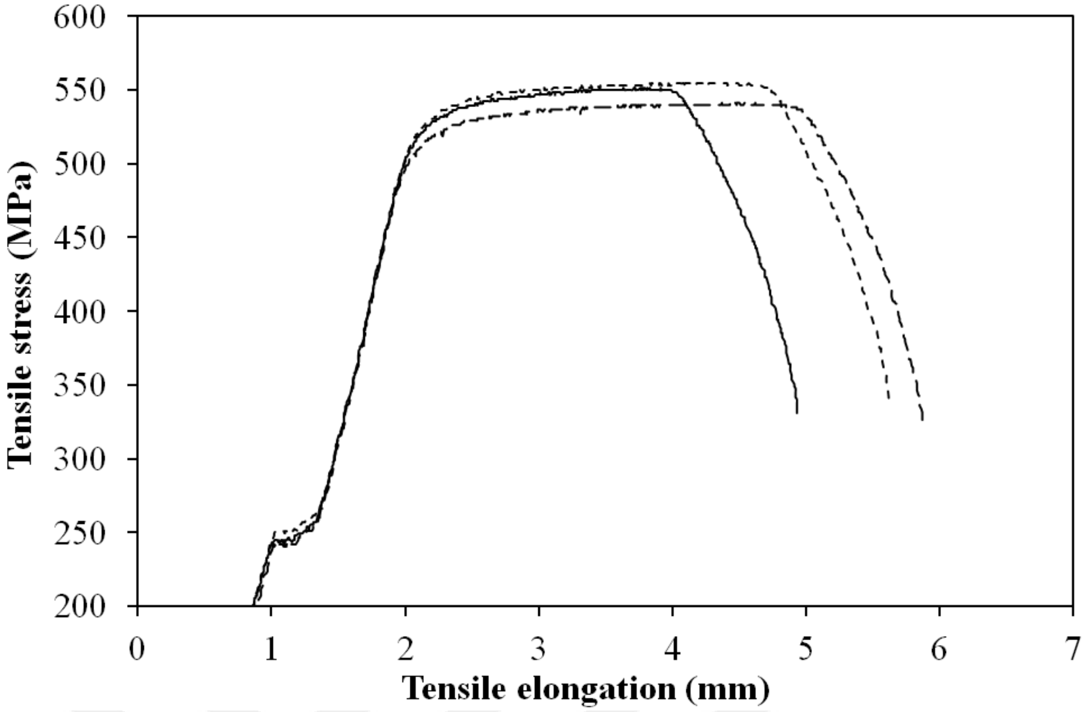

Figure 7.5 Coupon test stress–elongation curves for 5.5 mm steel bars

7.2.1.2 Lightweight Aggregate Concrete (LWC)

The pumice type used as lightweight aggregate in the manufacture of the LWC used has a maximum aggregate size of 10 mm. In order to create LWC with acceptable structural properties, the mix design of the LWC included cement, pumice LWA, water, silica fume (SF), fine crushed sand (CS), and hyperplasticizer (SP); Table 7.3 provides details about the LWC mix. The dry unit weight of LWC was 1753 kg/m^3. The standard cylinder specimens, 100×200 mm, were filled in three layers. After each layer, the concrete was carefully compacted to excrete entrapped air. After curing, concrete cylinder specimens were tested according to the ASTMC39/C39M-15 (2015) specification. According to the compression test, the average compressive strength of the LWC used was 30.58 MPa.

Table 7.3 LWC mix proportions

Mix proportions	Cement	SF	LWA	Water	CS	SP
Ratio	1	0.25	0.395	0.25	0.592	0.013

7.2.2 RLWCFST Specimens and the Testing Program

Due to the relatively small size of steel tube diameter, the tied type of reinforcement was used. Four longitudinal steel bars with diameters of 8 and 12 mm were used, and closed ties made with steel bars 5.5 mm in diameter were used to form transverse reinforcement with 60 mm between ties, as shown in Figure 7.6.

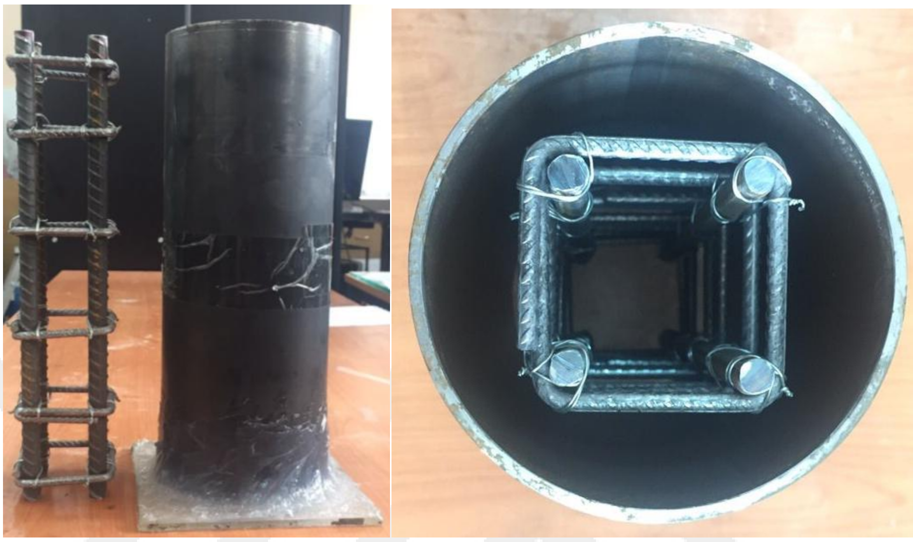

Figure 7.6 Reinforcement and steel tube for a specimen with *L/D* = 2.62

After completing the concrete pouring and curing processes, and the concrete surface of each column was leveled using high-strength epoxy. The RLWCFST column specimens were then ready for testing (Figure 7.7).

Specimens were accurately centered in the testing machine to cancel any opportunity of eccentric loading and inducing an associated bending effect. The testing machine capacity is 3000 kN; displacement-controlled loading at a rate of 0.5 mm/min was used for all column specimens and displacement transducers were installed to record the end shortening of the specimen. Compression loading against end shortening data was recorded for all specimens to allow discussion of column behavior in the pre- and post-collapse regions. Figure 7.8 shows a representative specimen during testing.

Figure 7.7 RLWCFST specimens

Figure 7.8 RLWCFST specimen testing

After preparation of the hollow steel tubes according to the test requirements, three different *L/D* ratios were selected to investigate the various types of failure performance. Each group consisted of two different thicknesses and LWC reinforced by two different types of steel bar in addition to the control specimen. Table 7.4 shows the properties of the tested RLWCFST columns. The specimen naming system included *L/D* ratio, *D/t* ratio, the diameter of longitudinal steel reinforcement bar. For example, the specimen name 2.62-35.60-C refers to an *L/D* ratio of 2.62, *D/t* ratio of 35.60, and control specimen (plain concrete core); specimen name 8.40-19.70-12mm, on the other hand, denotes an *L/D* ratio of 8.40, *D/t* of 19.70, and a 12 mm bar diameter.

Table 7.4 Properties of RLWCFST specimens

Specimen	*t* (mm)	D_{sr}* (mm)	*L* (mm)	*D/t*	*L/D*	f_y MPa	f_{ysr}** MPa
2.62-35.60-C	3.21	0	300	35.60	2.62	465	0.0
2.62-35.60-8mm	3.21	8	300	35.60	2.62	465	534
2.62-35.60-12mm	3.21	12	300	35.60	2.62	465	470
2.62-19.70-C	5.80	0	300	19.70	2.62	440	0.0
2.62-19.70-8mm	5.80	8	300	19.70	2.62	440	534
2.62-19.70-12mm	5.80	12	300	19.70	2.62	440	470
5.25-35.60-C	3.21	0	600	35.60	5.25	465	0.0
5.25-35.60-8mm	3.21	8	600	35.60	5.25	465	534
5.25-35.60-12mm	3.21	12	600	35.60	5.25	465	470
5.25-19.70-C	5.80	0	600	19.70	5.25	440	0.0
5.25-19.70-8mm	5.80	8	600	19.70	5.25	440	534
5.25-19.70-12mm	5.80	12	600	19.70	5.25	440	470
8.40-35.60-C	3.21	0	960	35.60	8.40	465	0.0
8.40-35.60-8mm	3.21	8	960	35.60	8.40	465	534
8.40-35.60-12mm	3.21	12	960	35.60	8.40	465	470
8.40-19.70-C	5.80	0	960	19.70	8.40	440	0.0
8.40-19.70-8mm	5.80	8	960	19.70	8.40	440	534
8.40-19.70-12mm	5.80	12	960	19.70	8.40	440	470

*D_{sr} longitudinal steel bar reinforcement diameter, **f_{ysr} longitudinal steel bar yield strength.

7.2.3 Test Results and Discussion

The results of testing six LWCFST columns and twelve RLWCFST columns are reported as end-shortening against compression loading curves, and failure modes are reported according to the effect of the geometrical and mechanical properties of the CFST column specimens.

7.2.3.1 End-Shortening Versus Compression Loading Curves

It is appropriate to address CFST columns according to their *L/D* ratio to control for the behavior of composite columns. According to the literature, columns with $L/D \leq 4$ are defined as short, while those with $L/D > 4$ are defined as long (Li *et al.*, 2015; Hoang and Fehling, 2017b).

In this study, columns were classified according to literature precedent and their failure patterns as short, medium, or long; short columns are susceptible to local materials failure, while long columns are susceptible to global or elastic buckling failure modes. Medium columns are columns that exhibited the combined effect of local material failure and global buckling failure; most columns tested fell in this range.

- **Compression behavior of short columns with *L/D* ratio equal to 2.62:**

Figure 7.9 shows the response of short specimens with *L/D* equal to 2.62. The improvement in compression capacity is evident between the control specimens and the reinforced specimens, and the difference increases as the area of reinforcement increases. The post-peak behavior also differed between thin specimens (*D/t* = 35.60) and thick specimens (*D/t* = 19.70). Thin control and reinforced specimens showed a sudden reduction in compression loading after reaching their compressive capacity. This behavior was a result of the structural weakness of the lightweight aggregate and the contribution of the *D/t* ratio. The presence of steel reinforcement could not prevent this discharge in capacity, but it did make it more smooth and gradual. For thick specimens, the contribution of steel tube thickness was clear; there was no sudden loss in compression loading in addition to the increase in compression capacity of the specimen. However, all reinforced specimens showed an increase in initial stiffness compared to control specimens.

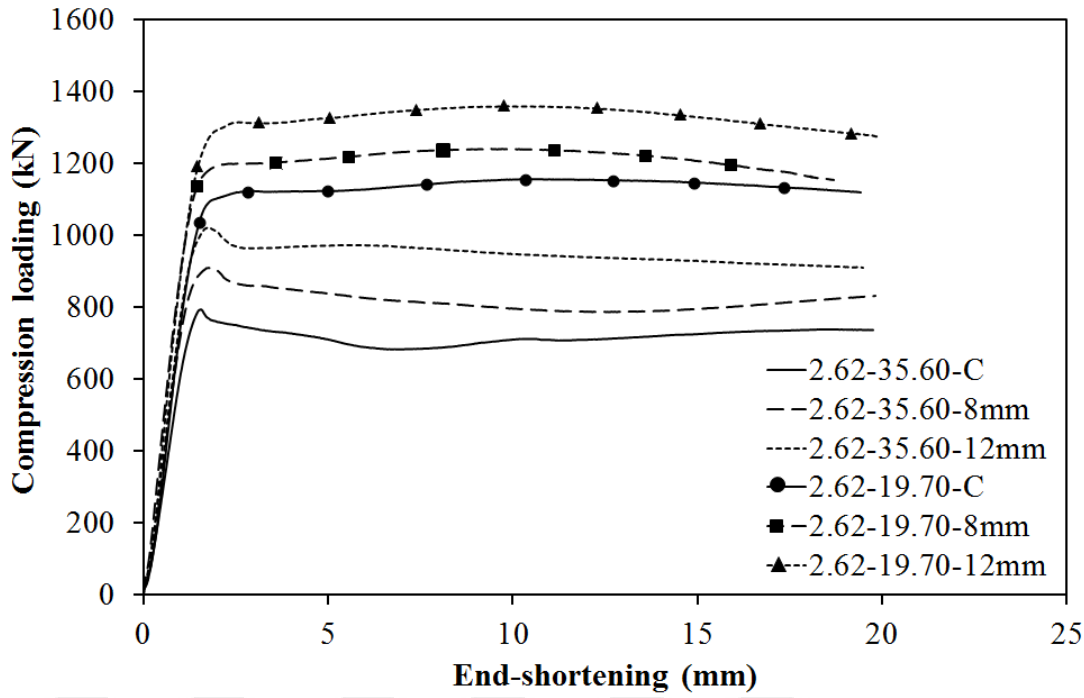

Figure 7.9 Load–shortening curves for columns with *L/D* = 2.62

- **Compression behavior of columns with *L/D* ratio equal to 5.25:**

Figure 7.10 presents the response of medium columns (*L/D* = 5.25). Their behavior is a combination of that of short and long columns. Among thin specimens (*D/t* = 35.60), specimen (5.25-35.60-C) showed a sudden loss in loading after reaching its compressive capacity, while reinforced specimens (e.g. 5.25-35.60-8mm, and 5.25-35.60-12mm) exhibited no such sudden reduction in loading. This difference in behavior reveals the impact of both *L/D* ratio and reinforcement on the column's response: for the control column, its *L/D* ratio governed its behavior, which was similar to that of its counterpart short columns (*L/D* = 2.62). For reinforced specimens, though, the steel reinforcement governed their behavior, increasing compression capacity and changing the failure modes by improving the mechanical properties of the LWC; no improvement in the initial stiffness was observed for these specimens. For thick specimens (*D/t* = 19.7), the initial stiffness of reinforced specimens was higher, and the contribution of both steel tube thickness and reinforcement is clear in the responses of these columns.

- **Compression behavior of columns with *L/D* ratio equal to 8.40:**

Long columns (*L/D* = 8.40) exhibited an increase in initial stiffness and compression capacity when the area of steel reinforcement was increased for both thin and thick specimens (Figure 7.11). The behavior of the thin specimens was similar to that of counterpart specimens in previous groups, where local material failure controlled, leading to a smoother reduction in load after reaching peak load. There was no sudden reduction in loading for thick specimens, and they exhibited a smoother transition from the pre-peak to the post-peak region. Column length governed this behavior, which differed markedly from the behavior of columns in the short and medium groups.

7.2.3.2 Failure Modes

The failure modes of RLWCFST columns are arranged for easy comparison according to *L/D* ratio.

- **Failure modes of RLWCFST columns with *L/D* ratio equal to 2.62:**

The failure modes of RLWCFST columns with *L/D* equal to 2.62 are illustrated in Figure 7.12. The typical failure mode for these columns was local materials failure. Specimens with *D/t* equal to 35.60 showed more characteristics of local failure in contrast to specimens with *D/t* = 19.70. The steel reinforcement bars governed the failure behavior for specimens with *D/t* of 35.60, as shown in Figures 7.12a–c. For the unreinforced specimen, an elephant foot buckling mode was observed. Reinforced specimens showed a different failure mode; diagonal cracks formed in these columns, where the concrete core was under two confinement effects: from the steel tube and from transverse steel. The difference in failure modes between control and reinforced specimens explains the difference in the transition from pre-peak to post-peak regions for these specimens, as shown in Figure 7.9. However, the behavior was different for specimens with *D/t* = 19.70, as shown in Figures 7.12d–f, where the thickness of the steel tubes controlled the failure mode. All of these specimens showed similar failure modes, as shown by their compression loading curves (Figure 7.9).

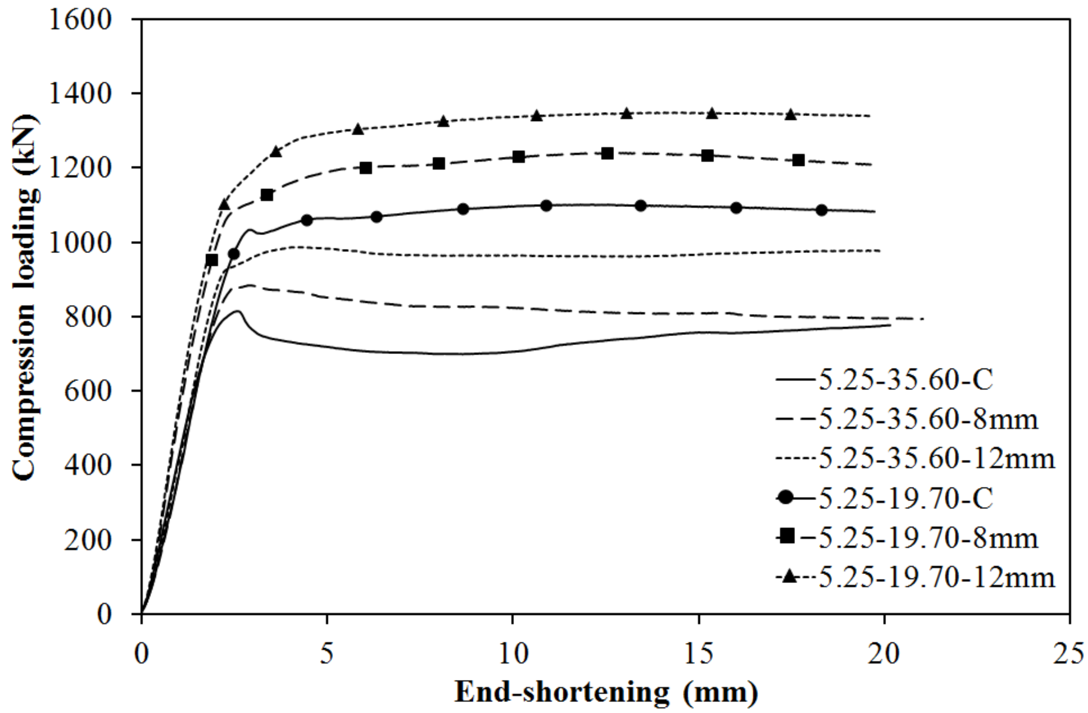

Figure 7.10 Load–shortening curves for columns with *L/D* = 5.25

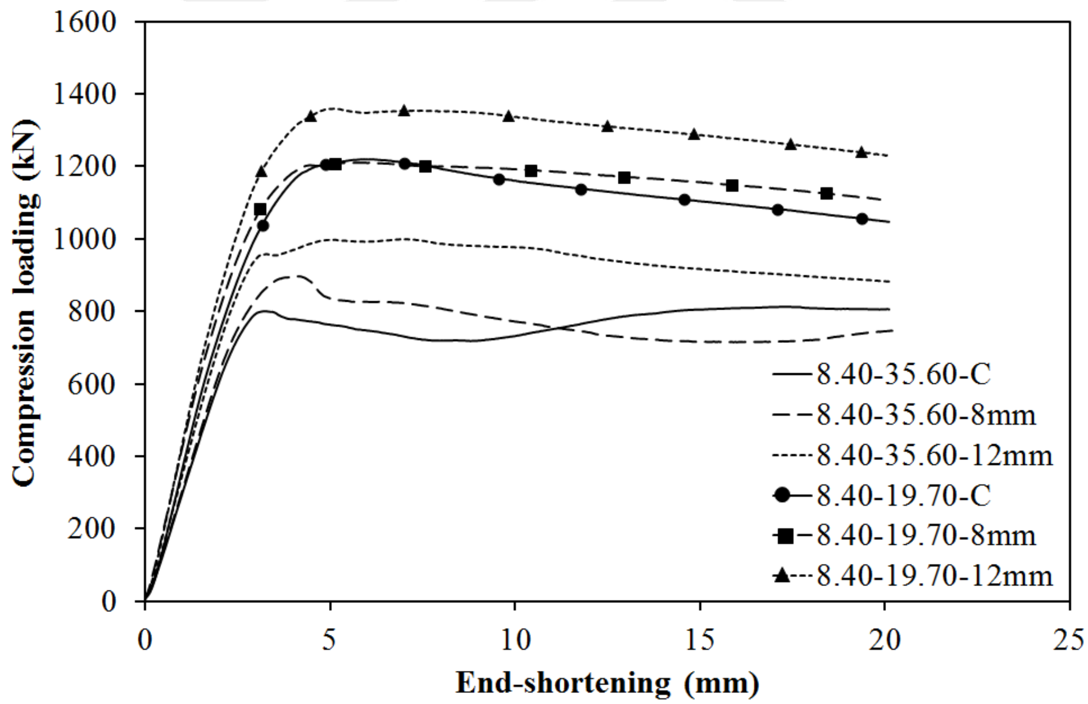

Figure 7.11 Load–shortening curves for columns with *L/D* = 8.40

- **Failure modes of RLWCFST columns with *L/D* ratio equal to 5.25:**

The failure modes of the RLWCFST specimens with *L/D* ratio of 5.25 are shown in Figure 7.13. Local material failure still governed the failure modes of the control specimen (Figure 7.13a), and this behavior explained the sudden reduction in loading after peak load was reached (Figure 7.10). The reinforced specimens showed a diagonal crack in the concrete core (Figures 7.13b, c) in addition to overall buckling without a sudden reduction in the loading (Figure 7.10). For the specimens with *D/t* = 19.70, the control specimen also showed local material failure, differing from that of the control specimen with *D/t* = 35.6 (5.25-35.60-C). The reinforced specimens, though, showed both local buckling and overall buckling. Medium specimens exhibited a combination of the features of short and long specimens; both materials failure and geometric instability were in evidence.

- **Failure modes of RLWCFST columns with *L/D* ratio equal to 8.40:**

Figure 7.14 shows the failure modes of long specimens. For specimens with *D/t* = 35.60, local buckling controlled. It also controlled the failure behavior of the control specimen (8.40-35.60-C), as shown in Figure 7.14a. However, local and global buckling occurred in reinforced specimens (Figures 7.14b, c). Even in the presence of steel reinforcement, as a result of the porous structure of lightweight aggregate, the LWC core was not able to provide full support to the steel tube. Thus, local crushing of lightweight aggregate occurred before the column reached its compression capacity. On the other hand, all thick specimens (*D/t* = 19.70) demonstrated the global buckling; the control specimen (8.40-19.70-C, Figure 7.14d) showed greater global bucking than reinforced specimens (Figures 7.14e, f).

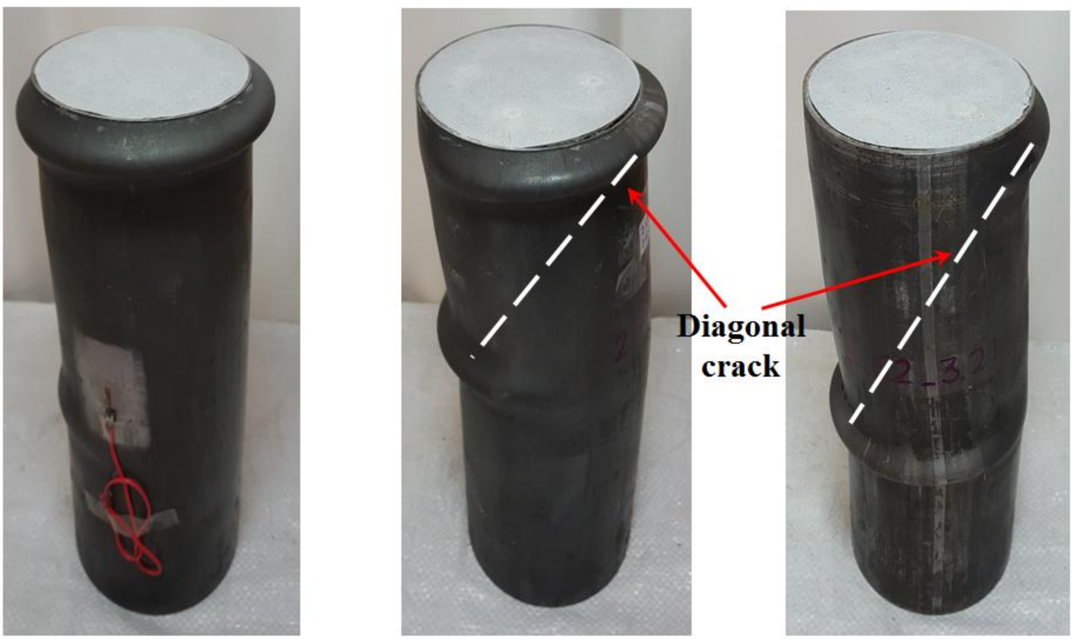

(a) 2.62-35.60-C (b) 2.62-35.60-8mm (c) 2.62-35.60-12mm

(d) 2.62-19.70-C (e) 2.62-19.70-8mm (f) 2.62-19.70-12mm

Figure 7.12 Failure modes of short columns

(a) 5.25-35.60-C (b) 5.25-35.60-8mm (c) 5.25-35.60-12mm

(d) 5.25-19.70-C (e) 5.25-19.70-8mm (f) 5.25-19.70-12mm

Figure 7.13 Failure modes of medium columns

(a) 8.40-35.60-C (b) 8.40-35.60-8mm (c) 8.40-35.60-12mm

(d) 8.40-19.70-C (e) 8.40-19.70-8mm (f) 8.40-19.70-12mm

Figure 7.14 Failure modes of long columns

7.2.3.3 Performance Indices

The presence of longitudinal steel reinforcement not only decreased crack propagation and prevented sudden strength loss, but also appeared to enhance the mechanical properties of the concrete core, such as its strength and ductility. In addition, the fire resistance of similarly reinforced CFST columns increases significantly (Kodur and Lie, 1995; Hamidian *et al.*, 2016). In this section, some derived performance indices such as toughness (energy absorption), ductility index (*DI*), compression capacity improvement index (*CI-I*), and *DI* improvement (*DI-I*) were calculated to examine the impact of various factors on the response of RLWCFST columns; the results are summarized in Table 7.5. *DI* was calculated using Equation 7.2:

$$DI = \frac{\Delta_{85\%}}{\Delta_{exp.}} \tag{7.1}$$

where $\Delta_{exp.}$ is the end-shortening at the maximum compression loading and $\Delta_{85\%}$ is the end-shortening when the compression loading falls to 85% of the maximum load. Note that when the loading failed to capture 85% of N_{exp}, $\Delta_{85\%}$ was considered the final value of end-shortening.

$$CI - I = \frac{N_{RLWCFST} - N_{LWCFST}}{N_{LWCFST}} \times 100 \tag{7.2}$$

$$DI - I = \frac{DI_{RLWCFST} - DI_{LWCFST}}{DI_{LWCFST}} \times 100 \tag{7.3}$$

Table 7.5 Summary of results for RLWCFST columns

Specimen	α	$N_{exp.}$ (kN)	$\Delta_{exp.}$ (mm)	*CI-I* (%)	χ (kN·mm)	*DI*	*DI-I* (%)
2.62-35.60-C	0.00	793.91	1.56	----	13710.97	3.06	----
2.62-35.60-8mm	11.75	910.31	1.76	14.66	15714.84	4.06	32.80
2.62-35.60-12mm	23.29	1021.97	1.73	28.73	17806.67	5.60	83.06
2.62-19.70-C	0.00	1154.95	10.35	----	20929.54	6.22	----
2.62-19.70-8mm	12.97	1239.44	9.31	7.32	21494.17	6.50	4.46
2.62-19.70-12mm	25.70	1359.94	9.87	17.75	25105.67	6.78	8.93
5.25-35.60-C	0.00	814.54	2.58	----	13841.37	3.31	----
5.25-35.60-8mm	11.75	884.48	2.87	8.45	16162.65	4.18	26.27
5.25-35.60-12mm	23.29	986.06	4.11	20.91	17904.04	4.93	48.72
5.25-19.70-C	0.00	1102.74	12.56	----	19660.87	3.20	----
5.25-19.70-8mm	12.97	1239.05	12.71	12.36	22222.50	3.28	2.43
5.25-19.70-12mm	25.70	1349.25	14.26	22.35	23925.76	3.32	3.62
8.40-35.60-C	0.00	812.05	17.29	----	14290.77	1.16	----
8.40-35.60-8mm	11.75	897.94	4.13	10.58	14396.25	1.94	66.60
8.40-35.60-12mm	23.29	998.57	6.99	22.97	17440.52	2.43	108.58
8.40-19.70-C	0.00	1219.64	5.90	----	20603.60	2.62	----
8.40-19.70-8mm	12.97	1209.42	5.89	0.00	21262.11	3.38	28.98
8.40-19.70-12mm	25.70	1361.35	5.12	11.62	23693.07	3.53	34.75

As shown in Table 7.5, the end-shortening ($\Delta_{exp.}$) results for specimens with *D/t* = 19.70 offer more plastic behavior before reaching their compression capacity compared to specimens with *D/t* = 35.60, which experience little plastic behavior before reaching their compression capacity. It is also apparent that compression capacity and initial stiffness improved with an increase in tube thickness; this behavior was observed for all specimens except one, 8.40-35.60-C.

Toughness, or energy absorption (χ), is known as the capacity of material to absorb energy in the plastic region up to rupture, where its contribution to the ductility of a structure is significant. Toughness can be estimated by calculating the area under a stress–strain or load–deformation curve up to a specified deformation value (Ezeldin and Balaguru, 1992; Chao *et al.*, 2012). In this study, numerical calculations using the trapezoidal rule formula were used to estimate the toughness of composite column specimens up to a specific value of end-shortening, as shown in Table 7.5. The area under the compression loading curve increased with an increase in the area of steel reinforcement. The specimen (2.62-19.70-12mm) gives the maximum toughness value, and as the results of compressive capacity, the reinforced specimens with *D/t* = 35.60 presented a higher toughness improvement ratio than the reinforced specimens with *D/t* = 19.70.

For a more meaningful measurement of the effect of the reinforcement ratio and the *D/t* ratio on the performance of composite columns, the steel-bar contribution (α) was considered. The value of α represents the steel-bar reinforcement ratio ($\rho = A_{sr}/A_c$) multiplying by the corresponding yield strength (f_{yr}); α changes with tube thickness and the yield strength of the steel-bar. Each steel-bar diameter (8mm and 12mm) has two different values of α due to the change in *D/t* ratio (Table 7.5).

The compression capacity of reinforced specimens is greater than that of the unreinforced or control specimens. Figure 7.15 shows the effect of steel-bar contribution (α) on the compression capacity improvement index (*CI-I*) for short, medium, and long columns. The contribution of steel-bar reinforcement had a significant effect on the improvement in compression capacity, and this effect differed according to the *L/D* ratio; among short columns, those with *D/t* = 35.60 ($\alpha = 11.75$ and 23.29) recorded a higher compression capacity improvement compared to columns with *D/t* = 19.70 ($\alpha = 12.97$ and 25.70), Figure (7.15a). This means that steel bar reinforcement had a significant impact on compression capacity for short columns with thin steel tubes where the dominant failure mode was material failure.

This behavior was different for medium columns, which presented a combination of the behavior of short and long columns. Medium columns with *D/t* = 19.70 recorded higher compression capacity than those with *D/t* = 35.60 (Figure 7.15b). These specimens exhibited a combined failure mode, as described in Section 7.2.3.2.

Among long columns, specimens with D/t = 35.60 again gave higher compression capacity improvement than specimens with D/t = 19.70. Geometric failure was the major failure mode of these specimens.

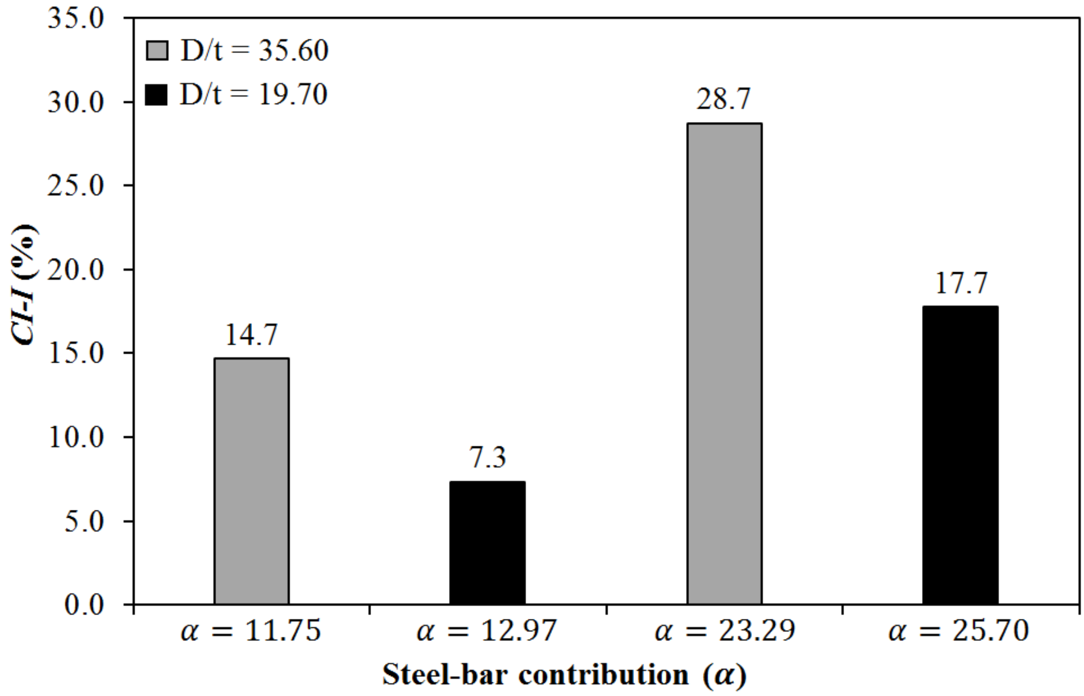

(a) Steel bar contribution (α) versus *CI-I* with *L/D* = 2.62

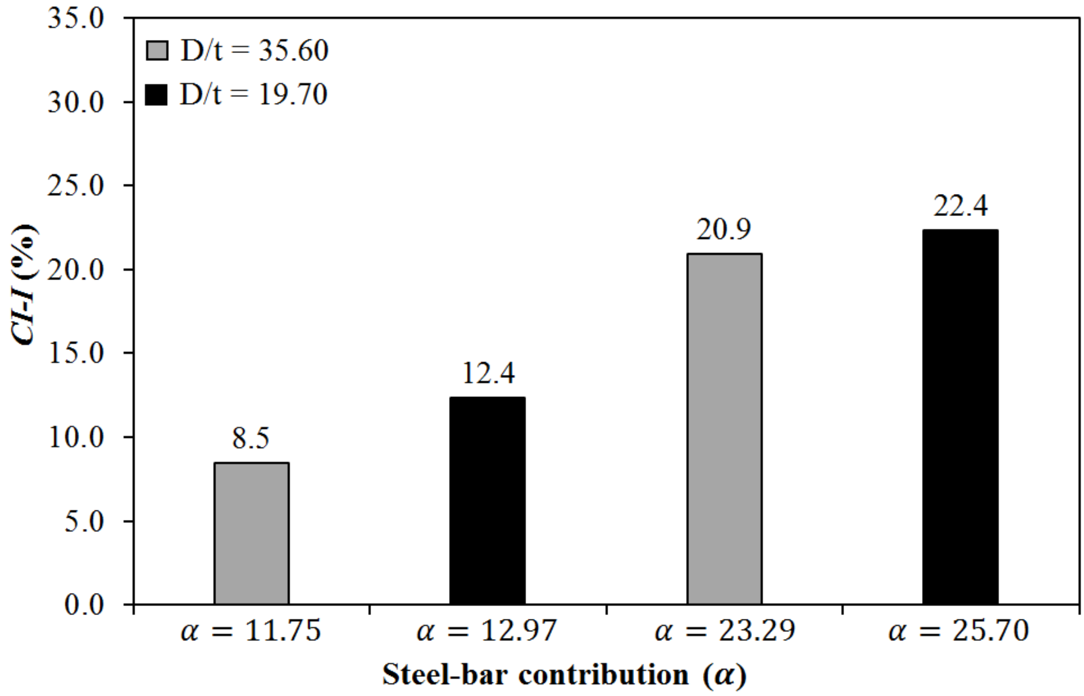

(b) Steel bar contribution (α) versus *CI-I* with *L/D* = 5.25

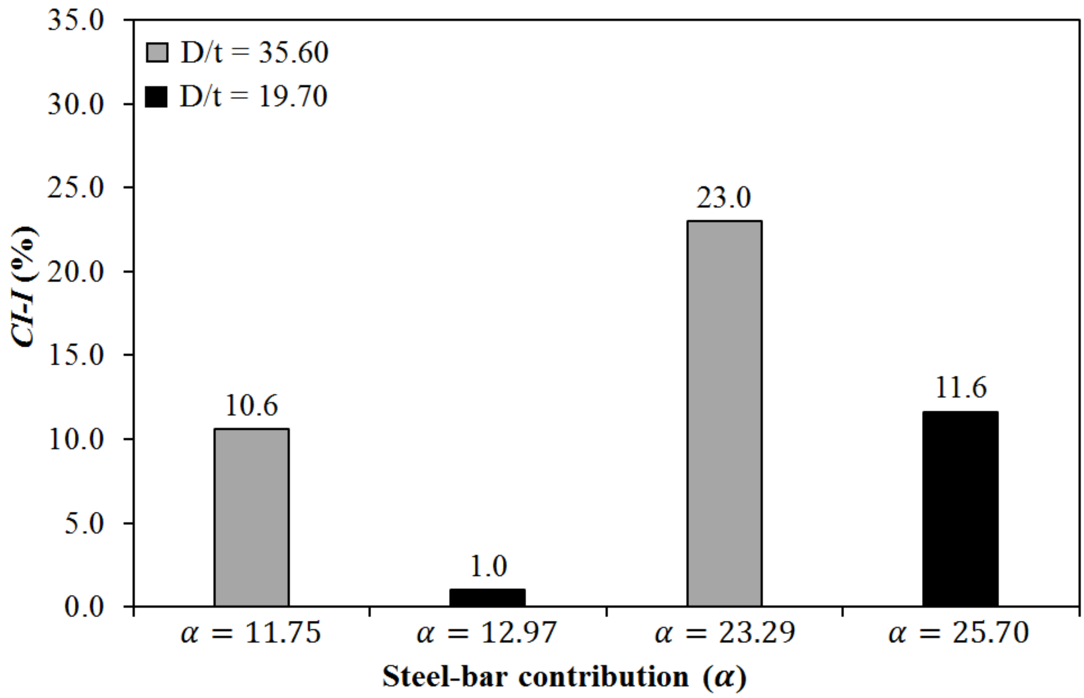

(c) Steel bar contribution (α) versus *CI-I* with *L/D* = 8.40

Figure 7.15 Steel bar contribution (α) versus *CI-I*

As shown in Figure 7.15 and Table 7.5, short specimens with *L/D* = 2.62 had a higher compression capacity improvement index (*CI-I*) than the corresponding medium-length (*L/D* = 5.25) and long (*L/D* = 8.40) specimens with *D/t* = 35.60. Medium-length specimens showed higher improvement in compression capacity than short and long specimens.

Ductility index *DI*, as mentioned before, is used to estimate the ability of the member to undergo large deformations beyond its elastic limit. As presented in Table 7.5, if compared within the same group, such as unreinforced specimens with the same *L/D* ratio, *DI* increases when *D/t* decreases. *DI* also improves for reinforced specimens compared to unreinforced specimens with the same *D/t* ratio, and increases when steel bar diameter increases. It worth noting that reinforced specimens with *D/t* = 35.60 showed a significant increase in ductility index improvement (*DI-I*) compared to reinforced specimens with *D/t* = 19.70, and this improvement was higher for larger steel-bar contribution, α (Figure 7.16 and Table 7.5).

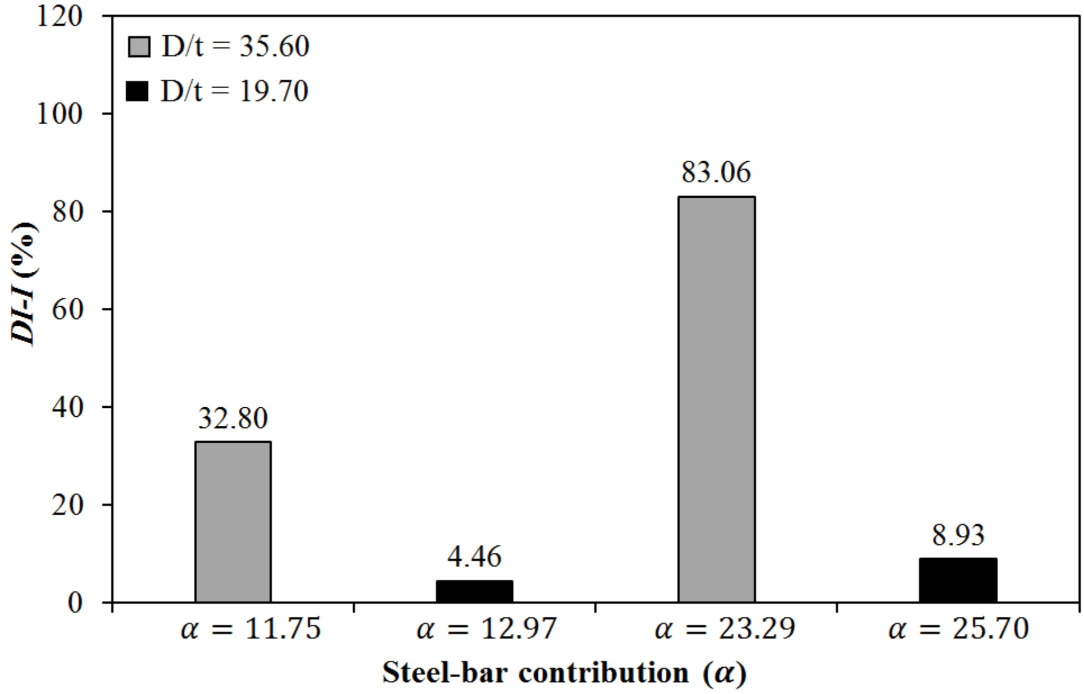

(a) Steel bar contribution (α) versus *DI-I* with *L/D* = 2.62

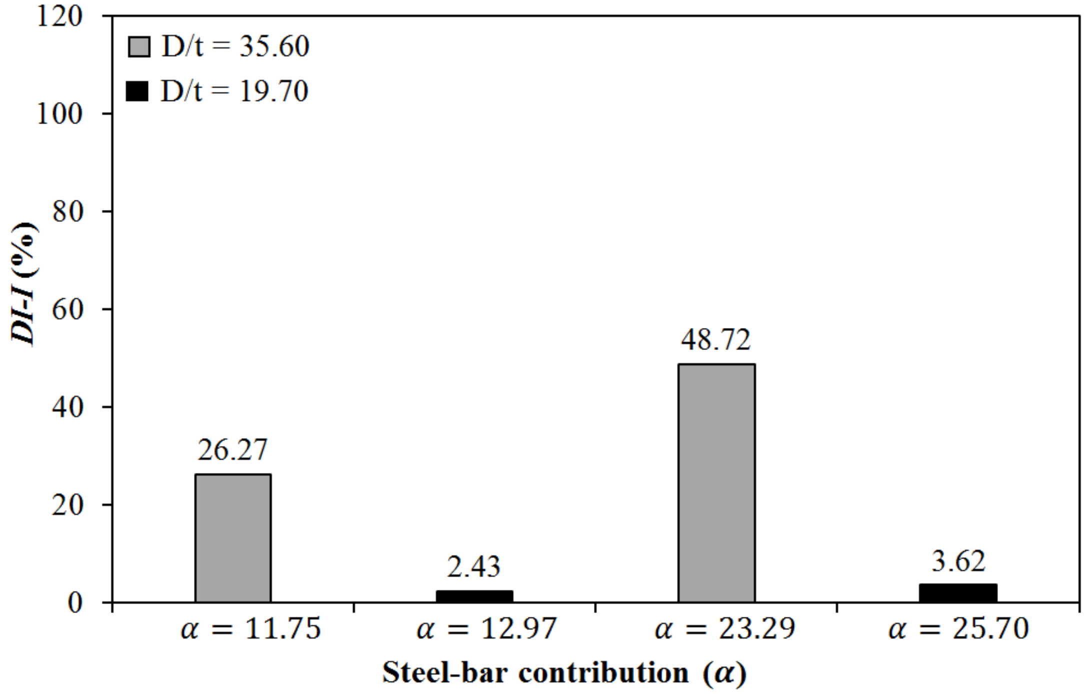

(b) Steel bar contribution (α) versus *DI-I* with *L/D* = 5.25

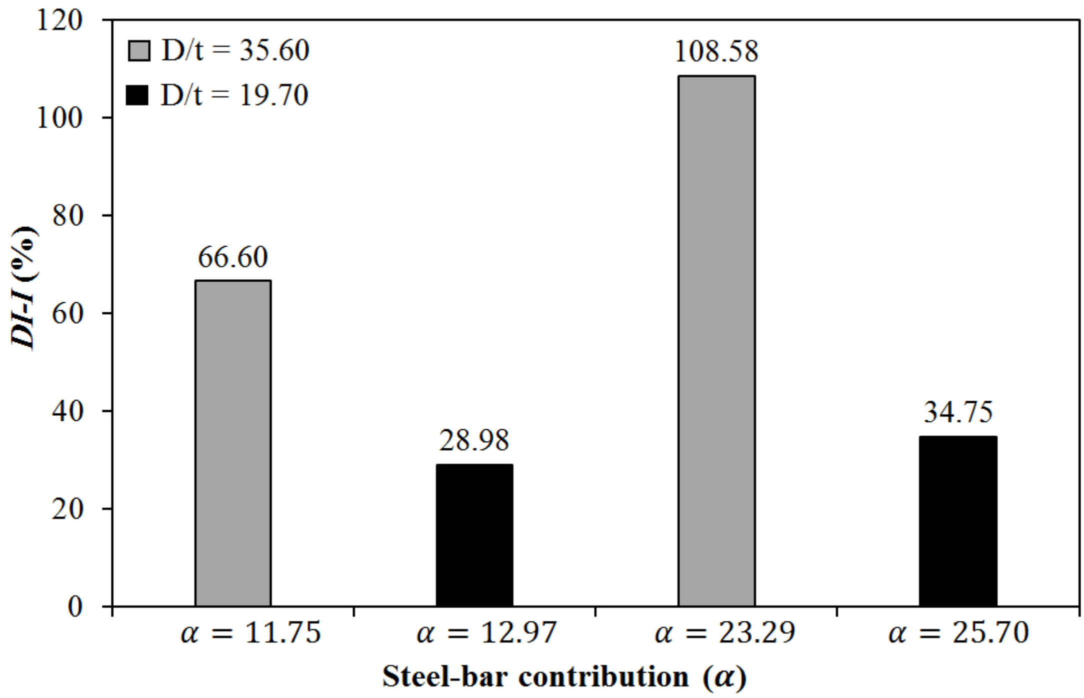

(c) Steel bar contribution (α) versus *DI-I* with *L/D* = 8.40

Figure 7.16 Steel bar contribution (α) versus *DI* improvement

Furthermore, the *D/t* ratio also affected the ductility index for columns with the same *L/D* ratio. Figure 7.17 shows the relation between steel bar contribution (α) and ductility index (*DI*) for specimens with *D/t* = 35.60 and *D/t* = 19.70. It is significant to note that the behavior of medium specimens changed according to their *D/t* ratio. Specimens with *D/t* = 35.60 behaved as short columns (Figure 7.17a), while specimens with *D/t* = 19.70 behaved as long specimens (Figure 7.17b). However, the ductility increased as the steel bar contribution increased for all specimens.

The use of thick steel tubes is a good choice to increase the compression capacity of the CFST columns, but it isn't always the most economical choice. For the reinforced concrete specimens, the concrete core was under the confinement of both steel reinforcement and the outer steel tube. Therefore, the presence of steel bar reinforcement enhanced the compression capacity of CFST columns, improving the mechanical properties of the concrete core. This behavior was especially marked for medium-length columns (*L/D* = 5.25, Figure 7.10) where the presence of steel bars precluded the sudden loss of loading for thin specimens. But as mentioned before, there are some difficulties involved in using a reinforced concrete core, such as an increase in the self-weight of the composite column in addition to the difficulties of pouring concrete in a steel tube with relatively small dimensions. These factors encourage the use of a high-performance concrete, such as self-compacted lightweight aggregate concrete.

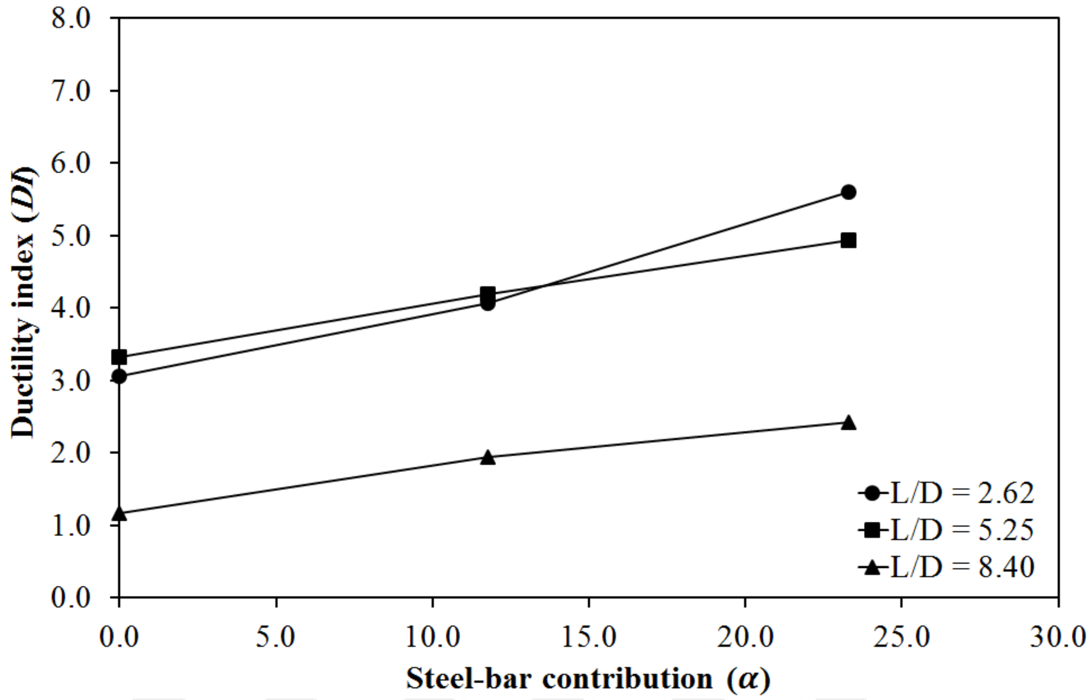

(a) Steel bar contribution versus *DI* with *D/t* = 35.60

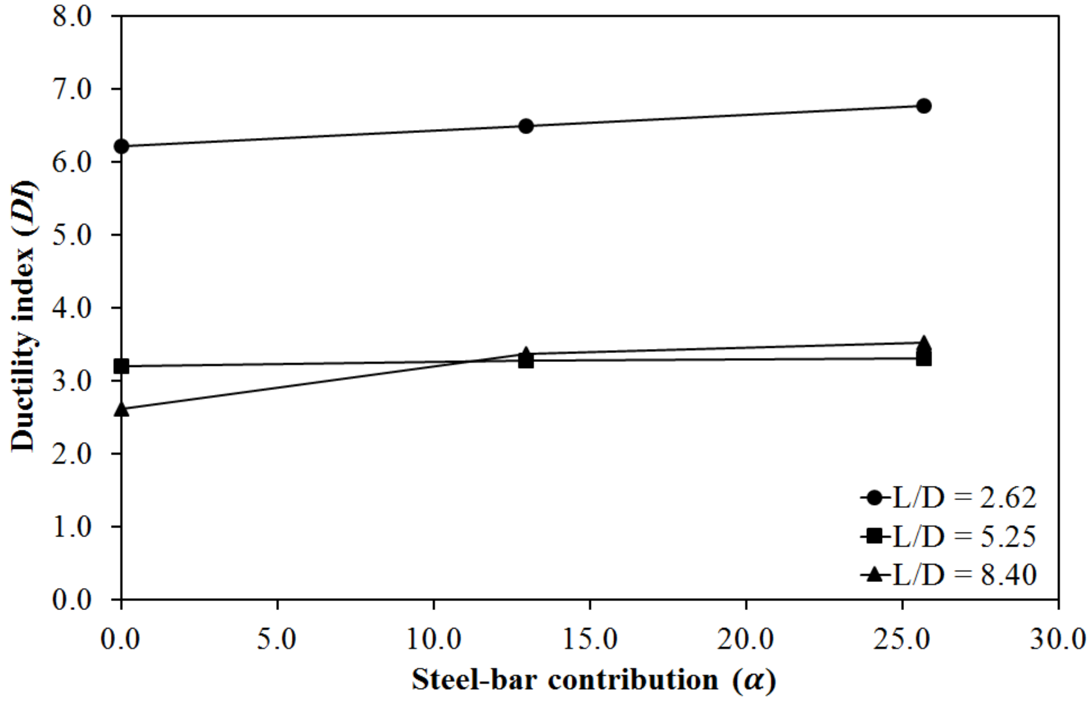

(b) Steel bar contribution versus *DI* with *D/t* = 19.70

Figure 7.17 Steel-bar contribution (α) versus ductility index (*DI*)

7.2.4 Design Specifications Predictions Versus Experiments Results

Many design specifications have been suggested to determine the capacity of CFST columns. ANSI/AISC360-16 (2016) and Eurocode4 (2004) are the design specification methods employed to perform some assessments for comparison with the experimental results of this study. These specifications consider the effect of longitudinal steel reinforcement in their calculations (*for details about the calculations see Chapter Three*).

The formulations of AISC360-16 and EC4 consider the impact of the longitudinal steel reinforcement on the capacity of CFST columns, where there is no effect of transverse reinforcement. However, in reality the confinement of the concrete core increases due to transverse reinforcement in addition to the confinement offered by the steel tube. Comparisons between the experimental results and design specifications predictions are presented in Table 7.6. Such comparisons are important to create a basis for design, especially because these specifications do not have a direct focus on columns constructed using LWC.

The error ratio ($N_{code}/N_{exp.}$) of the predicted results was calculated as described in Chapter Five (Equation 5.8) and Chapter Six. An error ratio less than one represents a conservative prediction on the safe side, while error ratio greater than one represents an overestimate, a prediction on the unsafe side.

For the AISC 360-16 specification, the ratio between design specification predictions and the experimental results ranged from 0.87 to 0.99, with a total average of 0.92. These results are conservative predictions, and the predictions of AISC360-16 specification are acceptable for RLWCFST columns with an average 8% difference on the safe side from experimental results. AISC360-16 also provided conservative predictions for short, medium, and long columns, with averages of 0.94, 0.94, and 0.90, respectively, all estimates on the safe side. However, the effect of the column's length is different between both design codes; this difference has an effect on calculation of compression capacity and the confinement effect. These variations are close to each other, as evidenced by the small standard deviation of AISC360-16 predictions (Table 7.6).

For predictions using EC4, the ratio between design specification predictions and the experimental results ranged between 0.94 and 1.35 with a total average of 1.13. The EC4 predictions are unconservative on average by 13%. However, the results of EC4 were different for short, medium, and long columns, with averages of 1.29, 1.14, and 0.97, respectively. The predictions for both short and medium specimens were unconservative, meaning that EC4 overpredicted by an average of 14% for short columns and 29% for medium columns. For long specimens it gave conservative predictions, on average 3.0% on the safe side. These variations are due to the effect of relative slenderness or the length influence on the confinement behavior, in addition to the mechanical and geometrical properties of composite section. These variations are clear in the high value of total standard deviation of EC4 predictions (Table 7.6).

These behaviors for both AISC360-16 and EC4 can be seen in Figures 7.18 and 7.19, which represent the comparison between the experimental results and the estimations of AISC360-16 and EC4, respectively. The data located above the equality line represent unsafe predictions. As shown in Figure 7.18, all predictions of AISC360-16 for short, medium, and long columns fell on the safe side. The margin of safety was especially large for long columns. Figure 7.19 shows the different behavior for EC4 predictions. There, the predictions for short and medium columns were located in the unsafe region, while the predictions for long columns fell in the safe region and gave a smaller standard deviation (Table 7.6).

Table 7.6 Experimental results compared with predictions of codes

Specimen	$N_{exp.}$ (kN)	$N_{AISC}/N_{exp.}$	$N_{EC4}/N_{exp.}$
2.62-35.60-C	793.91	0.99	1.35
2.62-35.60-8mm	910.31	0.93	1.27
2.62-35.60-12mm	1021.97	0.90	1.21
2.62-19.70-C	1154.95	0.96	1.34
2.62-19.70-8mm	1239.44	0.94	1.31
2.62-19.70-12mm	1359.94	0.91	1.24
5.25-35.60-C	814.54	0.95	1.15
5.25-35.60-8mm	884.48	0.94	1.15
5.25-35.60-12mm	986.06	0.92	1.10
5.25-19.70-C	1102.74	0.99	1.21
5.25-19.70-8mm	1239.05	0.93	1.14
5.25-19.70-12mm	1349.25	0.91	1.10
8.40-35.60-C	812.05	0.93	0.99
8.40-35.60-8mm	897.94	0.90	0.99
8.40-35.60-12mm	998.57	0.88	0.95
8.40-19.70-C	1219.64	0.87	0.94
8.40-19.70-8mm	1209.42	0.93	1.01
8.40-19.70-12mm	1361.35	0.88	0.94
μ (Short)		0.94	1.29
σ		0.031	0.055
μ (Medium)		0.94	1.14
σ		0.029	0.041
μ (Long)		0.90	0.97
σ		0.025	0.032
μ (Total)		**0.92**	**1.13**
σ		**0.03**	**0.14**

μ: average, σ: standard deviation

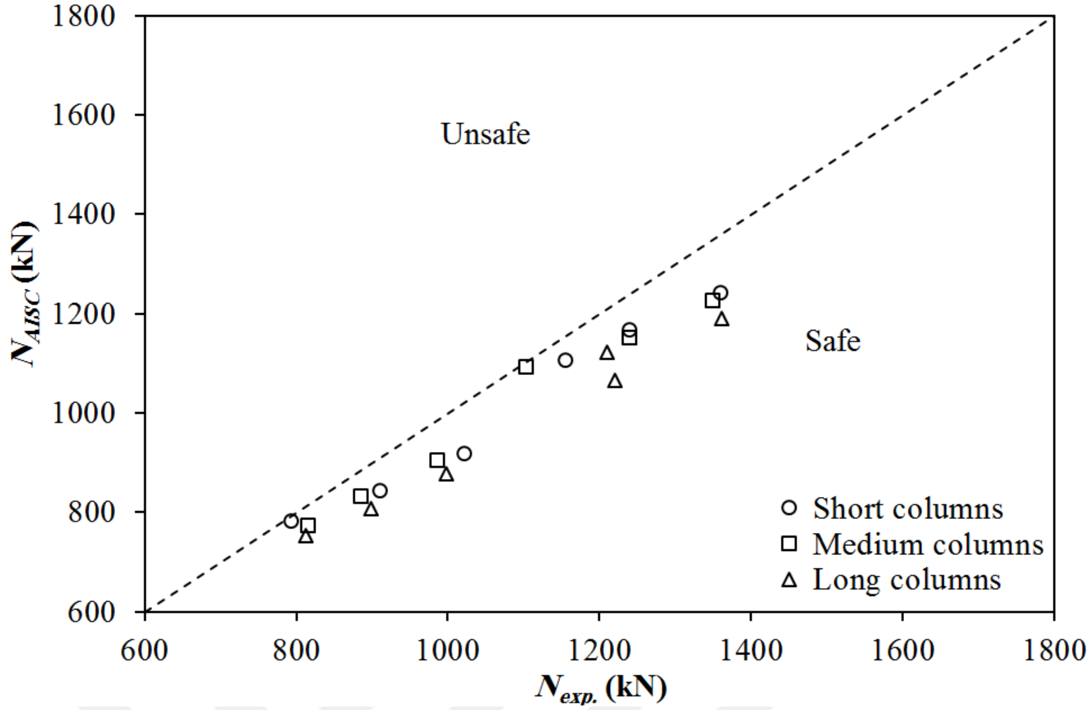

Figure 7.18 Comparison of $N_{exp.}$ and N_{AISC}

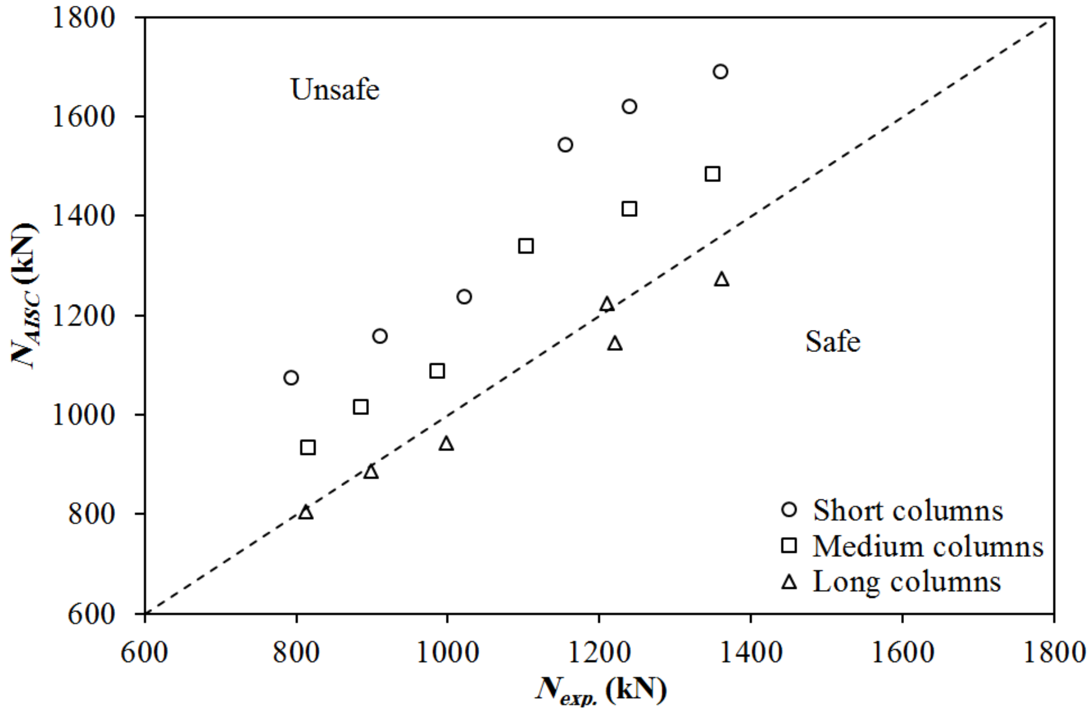

Figure 7.19 Comparison of $N_{exp.}$ and N_{EC4}

7.3 Summary and Conclusion

Recently, due to the increasing size of modern structures, the use of CFST columns have become increasingly popular, especially in seismically active regions. Since CFST columns have smaller cross-sections compared to reinforced concrete structures they offer a reduced self-weight. Further reduction of the self-weight of structures is desirable, especially in seismically active regions; reducing the self-weight of the concrete core also reduces construction costs. Thus, lightweight aggregate concrete has attractive characteristics which lead to improvements in the structural performance of CFST columns.

Reinforced CFST members, as a new kind of CFST column, may be especially useful in large-scale structures. They can be used reduce the self-weight and improve the seismic resistance of the composite structure. In the case of LWCFST columns, no previous study has dealt with reinforced LWC, where the use of reinforced LWC is not the only factor improving the performance of the column specimens. Therefore, an experimental investigation on the response of unreinforced and reinforced lightweight aggregate concrete-filled circular steel tube columns under axial compression was carried out. As reported by the test results, the following conclusions could be drawn:

- The presence of steel-bar reinforcement increases the compression capacity, ductility, toughness of the resulting composite column.
- Short specimens with L/D = 2.62 and D/t = 35.60 showed a discharge in compression capacity after reaching peak load, but reinforced specimens presented more smooth and gradual behavior. Specimens with D/t = 19.70 did not show this drop in capacity, and local materials failure was the major failure mode of short specimens.
- Medium specimens with L/D = 5.25 showed mixed failure modes, combining local and global buckling. For control specimens, though, local buckling governed. Reinforced medium specimens showed failure modes of local and global buckling.
- Long specimens with L/D = 8.40 and D/t = 35.60 behaved similarly to the medium specimens. The observed failure modes were local buckling for control specimens, and a combination of local and global buckling for reinforced specimens, while specimens with D/t = 19.70 succumbed to global buckling.
- The use of a thinner steel tube provides reinforcement for short and long columns. The improvement in compression capacity is better when a thin steel tube and reinforced LWC are combined, and the improvement increases with

increasing steel-bar contribution. The behavior of medium-length columns was in contrast; there, the thick steel tube gave a higher improvement in capacity, but the increase in contribution from steel-bar reinforcement combined with a thin steel tube can enhance the behavior of columns in this length range without the use of a thicker steel tube, as described in Figure 7.14b.

- The results for all columns revealed that the use of a hollow thin steel tube filled with reinforced LWC provided excellent improvement in column ductility.
- The AISC360-16 provided predictions with an average 8% conservative deviation from the experimental results, while the EC4 presented predictions with average unconservative deviations of 13%.
- All predictions of the AISC360-16 for short, medium, and long columns were located in the safe region. In contrast, only the EC4 predictions for long columns were located in the safe region, whilst those for short and medium columns were located in the unsafe region. These variations are due to the effect of relative slenderness or the length impact on the confinement behavior of the composite columns.

CHAPTER 8

CONCRETE-FILLED DOUBLE CIRCULAR STEEL TUBE (CFDCST) STUB COLUMNS – FULL (INTACT) AND REPAIR CONFIGURATIONS

8.1 General

Throughout the previous chapters of this thesis, the performance of single CFST columns—both conventional CFST columns and reinforced CFST columns with different types of concrete core—were investigated under different conditions. This chapter will focus on a new configuration of CFST stub columns.

Rapid growth in civil engineering structures, such as bridges with large spans and skyscrapers, has required CFST columns with a larger cross-section to offer higher weight-bearing capacity. The diameter of CFST columns in the field has reached up to 1600 mm, like this diameter may affect the useful internal space of the building and high hazard of material failure (Cai *et al.*, 2015). Consequently, a new configuration of CFST column is required to satisfy this increase in load.

Much research has been focused on improving the strength capacity, ductility, and confinement effect to reduce the cross-sectional dimensions and self-weight of CFST columns under different loading conditions. These approaches have followed different approaches, such as the use of external rings (Lai and Ho, 2014, 2015), internal steel-bar reinforcement (Xiamuxi and Hasegawa, 2012; Hamidian *et al.*, 2016), internal steel sections (Wang *et al.*, 2004; Zhu *et al.*, 2010; Chang *et al.*, 2012; Xu *et al.*, 2014; Cai *et al.*, 2015), and stiffeners (Dabaon *et al.*, 2009; Tao *et al.*, 2009; Ding *et al.*, 2018).

The essential function of CFST columns is to support load; this type of composite structure is considered superior due to its interaction between steel and concrete that increase its bearing capacity. But there is a defect in the performance of these structures at the elastic stage of loading; the confinement effect is not active in this stage because of the variation in Poisson's ratio of concrete core and steel.

In this stage, the lateral expansion of the steel tube is bigger than that of the concrete core until initial cracks form in the concrete core and allow the concrete to expand more than the steel tube (Kwan *et al.*, 2016). This behavior is more critical with high-strength concrete cores (Lai and Ho, 2014). This behavior has motivated the use of external rings in CFST column construction described in the literature (Lai and Ho, 2014; Kwan *et al.*, 2016).

Another critical behavior of CFST columns is its fire resistance. CFST columns provide better fire resistance than reinforced concrete or bare steel columns; the steel tube prevents the concrete core from spalling and the thermal structural interaction between steel tube and concrete core is beneficial (Kodur, 1998; Lu *et al.*, 2009; Song *et al.*, 2010). However, the major shortcoming of CFST is the reduction in strength experienced by the steel tube under specific fire conditions, which may affect the post-fire performance of CFST columns (Wang *et al.*, 2004). Therefore, many studies have sought approaches to improve the fire resistance of CFST columns, such as the use of internal steel sections (Wang *et al.*, 2004; Zhu *et al.*, 2010; Cai *et al.*, 2015), double-skin CFST columns (Lu *et al.*, 2010; Li *et al.*, 2012), steel-bar reinforced concrete core (Lie and Kodur, 1996), and concrete cores reinforced with steel fibers (Kodur and Lie, 1996).

However, new CFST columns configurations have the potential to improve the strength, ductility, stiffness, and interaction between the steel tube and concrete core in the elastic stage in addition to enhancing fire resistance. A new CFST column configuration, concrete-filled double steel tubular (CFDST) columns, has been designed with this end in mind. These columns have the same profile as concrete-filled double-skin steel tube columns except that in this case the inner tube is also filled with concrete. Figure 8.1 shows different circular cross-sections configurations of CFST columns.

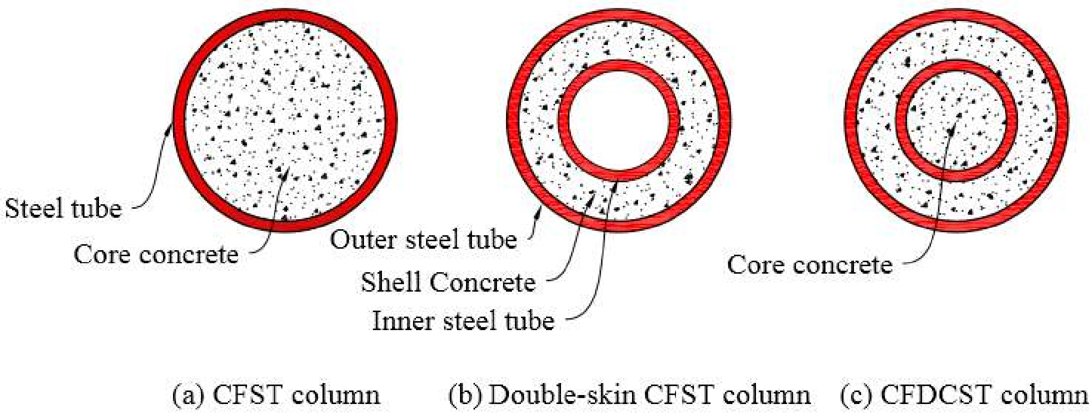

Figure 8.1 CFST column configurations

Compared to classic CFST columns, the total amount of concrete required can be reduced by using an inner steel tube filled with concrete, leading to decreased self-weight of the final member (Wan and Zha, 2016). In addition, two different concrete strengths or types can be combined in this column, and two different strengths and geometries of outer and inner steel tubes can be used. CFDST columns have better ductility performance and fire and post-fire resistance because the inner steel tube is preserved by both the shell concrete and outer steel tube. Moreover, the compression response of CFDST columns is much better than that of CFST columns, because the inner tube has support from both core and shell concrete. Composite action can be achieved in the elastic and plastic stages, especially in the external and internal circular cross-sections.

CFDST columns have been used for building in Germany, as reported by Roik and Bergmann (1985); the columns must provide fire resistance and support a vertical load of 8000 kN with a diameter limited to 600 mm. To satisfy these requirements, CFDST columns with circular cross-sections of both the external and internal tubes were used (Qian *et al.*, 2014).

As mentioned in Chapter 2, until now, few types of research have been conducted to study the performance of CFDST columns. Therefore, the work described in this Chapter studied the behavior of concrete-filled double circular steel tube (CFDCST) stub columns, in which the circular cross-sections of both the inner and outer steel tubes provide better confinement for both core and shell concrete.

8.2 Aim of this Work

The main aims of this study are two parts: The first is to investigate the behavior of CFDCST stub columns. A comprehensive experimental program was carried out to satisfy this aim, in which CFDCST stub columns were prepared and tested under axial compressive loading to methodically study the pre-collapse, collapse, and post-collapse behaviors.

Different materials and geometric characteristics of both steel tube and concrete were used to construct the specimens. Two various concrete strengths (normal- and high-strength concrete) were used for both the core and shell regions, and two different outer steel tube thicknesses were used to study their contribution to the confinement effect and compression capacity of the columns. This experimental program studied the impact of three various parameters on the behavior of the composite column: (1) outer steel tube characteristics, (2) core concrete strength, and (3) shell concrete strength.

As mentioned in Chapter Two, a CFST system has been used to repair and strengthen reinforced concrete columns (Sezen and Miller, 2011; Lu *et al.*, 2015a, 2015b). Therefore, the second goal of this study is investigating the possibility of CFDCST column concept for the repair of deformed CFST columns.

To that end, CFST stub columns were loaded up to a specific portion of the compression capacity to develop plastic deformation in the columns, after which the load was released. Then, the deformed column was centered within a larger steel tube and the shell regions between the inner and outer steel tubes filled with concrete. Fresh concrete took the shape of the deformed inner steel tube. Various concrete strengths and different outer steel tube thickness could be used. After the shell concrete finished curing, the repaired column specimens were ready for testing.

Using steel tube and concrete with the same properties for both aims of the study helped to examine the performance of repaired CFDCST columns relative to intact CFDCST columns. This study seeks to fill a gap in research, providing information about the performance of a novel type of CFST columns and facilitating their use in civil engineering applications.

8.3 Experimental Work

The experimental program of this study was a methodical procedure intended to investigate the performance of intact and repaired CFDCST stub columns in a way that allows rational comparison between them. The selected geometric and material properties helped to satisfy these goals. Figure 8.2 shows a cross-section and model of a CFDCST stub column.

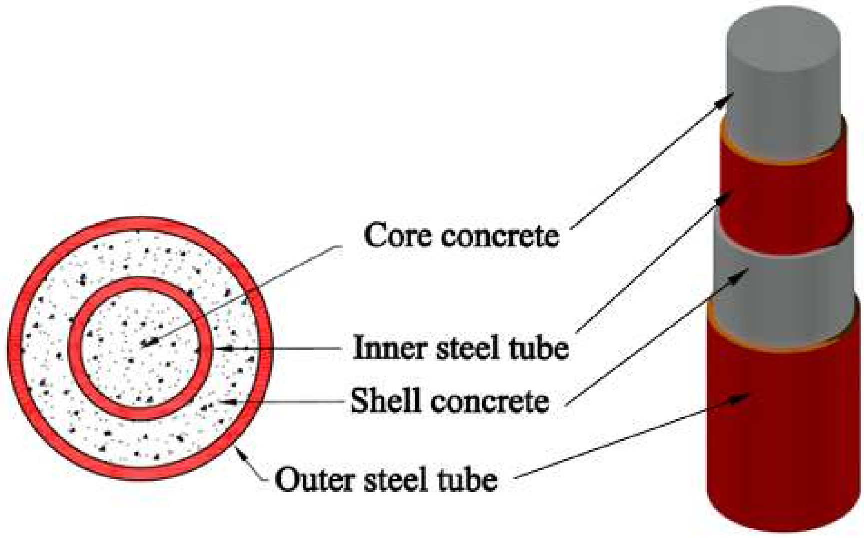

Figure 8.2 Cross-section and model of CFDCST stub column

8.3.1 Materials Properties

8.3.1.1 Steel

For intact specimens, a single inner steel tube with a cross-section of 88.90×4.25 mm was used. For the outer steel, two tubes with the same outer diameter and two different thicknesses were used, with cross-sections of 139.70×5.87 mm and 139.70×3.30 mm. During preparation of these steel tubes, some tensile coupon specimens were prepared according to ASTME8/E8M-16 (2016) to measure the mechanical properties of these steel tubes. The stress–elongation curves from coupon tests are shown in Figures 8.3–8.5, and the mechanical properties of the steel tube sections are summarized in Table 8.1.

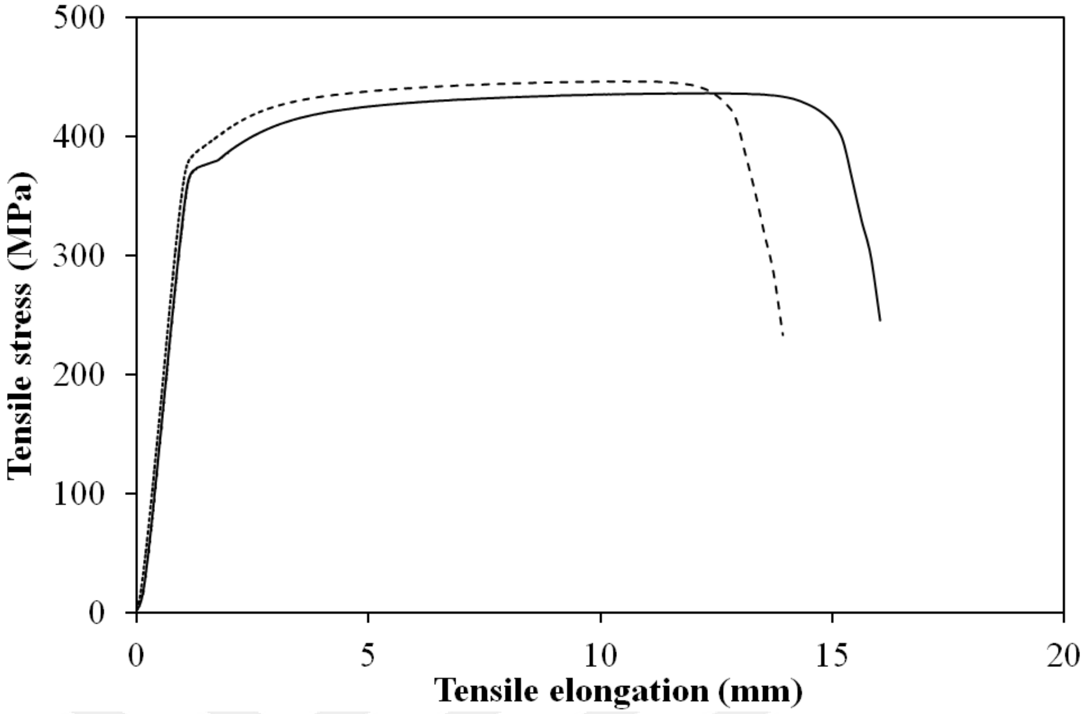

Figure 8.3 Coupon test stress–elongation curves for 88.90 × 4.25 mm

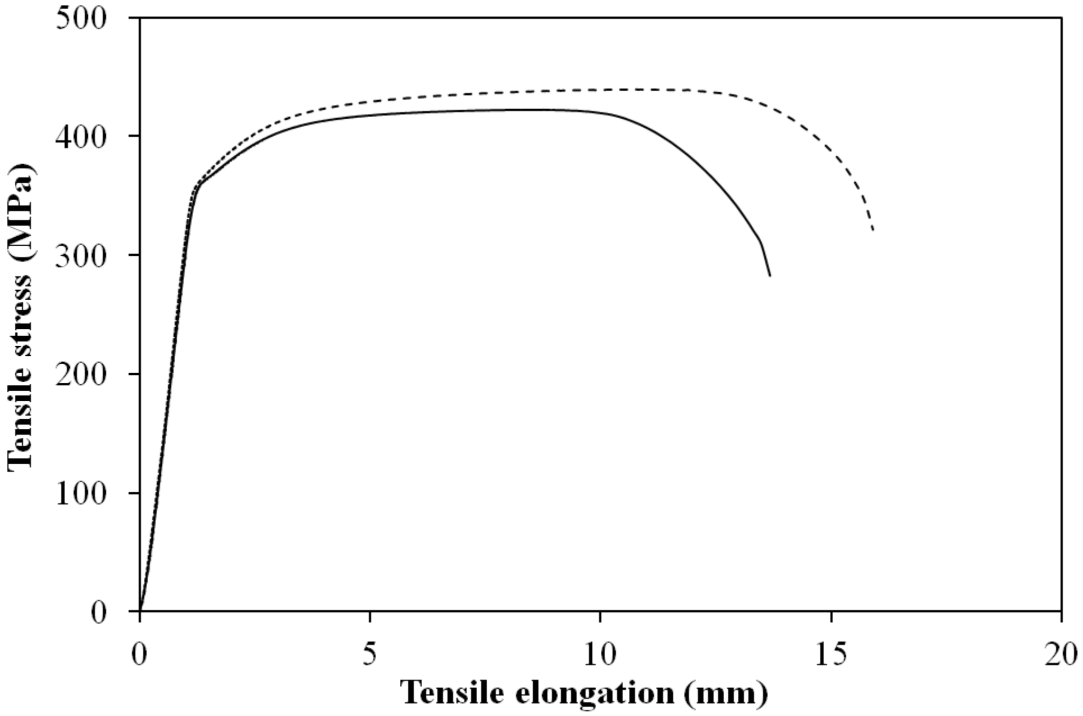

Figure 8.4 Coupon test stress–elongation curves for 139.70 × 5.87 mm

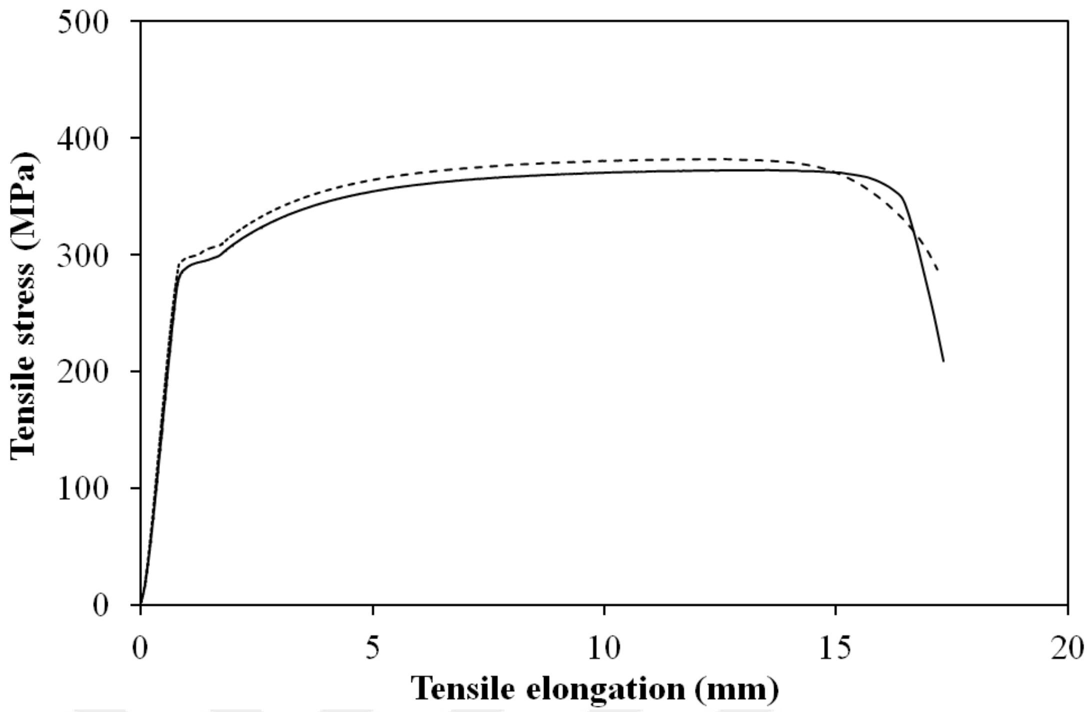

Figure 8.5 Coupon test stress–elongation curves for 139.70 × 3.30 mm

Table 8.1 Mechanical properties of steel tube sections

Section	D (mm)	t (mm)	f_y (MPa)	f_u (MPa)	E_s (GPa)
88.90×4.25	88.90	4.25	375	441	200
139.70×5.87	139.70	5.87	355	431	200
139.70×3.30	139.70	3.30	290	378	200

8.3.1.2 Concrete

Two various concrete mixes (normal- and high-strength) were used. The coarse and fine aggregates were river aggregates with a rounded shape; the maximum aggregate size of the coarse aggregate was 10 mm. These limitations were intended to ensure good compaction of fresh concrete poured in the columns, especially in the narrow spaces of the shell region. In addition to the traditional materials incorporated in the mix design, hyper-plasticizer was used in both mixes to create highly workable fresh concrete.

The standard cylinder specimens (100×200 mm) were filled in three layers. After each layer, the concrete was carefully compacted to excrete entrapped air. When the curing process was complete, the concrete cylinder specimens were tested according to ASTMC39/C39M-15 (2015). The compressive concrete strengths of the two mixes used are 30.55 MPa (Table 8.2) and 68.09 MPa (Table 8.3).

Table 8.2 Mix proportions for concrete with f_c of 30.55 MPa

Cement	Coarse aggregate	Fine aggregate	Water	Hyper-plasticizer
1	3.0	2.20	0.50	0.0035

Table 8.3 Mix proportions for concrete with f_c of 68.09 MPa

Cement	Coarse aggregate	Fine aggregate	Water	Hyper-plasticizer
1	2.62	1.80	0.34	0.01

The configuration of CFDCST columns offers an opportunity to use different concrete strengths for the same specimen: normal-strength (NS) concrete for core and high-strength (HS) concrete for the shell, or vice versa.

8.3.2 Column Specimens Preparation

All specimens had the same length (270 mm) to ensure their status as stub columns and to prevent the contribution of a global buckling failure mode. As mentioned in the previous chapters, before to pouring the fresh concrete, the ends of the steel tube were machined to guarantee full touch with the ends of the testing machine to help offer reliable results (Ziemian, 2010). The thick glass plates were used at the bottom ends of the small and large tubes and connected to the ends by using silicone to restrain the wet concrete during the casting and provide a flat surface of concrete at the bottom end of the column.

The manufacturing process for CFDCST stub columns was according to the following procedure: First, the smaller (88.90 mm diameter) steel tubes were filled with fresh concrete in five layers, with the concrete compacted manually after each layer. Then, the minimum sufficient time was permitted between pouring of the core concrete and shell concrete to ensure the same curing condition for both concretes. After completing the preparing of the core concrete, the silicone from the bottom end of the smaller diameter steel tubes was removed and cleaned. When the setting of core concrete was finished, the inner columns were centered inside the larger-diameter steel tubes. Following the same procedure as for the inner columns, the shell zones were filled with five layers of fresh concrete, with the fresh shell concrete compacted after addition of each layer.

The flat surfaces at the upper ends of the columns were as important as those of the bottom ends. To assure their quality, fresh concrete was not poured up to the end of the columns. The top last 3–4 mm of each column was left empty and the space filled with high-strength leveling epoxy after the curing process was complete.

In addition to the CFDCST columns, single-wall CFST specimens with dimensions corresponding to both the interior and exterior tubes of the intact CFDCST columns were manufactured and tested to investigate the separate contributions of the inner and outer columns. Figure 8.6 shows the single-wall CFST columns specimens for both steel tube diameters (88.90 mm and 139.70 mm) before testing, while Figure 8.7 shows the intact CFDCST columns specimens before testing.

8.3.3 Test Program

Specimens were accurately centered in the testing machine to cancel any eccentricity of loading and associated bending effects. The testing machine capacity is 3000 kN; displacement-controlled loading at a rate of 0.5 mm/min was applied to all column specimens and compression loading versus end-shortening data for all specimens was recorded to allow discussion of the behavior of columns in both the pre- and post-collapse regions; Figure 8.8 shows the experimental setup used for testing column specimens.

Figure 8.6 Single CFST columns before testing

Figure 8.7 Intact CFDCST columns specimens before testing

Figure 8.8 Column specimen testing

For repair testing, however, specimens of the smaller diameter steel tubes were filled with both concrete classes (30.55 MPa and 68.09 MPa) and tested up to a fraction of compression capacity with the same rate of loading. When the maximum loading was reached, the load was released and after a period of waiting to permit any possible spring-back behavior of the steel tubes, deformed CFST columns were centered in larger diameter steel tubes. The shell region was then filled with concrete, and after the resulting repaired columns specimens cured, they were tested. Testing was to failure, with both pre- and post-collapse behaviors recorded.

Table 8.4 and Figure 8.9 identify columns using the labeling system followed in this study. It includes the type of core concrete (CC), shell concrete (SC), and outer steel tube thickness (OT). For example, specimen name CC1-SC2-OT1 describes the CFDCST column with a core concrete strength of 30.55 MPa, shell concrete strength of 68.09 MPa, and outer steel tube with the thinner thickness (3.30 mm). The numbers 1 and 2 refer to the weaker and stronger properties, respectively. A suffix of "R" is used to denote repaired CFDCST columns. For the CFST specimens, the inner column specimens (smaller diameter steel tube) were labeled as 1 or 2 to refer to the concrete class (normal- or high-strength concrete), the steel tube thickness was not mentioned because it is a single tube, and the suffix "R" was used to differentiate between fully and partially tested specimens used for repair testing, e.g. 1-R or 2-R. For single CFST specimens with larger-diameter steel tubes, a two-class labeling system was used, e.g. 1-2, which means the core concrete was the 30.55 MPa mix, and the outer steel tube thickness was 5.87 mm.

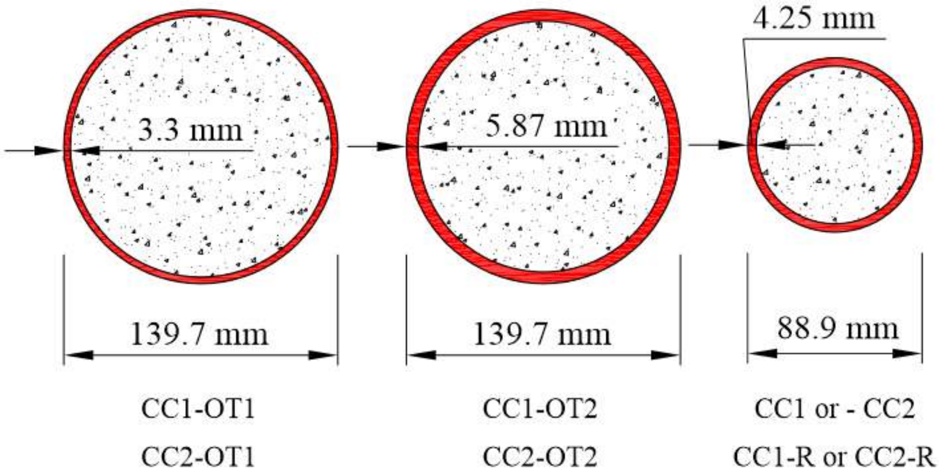

(a) Single CFST column cross-sections

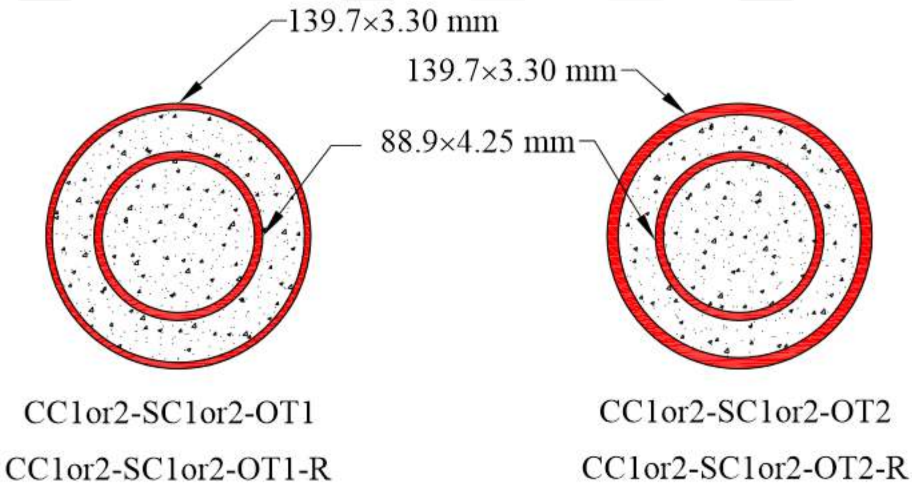

(b) CFDCST column cross-sections

Figure 8.9 Columns cross-sections in intact and repaired cases

Table 8.4 Properties of stub column specimens

Column	Inner column				Outer columns				Test case	$N_{exp.}$ (kN)
	f_c (MPa)	D_{inner} (mm)	t_{inner} (mm)	f_y (MPa)	f_c (MPa)	D_{outer} (mm)	t_{outer} (mm)	f_y (MPa)		
CC1-SC1-OT1	30.55	88.9	4.25	375	30.55	139.7	3.30	290	Full	1435.05
CC1-SC1-OT2	30.55	88.9	4.25	375	30.55	139.7	5.87	355	Full	1979.43
CC1-SC2-OT1	30.55	88.9	4.25	375	68.09	139.7	3.30	290	Full	1606.89
CC1-SC2-OT2	30.55	88.9	4.25	375	68.09	139.7	5.87	355	Full	2044.44
CC2-SC1-OT1	68.09	88.9	4.25	375	30.55	139.7	3.30	290	Full	1570.15
CC2-SC1-OT2	68.09	88.9	4.25	375	30.55	139.7	5.87	355	Full	2153.11
CC2-SC2-OT1	68.09	88.9	4.25	375	68.09	139.7	3.30	290	Full	1784.38
CC2-SC2-OT2	68.09	88.9	4.25	375	68.09	139.7	5.87	355	Full	2274.77
CC1-OT1	30.55	–	–	–	–	139.7	3.30	290	Full	923.57
CC1-OT2	30.55	–	–	–	–	139.7	5.87	355	Full	1480.54
CC2-OT1	68.09	–	–	–	–	139.7	3.30	290	Full	1372.87
CC2-OT2	68.09	–	–	–	–	139.7	5.87	355	Full	1884.09
CC1	30.55	88.9	4.25	375	–	–	–	–	Full	723.68
CC2	68.09	88.9	4.25	375	–	–	–	–	Full	844.35
CC1-R	30.55	88.9	4.25	375	–	–	–	–	Partial	625.00
CC1-R	30.55	88.9	4.25	375	–	–	–	–	Partial	625.73
CC1-R	30.55	88.9	4.25	375	–	–	–	–	Partial	623.65
CC1-R	30.55	88.9	4.25	375	–	–	–	–	Partial	624.86
CC2-R	68.09	88.9	4.25	375	–	–	–	–	Partial	727.93
CC2-R	68.09	88.9	4.25	375	–	–	–	–	Partial	732.41
CC2-R	68.09	88.9	4.25	375	–	–	–	–	Partial	727.03
CC2-R	68.09	88.9	4.25	375	–	–	–	–	Partial	726.21
CC1-SC1-OT1-R	30.55	88.9	4.25	375	30.55	139.7	3.30	290	Full	1483.28
CC1-SC1-OT2-R	30.55	88.9	4.25	375	30.55	139.7	5.87	355	Full	1969.89
CC1-SC2-OT1-R	30.55	88.9	4.25	375	68.09	139.7	3.30	290	Full	1576.73
CC1-SC2-OT2-R	30.55	88.9	4.25	375	68.09	139.7	5.87	355	Full	2115.89
CC2-SC1-OT1-R	68.09	88.9	4.25	375	30.55	139.7	3.30	290	Full	1553.42
CC2-SC1-OT2-R	68.09	88.9	4.25	375	30.55	139.7	5.87	355	Full	2105.73
CC2-SC2-OT1-R	68.09	88.9	4.25	375	68.09	139.7	3.30	290	Full	1837.57
CC2-SC2-OT2-R	68.09	88.9	4.25	375	68.09	139.7	5.87	355	Full	2259.66

8.3.4 Results and Discussion

In this section, the results of testing the CFDCST column specimens are presented as end-shortening against compression loading curves, and failure modes are discussed according to the impact of the geometrical and mechanical properties of the columns specimens. The compression loading against end-shortening curves for CFDCST columns are discussed to facilitate discussion of the compression behavior, ductility, and stiffness of the specimens as it relates to the parameters of core concrete compressive strength, shell concrete compressive strength, and outer steel tube thickness. The performance of CFDCST columns is compared to CFST columns with steel tubes of larger diameter to investigate the effect of the inner columns, where the presence of the inner columns shows the significance of CFDCST configuration. The results are summarized in Table 8.5.

8.3.4.1 Columns Filled with NS Core Concrete

- **End-shortening versus compression loading curves**

The compression behavior of columns with normal-strength (NS) core concrete is given in Figure 8.10. This group of specimens offers excellent ductility because the core is normal-strength concrete, which possesses higher ductility than high-strength concrete (De Oliveira *et al.*, 2009; Ekmekyapar and AL-Eliwi, 2016). The compression capacity of specimen CC1 was 723.68 kN. While for specimens CC1-OT1 and CC1-OT2 were 923.57 kN and 1480.54 kN, respectively. This change in the cross-section dimension and steel yield strength of the tube led to improving the capacities by 25.72% and 101.54% compared to specimen CC1.

The improvement in compression capacities detailed above is due to the dimension and yield strength of the steel tube. In contrast, the compression capacities of CFDCST specimens CC1-SC1-OT1, CC1-SC1-OT2, CC1-SC2-OT1, and CC1-SC2-OT2 were 1435.05 kN, 1979.44 kN, 1606.89 kN, and 2044.44 kN, respectively. The values for those specimens were compared to specimen CC1 to examine the effect of CFDCST configuration on their capacity improvements of 98.3–182.5%. These levels of improvement are relatively high; the smallest specimen provided approximately double the capacity of specimen CC1. Overall, CFDCST specimens provided much higher initial stiffness compared to CFST specimens, and their toughness increased significantly due to the use of inner columns (Figure 8.10).

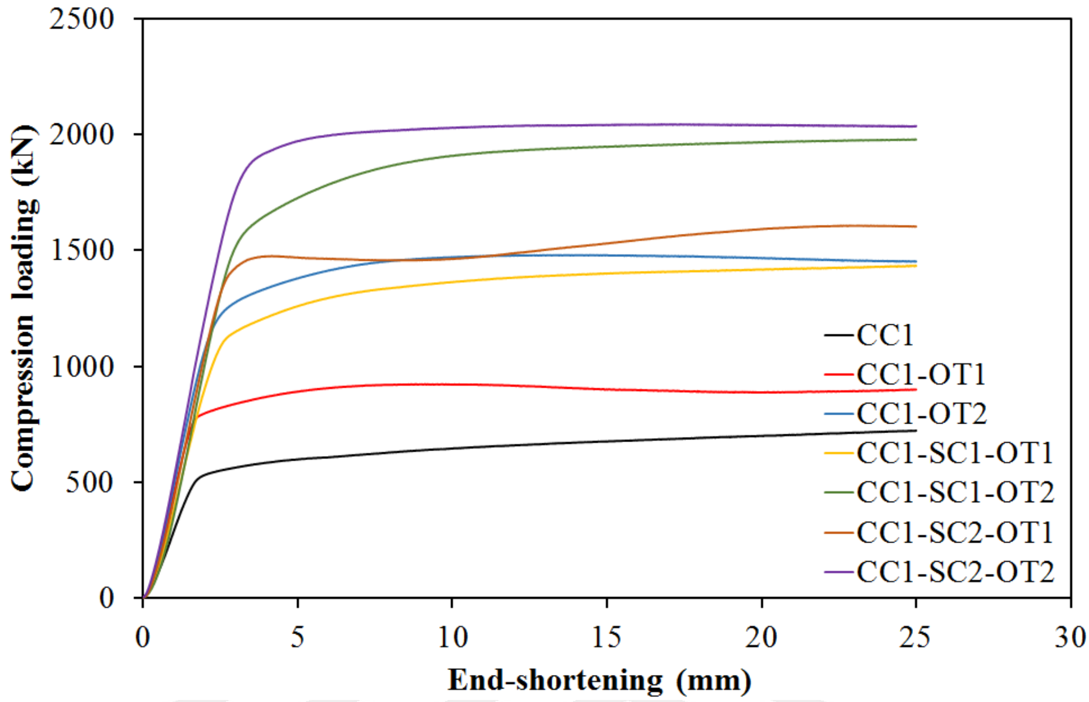

Figure 8.10 Load–shortening curves for columns NS core concrete

The differences between the capacities of specimens CC1-OT1 and CC1-OT2 and specimens CC1-SC1-OT1, CC1-SC1-OT2, CC1-SC2-OT1, and CC1-SC2-OT2 highlighted the considerable contribution of the inner specimens (CC1) on the performance of the CFDCST specimens as a whole (Figure 8.11). The CFDCST specimens provided 511.48 kN, 489.89 kN, 683.32 kN, and 563.89 kN increments in compression capacity due to the contributions of the CC1 specimens. These contributions indicate that the inner specimens take load approximately to their squash limits in addition to providing further confinement of both core and shell concretes.

Another indication can be seen, that the inner specimens have more effect on the CFDCST specimens with thinner outer steel tube as shown in Figure 8.11. Through exploring the effect of other parameters, it can be deduced that the external steel tube characteristics have a larger contribution than shell concrete strength. The increment in thickness and yield strength of the outer steel tube in CFDCST specimen with shell concrete provided a 37.94% enhancement in capacity (comparison of specimens CC1-SC1-OT1 and CC1-SC1-OT2), whilst the enhacement in compression capacity is

27.23% for CFDCST specimen with high-strength shell concrete (comparison of specimens CC1-SC2-OT1 and CC1-SC2-OT2, Figure 8.11).

In turn, the specimens with high-strength shell concrete gave the capacity improvement of 11.97% with thinner outer steel tube (comparison of specimens CC1-SC1-OT1 and CC1-SC2-OT1) and this enhancement is 3.28% with thicker outer steel tube (comparison of specimens CC1-SC1-OT2 and CC1-SC2-OT2, Figure 8.11). The local buckling of thinner outer tubes has a significant effect on this behavior.

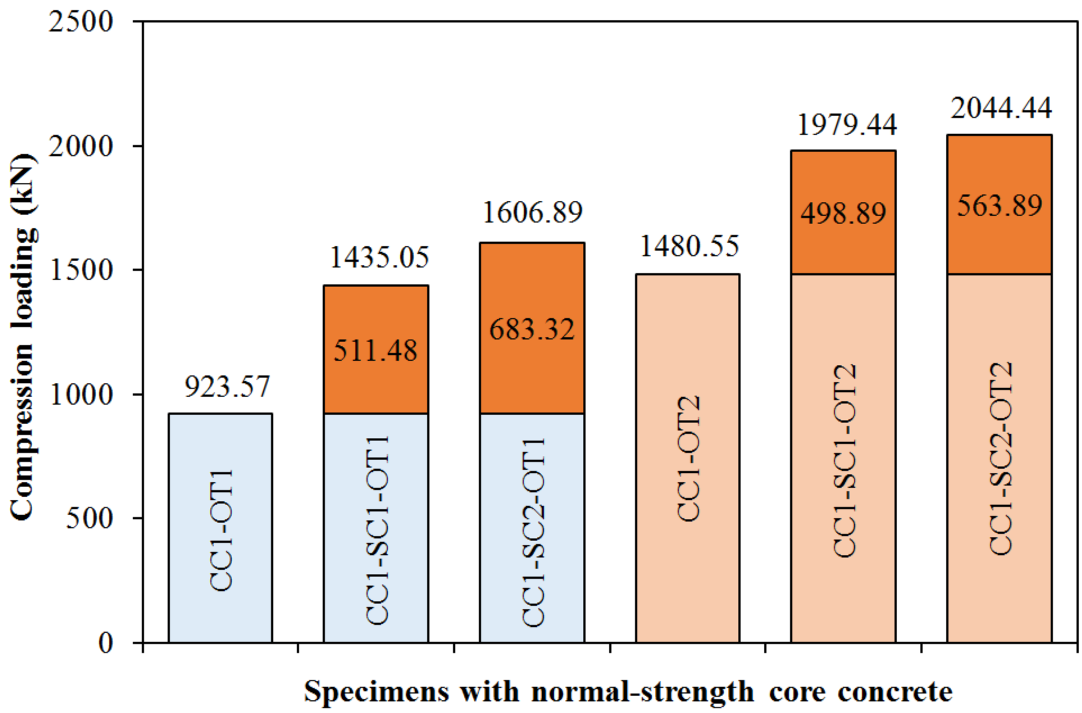

Figure 8.11 Compression capacities increment with NS core concrete

- **Failure modes**

Figure 8.12 describes the failure modes of this group of specimens. Local failure of the steel is evident for the specimens with thin outer steel tubes, where it takes a crippling shape. A failure mode of crushing followed by shear failure was noted for the concrete. It is also worth noting that the presence of an inner column tube could not prevent the shear failure of the concrete. Additionally, the distortions of the specimens with thin outer steel tubes were distributed over larger regions of the specimen, while for the specimens with thick outer steel tubes the deformations were over specific regions. This behavior indicates that the thicker outer steel tube had an outstanding confinement effect and governed the failure modes of both the shell concrete and the inner tube.

Figure 8.13 shows the sectional view of the tested specimens CC1-SC2-OT1 and CC1-SC1-OT2. The smoother surface of the inner surface of the shell concrete reflects good compaction of the concrete in shell region. This sectional view also shows the interaction between the inner tube and the shell concrete, and between the outer tube and the shell concrete. The friction between the inner steel tube and the shell concrete left black signs on the inner surface of the shell concrete, visible in Figure 8.13. These black signs and the shapes of the shell concrete indicates that the shell concretes played a significant role in supporting the inner steel tubes.

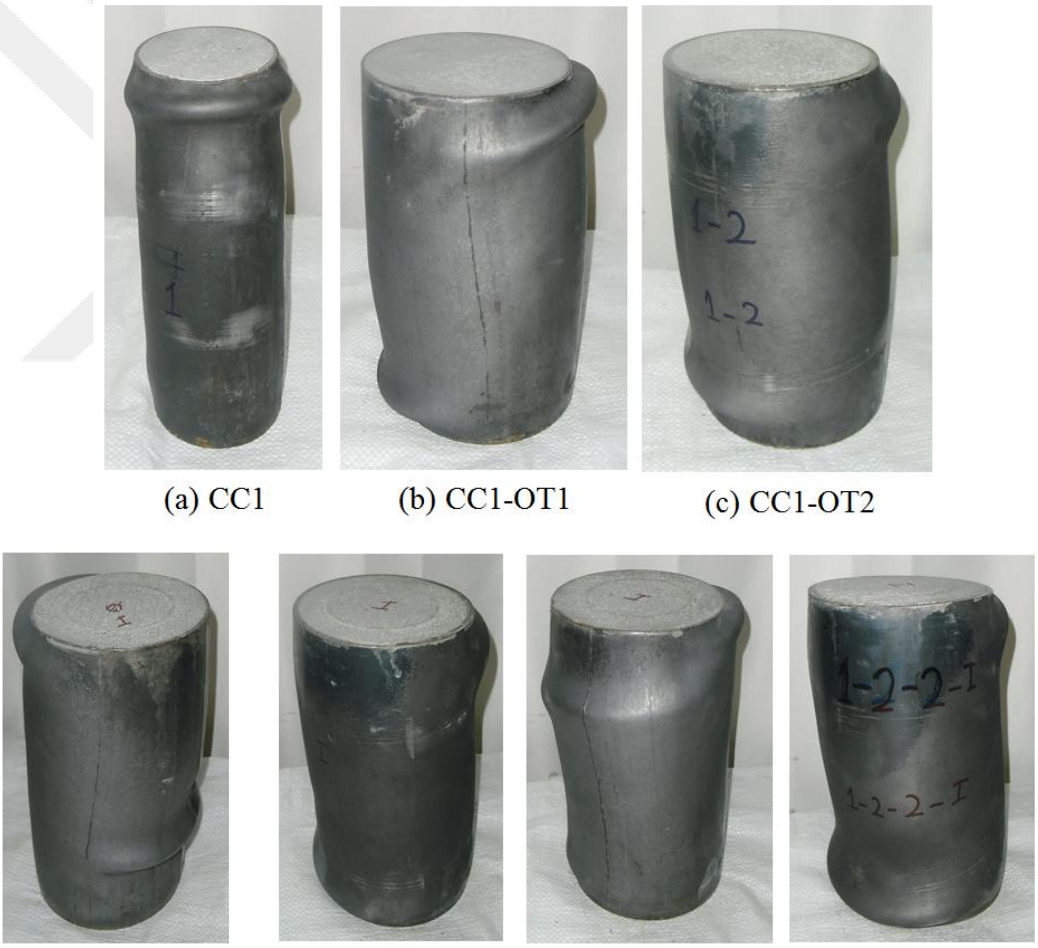

(a) CC1 (b) CC1-OT1 (c) CC1-OT2

(d) CC1-SC1-OT1 (e) CC1-SC1-OT2 (f) CC1-SC2-OT1 (g) CC1-SC2-OT2

Figure 8.12 Failure modes of columns with NS core concrete

(a) CC1-SC2-OT1 (b) CC1-SC1-OT2

Figure 8.13 Failure modes of columns CC1-SC2-OT1 and CC1-SC1-OT2

8.3.4.2 Columns Filled with HS Core Concrete

- **End-shortening versus compression loading curves**

The compression behavior of the columns with high-strength (HS) core concrete is described in Figure 8.14. Specimen CC2 showed a compression capacity of 844.35 kN, a 120.67 kN (16.67%) increment in capacity compared to specimen CC1. Despite this increment in capacity, specimen CC1 showed superior ductility (Figures 8.10 and 8.14). Due to the high strengths of this group of the specimens and for safety purposes. The hydraulic arrangement and software of the testing machine do not provide the displacement rate after reaching 2200 kN; after that point, only a very slow rate of displacement is provided by the testing machine. This affected the data for specimen CC2-SC2-OT2, which reached its compression capacity after 2200 kN.

CFST specimens CC2-OT1 and CC2-OT2 offered compression capacities of 1372.88 kN and 1884.10 kN, respectively. These capacities were compared to the capacities of specimens CC2-SC1-OT1, CC2-SC2-OT1, CC2-SC1-OT2, and CC2-SC2-OT2 to examine the contributions of the core CC2 specimens (Figure 8.15). The CFDCST specimens provided 197.28 kN, 411.51 kN, 269.02 kN, and 390.68 kN, respectively, increments in compression capacities due to contributions of the CC2 specimens. It is significant to mention that the contributions of CC2 specimen are unlike the contribution of CC1 specimens, as shown in Figures 8.11 and 8.15; for CFDCST specimens with normal-strength core concrete, the inner steel tube offered more confinement to both the shell and core concretes. From these results we can conclude that normal-strength core concrete provides better confinement and higher initial stiffness compared to high-strength core concrete. However, the presence of an inner steel tube enhances the ductility and toughness of the composite columns (Figure 8.14).

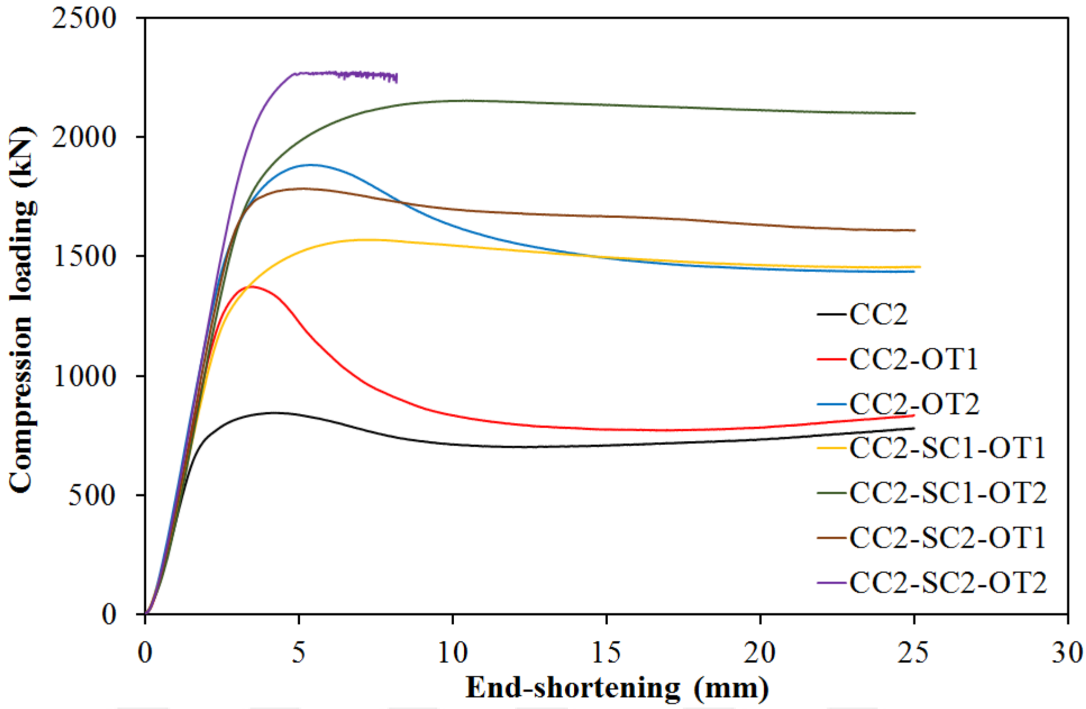

Figure 8.14 Load–shortening curves for columns with HS core concrete

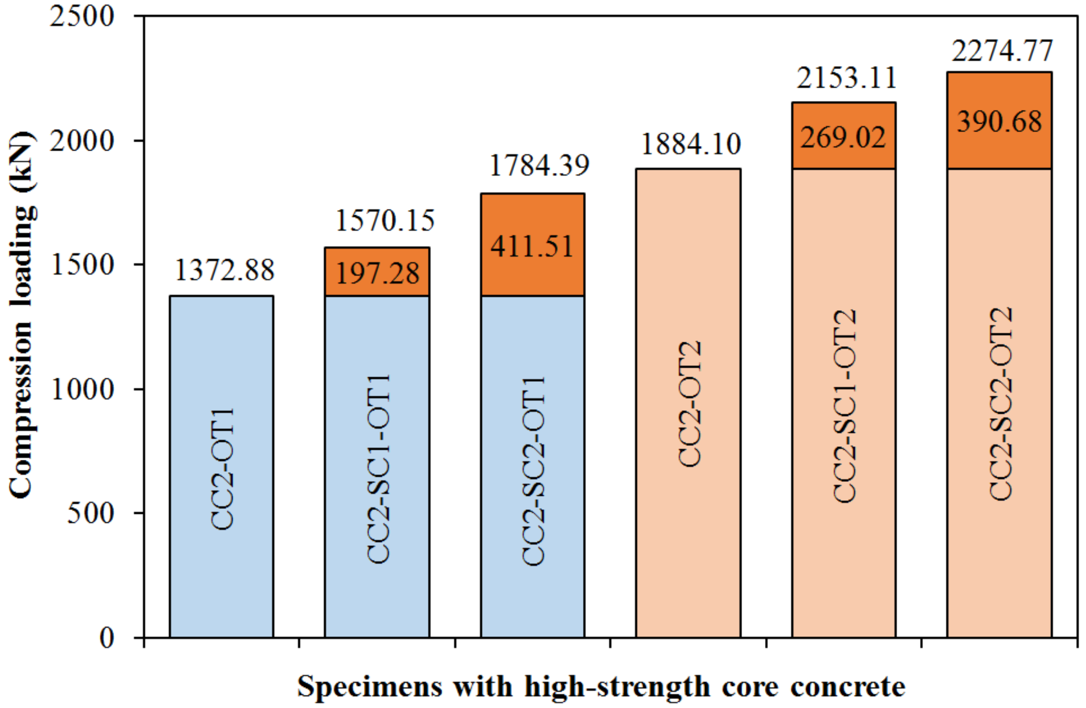

Figure 8.15 Compression capacities increment with HS core concrete

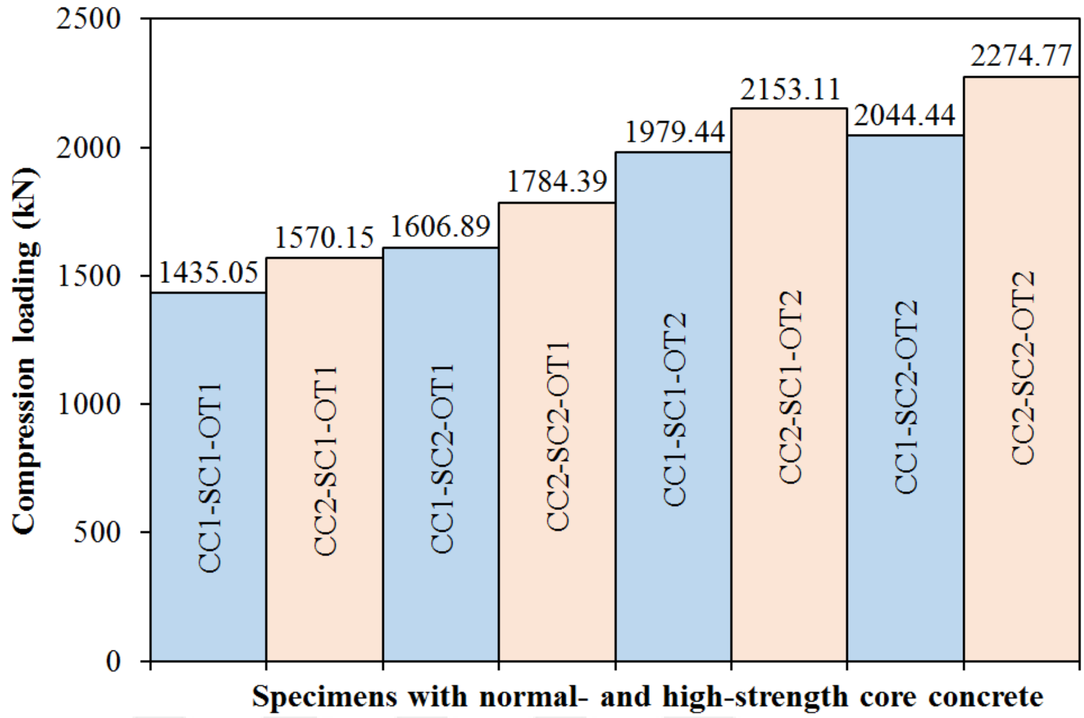

Figure 8.16 Capacity comparison for intact CFDCST specimens

CFDCST specimens CC2-SC1-OT1, CC2-SC2-OT1, CC2-SC1-OT2, and CC2-SC2-OT2, recorded compression capacities of 1570.15 kN, 1784.39 kN, 2153.11 kN, and 2274.77 kN, respectively. Where, these specimens offered compression capacities increment of 135.10 kN (9.41%), 177.50 kN (11.05%), 173.67 kN (8.77%), and 230.33 kN (11.27%), respectively, compared to corresponding CFDCST specimens with normal-strength core concrete. These results indicate the strong contributions of the shell concrete and outer steel tube in confining the core concrete and suggest that high compression capacity can be achieved using the CFDCST column configuration (Figure 8.16).

In this set of CFDCST specimens, the outer steel tube again has the higher contribution impact on the behavior of these composite columns compared to other parameters. Among the specimens with normal-strength shell concrete, specimen CC2-SC1-OT2 provided an increment in the capacity of 37.13% compared to specimen CC2-SC1-OT1. For specimens with high-strength shell concrete (comparison of CC2-SC2-OT2 and CC2-SC2-OT1), the percentage of increment of compression capacity is 27.48%. It is very interesting to note that the percentage changes in compression capacity of specimens with high-strength concrete core of the same level as those of specimens with normal-strength core concrete. Thus, it can be deduced that the contribution of the outer steel tube is the same for both normal and high-strength core concrete in CFDCST columns.

When examining the contribution of shell concrete to improvements in compression capacity, it was noted that the specimen with high-strength shell concrete and a thin outer steel tube (CC2-SC2-OT1) offered an increase in compression capacity of 13.64% over the corresponding specimen with normal-strength shell concrete and a thinner outer steel tube (CC2-SC1-OT1). The compression capacity improved by 5.65% for specimens with thicker outer steel tubes.

- **Failure modes**

Failure modes of specimens with high-strength core concrete are similar to those of specimens with normal-strength core concrete, as shown in Figure 8.17. Local crushing of concrete with associated shear failure combined with yielding, local failure of the steel tube, was noted. The thinner outer steel tube could not prevent the shear failure type of concrete and displayed local deformations apparently.

Sectional views of specimens CC2-SC2-OT1 and CC2-SC1-OT2 show good compaction of their shell regions (Figure 8.18). As concluded before, the thickness of the outer steel tube is the most important factor influencing the confinement of CFDCST specimens; this behavior is explicit in deformations of the inner tube, shell concrete, and the outer tube.

Again, as in the previous set of specimens, the friction between the inner steel tube and the shell concrete left black signs on the inner surface of the shell concrete (Figure 8.18). As mentioned above, these black signs and the shapes of the shell concrete indicate that shell concrete played a significant role in supporting the inner steel tubes. Deformations of the inner steel tube, shell concrete, and the outer steel tube were concentrated over a specific region of failure (Figure 8.17), as was also observed for the previous set of specimens (Figure 8.12).

The failure modes discussed here are those of CFDCST stub columns. Stub columns have a length-to-diameter (*L/D*) ratio chosen to limit the failure modes to local material failures in the steel tubes and concrete. This configuration prevents the overall buckling modes and mixed instability modes (overall buckling combined with local materials failure). With an increased *L/D* ratio, the behavior of CFDCST columns is totally different, and depending on this ratio the column will experience mixed failure modes or failure via global instability. Also, as has been discussed earlier, an increase in the *L/D* ratio leads to a reduce in the compression capacity of composite columns.

(a) CC2 (b) CC2-OT1 (c) CC2-OT2

(d) CC2-SC1-OT1 (e) CC2-SC1-OT2 (f) CC2-SC2-OT1 (g) CC2-SC2-OT2

Figure 8.17 Failure modes of columns with HS core concrete

(a) CC2-SC2-OT1 (b) CC2-SC1-OT2

Figure 8.18 Failure modes of columns CC2-SC2-OT1 and CC2-SC1-OT2

8.3.4.3 Parameters Contributions Ranking

In this study, three different parameters were found to affect the compression behavior of CFDCST stub columns: core concrete compressive strength, shell concrete compressive strength, and outer steel tube characteristics. The impact of each factor on the performance of these composite columns has been discussed in relation to compression behavior curves and observed failure modes. To facilitate a more detailed understanding of behaviors, statistical analysis was performed. An ANalysis Of VAriance (ANOVA) was conducted on the experimental results to understand the contribution of each factor to the compression capacity of CFDCST stub columns (Roy, 2010).

In statistical processing, each parameter was investigated at only two levels. The lower and upper boundary represent the first and second level, respectively. For concrete, two classes, normal- and high-strength, were used for the core and shell regions, and two thickness of outer steel tube were used. Therefore, for more accurate calculations both the geometric and mechanical properties of the outer steel tube were taken into consideration.

The squash load (cross-sectional area of outer steel tube multiplied by the steel yield strength, $A_s f_y$) of the outer steel tube was considered to represent the lower and upper limits of the outer steel tube. It is worth mention that the difference in thickness between the two outer steel tubes led to a small difference in the areas of the shell regions. This difference was ignored to simplify the statistical analysis since its effect is very small compared to the effect of the direct properties of the outer steel tube. Table 8.5 provides the lower and upper limits of the parameters.

Table 8.5 Limits of CFDCST column parameters

CFDCST parameter	Lower limit	Upper limit
Core concrete strength (MPa)	30.55	68.09
Shell concrete strength (MPa)	30.55	68.09
Outer steel tube squash load (kN)	1414 mm^2×290 MPa	2468 mm^2×355 MPa

The parameters and their limits used in the statistical analysis (ANOVA) connected with the compression capacities resulted from the experimental test are listed in Table 8.6, while Table 8.7 presents the results of ANOVA analysis. As shown in Table 8.7, the squash load of the outer steel tube has the most significant effect on compression capacity. The parameter second in importance is the core concrete compressive strength, followed by the shell concrete compressive strength, which has a smallest influence on the compression capacity of CFDCST stub columns.

The data in Table 8.7 also clarify the interaction between parameters. The ANOVA results show that interaction between the different parameters had no significant effect on the compression capacity of CFDCST columns; all interactions had contribution values smaller than 1%.

It worth mention that the ranked effect of parameters on the compression capacity of composite columns is not general; it depends on the number of parameters and their ranges. But these results give significant indications for developing the future designs of CFDCST stub columns.

Table 8.6 CFDCST column properties included in statistical analysis

CFDCST columns	Core f_c (MPa)	Shell f_c (MPa)	Outer steel tube squash load (kN)	Compression capacity (kN)
CC1-SC1-OT1	30.55	30.55	1414×290	1435.05
CC1-SC1-OT2	30.55	30.55	2468×355	1979.44
CC1-SC2-OT1	30.55	68.09	1414×290	1606.89
CC1-SC2-OT2	30.55	68.09	2468×355	2044.44
CC2-SC1-OT1	68.09	30.55	1414×290	1570.15
CC2-SC1-OT2	68.09	30.55	2468×355	2153.11
CC2-SC2-OT1	68.09	68.09	1414×290	1784.39
CC2-SC2-OT2	68.09	68.09	2468×355	2274.77

Table 8.7 Statistical results for the capacity of CFDCST columns

CFDCST parameter	DF	Sum of squares	Contribution (%)
Core f_c (MPa)	1	64190	10.02
Shell f_c (MPa)	1	41004	6.4
Outer steel tube squash load (kN)	1	528021	82.44
Interactions:			
Core f_c × Shell f_c	1	1226	0.19
Core f_c × outer tube squash load	1	1044	0.16
Shell f_c × outer tube squash load	1	4971	0.78
Error	1	25	0.0
Total	7	640482	100

8.3.5 CFST Columns as Repair Configuration

During the service life of structures, especially public structures, they are subjected to high stresses due to increasing different load conditions. Under these loads, unacceptable deformations which could impair the performance of the structures might develop. Sometimes, rebuilding affected structures is not ideal solution. This motivates another solution, strengthening or repairing these structures. If the elements of these structures have not lost their full strength, repair could be more economical than rebuilding.

To that end, the CFST configuration has been applied in repairing and strengthening arrangements for reinforced concrete columns (Sezen and Miller, 2011; Lu *et al.*, 2015a, 2015b). This suggests by extension that a CFDCST column configuration could be used in repairing or strengthening deformed CFST columns. The bigger size steel tube could surround the deformed CFST column, the fresh concrete poured in shell region between these two tubes and this concrete can take the form of a deformed inner CFST column, resulting in a repaired column.

8.3.5.1 Experimental and Test Program of the Repairing Configuration

In this part of the study, eight hollow steel tubes were prepared; four were filled with normal-strength concrete (CC1-R), and four with high-strength concrete (CC2-R), as shown in Table 8.4. These eight CFST columns were loaded up to 85% of their compression capacity. There were two reasons for this choice of percentage of total capacity: First, this level covers the elastic stage of loading and shows the column deformation at the level of plastic behavior. Second, at this level of loading, the CFST column does not reach its ultimate capacity and the retained capacity will be beneficial in the repair configuration.

There is another significant point; the deformation performance of the CFST stub column with normal-strength concrete is significantly different from that of one made with high-strength concrete. Normal-strength CFST stub columns show ductile behavior and reach compression capacity with high levels of axial and lateral deformations, while high-strength CFST stub columns have brittle behavior and achieve the compression capacity with very little axial and lateral deformation (Figure 8.19). For normal-strength CFST stub columns, extra lateral deformation happened when the column was loaded to more than 85% of ultimate capacity. It was then very hard to enclose the distorted column with an appropriate diameter of outer steel tube. So, the 85% of compression capacity was chosen as a reasonable and acceptable ratio for both normal and high-strength CFST stub columns to facilitate their repair.

Curves of end-shortening behavior as a function of compression loading were saved for columns which were loaded to 85% of the compression capacities. After the load was applied, the deformed columns were left for a specific time to allow the spring-back behavior of tested columns to appear. If the repair procedure was started immediately after testing, the spring-back behavior might cause cracks in shell concrete and weaken the bond between the shell concrete and steel tubes.

Next, deformed CFST stub columns were centered in a bigger size steel tube and fill the shell region with fresh concrete. After curing, eight composite columns were tested to failure, and their compression behavior curves recorded. This was intended to study the performance of the repaired columns and compared to the performance of CFDCST columns discussed in previous sections. Figure 8.20 shows the repaired specimens before testing.

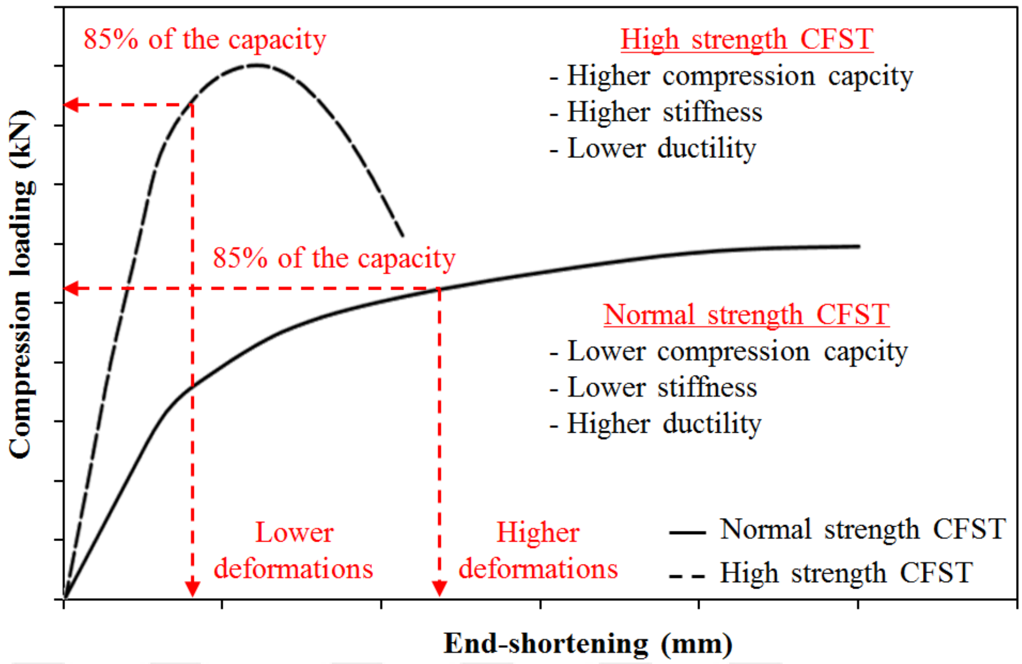

Figure 8.19 Behaviors of normal- and high-strength CFST stub columns

Figure 8.20 Composite columns of repair configuration before testing

8.3.5.2 Repaired Columns Filled with NS Core Concrete

- **End-shortening versus compression loading curves**

The compression behaviors of repaired columns with normal-strength (NS) core concrete compared to corresponding CFDCST columns and columns loaded up to 85% of the compression capacity (Figures 8.21–8.24 and Table 8.8). These comparisons were done to allow comparison and discussion of the ductility and stiffness behaviors of repaired and corresponding intact CFDCST columns.

Table 8.8 Results of stub columns specimens

Specimens	$N_{exp.}$ (kN)	Specimens	$N_{exp.}$ (kN)
CC1	723.69	CC2	844.35
CC1-R	625.01	CC2-R	727.94
CC1-R	625.74	CC2-R	732.41
CC1-R	623.65	CC2-R	727.03
CC1-R	624.86	CC2-R	726.22
CC1-OT1	923.57	CC2-OT1	1372.88
CC1-OT2	1480.55	CC2-OT2	1884.10
CC1-SC1-OT1	1435.05	CC1-SC1-OT1-R	1483.29
CC1-SC1-OT2	1979.44	CC1-SC1-OT2-R	1969.90
CC1-SC2-OT1	1606.89	CC1-SC2-OT1-R	1576.73
CC1-SC2-OT2	2044.44	CC1-SC2-OT2-R	2115.89
CC2-SC1-OT1	1570.15	CC2-SC1-OT1-R	1553.42
CC2-SC1-OT2	2153.11	CC2-SC1-OT2-R	2105.73
CC2-SC2-OT1	1784.39	CC2-SC2-OT1-R	1837.58
CC2-SC2-OT2	2274.77	CC2-SC2-OT2-R	2259.66

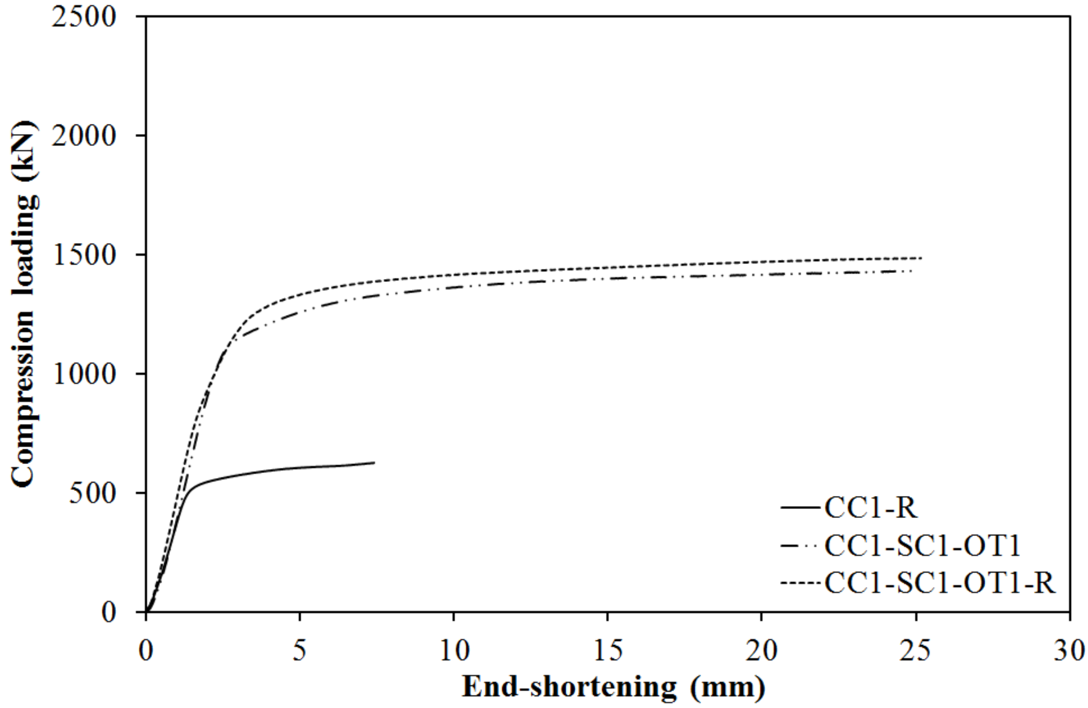

Figure 8.21 Load–shortening curves for CC1-SC1-OT1-R

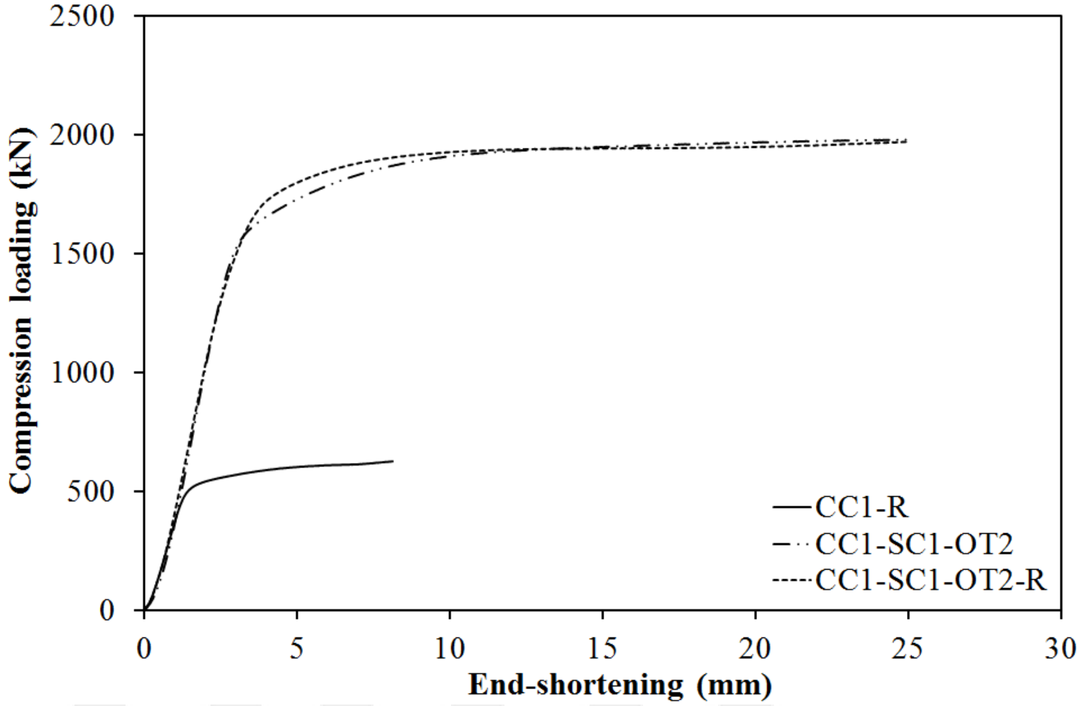

Figure 8.22 Load–shortening curves for CC1-SC1-OT2-R

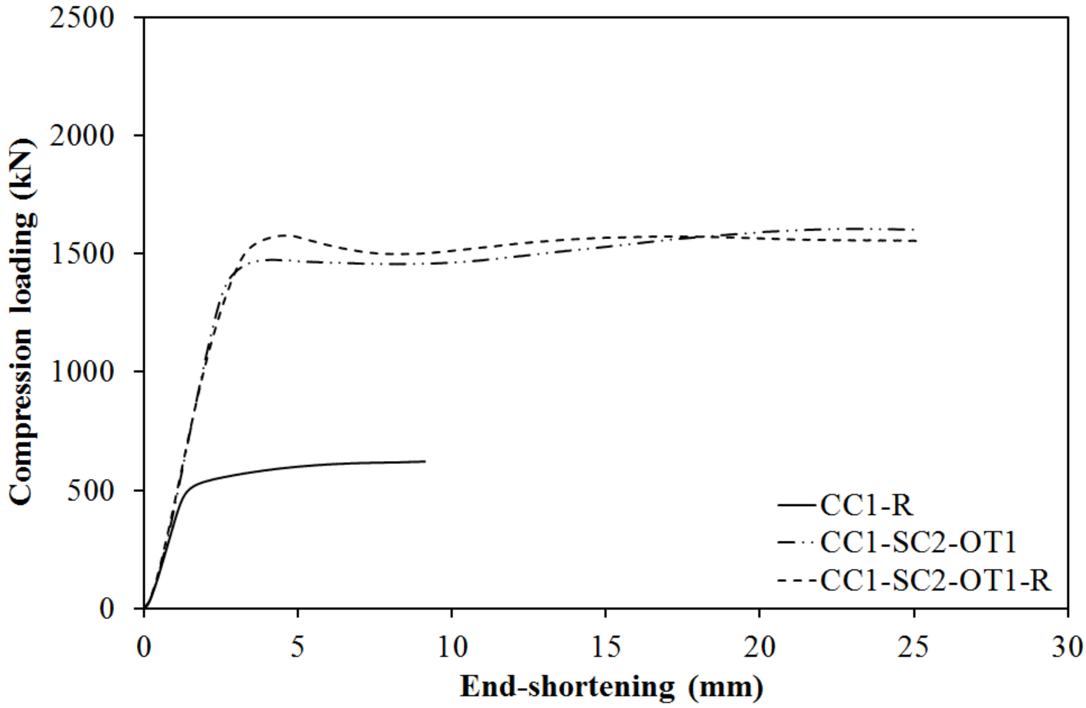

Figure 8.23 Load–shortening curves for CC1-SC2-OT1-R

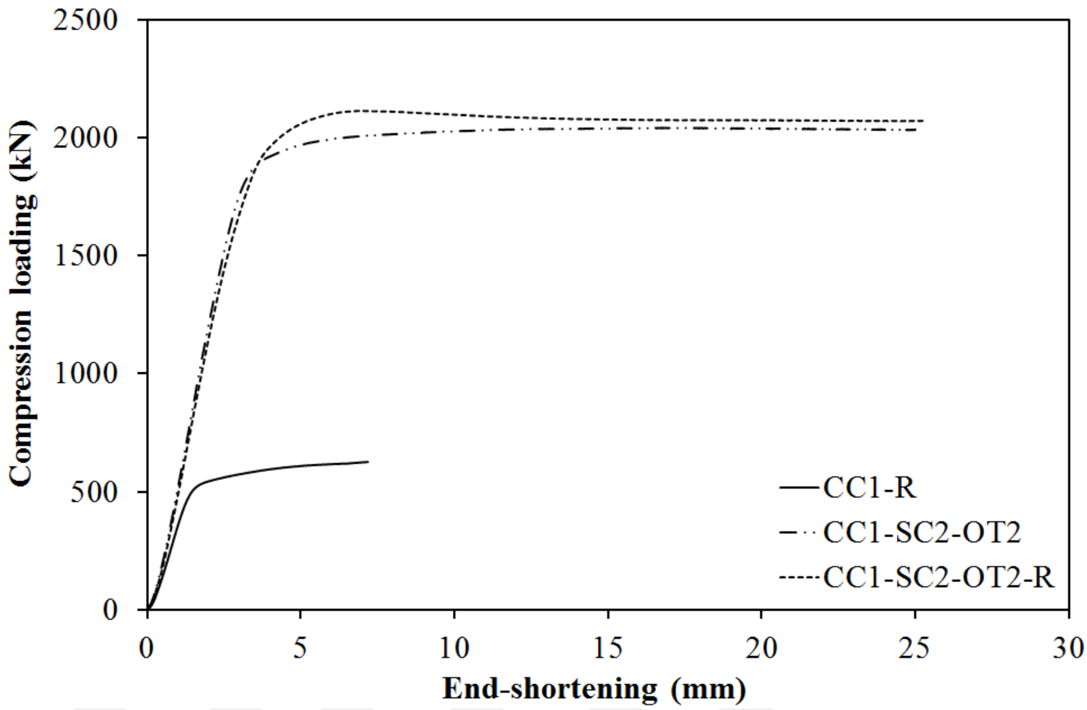

Figure 8.24 Load–shortening curves for CC1-SC2-OT2-R

The deformed CFST columns filled with normal-strength concrete examined a significant value of plastic deformations at 85% of the compression capacity. Four CC1-R specimens tested to 85% of their compression capacity experienced end-shortening ranging from 7.18 to 9.10 mm (Figures 8.21–8.24), and these levels of deformation caused visible permanent lateral deformation. It can be clearly noted based on Figures 8.21–8.24 that the repaired specimens have stiffness and ductility very close to that of their CFDCST counterparts.

Figure 8.25 illustrates the compression capacities and the capacity differences between repaired stub columns CC1-SC1-OT1-R, CC1-SC1-OT2-R, CC1-SC2-OT1-R, and CC1-SC2-OT2-R and the corresponding CFDCST columns. According to this comparison, it can be deduced that the repaired specimens offer a very close compression performance to the counterpart CFDCST columns. Also, it is important to note there is no contrary effect of the inner columns due to their plastic deformation on the outer tube and shell concrete. This behavior may stem from the mechanical properties of the steel, where the CFST columns were not completely tested to failure, which means that strength was reserved to allow the steel and concrete to stand up under compression.

The smaller diameter tube is classified as compact according to AISC360-16 due to its geometric and mechanical properties. When the compact circular section had a sufficient thickness, it enabled the steel to exhibit enhanced yield strength under longitudinal compression, and confined the concrete core to maximize its compressive strength ($0.95f_c$) (ANSI/AISC360-16, 2016).

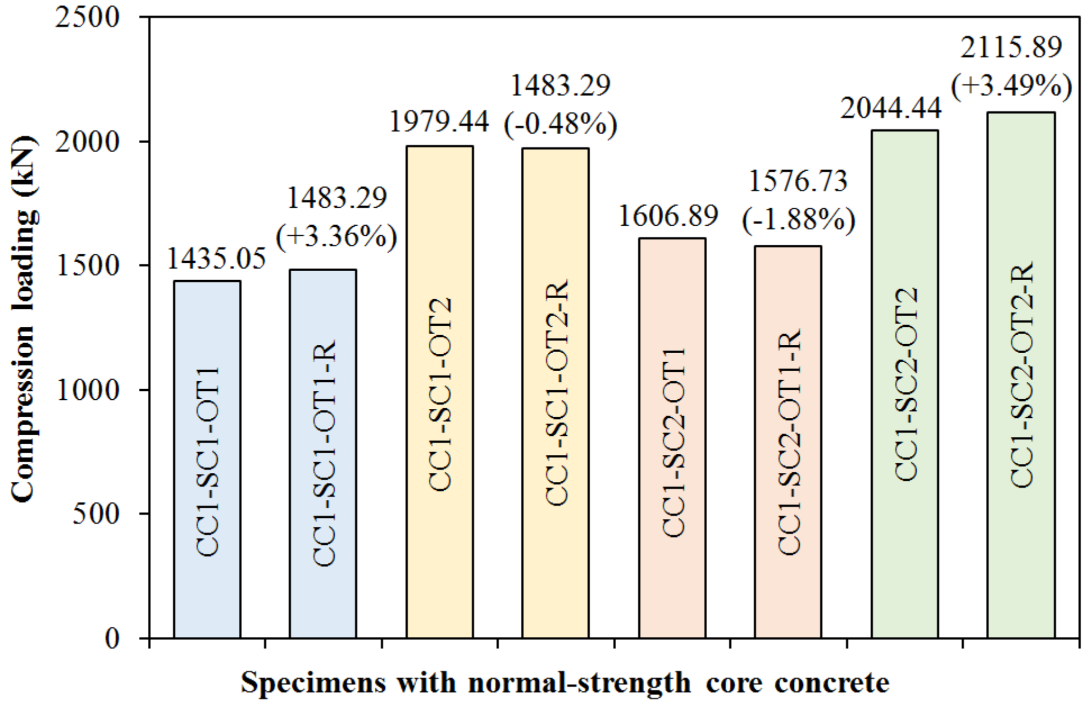

Figure 8.25 CFDCST and repaired specimens with NS core concrete

- **Failure modes**

Figure 8.26 illustrates the failure modes of repaired specimens. Again, local materials failure was observed. Concrete crushing had a larger contribution to the failure modes of these specimens, while shear failure was more dominant in the corresponding CFDCST specimens. The specimen with thinner outer steel tube and high-strength shell concrete (Figure 8.26c) showed a greater concentration of local materials failure compared to the specimen with normal-strength shell concrete (Figure 8.26a). In return, no difference in behavior was noticed for specimens with a thicker outer steel tube (Figures 8.26b and d).

In turn, for specimens with high-strength shell concrete, the failure modes differed according to the outer steel tube thickness, as shown in Figures 8.26c and d. No such difference was observed for specimens with normal-strength shell concrete; this behavior explains the interaction between the effect of outer steel tube thickness and the shell concrete compressive strength on the failure modes of repaired specimens.

Figure 8.26 Failure modes of repaired columns with NS core concrete

8.3.5.3 Repaired Columns Filled with HS Core Concrete

- **End-shortening against compression loading curves**

The compression behaviors of repaired columns with high-strength (HS) core concrete were compared to corresponding CFDCST columns and columns which loaded up to 85% of the compression capacity (Figures 8.27–8.30 and Table 8.8).

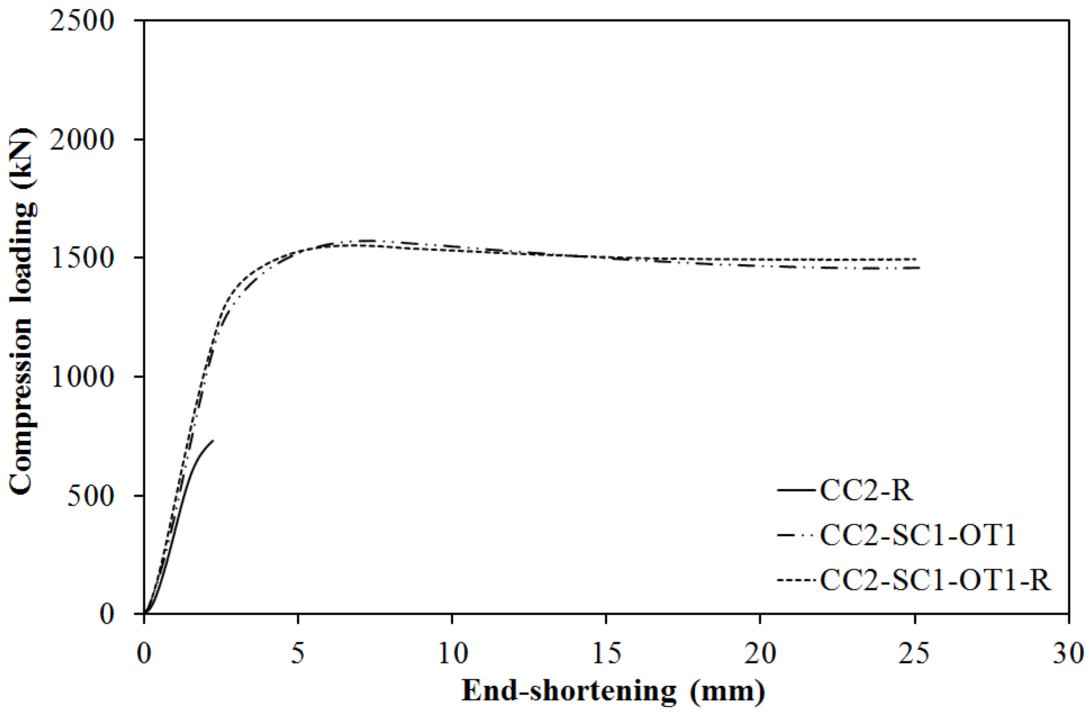

Figure 8.27 Load–shortening curves for CC2-SC1-OT1-R

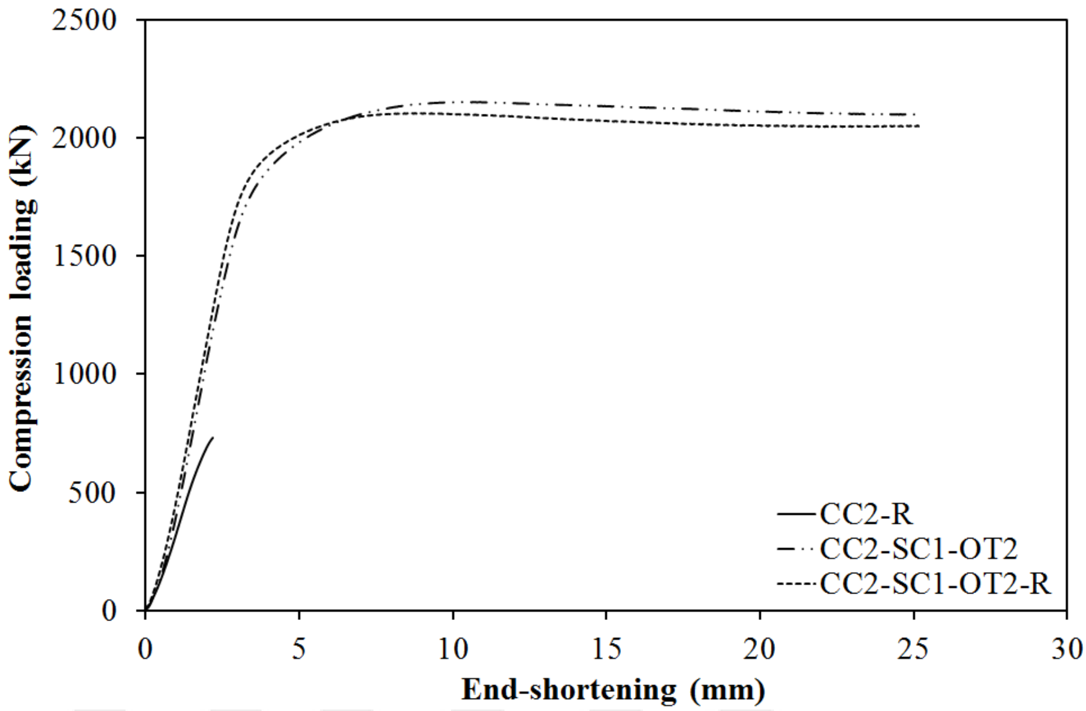

Figure 8.28 Load–shortening curves for CC2-SC1-OT2-R

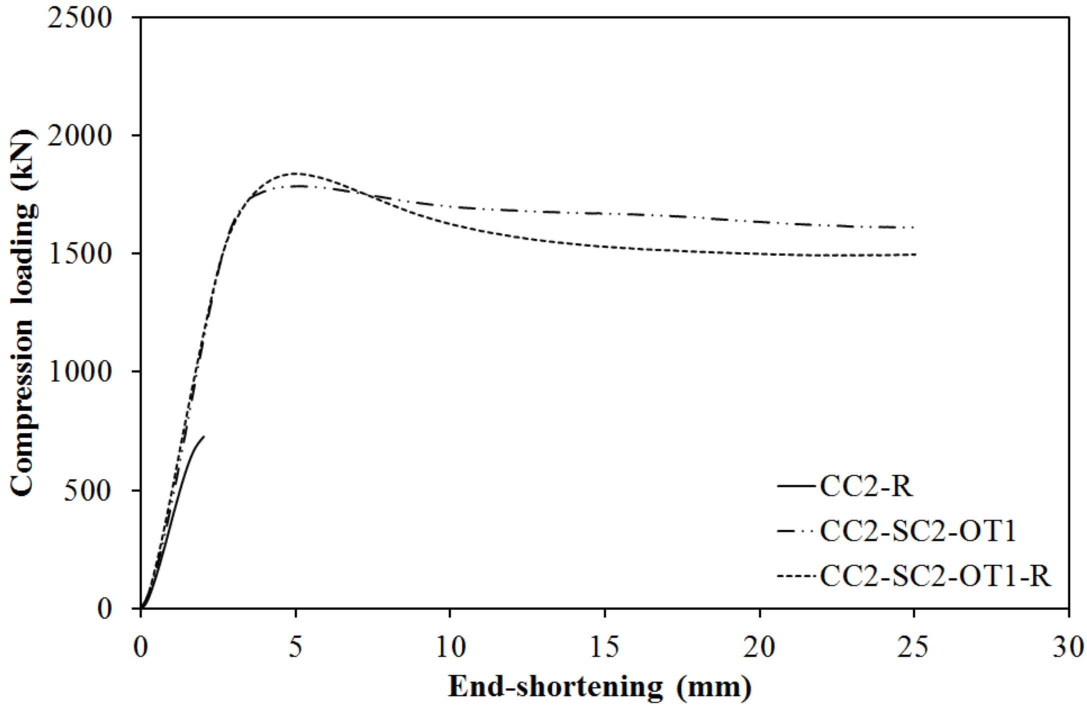

Figure 8.29 Load–shortening curves for CC2-SC2-OT1-R

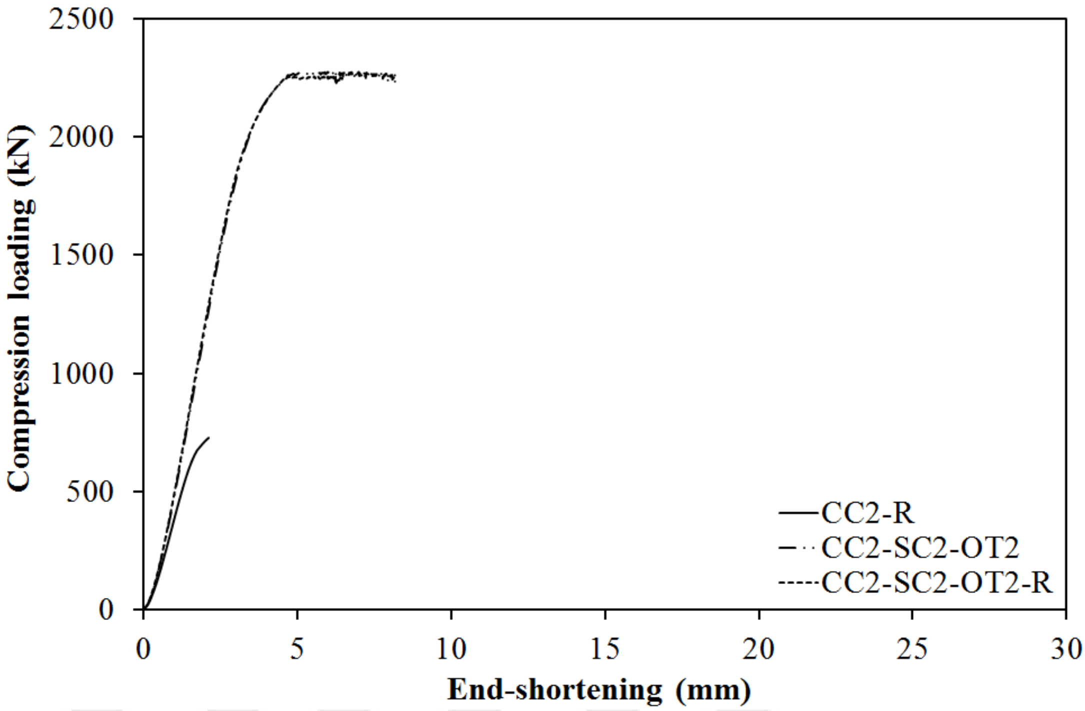

Figure 8.30 Load–shortening curves of CC2-SC2-OT2-R

As previously mentioned, high-strength CFST stub specimens reach their compression capacities at small levels of deformation (Figure 8.19). Therefore, the CC2-R specimens obtained 85% of compression capacity at levels of end-shortening varying from 2.03 mm to 2.24 mm. At this level of deformation, plastic deformation was observed for CFST stub specimens (e.g. CC2-R). Due to the small levels of deformation, the perpetual deformations were not highly obvious, unlike those in CFST specimens with normal-strength core concrete. The repaired specimens developed significant compression capacities, with values very close to those of the corresponding CFDCST specimens.

Figure 8.31 illustrates the compression capacities and the differences in capacity between the repaired stub columns—CC2-SC1-OT1-R, CC2-SC1-OT2-R, CC2-SC2-OT1-R, and CC2-SC2-OT2-R—and their CFDCST counterparts. According to this comparison, it can be deduced that the repaired specimens could offer very close compression performance to the corresponding CFDCST. Additionally, the stiffness and ductility behaviors of repaired specimens are very close to these of the CFDCST specimens (Figures 8.27–8.30).

As stub columns specimens with normal-strength core concrete, it can be concluded that the stub columns specimens with high-strength core concrete can be repaired by using larger diameter circular steel tube and infill the shell region by normal or high-strength concrete.

- **Failure modes**

Figure 8.32 presents the failure modes of repaired specimens with high-strength core concrete. Again, the crushing of concrete governed the failure modes, as the repaired specimens were prepared with normal-strength core concrete.

The specimen with thinner outer steel tube and high-strength shell concrete (Figure 8.32c) shows more concentration of local materials failure at the bottom of the specimen compared to the specimen with normal-strength shell concrete (Figure 8.32a). No visible failure mode was found for specimen CC2-SC2-OT2-R (Figure 8.32d) due to safety constraints of the testing machine, as mentioned in Section 8.3.4.2. Specimen CC2-SC1-OT2-R (Figure 8.32b) showed deformation similar to that of specimen CC2-SC1-OT1-R (Figure 8.32a). These specimens show the effect of normal and high-strength shell concretes on the failure modes of the specimens for both thin and thick outer steel tubes (Figure 8.32a–c).

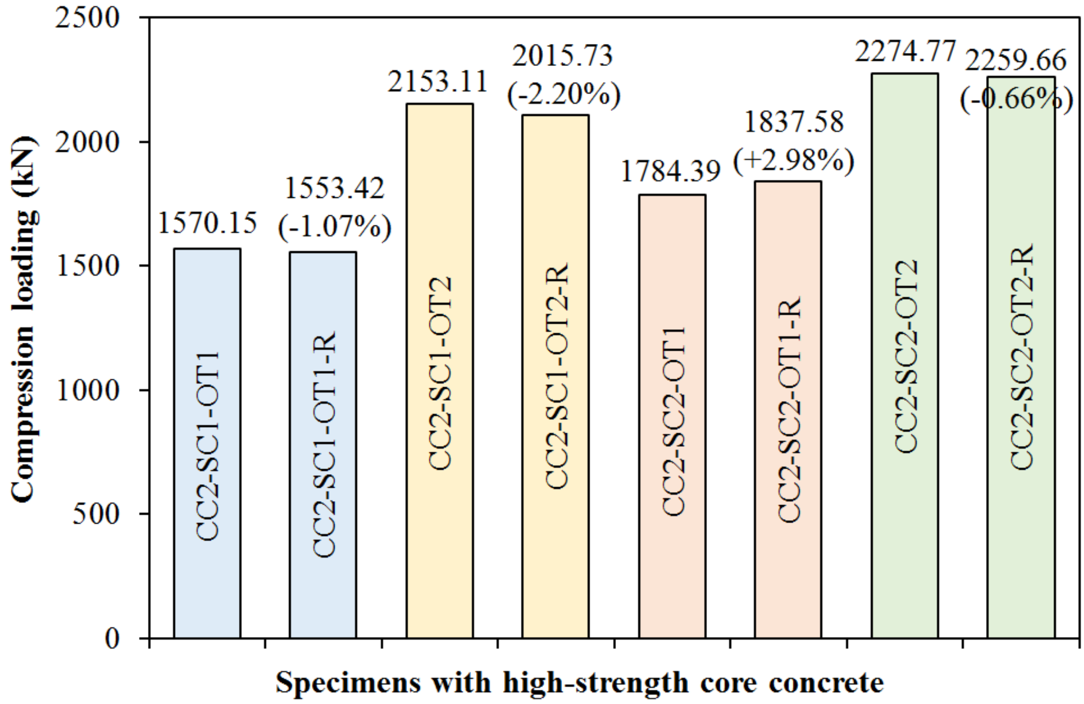

Figure 8.31 CFDCST and repaired columns with HS core concrete

(a) CC2-SC1-OT1-R (b) CC2-SC1-OT2-R (c) CC2-SC2-OT1-R (d) CC2-SC2-OT2-R

Figure 8.32 Failure modes of repaired columns with HS core concrete

8.4 Summary and Conclusion

The rapid growth in construction technology has stimulated structural engineers to develop new approaches, especially applications for composite structures. CFST columns are considered important members of the family of composite columns. Changes in structure design and size, such as long-span bridges and high-rise buildings required CFST columns with a larger cross-section to support the resulting heavy loads. Concrete-filled double steel tubular (CFDST) columns are a new configuration developed to satisfy these requirements with lower material usage and potentially lower self-weight. This configuration can be used in design or as a repair form.

This chapter investigated the capability of concrete-filled double circular steel tube stub columns through experimental and statistical analysis to develop them for use in composite structure applications. Concrete with normal and high compressive strengths were used for the shell and core regions, and two different outer steel tubes with the same diameter but with different properties (one with a smaller thickness and lower yield strength, and one with higher thickness and higher yield strength) were used, while one steel tube (with the same diameter and properties) was used as an inner tube.

These geometric and materials properties were selected with the aim to experimentally determine the impact of each factor on the compression performance of the resulting column. Statistical analysis was used to estimate the contribution of each parameter to the compression capacities of the tested columns. An additional investigation was carried out to explore the possibility of CFDCST configuration in repairing deformed

CFST columns. Based on the results of the two parts of this study, the following conclusions can be drawn:

- The CFDCST column configuration is efficient in enhancing compression, ductility, and stiffness performance over that of the corresponding CFST column. The use of this configuration minimizes the cross-sectional dimension of composite columns with equivalent performance.
- The presence of the inner steel tube divides the infill concrete into two parts: shell and core regions. This offers the option to use different concrete types and classes with various properties to fill the outer and inner steel tubes.
- The experimental results confirmed that the inner steel tube provided a full contribution to confine both the core and shell concrete, especially when normal-strength concrete was used in the shell and core regions.
- The contribution of the inner steel tube clearly improved the ductility and toughness of the composite columns especially with high-strength concrete in core and shell regions.
- The failure modes of stub CFDCST columns follow the failure behavior of stub CFST columns; local materials failure was observed.
- The sectional view of the tested columns revealed that the thicker outer steel tubes provided superior confinement of and good interaction between the shell concrete and the inner tube.
- The significant contribution of the outer steel tube is undeniable; the results of the statistical analysis showed it has the greatest effect on the compression capacity of CFDCST stub columns. The strength of the core and shell concretes have the second and third most important effects on compression capacity, respectively.
- The experimental results clarified that the using the CFDCST configuration for repair had high potential in repairing deformed CFST columns. Both the outer steel tube and shell concrete provided significant improvement in compression capacity and compensated for the deformation of the repaired CFST columns.
- The behavior of CFST stub columns with high-strength core concrete is different from the behavior of those filled with normal-strength core concrete.

Normal-strength CFST stub columns experienced high plastic deformation comapred to high-strength CFST stub columns.

- The values for compression capacity, ductility, and the stiffness performances of repaired columns was very close to that of the corresponding CFDCST columns.
- Repaired CFDCST columns with both normal-strength shell concrete and high-strength shell concrete exhibited performance very close to that of the corresponding CFDCST stub columns.

CHAPTER 9

SUMMARY, CONCLUSIONS, AND RECOMMENDATIONS FOR FURTHER STUDY

9.1 Summary

The goal of this thesis was to investigate the compressive behavior and confinement effect under axial loading of concrete-filled steel tube (CFST) columns. The other chapters of this thesis described the use of various types of concrete—normal-weight, lightweight, self-compacted, and high-performance concrete—with different compressive strengths to fill circular, hollow steel tubes to form CFST columns.

In addition to the classical CFST column configurations, a new configuration concept was applied to enhance the behavior of composite columns: concrete-filled double steel tubular (CFDST) columns. This new technique was also used to repair deformed CFST columns. For assessment, the test results compared with results of the AISC360-16, Eurocode 4 (EC4), AS5100.6, and AIJ2001 design specifications. The present thesis contributed to fill the gap of research in CFST columns applications.

In total, 82 CFST column specimens were tested. These tests were distributed between studies, with the tests described in four chapters—Chapter Five through Chapter Eight.

In a brief recapitulation, Chapter Five has two parts. The first focused on the effect of the different parameters: *L/D* ratio, *D/t* ratio, steel tube yield strength (f_y), and concrete compressive strength (f_c) on the behavior and the confinement effect of circular CFST columns. These properties are close to and out the limitations of the four design codes specifications (AISC16-360, EC4, AS5100.6, and AIJ2001). For this purpose, 18 CFST specimens were tested, with three *L/D* ratios, including short, medium, and long columns and two *D/t* ratios. This choice of parameters allowed observation of the confinement effect.

Concrete mixes of three different strengths were selected; two possess strengths very close to upper limits of the design codes included in this study, while, the third is beyond the limits of these codes. Two European steel specifications (S235 and S355) were used to address different confinement conditions.

The second part of the work described in Chapter Five concentrated on assessment of the predictions of design code specifications and a examine of the impact of each factor on the compression behavior and confinement effect within CFST columns. This aim was addressed by collecting 1036 results from experimental studies reported in the literature, as well as the results for 18 CFST columns described in the first part of the chapter. The resulting database included a wide range of parameters of circular CFST columns tested under axial compression.

The work described in Chapter Six studied the effect of two different infilled concrete types—self-compacted concrete and lightweight aggregate concrete—on the performance of CFST circular columns. LWC was observed to contribute to a reduction in the self-weight of CFST columns while improving the performance of columns, especially in seismically active regions. SCC also represents a compelling development in concrete technology; it can flow, compact, and fill a formwork, mold, or steel tube under only its own weight, with no vibration required. This property of SCC makes it an attractive choice for use in building CFST members to improve the construction process.

Although based on these test results and a survey of the literature it can be seen that LWC and SCC offer superior properties, there is a lack of studies about the application of these types of concrete for CFST columns. This study attempted to provide data to help fill this research gap. For this purpose, sixteen hollow steel columns filled with LWC and SCC were tested to study the response of LWCFST and SCCFST columns under axial compression loading. Specimens with four different *L/D* ratios were used in this experimental study to observe the behavior of short, medium, and long columns; the specimens also had three different *D/t* ratios. The predictions of design codes AISC16-360, EC4, and AIJ2001, codes established for normal-weight CFST columns, were compared to the experimental results for columns built with LWC and SCC.

Chapter Seven discussed the contribution of steel-bar reinforcement on the compressive performance of LWCFST columns subjected to axial loading. Generally, such reinforcement is used in piles, caissons, and bridge piers to improve strength and help with their connection to other elements. In spite of the fact that such reinforcement is an excellent structural engineering solution, few experimental studies have examined the performance of reinforced CFST columns. Furthermore, no previous study has dealt with RLWCFST columns.

Therefore, the study described in Chapter Seven attempted to gather data to help fill this research gap. It aimed to (1) explore the experimental behavior of RLWCFST circular columns with three different *L/D* ratios, two different *D/t* ratios, and two different diameters of longitudinal steel bars; (2) compare the response of RLWCFST columns to the corresponding LWCFST columns; and (3) investigate the appropriateness of the AISC360-16 and EC4 design codes for predicting the compression capacity of LWCFST and RLWCFST columns.

Chapter Eight studied a new configuration concept for CFST columns. The essential function of the CFST is bearing loads. With the increasing load of new structures with larger spans or greater heights, the cross-sectional dimensions of load-bearing columns must increase, leading to a corresponding increase in self-weight and the cost of construction. Concrete-filled double steel tubular (CFDST) columns were envisioned and developed as a new configuration to satisfy load-bearing requirements without the drawbacks. In this study, this configuration used both alone and as an approach to repair damaged CFST columns.

The first part of this study investigated the capacity and properties of concrete-filled double circular steel tube stub columns using experimental testing and statistical analysis. Selected geometric and materials properties were selected with the aim to examine the effect of each factor on the compression response of the column. The potential of the CFDCST configuration as a method for repairing deformed CFST columns was also investigated. Statistical analysis of the experimental results examined the contribution of each parameter to the compression capacities of the columns.

9.2 Conclusions

According to the studies reported in this thesis, the following general conclusions can be drawn:

1. The structural properties of CFST members are improved by their “composite action”, interactions between the outer steel tube and core concrete. CFST columns can be considered as an alternative for applications in which bare steel or reinforced concrete columns would otherwise be used. The composite column merges the best features of both steel and concrete in a single structural element.

2. The mechanical and geometrical properties of the steel tube affect the behavior of CFST columns. A thicker steel tube with higher yield strength provide higher compression capacity and an increased confinement effect than a thinner steel tube with lower yield strength. In addition, the cross-section dimension of a CFST column affects the behavior of the columns; compression capacity increases as the cross-section dimension increases.

3. The concrete compressive strength affects the behavior of and the confinement effect within CFST columns. High-strength concrete provides higher compressive capacity but a weaker confinement effect compared to normal-strength concrete, which provides a stronger confinement effect.

4. Column length has a significant impact on the response of CFST columns. Short columns present higher compression capacities and confinement effects than long columns.

5. The failure modes of CFST columns change according to their length. Short columns fail by local materials failure of steel tube and concrete. Long or slender columns fail by flexural or overall buckling.

6. Medium-length CFST columns offer behavior that is a combination of that of short and long columns; local and global buckling failure modes can be observed in the same column. Either local materials failure modes or global failure modes can govern for columns of the same length based on its other

properties, such as the thickness and yield of the steel tube or on the type of core concrete used.

7. The type of concrete also affects the performance of CFST columns. LWCFST columns provide lower compressive capacity, initial stiffness, ductility, and confinement effect compared to SCCFST columns. However, SCC offers other advantages: it can flow into place under only its self-weight, which eases the construction process. This option is significant, particularly in CFST construction due to the relatively small cross sections of the steel tubes. The use of LWC leads to a reduction in the self-weight of the structure and increases its strength to weight ratio, important in heavy structures. Additionally, the use of LWC offers improvements in the static, dynamic and thermal properties of the final structure.

8. LWCFST columns can experience discharge in compression loading after reaching their compression capacity because of the porous structure of the pumice lightweight aggregate. SCCFST columns did not exhibit the same behavior.

9. For LWCFST columns with pumice lightweight aggregate concrete, local materials failure governs the failure behavior, even for long columns. This behavior means the weakness of this type of concrete must be considered before its use in long CFST columns. Among SCCFST columns, even long columns showed good interaction between steel and concrete based on the strength index of these columns, which had values greater than one. This means SCC is an appropriate concrete type for use in CFST columns.

10. The use of steel-bar reinforcement increases the compression capacity, ductility, and toughness of RLWCFST columns and improves the mechanical properties of LWC.

11. For RLWCFST columns, the use of the steel-bar reinforcement affected the failure modes of the columns along with *D/t* ratios controlled the compression behavior curves, where the curves were more smooth and gradual in the presence of reinforcement.

12. The contribution of steel-bar reinforcement for both short and long columns is more significant when combined with the use of thin outer steel tubes. However, for medium-length columns, a thick steel tube combined with steel-bar reinforcement offered a higher improvement in the compression capacity improvement ratio. For medium-length columns with thin steel tubes, the compression capacity can be enhanced by increasing the steel-bar ratio.

13. The contribution of steel-bar reinforcement combined with a thin steel tube for medium-length RLWCFST columns exhibited a higher ductility improvement ratio compared with its use with a thick steel tube.

14. The most significant difference between the codes is their consideration of the confinement effect. AISC360-16 allows for an increase in the concrete core stress the due to transverse confinement by increasing the multiplier of the capacity equation from 0.85 to 0.95 for circular cross-section, while AIJ2011 uses a constant confinement factor of 0.27 in its calculations only for columns with circular cross-sections. EC4 and AS5100.6 consider the confinement effect in their calculations if the value of the slenderness ratio, $\bar{\lambda}$, is less than or equal to 0.5.

15. The CFDCST column configuration is very efficient in enhancing compression, ductility and stiffness performance. The use of this configuration leads to the potential to minimize the cross-sectional dimension of composite columns.
16. According to the statistical comparison with the collected database, the predictions of AS5100.6 and EC4 are in better agreement with experimental results even for properties beyond their limits. In future, these codes could change their limits to cover a wider range of CFST columns properties. While AISC360-16 and AIJ2001 give conservative predictions for CFST columns within and beyond their design code limits, this indicates that more attention should be paid to the confinement effect for circular CFST columns in both codes.
17. The CFDCST stub column configuration proved very effective in offering improved compression, ductility, and stiffness performance over the

corresponding CFST columns. The use of this configuration can allow minimization of the cross-sectional dimension of composite columns.

18. In this new configuration, there is a possibility to use different types and different concrete compressive strength for both the core and shell zones due to presence of the inner steel tube. Steel tubes with different properties can be used for both the outer and inner tubes. The experimental results confirmed that the inner steel tube provided full contribution to confine both core and shell concrete especially when using normal-strength concrete in shell and core regions.
19. The experimental results presented that using the CFDCST configuration in the repair process worked well in the repair of deformed CFST columns. Both the outer steel tube and shell concrete provided significant improvements in compression capacity and compensated for the deformation of the repaired CFST.

9.3 Recommendations for Further Study

Throughout this thesis, study of the compressive behavior of CFST columns subjected to axial loading included various types of concrete. They included concretes of different types—normal-weight, lightweight aggregate, self-compacted, and high-performance concrete—and different concrete compressive strengths—from normal- to ultra-high-strength concrete. In addition, a new column configuration, concrete-filled double circular steel tubes stub columns were examined, and the use of this new configuration in the repair process for CFST columns studied. Further studies are important to build a full picture and give a better understanding of the behavior of CFST columns and provide guidelines for the design process.

Based on this work, further studies are important in following areas:

1. Materials properties – concrete and steel:
    a. Enhance the mechanical properties of lightweight aggregate concrete either by using artificial lightweight aggregate or by adding steel fiber-reinforced lightweight aggregate concrete.
    b. Develop a mix design for lightweight aggregate self-compacting concrete. This concrete would offer a combination of two advantages: light weight

and self-compaction ability. It can be developed in different grades, as both a normal-strength and high-strength concrete.

c. Develop the mechanical properties of existing self-compacted concrete by using steel-fiber-reinforced self-compacted concrete with various concrete compressive strengths.

d. Improve the mechanical properties of high-performance concrete and ultra-high-performance concrete.

e. Investigate the use of different kinds of concrete from those used in these studies, such as recycled aggregate concrete, geopolymer concrete, etc.

f. Use high-strength steel tubes and study the effect of this steel strength on the confinement effect in CFST columns.

2. Study the effect of imperfections in both steel tubes and concrete.
3. Study the effect of concrete shrinkage and creep. Shrinkage and creep affect the bonding strength between steel and the concrete core in CFST columns, and these behaviors lead to a reduction in compression capacity.
4. Perform fire resistance tests for different types of concrete. This is especially important for high-strength concrete, which has brittle behavior; further investigation is necessary to improve this behavior and determine how to prevent the concrete from exploding in fires.
5. Develop methods to increase the confinement effect in CFST columns by using external or internal reinforcement approaches, such as using external fiber reinforced polymer (FRP) jacketing, steel rings, or different internal reinforcing configurations.
6. Develop the concrete-filled double steel tube column concept by using different cross-section types for both the outer and inner tubes, as well as different material types for both tubes. These tests may include a mix of steel tubes with FRP tubes or other materials to improve the performance of this configuration.
7. Investigate the influence of length on the compressive performance of concrete-filled double steel tube columns.
8. Investigate the using of different techniques in repairing deformed CFST columns, such as FRP jacketing techniques.
9. All columns resulting from the further work suggested above can be studied under dynamic loading tests. The hysteretic response of columns is significant

for structures under seismic loading and high-rise building under wind loading, in addition to other accidental loads, such as impact loading. Therefore, the dynamic response of CFST columns is significant and must be investigated.

10. In addition to the experimental investigation, numerical investigation using finite element methods should be adopted to investigate the different cases of CFST columns which are difficult to carry out experimentally.
11. Develop the formulations of existing design codes, especially for recognizing the confinement and the length effects. Expand the limits of these codes to encompass columns with a wider range of material and geometric properties.

REFERENCES

ABAQUS. 2014. CAE6.14-4, Dassault Systèmes Simulia Corp. Providence, RI, USA.

Abdelgadir, E., Bohai, J., Zhongqiu, F., and Zhengqing, H. (2011). The behavior of lightweight aggregate concrete filled steel tube columns under eccentric loading. *Steel & Composite structures.* **11(6)**, 469-488.

Abed, F., AlHamaydeh, M., and Abdalla, S. (2013). Experimental and numerical investigations of the compressive behavior of concrete filled steel tubes (CFSTs). *Journal of Constructional Steel Research.* **80**, 429-439.

ACI211.1-91. 2002. Standard practice for selecting proportions for normal, heavyweight, and mass concrete. U.S.A.: American Concrete Institute.

ACI211.4R-08. 2008. Guide for selecting proportions for high-strength concrete using portland cement and other cementitious material. U.S.A.: American Concrete Institute.

ACI213R-03. 2003. Guide for structural lightweight-aggregate concrete. U.S.A.: American Concrete Institute.

ACI237R-07. 2007. Self-consolidating concrete. U.S.A.: American Concrete Institute.

ACI363R-10. 2010. Report on high-strength concrete. U.S.A.: American Concrete Institute.

AIJ2001. 2001. Architectural institute of Japan (AIJ) standard for structural calculation of steel reinforced concrete structures, 5th edition (in Japanese).

AL-Eliwi, B.J.M., Ekmekyapar, T., Faraj, R.H., Göğüş, M.T., and AL-Shaar, A.A.M. (2017). Performance of lightweight aggregate and self-compacted concrete-filled steel tube columns *Steel and Composite Structures.* **25(3)**, 299-314.

ANSI/AISC360-16. 2016. American institute of steel constrcution, specification for structural steel buildings. Chicago, Illinois, U.S.A.

ANSYS. 2016. Mechanical APDL theory reference version 17.2.

AS5100.6-2004. 2004. Australian standard bridge design part 6: Steel and composite construction. Sydney, Australia: Standards Australia Limited.

Aslani, F., Uy, B., Tao, Z., and Mashiri, F. (2015). Predicting the axial load capacity of high-strength concrete filled steel tubular columns. *Steel and Composite Structures.* **19(4)**, 967-993.

ASTMA370−17a. 2017. Standard test methods and definitions for mechanical testing of steel products. West Conshohocken, PA 19428-2959. United States.

ASTMC39/C39M-15. 2015. Standard test method for compressive strength of cylindrical concrete specimens. West Conshohocken, PA 19428-2959, United States.: ASTM International.

ASTMC39/C39M−15a. 2015. Standard test method for compressive strength of cylindrical concrete specimens. West Conshohocken, PA. U.S.A.: ASTM International.

ASTMC330/C330M-14. 2014. Standard specification for lightweight aggregates for structural concrete. West Conshohocken, PA. U.S.A.: ASTM International.

ASTMC494/C494M−17. 2017. Standard specification for chemical admixtures for concrete. West Conshohocken, PA, U.S.A.: ASTM International.

ASTMC617/C617M−15. 2015. Standard practice for capping cylindrical concrete specimens. West Conshohocken, PA. U.S.A.: ASTM International.

ASTME8/E8M-16. 2016. Standard test methods for tension testing of metallic material, ASTM International. West Conshohocken, PA 19428-2959. United States.

Attard, M.M., and Setunge, S. (1996). Stress-strain relationship of confined and unconfined concrete. *ACI Materials Journal.* **93(5)**, 432-441.

Baltay, P., and Gjelsvik, A. (1990). Coefficient of friction for steel on concrete at high normal stress. *Journal of Materials in Civil Engineering-ASCE.* **2(1)**, 46-49.

Beck, A.T., Oliveira, W.L.A.D., Nardim, S.D., and Debs, A.L.H.C.E. (2009). Reliability-based evaluation of design code provisions for circular concrete-filled steel columns. *Engineering Structures.* **31(10)**, 2299-2308.

Bohai, J., Zhongqiu, F., Qu, T., and Wang, M. (2013). Stability behavior of lightweight aggregate concrete filled steel tubular columns under axial compression. *Advanced Steel Construction.* **9(1)**, 1-13.

Bridge, R.Q., and O'Shea, M.D. 1997. Australian composite code concrete filled steel tubes – a comparison of international codes and practices. Paper presented at the International Conference on Composite Construction, Innsbruck, Austria.

Cai, J., Pan, J., and Wu, Y. (2015). Mechanical behavior of steel-reinforced concrete-filled steel tubular (SRCFST) columns under uniaxial compressive loading. *Thin-Walled Structures.* **97**, 1-10.

Caldarone, M.A. 2008. High-strength concrete: A practical guide: CRC Press.

Candappa, D.P., Setunge, S., and Sanjayan, J.G. (1999). Stress versus strain relationship of high strength concrete under high lateral confinement. *Cement and Concrete Research.* **29**, 1977–1982.

Chan, T.-M., Huai, Y.-M., and Wang, W. (2015). Experimental investigation on lightweight concrete-filled cold-formed elliptical hollow section stub columns. *Journal of Constructional Steel Research.* **115**, 434-444.

Chandra, S., and Berntsson, L. 2002. Lightweight aggregate concrete: Elsevier.

Chang, X., Liang, R.Z., Zhou, W., and Zhang, Y.-B. (2013). Study on concrete-filled stainless steel–carbon steel tubular (CFSCT) stub columns under compression. *Thin-Walled Structures.* **63**, 125-133.

Chang, X., Wei, Y.-Y., and Yun, Y.-C. (2012). Analysis of steel-reinforced concrete-filled-steel tubular (SRCFST) columns under cyclic loading. *Construction and Building Materials.* **28(1)**, 88-95.

Chao, S.H., Karki, N.B., Cho, J.S., and Waweru, R.N. 2012. Use of double punch test to evaluate the mechanical performance of fiber reinforced concrete High Performance Fiber Reinforced Cement Composites 6 (pp. 27-34): Springer.

Chen, J., Wang, Y., Roeder, C.W., and Ma, J. (2017). Behavior of normal-strength recycled aggregate concrete filled steel tubes under combined loading. *Engineering Structures.* **130**, 23-40.

Chen, Z.-p., Liu, F., Zheng, H.-H., and Xue, J.-Y. 2010. Research on the bearing capacity of recycled aggregate concrete-filled circle steel tube column under axial compression loading. Paper presented at the International conference on mechanic automation and control engineering (MACE), Wuhan, China.

Dabaon, M.A., El-Boghdadi, M.H., and Hassanein, M.F. (2009). Experimental investigation on concrete-filled stainless steel stiffened tubular stub columns. *Engineering Structures.* **31(2)**, 300-307.

Darwin, D., Dolan, C.W., and Nilson, A.H. 2016. Design of concrete structures (Fifteenth Edition ed.). U.S.A.: McGraw-Hill Education.

De Oliveira, W.L.A., De Nardin, S., de Cresce El Debs, A.L.H., and El Debs, M.K. (2009). Influence of concrete strength and length/diameter on the axial capacity of CFT columns. *Journal of Constructional Steel Research.* **65(12)**, 2103-2110.

Ding, F.-x., Zhu, J., Cheng, S., and Liu, X. (2018). Comparative study of stirrup-confined circular concrete-filled steel tubular stub columns under axial loading. *Thin-Walled Structures.* **123**, 294-304.

Dundu, M. (2012). Compressive strength of circular concrete filled steel tube columns. *Thin-Walled Structures.* **56**, 62-70.

EFNARC. 2005. Specifications and guidelines for self-compacting concrete-specification, production and use. English ed. The European Federation of Specialist Construction Chemicals and Concrete Systems.

Ekmekyapar, T. (2016). Experimental performance of concrete filled welded steel tube columns. *Journal of Constructional Steel Research.* **117**, 175-184.

Ekmekyapar, T., and AL-Eliwi, B.J.M. (2016). Experimental behaviour of circular concrete filled steel tube columns and design specifications. *Thin-Walled Structures.* **105**, 220-230.

Ekmekyapar, T., and AL-Eliwi, B.J.M. (2017). Concrete filled double circular steel tube (CFDCST) stub columns. *Engineering Structures.* **135**, 68-80.

Ellobody, E., and Young, B. (2006). Nonlinear analysis of concrete-filled steel SHS and RHS columns. *Thin-Walled Structures.* **44(8)**, 919-930.

Ellobody, E., Young, B., and Lam, D. (2006). Behaviour of normal and high strength concrete-filled compact steel tube circular stub columns. *Journal of Constructional Steel Research.* **62(7)**, 706-715.

EN10219. 2006. EN 10219, Cold formed welded structural hollow sections of non-alloy and fine grain steels. CEN, Brussels: European Standard.

Endo, T., Shioi, Y., Hasegawa, A., and Wang, H.J. 2000. Experimental study on reinforced concrete filled steel tubualr structure. Paper presented at the 25th Conference on Our World in Concrete and Structures, Singapore.

Eurocode2. 2004. Design of concrete structures - EN 1992-1-1Part 1-1: Generalrules and rules for buildings Brussels: European Committee for Standardization (CEN).

Eurocode3. 2005. Design of steel structures – EN 1993-1-1 Part 1.1: Generalrules and rules for buildings. Brussels: European Committee for Standardization (CEN).

Eurocode4. 2004. Design of composite steel and concrete structures, EN 1994-1-1:2004 Part 1-1: General rules and rules for buildings. Brussels: European Committee for Standardization (CEN).

Ezeldin, A.S., and Balaguru, P.N. (1992). Normal- and high-strength fiber-reinforced concrete under compression. *Journal of Materials in Civil Engineering, ASCE.* **4(4)**, 415-429.

Fu, Z., Ji, B., Lv, L., and Zhou, W. (2011). Behavior of lightweight aggregate concrete filled steel tubular slender columns under axial compression. *Advanced Steel Construction.* **7(2)**, 144-156.

Fujii, K. 1994. Structural and ultimate behavior of two types of mortar filled steel tubes in compression. Paper presented at the Proceedings of the 4th ASCCS International Conference, Košice, Slovakia.

Furlong, R.W. (1968). Strength of steel-encased concrete beam-columns. *Journal of Structural Divison ASCE.* **93(5)**, 113-124.

Gardner, N.J., and Jacobson, E.R. (1967). Structural behavior of concrete filled steel tubes. *ACI Journal Proceedings.* **64(7)**, 404-413.

Georgios, G., and Lam, D. (2004). Axial capacity of circular concrete-filled tube columns. *Journal of Constructional Steel Research.* **60(7)**, 1049-1068.

Ghannam, S., Jawad, Y.A., and Hunaiti, Y. (2004). Failure of lightweight aggregate concrete-filled steel tubular columns. *Steel and Composite Structures.* **4(1)**, 1-8.

Guler, S., Çopur, A., and Aydogan, M. (2012). Flexural behaviour of square UHPC-filled hollow steel section beams. *Structural Engineering and Mechanics.* **43(2)**, 225-237.

Guler, S., Çopur, A., and Aydogan, M. (2013). Axial capacity and ductility of circular UHPC-filled steel tube columns. *Magazine of Concrete Research.* **65(15)**, 898-905.

Gupta, P.K., Sarda, S.M., and Kumar, M.S. (2007). Experimental and computational study of concrete filled steel tubular columns under axial loads. *Journal of Constructional Steel Research.* **63(2)**, 182-193.

Hamidian, M.R., Jumaat, M.Z., Alengaram, U.J., Ramli Sulong, N.H., and Shafigh, P. (2016). Pitch spacing effect on the axial compressive behaviour of spirally reinforced concrete-filled steel tube (SRCFT). *Thin-Walled Structures.* **100**, 213-223.

Han, L.-H. (1997). Theoretical analyses and experimental researches for the behaviors of high strength concrete filled steel tubes subjected to axial compression. *Industrial construction.* **27**, 39-44 [in Chinese].

Han, L.-H. (1998). Fire resistance of concrete filled steel tubular columns *Advances in Structural Engineering.* **2(1)**, 35-40.

Han, L.-H. (2000). Tests on concrete filled steel tubular columns with high slenderness ratio. *Advances in Structural Engineering.* **3(4)**, 337-344.

Han, L.-H. (2002). Tests on stub columns of concrete-filled RHS sections. *Journal of Constructional Steel Research.* **58**, 353–372.

Han, L.-H., and Huo, J.-s. (2003). Concrete-filled hollow structural steel columns after exposure to iso-834 fire standard. *Journal of Structural Engineering ASCE.* **129(1)**, 68-78.

Han, L.-H., Jiang, S., Cao, Y., and Yuan, Y. (1999). Experimental studies on the behavior and strength of very slender concrete filled steel tubular columns. *Steel construction.* **14(2)**, 21-25 [in Chinese].

Han, L.-H., Wei, L., and Reidar, B. (2014). Developments and advanced applications of concrete-filled steel tubular (CFST) structures: Members. *Journal of Constructional Steel Research.* **100**, 211-228.

Han, L.-H., and Yao, G.-H. (2003). Behaviour of concrete-filled hollow structural steel (HSS) columns with pre-load on the steel tubes. *Journal of Constructional Steel Research.* **59(12)**, 1455-1475.

Han, L.-H., and Yao, G.-H. (2004). Experimental behaviour of thin-walled hollow structural steel (HSS) columns filled with self-consolidating concrete (SCC). *Thin-Walled Structures.* **42(9)**, 1357-1377.

Han, L.-H., Yao, G.-H., Chen, Z.-B., and Yu, Q. (2005a). Experimental behaviours of steel tube confined concrete (STCC) columns. *Steel and Composite Structures.* **5(6)**, 459-484.

Han, L.-H., Yao, G.-H., and Zhao, X.-L. (2005b). Tests and calculations for hollow structural steel (HSS) stub columns filled with self-consolidating concrete (SCC). *Journal of Constructional Steel Research.* **61(9)**, 1241-1269.

Han, L.-H., Zhao, X.-L., and Tao, Z. (2001). Tests and mechanics model for concrete-filled SHS stub columns, columns and beam-columns. *Steel and Composite Structures.* **1(1)**, 51-74.

Hassanein, M.F., Elchalakani, M., and Patel, V.I. (2017). Overall buckling behaviour of circular concrete-filled dual steel tubular columns with stainless steel external tubes. *Thin-Walled Structures.* **115**, 336-348.

Hassanein, M.F., Kharoob, F.O., and Liang, Q.Q. (2013). Behaviour of circular concrete-filled lean duplex stainless steel–carbon steel tubular short columns. *Engineering Structures.* **56**, 83-94.

Hicks, S.J., and Newman, G.M. 2002. Design guide for SHS concrete filled columns U.K.: Corus Tubes.

Hoang, A.L., and Fehling, E. (2017a). Numerical study of circular steel tube confined concrete (STCC) stub columns. *Journal of Constructional Steel Research.* **136**, 238-255.

Hoang, A.L., and Fehling, E. (2017b). A review and analysis of circular UHPC filled steel tube columns under axial loading. *Structural Engineering and Mechanics.* **62(4)**, 417-430.

Hu, H.-T., Huang, C.-S., Wu, M.-H., and Wu, Y.-M. (2003). Nonlinear analysis of axially loaded concrete-filled tube columns with confinement effect. *Journal of Structural Engineering ASCE.* **129(10)**, 1322–1329.

Imran, I., and Pantazopoulou, S.J. (1996). Experimental study of plain concrete under triaxial stress. *ACI Structural Journal.* **93(6)**, 589-601.

Kato, B. (1995). Compressive strength and deformation capacity of concrete-filled tubular stub columns (Strength and rotation capacity of concrete-filled tubular columns, Part 1). *Journal of Structural and Construction Engineering, AIJ.* **468**, 183-191 [in Japanese].

Kato, B. (1996). Column curves of steel-concrete composite members. *Journal of Construction and Steel Research.* **39(2)**, 121-135.

Kloppel, V.K., and Goder, W. (1957). An investigation of the load carrying capacity of concrete-filled steel tubes and development of design formula. *Der Stahlbau.* **26 (2)**, 44-50.

Knowles, R.B., and Park, R. (1969). Strength of concrete filled steel tubular columns. *Journal of the Structural Division ASCE.* **95(12)**, 2565-2588.

Knowles, R.B., and Park, R. (1970). Axial load design for concrete filled steel tubes. *Journal of the Structural Division ASCE.* **96(10)**, 2125-2153.

Kodur, V.K.R. (1998). Performance of high strength concrete-filled steel columns exposed to fire. *Candain Journal of Civil Engineering.* **25**, 975-981.

Kodur, V.K.R., and Lie, T.T. (1995). Fire performance of concrete-filled hollow steel columns *Journal of Fire Protection Engineering.* **7(3)**, 89-97.

Kodur, V.K.R., and Lie, T.T. (1996). Fire resistance of circular steel column filled with fiber-reinforced concrete. *Journol of Structural Engineering, ASCE.* **122(7)**, 776-782.

Köksal, F., Altun, F., Yiğit, İ., and Şahin, Y. (2008). Combined effect of silica fume and steel fiber on the mechanical properties of high strength concretes. *Construction and Building Materials.* **22(8)**, 1874-1880.

Kosmatka, S.H., and Wilson, M.L. 2011. Design and control of concrete mixtures, the guide to applications, methods, and materials (Fifteenth Edition ed.). U.S.A.: Portland Cement Association.

Kwan, A.K.H., Dong, C.X., and Ho, J.C.M. (2016). Axial and lateral stress–strain model for circular concrete-filled steel tubes with external steel confinement. *Engineering Structures.* **117**, 528-541.

Lachemi, M., Hossain, K.M.A., and Lambros, V.B. (2006a). Axial load behavior of self-consolidating concrete-filled steel tube columns in construction and service stages *ACI Structural Journal.* **103(1)**, 38-47.

Lachemi, M., Hossain, K.M.A., and Lambros, V.B. (2006b). Self-consolidating concrete filled steel tube columns-design equations for confinement and axial strength. *Structural Engineering and Mechanics.* **22(5)**, 541-562.

Lai, M.H., and Ho, J.C.M. (2014). Confinement effect of ring-confined concrete-filled-steel-tube columns under uni-axial load. *Engineering Structures.* **67**, 123-141.

Lai, M.H., and Ho, J.C.M. (2015). Optimal design of external rings for confined CFST columns. *Magazine of Concrete Research.* **67(19)**, 1017-1032.

Lai, Z., and Varma, A.H. (2015). Noncompact and slender circular CFT members: Experimental database, analysis, and design. *Journal of Constructional Steel Research.* **106**, 220-233.

Li, B., and Hao, R.-x. (2005). The analysis of concrete filled steel tube column carrying capacity *Journal of Baotou University of Iron and Steel Technology.* **24(1)**, 5-8 [in Chinese].

Li, B., and Wen, Y. (2003). Experimental study on bearing capacity of long concrete filled steel tubular columns with axial compression. *Earthquake Engineering and Engineering Vibration.* **23(5)**, 130-133 [in Chinese].

Li, N., Lu, Y.-Y., Li, S., and Liang, H.-J. (2015). Statistical-based evaluation of design codes for circular concrete-filled steel tube columns. *Steel and Composite Structures.* **18(2)**, 519-546.

Li, W., Han, L.-H., and Zhao, X.-L. (2012). Axial strength of concrete-filled double skin steel tubular (CFDST) columns with preload on steel tubes. *Thin-Walled Structures.* **56**, 9-20.

Liao, F.-Y., Han, L.-H., and Tao, Z. (2013). Behaviour of CFST stub columns with initial concrete imperfection: Analysis and calculations. *Thin-Walled Structures.* **70**, 57-69.

Lie, T.T., and Kodur, V.K.R. (1996). Fire resistance of steel columns filled with bar-reinforced concrete. *Journal of Structural Engineering, ASCE.* **122(1)**, 30-36.

Liew, J.Y.R., and Xiong, D.X. (2009). Effect of preload on the axial capacity of concrete-filled composite columns. *Journal of Constructional Steel Research.* **65(3)**, 709-722.

Liew, J.Y.R., and Xiong, D.X. (2012). Ultra-high strength concrete filled composite columns for multi-storey building construction. *Advances in Structural Engineering.* **15(9)**, 1487-1503.

Liew, J.Y.R., and Xiong, M. 2015. Design guide for concrete filled tubular members with high strength materials to eurocode 4. Singapore: Research Publishing Services.

Liew, J.Y.R., Xiong, M., and Xiong, D. (2016). Design of concrete filled tubular beam-columns with high strength steel and concrete. *Structures.* **8**, 213-226.

Lin, C.Y. 1988. Axial capacity of concrete infilled cold-formed steel columns. Paper presented at the Ninth International Specialty Conference on Cold-Formed Steel Structures, St. Louis, Missouri, U.S.A.

Lin, M.-L., and Tsai, K.-C. 2001. Behaviour of double-skinned composite steel tubular columns subjected to combined axial and flexural loads. Paper presented at the In: Proceedings of the first international conference on the steel and composite structures, Pssan, Korea.

Lu, H., Han, L.-H., and Zhao, X.-L. (2010). Fire performance of self-consolidating concrete filled double skin steel tubular columns: Experiments. *Fire Safety Journal.* **45(2)**, 106-115.

Lu, H., Zhao, X.-L., and Han, L.-H. (2009). Fire behaviour of high strength self-consolidating concrete filled steel tubular stub columns. *Journal of Constructional Steel Research.* **65(10-11)**, 1995-2010.

Lu, Y.-Y., Liang, H.-J., Li, S., and Li, N. (2015a). Axial behavior of RC columns strengthened with SCC filled square steel tubes. *Steel and Composite Structures.* **18(3)**, 623-639.

Lu, Y.-Y., Liang, H.-J., Li, S., and Li, N. (2015b). Eccentric strength and design of RC columns strengthened with SCC filled steel tubes. *Steel and Composite Structures.* **18(4)**, 833-852.

Mander, J.B., Priestley, M.J.N., and Park, R. (1988). Theoretical stress-strain model for confined concrete. *Journal of Structural Engineering ASCE.* **114(8)**, 1804-1826.

Mathias, J. 2002a. Composite action and confinement effect in tubular steel - concrete columns. (Doctor of Philosophy Ph.D. Thesis), Chalmers University of Technology, Göteborg (Sweden).

Mathias, J. (2002b). The efficiency of passive confinement in CFT columns. *Steel and Composite Structures.* **2(5)**, 379-396.

Mathias, J. (2003). Composite action in connection regions of concrete-filled steel tube columns. *Steel and Composite Structures.* **3(1)**, 47-64.

Mathias, J., and Gylltoft, K. (2001). Structural behavior of slender circular steel-concrete composite columns under various means of load application. *Steel and Composite Structures.* **1(4)**, 393-410.

Mathias, J., and Gylltoft, K. (2003). Mechanical behavior of circular steel – concrete composite stub columns. *Journal of Structural Engineering, ASCE.* **128(8)**, 1073-1081.

Matsui, C., and Tsuda, K. 1996. Strength and behavior of slender concrete filled steel tubular columns. Paper presented at the Proceedings of The Second International Symposium on Civil Infrastructure Systems, Hong Kong, China.

Mo, K.H., Alengaram, U.J., and Jumaat, M.Z. (2016). Bond properties of lightweight concrete – A review. *Construction and Building Materials.* **112**, 478-496.

Mo, K.H., Ling, T.-C., Alengaram, U.J., Yap, S.P., and Yuen, C.W. (2017). Overview of supplementary cementitious materials usage in lightweight aggregate concrete. *Construction and Building Materials.* **139**, 403-418.

Moon, J., Kim., J.J., Lee, T.-H., and Lee, H.-E. (2014). Prediction of axial load capacity of stub circular concrete-filled steel tube using fuzzy logic. *Journal of Constructional Steel Research.* **101**, 184-191.

Moon, J., Lehman, D.E., Roeder, C.W., and Lee, H.-E. (2013). Strength of circular concrete-filled tubes with and without internal reinforcement under combined loading. *Journal of Structural Engineering.* **139(12)**, 1-12.

Mouli, M., and Khelafi, H. (2007). Strength of short composite rectangular hollow section columns filled with lightweight aggregate concrete. *Engineering Structures.* **29(8)**, 1791-1797.

Neogi, P.K., San, H.K., and Chapman, J.C. (1969). Concrete filled tubular steel columns under eccentrical loading. *Journal of the Structural Engineer.* **47(5)**, 187-195.

Neville, A.M. 2011. Properties of concrete (Vol. 5). England: Pearson Education Limited.

O'Shea, M.D., and Bridge, R.Q. 1994, October 18-19, 1994. Tests of thin-walled concrete-filled steel tubes. Paper presented at the Twelfth International Specialty Conference on Cold-Formed Steel Structures, St. Louis, Missouri, U.S.A.

O'Shea, M.D., and Bridge, R.Q. 1997. The design for local buckling of concrete filled steel tubes. Paper presented at the Composite Construction - Conventional and Innovate, Innsbruck, Austria.

O'Shea, M.D., and Bridge, R.Q. (2000). Design of circular thin-walled concrete filled steel tubes *Journal of Structural Engineering ASCE.* **126(11)**, 1295-1303.

Oehlers, D.J., and Bradford, M.A. 1995. Composite steel and concrete structural members: Fundamental behaviour (First Edition ed.). U.K.: PERGAMON.

Oehlers, D.J., and Bradford, M.A. 2002. Elementary behaviour of composite steel and concrete structural members. U.K.: Butterworth-Heinemann.

Oliveira, W.L.A.D., Nardin, S.D., Debs, A.L.H.d.C.E., and Debs, M.K.E. (2010). Evaluation of passive confinement in CFT columns. *Journal of Constructional Steel Research.* **66(4)**, 487-495.

Pagoulatou, M., Sheehan, T., Dai, X.H., and Lam, D. (2014). Finite element analysis on the capacity of circular concrete-filled double-skin steel tubular (CFDST) stub columns. *Engineering Structures.* **72**, 102-112.

Patel, V.I. 2013. Nonlinear inelastic analysis of concrete-filled steel tubular slender beam-columns. (Doctor of Philosophy Ph.D. Thesis), Victoria University, Australia.

Portolés, J.M., Romero, M.L., Bonet, J.L., and Filippou, F.C. (2011). Experimental study of high strength concrete-filled circular tubular columns under eccentric loading. *Journal of Constructional Steel Research.* **67(4)**, 623-633.

Portolés, J.M., Serra, E., and Romero, M.L. (2013). Influence of ultra-high strength infill in slender concrete-filled steel tubular columns. *Journal of Constructional Steel Research.* **86**, 107-114.

Qian, J., Li, N., Ji, X., and Zhao, Z. (2014). Experimental study on the seismic behavior of high strength concrete filled double-tube columns. *Earthquake Engineering and Engineering Vibration.* **13(1)**, 47-57.

Qu, X., Chen, Z., Nethercot, D.A., Gardner, L., and Theofanous, M. (2013). Load-reversed push-out tests on rectangular CFST columns. *Journal of Constructional Steel Research.* **81**, 35-43.

Rabbat, B.G., and Russell, H.G. (1985). Friction coefficient of steel on concrete or grout. *Journal of Structural Engineering-ASCE.* **111(3)**, 505-515.

Ramachandran, V.S. 1996. Concrete admixtures handbook: Properties, science and technology: William Andrew.

Richart, F.E., Brandzaeg, A., and Brown, R.L. (1928). A study of the failure of concrete under combined compressive stresses. *Bull. 185. Champaign, IL, USA: University of Illinois Engineering Experimental Station*.

Roeder, C.W., Cameron, B., and Brown, C.B. (1999). Composite action in concrete filled tubes. *Journal of Structural Engineering ASCE.* **125(5)**, 477-484.

Roeder, C.W., Lehman, D.E., and Thody, R. (2009). Composite action in CFT components and connections. *ENGINEERING JOURNAL.* **Fourth Quarter**, 229-242.

Roik, K., and Bergmann, R. 1985. Composite columns—design and examples for construction. Paper presented at the Composite and mixed construction.

Roy, R.K. 2010. A primer on the Taguchi method: Society of Manufacturing Engineers.

Russell, H.G. (1999). ACI defines high-performance concrete. *Concrete International.* **21(2)**.

Saisho, M., Abe, T., and Nakaya, K. (1999). Ultimate bending strength of high-strength concrete filled steel tube column. *Journal of Structural and Construction Engineering, AIJ.* **523**, 133-140 [in Japanese].

Sakino, K., and Hayashi, H. 1991. Behavior of concrete filled steel tubular stub columns under concentric loading. Paper presented at the Proceeding of the 3rd international conference on steel–concrete composite structures.

Sakino, K., Nakahara, H., Morino, S., and Nishiyama, I. (2004). Behavior of centrally loaded concrete-filled steel-tube short columns. *Journal of Structural Engineering ASCE.* **130(2)**, 180-188.

Schneider, H. 2006. Zum tragverhalten kurzer, umschnürter, kreisförmiger, druckglieder aus ungefasertem UHFB. (Doctoral Dissertation [In German]), University of Leipzig, Leipzig, Germany.

Schneider, S.P. (1998). Axially loaded concrete filled steel tube *Journal of Structural Engineering, ASCE.* **124(10)**, 1125-1138.

Sezen, H., and Miller, E.A. (2011). Experimental evaluation of axial behavior of strengthened circular reinforced-concrete columns. *Journal of Bridge Engineering.* **16(2)**, 238-247.

Shams, M., and Saadeghvaziri, M.A. (1997). State of the art of concrete-filled steel tubular columns. *ACI Structural Journal.* **94(5)**, 558-571.

Shanmugam, N.E., and Lakshmi, B. (2001). State of the art report on steel–concrete composite columns. *Journal of Constructional Steel Research.* **57**, 1041–1080.

Shaohuai, C., and Wanli, G. (1985). Behaviour and ultimate strength of long concrete-filled steel tubular columns. *Journal of Building Structures.* **1**, 32-40 [in Chinese].

Skazlić, M., Serdar, M., and Bjegović, D. 2008. Influence of test specimen geometry on compressive strength of ultra high performance concrete. Paper presented at the Second International Symposium on Ultra High Performance Concrete.

Song, T.-Y., Han, L.-H., and Yu, H.-X. (2010). Concrete filled steel tube stub columns under combined temperature and loading. *Journal of Constructional Steel Research.* **66(3)**, 369-384.

Tan, K. (2006). Analysis of formulae for calculating loading bearing capacity of steel tubular high strength concrete. *Journal of Southwest University of Science and Technology.* **21(2)**, 7-10 [in Chinese].

Tan, K.F., Pu, X.C., and Cai, S.H. (1999). Study on the mechanical properties of steel extra-high strength concrete encased in steel tubes. *Journal of Building Structures.* **20(1)**, 10-15 [in Chinese].

Tao, Z., Han, L.-H., Uy, B., and Chen, X. (2011). Post-fire bond between the steel tube and concrete in concrete-filled steel tubular columns. *Journal of Constructional Steel Research.* **67(3)**, 484-496.

Tao, Z., Han, L.-H., and Zhao, X.-L. (2004). Behaviour of concrete-filled double skin (CHS inner and CHS outer) steel tubular stub columns and beam-columns. *Journal of Constructional Steel Research.* **60(8)**, 1129-1158.

Tao, Z., Song, T.-Y., Uy, B., and Han, L.-H. (2016). Bond behavior in concrete-filled steel tubes. *Journal of Constructional Steel Research.* **120**, 81-93.

Tao, Z., Uy, B., Han, L.-H., and HE, S.-H. (2008). Design of concrete-filled steel tubular members according to the australian standard AS 5100 model and calibration *Australian Journal of Structural Engineering.* **8(3)**, 197-214.

Tao, Z., Uy, B., Han, L.-H., and Wang, Z.-B. (2009). Analysis and design of concrete-filled stiffened thin-walled steel tubular columns under axial compression. *Thin-Walled Structures.* **47(12)**, 1544-1556.

Tao, Z., Wang, Z.-B., and Yu, Q. (2013). Finite element modelling of concrete-filled steel stub columns under axial compression. *Journal of Constructional Steel Research.* **89**, 121-131.

Tomii, M., and Yoshimaro, K. 1977. Experimental studies one concrete filled steel tubular columns under concentric loading. Paper presented at the International

Colloquium on Stability of Structures Under Static and Dynamic Loads, Washington, DC.

Tue, N.V., Schneider, H., Simsch, G., and Schmidt, D. 2004. Bearing capacity of stub columns made of NSC, HSC and UHPC confined by a Steel Tube. Paper presented at the Proceedings of the International Symposium on Ultra High Performance Concrete, Kassel, Germany.

Uy, B., and Liew, J.Y.R. 2003. Composite steel – concrete structures. In W. F. C. a. J. Y. R. Liew (Ed.), The Civil Engineering Handbook (Second Edition ed., pp. 62). U.S.A: CRC PRESS.

Uy, B., Tao, Z., and Han, L.-H. (2011). Behaviour of short and slender concrete-filled stainless steel tubular columns. *Journal of Constructional Steel Research.* **67(3)**, 360-378.

Wan, C.-Y., and Zha, X.-X. (2016). Nonlinear analysis and design of concrete-filled dual steel tubular columns under axial loading. *Steel and Composite Structures.* **20(3)**, 571-597.

Wang, Q., Zhao, D., and Guan, P. (2004). Experimental study on the strength and ductility of steel tubular columns filled with steel-reinforced concrete. *Engineering Structures.* **26(7)**, 907-915.

Wang, Y.-B., Liew, J.Y.R., Lee, S.C., and Xiong, D.X. (2016). Experimental study of ultra-high-strength concrete under triaxial compression. *ACI Materials Journal.* **113(1)**, 105-112.

Wang, Y., Chen, J., and Geng, Y. (2015). Testing and analysis of axially loaded normal-strength recycled aggregate concrete filled steel tubular stub columns. *Engineering Structures.* **86**, 192-212.

Wang, Z.-B., Tao, Z., Han, L.-H., Uy, B., Lam, D., and Kang, W.-H. (2017a). Strength, stiffness and ductility of concrete-filled steel columns under axial compression. *Engineering Structures.* **135**, 209-221.

Wang, Z.-B., Tao, Z., and Yu, Q. (2017b). Axial compressive behaviour of concrete-filled double-tube stub columns with stiffeners. *Thin-Walled Structures.* **120**, 91-104.

Wille, K., Naaman, A.E., El-Tawil, S., and Parra-Montesinos, G.J. (2012). Ultra-high performance concrete and fiber reinforced concrete: achieving strength and ductility without heat curing. *Materials and Structures.* **45(3)**, 309-324.

Wille, K., Naaman, A.E., and Parra-Montesinos, G.J. (2011). Ultra-high performance concrete with compressive strength exceeding 150 mpa (22 ksi): A simpler way. *ACI Materials Journal.* **108(1)**, 46-54.

Xiamuxi, A., and Hasegawa, A. (2011). Compression test of RCFT columns with thin-walled steel tube and high strength concrete. *Steel and Composite Structures.* **11(5)**, 391-402.

Xiamuxi, A., and Hasegawa, A. (2012). A study on axial compressive behaviors of reinforced concrete filled tubular steel columns. *Journal of Constructional Steel Research.* **76**, 144-154.

Xincheng, P. 2012. Super-high-strength high performance concrete: CRC Press.

Xiong, M.-X., Xiong, D.-X., and Liew, J.Y.R. (2017). Axial performance of short concrete filled steel tubes with high-and ultra-high-strength materials. *Engineering Structures.* **136**, 494-510.

Xu, F., Chen, J., and Jin, W.-l. (2014). Experimental investigation of thin-walled concrete-filled steel tube columns with reinforced lattice angle. *Thin-Walled Structures.* **84**, 59-67.

Yahia, A., and Aïtcin, P.C. 2016. Self-consolidating concrete. In P.-C. Aïtcin and R. J. Flatt (Eds.), Science and Technology of Concrete Admixtures (pp. 491-502): Elsevier.

Yamamoto, T., Kawaguchi, J., and Morino, S. 2000, May 28-June 2, 2000. Experimental study of scale effects on the compressive behavior of short concrete-filled steel tube columns. Paper presented at the Composite Construction in Steel and Concrete IV, Banff, Alberta, Canada.

Yamamoto, T., Kawaguchi, J., and Morino, S. (2002). Experimental study of the size effect on the behaviour of concrete filled circular steel tube columns under axial compression. *Journal of Structural and Construction Engineering, AIJ.* **561**, 237–244 [in Japanese].

Yang, H., Lam, D., and Gardner, L. (2008). Testing and analysis of concrete-filled elliptical hollow sections. *Engineering Structures.* **30(12)**, 3771-3781.

Yang, Y.-F., and Han, L.-H. (2006a). Compressive and flexural behaviour of recycled aggregate concrete filled steel tubes (RACFST) under short-term loadings. *Steel and Composite Structures.* **6(3)**, 257-284.

Yang, Y.-F., and Han, L.-H. (2006b). Experimental behaviour of recycled aggregate concrete filled steel tubular columns. *Journal of Constructional Steel Research.* **62(12)**, 1310-1324.

Yang, Y.F., and Han, L.-H. (2012). Concrete filled steel tube (CFST) columns subjected to concentrically partial compression. *Thin-Walled Structures.* **50(1)**, 147-156.

Yi, S.-T., Yang, E.-I., and Choi, J.-C. (2006). Effect of specimen sizes, specimen shapes, and placement directions on compressive strength of concrete. *Nuclear Engineering and Design.* **236(2)**, 115-127.

Yu-Feng, A., Lin-Hai, H., and Xiao-Ling, Z. (2012). Behaviour and design calculations on very slender thin-walled CFST columns. *Thin-Walled Structures.* **53**, 161-175.

Yu, X., Tao, Z., and Song, T.Y. (2015). Effect of different types of aggregates on the performance of concrete-filled steel tubular stub columns. *Materials and Structures.* **49(9)**, 3591-3605.

Yu, Z.-W., Fa-xing, D., and S., C.C. (2007). Experimental behavior of circular concrete-filled steel tube stub columns. *Journal of Constructional Steel Research.* **63(2)**, 165-174.

Yu, Z., Ding, F., and Lin, S. (2002). Researches on behavior of high-performance concrete filled tubular steel short columns. *Journal of Building Structures.* **23(2)**, 41-47 [in Chinese].

Yu., Q., Tao, Z., and Wu, Y.-X. (2008). Experimental behaviour of high performance concrete-filled steel tubular columns. *Thin-Walled Structures.* **46(4)**, 362-370.

Zeghiche, J., and Chaoui, K. (2005). An experimental behaviour of concrete-filled steel tubular columns. *Journal of Constructional Steel Research.* **61(1)**, 53-66.

Zhang, S., and Wang, Y. (2004). Failure modes of short columns of high-strength concrete filled steel tubes. *China Civil Engineering Journal.* **37(9)**, 1-10 [in Chinese].

Zhao, X.-L., Wilkinson, T., and Hancock, G. 2005. Cold-formed tubular members and connections - structural behaviour and design. U.K.: Elsevier

Zhongqiu, F., Bohai, J., Lei, L., and Ming, Y. (2011b). The mechanical properties of lightweight aggregate concrete confined by steel tube *ASCE Geotechnical Special Publication.* **219**, 33-39.

Zhongqiu, F., Bohai, J., Lei, L., and Wenjie, Z. (2011a). Behavior of lightweight aggregate concrete filled steel tubular slender columns under axial compression *Advanced Steel Construction.* **7(2)**, 144-156.

Zhongqiu, F., Bohai, J., Zhou, Y., and Wang, X. (2011c). An experimental behavior of lightweight aggregate concrete filled steel tubular stub under axial compression *ASCE Geotechnical Special Publication.* **219**, 24-32.

Zhou, Y., Liu, X., Xing, F., Li, D., Wang, Y., and Sui, L. (2017). Behavior and modeling of FRP-concrete-steel double-skin tubular columns made of full lightweight aggregate concrete. *Construction and Building Materials.* **139**, 52-63.

Zhu, M., Liu, J., Wang, Q., and Feng, X. (2010). Experimental research on square steel tubular columns filled with steel-reinforced self-consolidating high-strength concrete under axial load. *Engineering Structures.* **32(8)**, 2278-2286.

Ziemian, R.D. 2010. Guide to stability design criteria for metal structures (Six Edition ed.). U.S.A: John Wiley & Sons, Inc.

CURRICULUM VITAE

PERSONAL INFORMATION

Name and Surname: Baraa Jabbar Mahmood AL-ELIWI

Nationality: IRAQI

Birth place and date: Mosul / IRAQ – January 02,1979

Marital status: Married

Email: baraa.aleliwi@gmail.com

EDUCATION

	Graduate School	Year
Master	Civil Engineering Department, College of Engineering, University of Mosul – IRAQ	2004
Bachelor	Civil Engineering Department, College of Engineering, University of Mosul – IRAQ	2001

WORK EXPERIENCE

	Place	Enrollment
2005 – 2011	Civil Engineering Department, College of Engineering, University of Mosul – IRAQ	Assistant Lecturer
2011 - Present	Civil Engineering Department, College of Engineering, University of Mosul – IRAQ	Lecturer

PUBLICATIONS

1. AL-Eliwi, B.J.M., Ekmekyapar, T., Faraj, R.H., Göğüş, M.T., and AL-Shaar, A.A.M. (2017). Performance of lightweight aggregate and self-compacted concrete-filled steel tube columns. *Steel and Composite Structures.* **25(3)**, 299-314.

2. Ekmekyapar, T., and Al-Eliwi, B.J.M. (2017). Concrete filled double circular steel tube (CFDCST) stub columns. *Engineering Structures.* **135**, 68-80.

3. Ekmekyapar, T., and Al-Eliwi, B.J.M. (2016). Experimental behaviour of circular concrete filled steel tube columns and design specifications. *Thin-Walled Structures.* **105**, 220-230.

4. AL-Eliwi, B.J.M., Ekmekyapar, T., and Daham, A.K. (2018). Behavior of steel-bar reinforced concrete-filled steel tube circular stub columns under axial loading. Paper presented at the 3rd International Conference on Civil and Environmental Engineering (ICOCEE), İzmir - Turkey.

5. AL-Eliwi, B.J.M., Ekmekyapar, T., and Ameen, Y.F.M. (2018). A study on performance of tied reinforced self-compacted concrete-filled steel tube circular stub columns. Paper presented at the 3rd International Conference on Civil and Environmental Engineering (ICOCEE 2018), İzmir - Turkey.

6. AL-Eliwi, B.J.M., Ekmekyapar, T., and Khudhur, E.S. (2017). Assessment of design specification predictions for the composite columns. Paper presented at the International Advanced Researches & Engineering Congress (IAREC 2017), Osmanye Korkut Ata University - Osmanye – Turkey.

7. AL-Eliwi, B.J.M., Ekmekyapar, T., and Al-Juboori, H.A.M.S. (2017). Comparison of AISC 360 – 16 and ec4 for the prediction of composite column capacity. Paper presented at the 2nd International Energy & Engineering Conference, Gaziantep University - Turkey.

8. AL-Eliwi, B.J.M. (2011). Nonlinear analysis of reinforced high strength concrete deep beams with openings. *Al-Rafidain Engineering Journal.* **20(4)**, 86-102.

9. AL-Eliwi, B.J.M., AL-Saffar, N.S., and AL-Jubori, N.H.J. (2010). Nonlinear finite element analysis of fibro-ferrocrete slabs. *The Iraqi Journal of Civil Engineering - IJCE.* **7(1)**, 29-41.

10. Ahmed, S.Y., and AL-Eliwi, B.J.M. (2010). Nonlinear finite element analysis of concrete beams reinforced with polymers re-bar. Paper presented at the 2nd Annual Scientific Conference of the College of Engineering Babylon Univervisty - Babylon - Iraq.

11. AL-Ta'an, S., and AL-Eliwi, B.J.M. (2008). Nonlinear finite elements analysis of partially prestressed fibrous concrete beams. Paper presented at the 7th International Congress, Concrete: Construction’s Sustainable Option, Dundee, United kingdom.

FOREIGN LANGUAGE

English

HOBBIES

1. Reading.
2. Computer software.